Photochemical and Photophysical Reaction Dynamics of Chemical and Biological Systems

Tesis Doctoral que presenta:

Felipe Zapata

Director de la Tesis Doctoral:

Luis Manuel Frutos

Departamento de Química Analítica, Química Física e Ingeniería Química

Doctorado en Química Fina

2014

Universidad de Alcalá

DEPARTAMENTO DE
QUÍMICA ANALÍTICA, QUÍMICA
FÍSICA E INGENIERÍA QUÍMICA
Edificio Polivalente
Carretera Madrid-Barcelona, Km. 33,600
28871 Alcalá de Henares (Madrid)
Telf. 91-8854 941

Aberto Escarpa Miguel, Director de la Comisión Académica del Programa de Doctorado en Química Fina

CERTIFICA:

Que el trabajo descrito en la presente memoria y titulado *" Photochemical and Photophysical Reaction Dynamics of Chemical and Biological Systems"* ha sido realizado por Felipe Zapata bajo la dirección del Dr. Luis Manuel Frutos Gaite y reúne a su entender todos los requisitos para su defensa y aprobación como Tesis Doctoral.

Y para que así conste a los efectos oportunos, firma el presente informe en Alcalá de Henares a 20 de Mayo de 2014.

Fdo. Alberto Escarpa Miguel

Universidad de Alcalá

DEPARTAMENTO DE QUÍMICA ANALÍTICA, QUÍMICA FÍSICA E INGENIERÍA QUÍMICA
Edificio Polivalente
Carretera Madrid-Barcelona, Km. 33,600
28871 Alcalá de Henares (Madrid)
Telf. 91-8854 941

Luis Manuel Frutos Gaite, Director de la Tesis Doctoral de Felipe Zapata

CERTIFICA:

Que el trabajo descrito en la presente memoria y titulado *" Photochemical and Photophysical Reaction Dynamics of Chemical and Biological Systems"* ha sido realizado por Felipe Zapata bajo la dirección del Dr. Luis Manuel Frutos Gaite y reúne a su entender todos los requisitos para su defensa y aprobación como Tesis Doctoral.

Y para que así conste a los efectos oportunos, firma el presente informe en Alcalá de Henares a 20 de Mayo de 2014.

Fdo. Luis Manuel FrutosGaite

A Mi Madre

Por Todo

Acknowledgements

Foremost, I would like to thank my supervisor, Professor Luis Manuel Frutos, for his guidance and support during this research, for encouraging me to follow my dreams. His patience and charisma have been a well of inspiration.

A special thanks to Professors Roland Lindh and Marcus Elstner, who kindly hosted me during my short research stay in their groups respectively at the University of Uppsala (Uppsala, Sweden) and the Karlsruhe Institute of technology (Karlsruhe, Germany).

The RESMOL group headquarters has provided a great environment to learn, talk about science and computers, discuss of politics and taste some good wines. None of this would have been possible without Professor Obis Castaño. I also want to thank the group members, especially to Cristina García-Iriepa, Alessio Valentini and Daniel Rivero, for all the constant feedback and interchange of ideas.

I would like to thank my friend Angel Alvarez, whom is the one responsible for introducing me to the world of computer science. Also I would like to thank my friend Marco Marazzi for his invaluable help and constant support.

I am grateful to my Colombian Friends: Andrea Pérez, Steven Roldan, Cristiam Santa, Lucas Blandon and Johnatan Diosa. Their friendship has been invaluable.

I thank my mother for all her patient, love and support. Also I would like to thank to my aunts, for their love and support.

Finally my gratitude and love to Natalia, for all her support.

Abstract

In this thesis we present a set of theoretical methodologies focused on photophysical and photochemical phenomena, which were implemented and subsequently applied to a collection of chemical and biological relevant systems.

The developments and applications are divided in four sections which are: energy transfer, dynamical studies of photoreactivity in biological systems, photochemical response to external forces and finally dynamical behaviour of molecular devices.

In the energy transfer section it is tackle the problem of finding which molecular coordinates modulates more efficiently the triplet energy transfer process (i.e. the triplet energy transfer reaction coordinate), together with a dynamical approach to the energy transfer at constant temperature.

The photochemical dynamics section firstly deals with the static and dynamical characterization of a minimal molecular model to study the phenomena of chemiluminescence and bioluminescence. Then the preliminary results of the simulations of fluorescence in the IrisFP are shown.

Subsequently the photodynamical response to external forces section contains a discussion on the effect of external forces in the reactivity of molecular systems, as well as change of spectroscopic properties.

Finally it is considered the design and operation of molecular motors control by light irradiation, where molecular simulations are used as a characterization tool of their properties.

Additionally, it was developed a set of programs focused on modularity, parallelism and readability, aiming to perform the numerical simulations described in this thesis.

List of Abbreviations

CASSCF Complete Active-Space Self-Consistent Field Method

CASPT2 Multiconfigurational Second-Order Perturbation Method

CI Conical Intersection

c-Stb Cis-Stilbene

DFT Density Functional Theory

FPs Photoactive Fluorescent Proteins

GHC Glasgow Haskell Compiler

HF Hartree-Fock

I/O Input/Output

MCSCF Multiconfigurational Self-Consistent Field

NAMD Non-Adiabatic Molecular Dynamics

PDT PhotoDynamic Therapy

PES Potential Energy Surface

RSNO R-substituted-Sulfur-Nitrosothiols

TD-DFT Time-Depended Density Functional Theory

TET Triplet Energy Transfer

TET-RC Triplet Energy Transfer – Reaction Coordinate

List of Publications

- M. A. Fernández-González, M. Marazzi, A. López-Delgado, F. Zapata, C. García-Iriepa , D. Rivero, O. Castaño, M. Temprado and L. M. Frutos. "*Structural Substituent Effect in the Excitation Energy of a Chromophore: Quantitative Determination and Application to S-Nitrosothiols"*. The Journal of Chemical Theory and Computation **2012**, 8, 3293–3302.
- C. García-Iriepa, M. Marazzi, F. Zapata, A. Valentini, D. Sampedro and L. M. Frutos. "*Chiral Hydrogen Bond Environment Providing Unidirectional Rotation in Photoactive Molecular Motors"*. Journal of Physical Chemistry Letters **2013**, 4, 1389-1396.
- P. Farahani, D. Roca-Sanjuán, F. Zapata and R. Lindh. "*Revisiting the Nonadiabatic Process in 1,2-Dioxetane".* The Journal of Chemical Theory and Computation **2013**, 9, 5404–5411.
- F. Zapata, M. Marazzi, O. Castaño, U. Acuña and L. M. Frutos. "*Definition and Determination of the Triplet-Triplet Energy Transfer Reaction Coordinate"*. The Journal of Chemical Physics **2014**, 140, 034102.
- F. Zapata, M. A. Fernández-Gonzáles, D. Rivero, A. Álvarez, M. Marazzi and L. M. Frutos. "*Towards an Optomechanical Control of Photoswitches by Tuning their Spectroscopical Properties: Structural and Dynamical Insights into Azobenzene"*. The Journal of Chemical Theory and Computation **2014**, 10, 312–323.
- C. García-Iriepa, M. Marazzi, F. Zapata, A. Valentini, D. Sampedro and L. M. Frutos. "*Molecular Design Concepts: Towards Highly Efficient Photoactive Molecular Motors*".
- F. Zapata, R. Palmeiro, O. Castaño and L. M. Frutos. "*Triplet Energy Transfer Reaction Coordinate Determined from Molecular Dynamics Simulations*"

Contents

Chapter 1: Introduction

"...how do we know what the ultimate good of Humanity will entail? We haven't at our disposal the infinite factors that the Machine has at its! Perhaps, to give you a not unfamiliar example, our entire technical civilization has created more unhappiness and misery than it has removed. Perhaps an agrarian or pastoral civilization, with less culture and less people would be better. If so, the Machines must move in that direction, preferably without telling us, since in our ignorant prejudices we only know that what we are used to, is good — and we would then fight change. Or perhaps a complete urbanization, or a completely caste-ridden society, or complete anarchy, is the answer. We don't know. Only the Machines know, and they are going there and taking us with them."

I, Robot. Isaac Asimov

In the picture: Alan Turing slate statue at Bletchley Park museum

In nature everything is in motion, change is the only permanent thing and we as humans try to understand the principles that govern such behaviour. In doing so, we create our own mental universes where we are free to subdivide the whole natural system into swallowable pieces. Once we have defined the boundaries of the subsystem of interest, we then endow the system with several ideal features (e.g. thermodynamic equilibrium, adiabatic electronic states, etc.) which allow us to reproduce some measurable properties using a mathematical framework.

This Ph.D. Thesis is then framed in the context of dynamical simulation of photoinduced physical and chemical processes, where the Born-Oppenheimer approximation is the basic theoretical support for the developments presented in this work. Together with it, Hamiltonian and non-Hamiltonian dynamical simulations were carried out to obtain statistics belonging to either microcanonical (NVE) or canonical ensembles (NVT).

In order to establish a framework in which the arguments of the present work are expanded, it is initially presented a chapter with a brief survey of the main methodologies used, as they are the Born-Oppenheimer molecular dynamics and the electronic structure methods. Also there are included the methods used to interpolate potential energy Surfaces (PES) as an alternative to expensive "on the fly" molecular dynamics. Finally in this methodology chapter is discussed the programming methods applied in the implementation of the discussed algorithms.

In the first part of this Ph.D. Thesis it is studied the energy transfer phenomenon, especially the triplet-triplet energy transfer (TET). This process is the most common and most important type of energy transfer, for instance in photosynthesis and energy transfer in molecular wires (Barigelletti and Flamigni 2000, Fraser, et al. 2001, Speiser 1996, You and Hsu 2011). Also, it is worth to notice that in the development of organic and polymer light-emitting diodes (OLEP/PLED), where triplet formation leads to a significant reduction in the theoretical efficiency of the device, being the modulation of triplet-triplet energy transfer a main objective in its improvement (Vura-Weis, et al. 2010). Moreover, It has been previously postulated that some molecular distortions of both donor and acceptor moieties involved in the process, lead to change in the amount of energy transferred, accounting for the experimental rate measures of TET and suggesting the possibility to module it (Frutos and Castano 2005). Since the early sixties it has been an

intense debate about the nature of the internal coordinates involved in the modulation of TET, being still an open question the identification of such coordinates and the qualitative contribution of them to the process. In this Ph. D. thesis we have addressed that question.

Subsequently, the second block of this work deals with dynamical processes on models systems to simulate biological phenomena. The first phenomenon studied is the chemiluminescence, which is process of light emission by an excited product of a chemical reaction, that when happens in living beings is called bioluminescence. In this last process it has been appointed the family of the 1,2-dioxetanes are responsible for the light emission . A minimal model of this molecule has been used to supply further information about the bioluminescence process.

On the other hand, the fluorescent proteins have become invaluable tools as biological markers (Shaner, et al. 2007), thanks to their versatility to emit at different wavelengths. Nevertheless, it is still a big challenge to design a fluorescent protein that absorb or emit to a given wavelength, since the mutations done in the genetic material which expresses the protein can result in a significantly environmental change, altering the behavior of the chromophore. A first step towards the design of such complex system is to understand the effect of the surroundings in the spectroscopic properties of the chromophore. In this Ph. D. we carried out a preliminary study in this line of reasoning.

In turn, the third block approach the role of external forces in both reactivity and changes in spectroscopic properties of molecular systems, providing the basis to suggest new systems which use external forces as the agent to change effectively some physical chemistry properties. The application of external forces to a molecular system, can result in quite interesting features as it is the geometric and energetic adjustment of both minima and transition states, due to the disruption generated by a mechanical force in the equilibrium geometries, enabling to modify the structure and the energy of both minima and transition states, which favor or hinder the reaction path of a molecule, changing completely the reactivity of a system (Konda, et al. 2013). In this work we have studied the change in reactivity due to external forces.

Also these geometrical disruptions can lead to significant change in the spectroscopical properties of the molecular system, opening the possibility to the design

of optomechanical control devices. Such possibility was explored using the azobenzene as a photoswitch under external forces.

Finally, on the last block it was approach the dynamical behavior of molecular devices as molecular motors and switches, which operate only in photoinduced cycles without any thermal step, using a chiral environment as the asymmetric agent responsible for the unidirectional rotation.

It is important to notice that regarding the programming tools developed to compute the results presented in this Ph.D. thesis, we made a special effort to introduce one of the most outstanding languages in regard to abstraction level, readability, parallelism, concurrency, automation, etc. Most important that the used language “per se”, it is the use of standard techniques in computer science to approach several well-known problems which appear in many fields being the computational chemistry one of them. And even though such problems are outside the scope of this Thesis, are nevertheless of primary importance in the development of simulation software.

1.1 Chapter Bibliography

Barigelletti, F.; Flamigni, L., Photoactive molecular wires based on metal complexes. *Chem. Soc. Rev.* **2000,** *29*, 1-12.

Fraser, N.; Hashimoto, H.; Cogdell, R., Carotenoids and bacterial photosynthesis: The story so far. *Photosynth. Res.* **2001,** *70*, 249-256.

Frutos, L. M.; Castano, O., A new algorithm for predicting triplet-triplet energy-transfer activated complex coordinate in terms of accurate potential-energy surfaces *J. Chem. Phys.* **2005,** *123*, 104108-104111.

Konda, S. S. M.; Brantley, J. N.; Varghese, B. T.; Wiggins, K. M.; Bielawski, C. W.; Makarov, D. E., Molecular Catch Bonds and the Anti-Hammond Effect in Polymer Mechanochemistry. *J. Am. Chem. Soc.* **2013,** *135*, 12722-12729.

Shaner, N. C.; Patterson, G. H.; Davidson, M. W., Advances in fluorescent protein technology. *J. Cell Sci.* **2007,** *120*, 4247-4260.

Speiser, S., Photophysics and Mechanisms of Intramolecular Electronic Energy Transfer in Bichromophoric Molecular Systems: Solution and Supersonic Jet Studies. *Chem. Rev.* **1996,** *96*, 1953-1976.

Vura-Weis, J.; Abdelwahed, S. H.; Shukla, R.; Rathore, R.; Ratner, M. A.; Wasielewski, M. R., Crossover from Single-Step Tunneling to Multistep Hopping for Molecular Triplet Energy Transfer. *Science* **2010,** *328*, 1547-1550.

You, Z.-Q.; Hsu, C.-P., Ab Inito Study on Triplet Excitation Energy Transfer in Photosynthetic Light-Harvesting Complexes. *The Journal of Physical Chemistry A* **2011,** *115*, 4092-4100.

Chapter 2: Methods

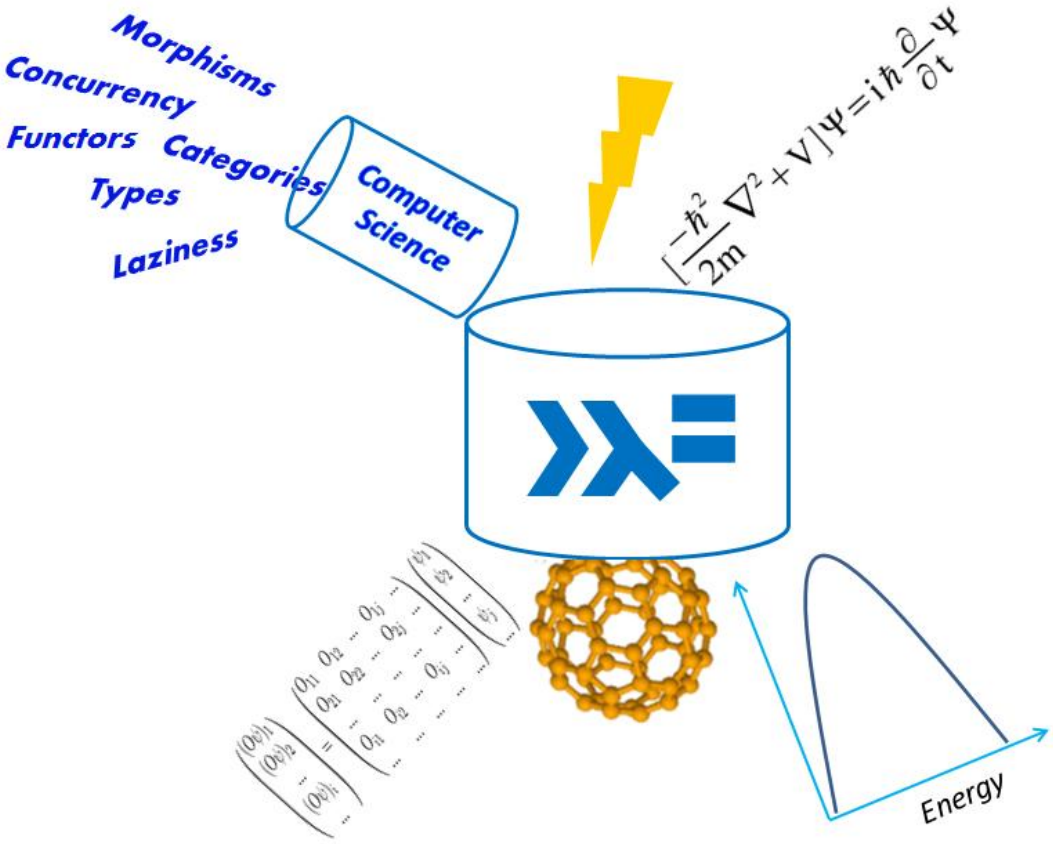

…To permit irresponsible authority is to sow disaster; to hold a man responsible for anything he does not control is to behave with blind idiocy. The unlimited democracies were unstable because their citizens were not responsible for the fashion in which they exerted their sovereign authority … other than through the tragic logic of history. The unique 'poll tax' that we must pay was unheard of. No attempt was made to determine whether a voter was socially responsible to the extent of his literally unlimited authority. If he voted the impossible, the disastrous possible happened instead – and responsibility was then forces on him willy-nilly and destroyed both him and his foundationless temple.

Starship Troppers. Robert Heinlein.

2.1 Molecular Dynamics

In principle the behaviour of a molecular system can be obtained solving the time-dependent Schrödinger equation involving the complete molecular hamiltonian, which completely determines the dynamical behaviour of all system's particles. Nevertheless, due to its enormous computational cost this mathematical treatment is restricted to systems with few atoms (Clary 2008). A bypass to ease the computational cost is the so called Born-Oppenheimer approximation, where the nuclei motion is decoupled from the electrons, as a consequence of the different time scales of motion between them, due to their mass difference (Born and Huang 1954). This approximation enables to simulate the molecular system dynamics using classical mechanics, constrained to an accurate description of the Potential Energy Surface (PES), which results directly from the Born-Oppenheimer approximation (Field 2007). Moreover, this treatment apart from being deterministic (we know in every step the position and velocity of the atoms and do not have a wave package propagating), cannot take into account quantum effects like the tunnel effect or the zero point vibrational energy. Besides, it must be introduced special treatments for the molecular phenomena where the Born-Oppenheimer approximation is no longer valid, like conical intersections or avoided crossings (Ben-Nun, et al. 2000, Worth and Cederbaum 2004). Despite the mentioned limitations, the Born-Oppenheimer molecular dynamics provides faithful results for the vast majority of chemistry.

The reliability of the dynamics depends on the PES accuracy to describe interactions among the system particles (Frenkel and Smit 2002, Griebel, et al. 2007), therefore is of central importance the use of accurate PESs, providing molecular forces that describe accurately the molecular systems interactions in an affordable computational time. There have been different approximations to determine forces in molecular dynamics; the first procedure consists in approximating molecular potential energy surfaces as a contribution of different interactions (usually bonding and non-bonding) obtained from experimental data or quantum-mechanical calculations, permitting the generation of force fields capable of reproducing many properties of the systems (Field 2007, Norrby and Brandt 2001). In these cases, there exist different force fields for different kind of systems, and usually they are limited to describe conformational changes rather than chemical processes. Among the existing force fields, it can be remarked AMBER for biological systems (Case, et al. 2006), CHARMM for

different chemical systems (Brooks, et al. 2009), OPLS for liquid simulations (Kaminski, et al. 2001), and many others for a large variety of problems.

On the other hand, a second approximation implies the calculation of the molecular forces in every step of the dynamics simulation (i.e. "on the fly" molecular dynamics) by using some ab-initio or any other electronic structure method, avoiding any analytical or numerical representation and describing only local properties of the PES (Bowman, et al. 2010).

There is a third possibility, which is actually a set of algorithms, to obtain an approximated PES through an interpolation of a set of points calculated at high level of theory and adjusted to minimize the error. The most outstanding interpolation methods are the reproducing kernel Hilbert space (Ho and Rabitz 1996), the neural networks (Witkoskie and Doren 2005), interpolating moving least squares (Maisuradze, et al. 2003), and the modified Shepard interpolation (Ischtwan and Collins 1994).

The disadvantage of the first strategy is its accuracy, which is in most cases limited to a qualitative description of the simulated processes and is also unable to accurately describe chemical reactions, intramolecular hydrogen bonds or predict excited state properties (Berendsen 1998, Cheatham and Young 2000); in the second strategy, the computational cost of molecular forces calculations using a high level of theory is unaffordable in many cases, especially for medium to large size systems and large simulation time (Hollebeek, et al. 1999). Moreover, the construction of a grid for the determination of PESs involves a very large set of parameters which are usually limited to few coordinates in small molecular systems. Besides, these mathematical approaches can produce different dynamical behaviour, due to small changes in the energy derivatives (Espinosa-Garcia, et al. 2012).

Moreover, the standard formulation of molecular dynamics results in trajectories belonging to the micro-canonical (NVE) ensemble. In this ensemble the number of particles, volume and total energy of the system is preserved. Nevertheless, most of the chemical experiments are carried out at constant temperature, which statistical behaviour is described by the canonical (NVT) ensemble. An approximation taking into account the temperature, was addressed by Andersen, whom introduced a thermostat in which the system is coupled to a heat bath driving the temperature to the desired value, where the

thermostat is represented by stochastic forces acting on some random picked particles generating a canonical distribution (Andersen 1980). The shortcoming of Anderson thermostats is its disability to calculate dynamics properties due to the stochastic forces which make the particles velocity incoherent between themselves (Frenkel and Smit 2002). An alternative is the extended Lagrangian methodology (Nosé 1984), in which an additional coordinate is introduced in the Lagrangian of the system. This methodology in conjunction with the development of non-Hamiltonian integrators have evolved to the Nosé-Hoover chain of thermostats, which is a widely used algorithm in the constant temperature molecular dynamics simulations (Tuckerman and Martyna 2000).

2.1.1 Born-Oppenheimer Molecular Dynamics

In order to establish the physical framework in which molecular dynamics is found, a brief account of the approximations starting from the non-relativist quantum mechanism formulation through the Schrödinger equation is described.

Time Dependent Schrödinger equation is given by

$$i\hbar\frac{\partial}{\partial t}\Phi\left(\mathbf{r}_n,\mathbf{R}_N;t\right)=\mathcal{H}\Phi\left(\mathbf{r}_n,\mathbf{R}_N;t\right) \tag{2.1.1}$$

Where $\mathbf{r_n}$ and $\mathbf{R_N}$ are the vectors containing the electron and nuclei coordinates, respectively. The Hamiltonian is formulated as

$$\sum_N\frac{\hbar^2}{2M_N}\nabla_N{}^2+\mathcal{H}_{elec}\left(\mathbf{r}_n,\mathbf{R}_N\right) \tag{2.1.2}$$

The electronic Hamiltonian $\mathcal{H}_{elec}$, the clamped nuclei part, includes electron-electron, electron-nuclear, nuclear-nuclear Coulomb interactions. Subsequently it is supposed that the exact solution for the time independent electronic Schrödinger equation can be found for a fixed position of the nuclei $\mathbf{R_N}$,

$$\mathcal{H}_{elec}\left(\mathbf{r}_n;\mathbf{R}_N\right)\Psi_k=\mathrm{E}_k\Psi_k\left(\mathbf{r}_n;\mathbf{R}_N\right) \tag{2.1.3}$$

These electronic wave functions must fulfill the orthonormal condition

$$\left\langle\Psi^*{}_i\middle|\Psi_j\right\rangle=\delta_{ij} \tag{2.1.4}$$

If all the electronic wave functions, called adiabatic eigenfunctions, are known for all possible nuclear configurations then the total wave function solution of equation (2.1.1) can be expressed by the following approximation introduced by Born (Born and Huang 1954),

$$\Phi\left(\mathbf{r}_n,\mathbf{R}_N;t\right)=\sum_{k=0}^{\infty}\Psi_k\left(\mathbf{r}_n;\mathbf{R}_N\right)\mathcal{X}\left(\mathbf{R}_N;t\right) \tag{2.1.5}$$

where χ are the nuclear wave functions, interpreted as the time-dependent expansion coefficients. Inserting the guess (2.1.5) into the time-dependent Schrödinger equation (2.1.1) and using the orthonormal condition (2.1.4) and integration over all the electron coordinates it is obtained a system of coupled differential equations

$$\left[-\sum_N\frac{\hbar^2}{2M_N}\nabla_N{}^2+\mathrm{E}_k\left(\mathbf{R}_N\right)\right]\mathcal{X}_k+\sum_j C_{kl}\mathcal{X}_j=i\hbar\frac{\partial\mathcal{X}_k}{\partial t} \tag{2.1.6}$$

where C_{kj} is the nonadiabatic coupling operator, defined by

$$C_{kj}=\left\langle\Psi_k{}^*\right|-\sum_N\frac{\hbar^2}{2M_N}\nabla_N{}^2\left|\Psi_j\right\rangle+\frac{1}{M_N}\sum_N\left\langle\Psi_k{}^*\right|-i\hbar\nabla_N\left|\Psi_j\right\rangle\left[-i\hbar\nabla_N\right] \tag{2.1.7}$$

The first term in the nonadiabatic coupling operator is the nuclei kinetic energy operator while the second depends on the momenta, whereas if the electronic wave function is real the second term equal zero.

A further approximation is needed to take into account only the kinetic matrix diagonal elements of the nonadiabatic coupling operator C_{kk}, which are correction to the kth adiabatic eigenvalue according to equation(2.1.6). Considering only diagonal elements implies that the nuclear propagation is carried out on a single quantum state and therefore the total wave function (2.1.5) is reduced to a product of the electronic and nuclear wave function

$$\Phi\left(\mathbf{r}_n,\mathbf{R}_N;t\right)\approx\Psi_k\left(\mathbf{r}_n;\mathbf{R}_N\right)\mathcal{X}\left(\mathbf{R}_N;t\right) \tag{2.1.8}$$

Born-Oppenheimer Molecular dynamics implies also to ignore the coupling nonadiabatic operator, and then equation (2.1.6) reduces to

$$\left[-\sum_{N}\frac{\hbar^2}{2M_N}\nabla_N{}^2+\mathrm{E}_k\left(\mathbf{R}_N\right)\right]\mathcal{X}_k=i\hbar\frac{\partial\mathcal{X}_k}{\partial t} \tag{2.1.9}$$

From this point onwards it only remains to show the feasibility to describe the molecular dynamics as classical particles, which required a more involving mathematical description as it has been shown elsewhere (Marx and Hutter 2009). The Resulting classical equation is given by

$$M_N\frac{d^2\mathbf{R}}{dt^2}=-\nabla_N V_k\left(\mathbf{r};\mathbf{R}\right) \tag{2.1.10}$$

Equation (2.1.10) describes a molecular system evolving according to the Newton Equations of motion under an effective potential V_k, which is obtained by solving the time dependent Schrödinger equation (2.1.3).

2.1.2 Non-Adiabatic Molecular Dynamics

The dynamical behavior of the vast majority of chemical systems can be rationalized under the Born-Oppenheimer approximation, but there are a set of interesting problems when coupling between nuclear and electronic movement cannot be longer neglected (e.g. inelastic collisions atom-atom / atom-molecule or the radiationless decay of excited states (Clary 2008, Kuppermann and Abrol 2003)). In general we are interested in the case where two electronic states are degenerated and this phenomenon involves only a subset on nuclear coordinates.

Therefore it is necessary a methodology that treats the degeneracy on those regions where the nuclei and electrons coupling is considerable and use the Born-Oppenheimer approximation for the rest of the phase space. To treat the coupling between nuclei and electrons there have been introduced a set of approximations, among them the diabatic states representation has been widely used, these diabatic states are chosen such that they may cross in the region where the coupling is not negligible, coupling effectively the electronic states involved in the transition (Köuppel, et al. 2007). The coupling between nuclei and electrons can lead to conical intersections and avoided crossings which are efficient channels for the deactivation of excited states (Worth and Cederbaum 2004). The details of such phenomenon has been intensively studied: (Ben-Nun, et al. 2000, Worth and Robb 2002).

In a seminal paper by Tully (Tully 1990), it was outlined the main desirable characteristics of an algorithm to carry out molecular dynamics simulations involving electronic transitions. These attributes are among others: computational affordability, branching of the trajectories in individual electronic states in weak electronic coupling areas, reversibility and inclusion of the quantum coherence. Following the afore mentioned criteria, in the present thesis we have used non-adiabatic molecular dynamics (NAMD), through application of the Tully's fewest switches algorithm (Tully 1990) with decoherence correction for the surface hop (Granucci and Persico 2007, Jaeger, et al. 2012) as implemented by (Valentini and Frutos 2012)

2.1.3 Classical Molecular Dynamics

On the other hand, Solution of the classical Hamiltonian equation depends on the chosen initial conditions, position and momenta, denoted as $\mathbf{R_0}$ and $\mathbf{P_0}$.The molecular system initial configuration at t_0 is a point in the phase space of dimensionality 6N (3N positions and 3N momenta), denoted as F($\mathbf{X_0}$) where

$$\mathbf{X}_0 = \mathbf{R}_1(0), .\mathbf{R}_N(0), \mathbf{P}_1(0), .., \mathbf{P}_N(0). \tag{2.1.11}$$

and N is the number of atoms. After Δt units of time, the molecular configuration has moved to the phase space point represented by $F(\mathbf{R_t},\mathbf{P_t})$, where the displacement vector can now be regarded as a coordinate transformation from t=0 to t and the phase space volume transformed according to

$$J(\mathbf{X}_0;\mathbf{X}_t) = \frac{\partial(\mathbf{X}_0)}{\partial(\mathbf{X}_t)}, \tag{2.1.12}$$

where **J** is the transformation Jacobian.

If the equation of motion is expressed in the general way,

$$\dot{\mathbf{X}} = \varphi(\mathbf{X}) = \left(-\frac{\partial \mathcal{H}}{\partial \mathbf{R}_1}, ..., -\frac{\partial \mathcal{H}}{\partial \mathbf{R}_N}, \frac{\partial \mathcal{H}}{\partial \mathbf{P}_1}, ..., \frac{\partial \mathcal{H}}{\partial \mathbf{P}_N} \right), \tag{2.1.13}$$

then the compressibility term is defined as,

$$k(\vec{X}, t) = \nabla_X \bullet \varphi. \tag{2.1.14}$$

Hamiltonian systems are incompressible meaning that previous expression is zero and the change of Jacobian with time expressed as,

$$\frac{d\mathbf{J}}{dt} = \mathbf{J}\nabla_X \bullet \varphi. \tag{2.1.15}$$

since the Jacobian transformation is constant in time for Hamiltonian systems, therefore Hamiltonian molecular dynamics must preserve the phase space (Tuckerman, et al. 1992). Accordingly when numerical integration is performed, an appropriate integration algorithm must be chosen such that preserved the volume of the phase space.

A Liouville Formulation of Time-Reversible Algorithms has been independently proposed by Tuckerman and Sexton (Sexton and Weingarten 1992, Tuckerman, et al. 1992). From the Liouville formulation and trotter Factorization it can be shown that the Velocity-Verlet algorithm is a volume preserving algorithm (Frenkel and Smit 2002), therefore the integration of the motion equations for molecular dynamics belonging to the microcanonical ensemble was carried out using the velocity-Verlet algorithm as described elsewhere (Swope, et al. 1982). The first step advances the positions and semi advances the velocities and then the force is calculated using the new positions. Finally, the velocity is semi advanced with the calculated forces.

In order to achieve the desired temperature, the initial conditions for constant energy simulations were obtained by scaling the velocity randomly and periodically, in such a way that the system increases its energy in small quantities followed by a relaxation period, until the system acquires the total required energy.

2.1.4 Non-Hamiltonian Dynamics

As it has been shown in section 2.1.3, Hamiltonian molecular dynamics preserved the phase space, but for non-Hamiltonian dynamics $\frac{dJ}{dt} \neq 0$ formal Integration of equation (2.1.15) results on the following expression,

$$J\left(\mathbf{X}_t;\mathbf{X}_0\right) = \exp\left(\int_0^t k(\mathbf{X}_\alpha,\alpha)d\alpha\right) \tag{2.1.16}$$

Assuming that the compressibility (2.1.14) can be regarded as the total time derivative of some function W, then $\kappa = \frac{dW}{dt}$ and the Jacobian is expressed by

$$\mathbf{J}\left(\mathbf{X}_t;\mathbf{X}_0\right) = \exp\left(\int_0^t \frac{dW}{dt}(\mathbf{X}_\alpha)d\alpha\right) = \exp\left(W\left(\mathbf{X}_t\right) - W\left(\mathbf{X}_0\right)\right). \tag{2.1.17}$$

Therefore for non-Hamiltonian dynamics the volume of the phase space transforms according to

$$d\mathbf{X}_t = \mathbf{exp}\left(W\left(\mathbf{X}_t\right) - W\left(\mathbf{X}_0\right)\right) d\mathbf{X}_0 \tag{2.1.18}$$

which after integration, results in the following conservation law,

$$\mathbf{e}^{-W\left(\vec{X}_t\right)} d\vec{X}_t = \mathbf{e}^{-W\left(\vec{X}_0\right)} d\vec{X}_0 \Rightarrow \sqrt{g\left(\vec{X}_t\right)} d\vec{X}_t = \sqrt{g\left(\vec{X}_0\right)} d\vec{X}_0 \tag{2.1.19}$$

the invariant metric introduced, named $\sqrt{g}$, can be used to formulate the general Liouville equation for non-Hamiltonian dynamics as follows,

$$\frac{\partial\left(f\sqrt{g}\right)}{\partial t} + \nabla_X \bullet \left(\dot{\mathbf{X}} f \sqrt{g}\right) = 0 \tag{2.1.20}$$

where ***f(X)*** is the phase space distribution. The ensemble average corresponding with this general Liouville equation is

$$\left\langle A \right\rangle = \frac{\int d\mathbf{X} \sqrt{g\left(\mathbf{X}\right)} A\left(\mathbf{X}\right) f\left(\mathbf{X}\right)}{\int d\mathbf{X} \sqrt{g\left(\mathbf{X}\right)} f\left(\mathbf{X}\right)} \tag{2.1.21}$$

if there are Nc quantities that must be conserved represented by

$$Z_i\left(\mathrm{X}\right) = C_i \forall i \in 1,..Nc \tag{2.1.22}$$

the partition function for non-Hamiltonian system is then given by,

$$\Omega\left(C_1,...,C_n\right) = \int d\mathrm{X} \sqrt{g\left(\mathrm{X}\right)} \prod_{i=1}^{Nc} \delta\left(Z_i\left(\mathrm{X}\right) - C_i\right) \tag{2.1.23}$$

using the previous partition function it is possible to obtain the canonical partition function (NVT) integrating over the dummy variables introduced to represent the thermostat as it will be described subsequently. For a detailed mathematical derivation of previous equations see (Tuckerman, et al. 2001).

In order to introduce the temperature as a constraint in the system, Nosé introduced a "dummy" coordinate in the classical Lagrangian in such a way that the new formulation can be expressed as,

$$\mathcal{L}_{Nose} = \sum_{i=1}^{N} \frac{m_i}{2} s^2 \left(\frac{d\mathbf{R}_i}{dt}\right)^2 - \mathcal{U}\left(\mathbf{R}^N\right) + \frac{Q}{2}\left(\frac{ds}{dt}\right)^2 - \frac{L}{\beta} \mathbf{ln}\, s \tag{2.1.24}$$

Where *s* is the additional variable which represents a thermostat, Q is a fictitious mass associated with *s*, L a parameter to be adjusted and β is the reciprocal temperature ($1/k_BT$). These kinds of Lagrangians are representative of those molecular dynamics simulations where the forces depend on the velocities. Further simplifications introduced by Hoover shown, that this Lagrangian produces a quantity that is conserved (Hoover and Hoover 2005), which is not a Hamiltonian since motion equations cannot be deduced from it, which can be formulated as

$$H_{Nose} = \sum_{i=1}^{N} \frac{\mathbf{p}_i^{\,2}}{2m_i} + \mathcal{U}\left(\mathbf{r}^N\right) + \frac{\xi^2 Q}{2} + L\frac{\ln s}{\beta} \tag{2.1.25}$$

Where $L=3N$ and $\xi = d\left(\ln s\right)/dt$. Hoover has shown that this equation is unique, meaning that other equation of the same form cannot produce a canonical ensemble (Hoover and Hoover 2005). A shortcoming of this development is that Nosé-Hoover algorithm can only generates a correct distribution if there is only one constant of motion. Tuckerman and co-workers proposed to couple the Nosé-Hoover thermostat to a chain of *M* thermostats to overcome this drawback (Tuckerman and Martyna 2000), resulting in the following motion equations

$$\frac{d\mathbf{R}_i}{dt} = \frac{\mathbf{P}_i}{m_i} \tag{2.1.26}$$

$$\frac{d\mathbf{P}_i}{dt} = \vec{F}_i - \frac{P\xi_1}{Q_1}\mathbf{P}_i \tag{2.1.27}$$

$$\frac{d\xi_k}{dt} = \frac{P\xi_k}{Q_k} \; \forall k \in 1,2..M \tag{2.1.28}$$

$$\frac{d\xi_k}{dt} = \frac{P\xi_k}{Q_k} \; \forall k \in 1,2..M \tag{2.1.29}$$

$$\frac{dP\xi_1}{dt} = \left(\sum_{i=1}^{N}\frac{P_i}{m_i} - 3Nk_BT\right) - \frac{P\xi_2}{Q_2}P\xi_1 \tag{2.1.30}$$

$$\frac{dP\xi_k}{dt} = \left(\frac{P^2\xi_{k-1}}{Q_{k-1}} - k_BT\right) - \frac{P\xi_{k+1}}{Q_{k+1}}P\xi_k \tag{2.1.31}$$

$$\frac{dP\xi_M}{dt} = \left(\frac{P^2\xi_{M-1}}{Q_{M-1}} - k_B T \right) \tag{2.1.32}$$

Where the quantity conserved is formulated as

$$\mathcal{H}_{NHC} = \mathcal{H}(\mathbf{R},\mathbf{P}) + \sum_{k=1}^{M} \frac{P^2\xi_k}{2Q_k} + 3Nk_B T\xi_1 + \sum_{k=2}^{M} k_B T\xi_k \tag{2.1.33}$$

using the partition function for non-Hamiltonian dynamics and the previous example the partition function for the canonical ensemble can be generated as shown by Tuckerman (Tuckerman and Martyna 2000).

Non-Hamiltonian Molecular dynamics required special integration methodologies, considering that forces depend on the velocities and subsequently algorithms as the velocity-Verlet must be iteratively resolved, losing time reversible properties. Therefore were introduced reversible integrators to extended systems, using the Liouville operator and the trotter factorization. A derivation of a family of integrator for the Nosé-Hoover Chain is described by (Martyna, et al. 1996).

On the other hand, the initial conditions for simulating the canonical ensemble are prepared getting random velocities from a Maxwell-Boltzmann distribution, assuming that every component of the velocity can be considered as an independent Gaussian random variable (Field 2007). In order to avoid misinterpretation and numerical drifting in the temperature, the motion and rotation of the center of mass is removed when there are not involved chemical reactions.

2.1.5 Quantum Mechanics/Molecular Mechanics Method

A hybrid Quantum Mechanics/Molecular Mechanics (QM/MM) model is composed by two subsystems: a QM region is focused on the description of a chemical reaction and the surrounding MM region is treated classically. Therefore, QM/MM methods are suitable to describe the environment effect on a particular molecular system, e.g. surrounding it by explicit solvent molecules, or considering the actual biomolecule where it is included (a base pair in DNA, an amino acid in a protein, etc.).

Different QM/MM schemes were designed and developed (Lin and Truhlar 2007). In this Thesis, we adopted an approach by which the Hamiltonian of the QM/MM model ($\hat{\mathbf{H}}_{tot}$) is a sum of three components:

$$\hat{\mathbf{H}}_{tot} = \hat{\mathbf{H}}_{QM} + \hat{\mathbf{H}}_{MM} + \hat{\mathbf{H}}_{QM/MM} \tag{2.1.34}$$

$\hat{\mathbf{H}}_{QM}$ is the Hamiltonian of the QM system in vacuum, while $\hat{\mathbf{H}}_{MM}$ refers to the MM region treated with a classical force field. The interaction between QM and MM regions is described by the term $\hat{\mathbf{H}}_{QM/MM}$:

$$\hat{\mathbf{H}}_{QM/MM} = \hat{\mathbf{V}}^{elec}_{QM/MM} + \hat{\mathbf{V}}^{nucl}_{QM/MM} + \hat{\mathbf{V}}^{vdw}_{QM/MM} + \hat{\mathbf{V}}^{bond}_{QM/MM} \tag{2.1.35}$$

by which electrostatic, nuclear, van der Waals and bonding interactions are taken into account, respectively. Especially, the electrostatic and nuclear terms are given by the following relations:

$$\hat{\mathbf{V}}^{elec}_{QM/MM} = \sum_{i}^{n} \sum_{A \in MM} \frac{q_A}{|\mathbf{r}_A - \mathbf{r}_i|} \tag{2.1.36}$$

$$\hat{\mathbf{V}}^{nucl}_{QM/MM} = \sum_{A}^{N} \sum_{B \in MM} \frac{Z_A q_B}{|\mathbf{R}_A - \mathbf{R}_B|} \tag{2.1.37}$$

$\hat{\mathbf{V}}^{elec}_{QM/MM}$ describes the interaction between the electrons of the QM region with the point charges (q_A) in the MM region; while $\hat{\mathbf{V}}^{nucl}_{QM/MM}$ is responsible for the interaction between the nuclei of the QM region (with Z_A being the proton number of nucleus A) and the B point charges of the MM region. For both electrostatic and nuclear terms the Electro-Static Potential Fitted (ESPF) method is applied (Ferré and Ángyán 2002): one-electron operators are added to $\hat{\mathbf{H}}_{QM}$ in order to calculate the interaction between the QM charges distribution and the MM electrostatic potential field, considered as an external field, resulting in the following interaction energy,

$$\Delta E = \sum_{\alpha} \sum_{\mu\nu} \mathrm{P}_{\mu\nu} Q^{\alpha}_{\mu\nu} V^{\alpha} \tag{2.1.38}$$

where $P_{\mu\nu}$ and $Q^{\alpha}_{\mu\nu}$ are the density matrix and multipole-like matrix elements interacting with the electrostatic potential V^{α} calculated at the point center α.

Van der Waals interactions are taken into account by a short-range Lennard-Jones term, assigning parameters to both QM and MM atoms,

$$\hat{\mathbf{V}}^{vdw}_{QM/MM} = \sum_{A>B} 4\varepsilon_{AB}\left[\left(\frac{\sigma_{AB}}{d_{AB}}\right)^{12} - \left(\frac{\sigma_{AB}}{d_{AB}}\right)^{6}\right] \tag{2.1.39}$$

where for every AB couple, ε is the potential well, σ is the finite distance at which the potential between A and B is zero, and d_{AB} is the distance between A and B.

If the frontier between QM and MM regions involves covalent bonds, an additional term $\left(\hat{\mathbf{V}}^{bond}_{QM/MM}\right)$ is added to $\hat{\mathbf{H}}_{tot}$, including some empirical bonded terms. The scheme used to treat the frontier bonds is called Link Atom (LA), where a monovalent atom (usually hydrogen) is used to saturate the QM system. Applying the Morokuma's scheme for LA positioning, the distance between LA and the first linked AM atom $\left(d_{QM_1-LA}\right)$ is modified with respect to the frontier QM and MM atoms $\left(d_{QM_1-MM_1}\right)$ while optimizing, thanks to a scaling factor (S_{LA}):

$$d_{QM_1-LA} = S_{LA} d_{QM_1-MM_1} \tag{2.1.40}$$

2.2 Electronic Structure Methodologies

Ab initio electronic structure calculations are mathematical approximations based only in physical constants (i.e. they do not depend on empirical parameterizations), which aim to solve the time-independent Schrödinger equation (2.1.3). The initial starting point for most method is the Hartree-Fock approximation, which established that the ground-state wavefunction Ψ_0 is determined by products of monoelectronic wavefunctions of the molecular orbitals. Within this approximation, the electronic field is determined by a self-consistent field method, where every single electron is moving under the mean-potential created by the other electrons. The wavefunction is built from Slater

determinants as an antisymmetrized product of spin orbitals (i.e. the product of a spatial orbital and a spin function):

$$\left|\Psi_0\right\rangle = (n!)^{\frac{1}{2}} \begin{pmatrix} \varphi_1(1) & \cdots & \varphi_n(1) \\ \vdots & \ddots & \vdots \\ \varphi_1(n) & \cdots & \varphi_n(n) \end{pmatrix} = \left|\varphi_1\varphi_2\cdots\varphi_n\right\rangle \tag{2.2.1}$$

The expected value of the energy is then calculated as

$$\mathrm{E} = \left\langle \Psi_0 \left| \hat{H} \right| \Psi_0 \right\rangle \tag{2.2.2}$$

Where the Hamiltonian can be expressed as follows:

$$\hat{H} = -\frac{1}{2}\sum_{\mathrm{N}} \nabla_{\mathrm{i}}^2 - \sum_{k=1}^{N}\sum_{i=1}^{n} \frac{Z_k}{\mathbf{R}_{ki}} + \sum_{j=1}^{n}\sum_{i\neq j}^{n} \frac{1}{\mathbf{r}_{ij}} \tag{2.2.3}$$

where *n* stands for the number of electron and N represents the number of nuclei. The first, second and third term on the right hand side of (2.2.3) are the electron kinetic energy operator, the nuclei-electron attraction potential operator and the electron-electron repulsion potential operator, respectively. This corresponds to the electronic Hamiltonian, since the nuclei kinetic energy is omitted, based on the Born−Oppenheimer approximation. Now we have all the elements to determine the energy of the system, by replacing (2.2.1) and (2.2.3) in (2.2.2), obtaining the following expression for the energy:

$$\mathrm{E}_0 = 2\sum_{i=1}^{n/2} HCore_{ij} + \sum_{j=1}^{n/2}\sum_{i=1}^{n/2} \left(2J_{ij} - K_{ij}\right) \tag{2.2.4}$$

Where $HCore_{ij}$ is the electronic energy of a single electron moving under the attraction of a nuclear "core", without interact with other electrons; J_{ij} is the so-called Coulomb integral, representing electrostatic repulsion between the electrons; K_{ij} is called the exchange integral, which is a pure quantum effect without similar in classical physics, standing for the correlation in the motion of the electrons with parallel spin which are correlated in the single determinant approximation of Hartree-Fock. The terms J_{ij} and K_{ij} take into account for the average electrostatic repulsion between electrons. The

energy is finally calculated by applying the variational principle (Szabo and Ostlund 1996).

2.2.1 The Complete Active-Space Self-Consistent Field Method

The principle of all Multiconfigurational Self-Consistent Field (MCSCF) methods is the expansion of a monoconfigurational HF wavefunction as a linear combination of Slater determinants. Among all MCSCF methods, the CASSCF method results in a MCSCF wavefunction generated by linear combination of configurations $\mathbf{\Phi}_k$, considering that each configuration corresponds to a different occupation of the molecular orbitals φ_i included in the so-called active space (Roos 2007), where each molecular orbital is a linear combination of atomic orbitals χ_μ :

$$\left|\mathbf{\Psi}_{CASSCF}\right\rangle = \sum_k A_k \left|\mathbf{\Phi}_k\right\rangle \tag{2.2.5}$$

$$\mathbf{\Phi}_k = A\prod_{i\subset k}\varphi_i \tag{2.2.6}$$

$$\varphi_i = \sum_\mu C_{\mu i}\chi_\mu \tag{2.2.7}$$

The optimization of $\mathbf{\Psi}_{CASSCF}$ is based, therefore, on the simultaneous variation of orbital coefficients $C_{\mu i}$ and configuration coefficients A_k, until reaching self-consistency. Once $\mathbf{\Psi}_{CASSCF}$ is optimized, the energy of the system is calculated as follows:

$$\mathrm{E} = \left\langle \Psi \left| \hat{H} \right| \Psi \right\rangle = \sum_{i,j} h_{ij} D_{ij} + \sum_{i,j,k,l} g_{ijkl} P_{ijkl} \tag{2.2.8}$$

Where h_{ij} and g_{ijkl} are the monoelectronic and bielectronic integrals, respectively:

$$h_{ij} = \left\langle \chi_i(1) \left| \hat{h} \right| \chi_J(1) \right\rangle \tag{2.2.9}$$

$$g_{ijkl} = \iint \varphi_i^*(\mathbf{q}_1)\varphi_j(\mathbf{q}_1)\mathbf{r}_{12}^{-1}\varphi_k^*(\mathbf{q}_2)\varphi_l(\mathbf{q}_2)\,d\mathbf{q}_1 d\mathbf{q}_2 \tag{2.2.10}$$

Where **r** is the position vector and **D** is the first order reduced density matrix, which is defined as a function of the expansion coefficients given by (2.2.5):

$$D_{ij} = \left\langle \Psi \left| \hat{E}_{ij} \right| \Psi \right\rangle = \sum_{K,L} A_K^* A_L D_{ij}^{KL} = \sum_{K,L} A_K^* A_L \left\langle \Phi_K \left| \hat{E}_{ij} \right| \Phi_L \right\rangle \qquad (2.2.11)$$

P is the second order reduced density matrix, with elements:

$$P_{ijkl} = \frac{1}{2} \sum_{K,L} A_K^* A_L \left\langle \Phi_K \left| \hat{E}_{ij} \hat{E}_{kl} - \delta_{kj} \hat{E}_{il} \right| \Phi_L \right\rangle \equiv \sum_{K,L} A_K^* A_L P_{ijkl}^{K,L} \qquad (2.2.12)$$

where $P_{ijkl}^{K,L}$ are defined as the bielectronic coupling coefficients. One of the characteristics of the CASSCF method is the selection of the configurations (i.e. the orbitals) to be included in the wavefunction. In principle, the active space could include all the orbitals, leading to a so called full CI (Configuration Interaction) treatment. Unfortunately, a full CI requires an unfeasibly high computational cost even for small size molecules, and therefore a limited number of orbitals have to be selected. The number and type of orbitals will depend on the chemical nature of the problem to be studied, in any case being necessary that all chemically relevant orbitals are part of the active space (e.g., for a conjugated hydrocarbon the active space should include all π and π* orbitals). Therefore, when applying the CASSCF method all orbitals will be divided into three groups: (i) inactive orbitals, which remain doubly occupied; (ii) virtual orbitals, which stay unoccupied; (iii) active orbitals, where all possible electronic excitations are allowed, resulting in a total number *N* of configuration state functions which form Ψ_{CASSCF}, given by the following formula (for a defined state multiplicity) (Cramer 2004):

$$N = \frac{n!(n+1)!}{\left(\frac{m}{2}\right)!\left(\frac{m}{2}+1\right)!\left(n-\frac{m}{2}\right)!\left(n-\frac{m}{2}+1\right)!} \qquad (2.2.13)$$

where n is the number of electrons and m the number of orbitals, usually indicated as CASSCF(*m*,*n*). With state-of-the-art computational resources, a CASSCF(4,4) is a straightforward task, being *N*=20, while a CASSCF(14,12) is highly demanding, being *N*=169884. Considering that the computational feasibility depends also on the basis set applied, we can nowadays set the upper limit to the size of the active space as a CASSCF(20,20).

2.2.2 The CASPT2 Method

One of the most convenient ways to include dynamical electron correlation effects in molecules is to apply a second order perturbation approach. In the CASPT2 method, a multiconfigurational CASSCF wavefunction $|\Psi_0\rangle$ is considered as zeroth order wavefunction for a second order perturbation approach correlation problem. The derived formulation was shown to be valid for any reference state built as a full CI wavefunction in a certain orbital sunspace (Andersson, et al. 1990).

$|\Psi_0\rangle$ is expanded in a configuration space which, for convenience, is divided into four subspaces: V_0 is the one dimensional space spanned by $|\Psi_0\rangle$ for the electronic state calculated; V_k is the orthogonal space to $|\Psi_0\rangle$ within the restricted full CI subspace used to generate the CASSCF wavefunction; V_{SD} is the space related to single and double excitation states generated from V_0; V_{TQ} is the space containing all higher order excitations not included in V_0, V_K and V_{SD}. It has to be noted that only the functions defined in the V_{SD} subspace interact with $|\Psi_0\rangle$ via the total Hamiltonian, and therefore it has to be considered that only V_0 contributes to the expansion of the first order wavefunction when formulating the zeroth order Hamiltonian.

Since the total dimension of the first order space corresponds to the dimension of V_{SD} (Andersson, et al. 1990),the first order wavefunction can be expanded into a set of functions $|\Psi_0\rangle$ from V_{SD}:

$$|\Psi_1\rangle = \sum_{j=1}^{M} C_j |\Psi_j\rangle \tag{2.2.14}$$

Where $M \geq V_{SD}$ dimension and the coefficients C_j are calculating by the solving the following system of linear equations:

$$\sum_{j=1}^{M} C_j \langle \Psi_i | H_0 - E_0 | \Psi_j \rangle = -\langle \Psi_i | H | \Psi_0 \rangle, i = 1,\ldots,M \tag{2.2.15}$$

Where the zeroth order energy can be readily calculated as:

$$E_0 = \langle \Psi_0 | H | \Psi_0 \rangle \tag{2.2.16}$$

It is reasonable to assume that, in the majority of cases, dimension and therefore the double excitation states will be linearly dependent. Such linear (and near linear) dependence can be removed by diagonalizing the overlap matris **S**

$$S_{ij} = \left\langle \Psi_i \middle| \Psi_j \right\rangle \tag{2.2.17}$$

and removing the eigenvectors corresponding to zero (or close to zero) eigenvalues. Eq. (2.2.14) can be then solved by transforming the CI space into a orthonormalized form, and the second order energy can be finally obtained. The resulting CASPT2 energy takes into account a weighted sum over all active orbitals, being this formulation valid for all types of electronic excitations.

Usually, the inclusion of dynamical electron correlation effects brings to quantitative results in photochemistry and photophysics, when compared to experimental data. The main drawbacks are a considerable larger time compare with CASSCF calculations and the lack of an analytical energy gradient for medium and large size active spaces.

2.2.3 Density Functional Theory

As a quantum chemical methodology, DFT is based on two theorems proved by Hohenberg and Kohn in 1964. The Hohenberg-Kohn existence theorem states that the energy of a molecular system depends on the ground-state electron density $\rho = \rho(\mathbf{q})$, since this density determines the Hamiltonian operator. Integration of the ground-state density gives the number of electrons that interact with each other and within an external potential (i.e. the attraction to the nuclei). The Hohenberg-Kohn existence theorem proves that the ground-state electron density determines the external potential, and therefore the Hamiltonian (Cramer 2004, Hohenberg and Kohn 1964).

By this formulation, the energy depends on the electron density, i.e. it is a density functional $\mathrm{E}[\rho]$:

$$\mathrm{E}[\rho] = T_e[\rho] + \int \rho(\mathbf{r}) v(\mathbf{r}) + \frac{1}{2} \iint \rho(\mathbf{q}_1) - \rho(\mathbf{q}_1) \frac{\rho(\mathbf{q}_1) - \rho(\mathbf{q}_1)}{|\mathbf{q}_1 - \mathbf{q}_2|} d\mathbf{q}_1 d\mathbf{q}_2 + E_{CE}[\rho] \tag{2.2.18}$$

where $T_e[\rho]$ is the electron kinetic energy, the second and third term on the right hand side are related to the classical electrostatic interaction between electrons, which is the correlation and exchange energy term, containing all non-classical electronic interactions. The exact formulation of this last term is not known; therefore it requires an approximate expression giving rise to different possible types of density functional.

The existence of an electron density as a fundamental quantity is thus a first step, which is followed by a demonstration that the electron density obeys to the variational principle, and it can be optimized. The Hohenberg–Kohn variational theorem assumes that a guess ground-state electron density is provided (thanks to the existence theorem), by which the proper number of electrons can be integrated. As a consequence, such electron density determines a guess wavefunction (Ψ_{guess}) and Hamiltonian $(\mathbf{H}_{guess})$, permitting the evaluation of the expected energy (E_{guess}), being greater than or equal to the ground-state true energy (E_0):

$$\left\langle \Psi_{guess} \middle| \widehat{\mathbf{H}}_{guess} \middle| \Psi_{guess} \right\rangle = E_{guess} \geq E_0 \tag{2.2.19}$$

By this procedure, it can be avoided to solve the Schrödinger equation to compute the energy, even if it does not have a consistent criterion to follow in order to choose the best electron densities that leads to reliable ground-state energy $(E_{guess} \approx E_0)$. Especially, a different approximation $E_{CE}[\rho]$ of can lead to a different final energy value, being necessary a careful decision of the density functional to be applied (i.e. a suitable density functional has to be calibrated for each set of molecules).

2.2.4 Crossings between Electronic States

As it has been discussed previously in the vicinity of an electronic state crossing the Born-Oppenheimer approximation is no longer valid, and it is necessary to take into account non-adiabatic effects to correctly describe photodynamical processes.

Two potential energy surfaces $E_1(\mathbf{q})$ and $E_2(\mathbf{q})$ intersect in a set of coordinates **q** where the energy for both states is equal. The subspace spanned by these coordinates could be expected a subspace of *3N-7* dimensions (being *3N-6* the degrees of freedom of the system). However, E_1 and E_2 are two solutions of the same eigenvalue problem given by a single Hamiltonian ***H***, and therefore they are not independent of each other, leading to an additional condition (Neumann and wigner 1929, Teller 1937).

The two intersecting adiabatic states Ψ_1 and Ψ_2 can be expressed as linear combinations of two diabatic orthogonal states Φ_1 and Φ_2 in the complementary hyperspace to the one spanned by all other eigenstates Ψ_n $(n \geq 3)$, for which the energies E_n $(n \geq 3)$ are non-degenerated with E_1 and E_2:

$$\Psi_1 = c_{11}\Phi_1 + c_{12}\Phi_2;\ \Psi_2 = c_{12}\Phi_1 + c_{22}\Phi_2 \tag{2.2.20}$$

By solving the eigenvalue problem given by the 2×2 matrix $H_{ij} = \langle \varphi_i | \hat{H} | \varphi_i \rangle$, the expansion coefficients and the corresponding energies (E_1 and E_2) can be determined. The matrix elements are therefore:

$$\begin{aligned} H_{11} &= \langle \Phi_1 | \hat{H} | \Phi_1 \rangle \\ H_{22} &= \langle \Phi_2 | \hat{H} | \Phi_2 \rangle \\ H_{12} &= \langle \Phi_1 | \hat{H} | \Phi_2 \rangle = H_{12} \end{aligned} \tag{2.2.21}$$

It can be demonstrated that E_1 and E_2 have the following expressions (Schelegel 1987):

$$E_{1,2} = \frac{(H_{11} + H_{22}) \pm \sqrt{(H_{11} - H_{22})^2 + 4{H_{12}}^2}}{2} \tag{2.2.22}$$

Therefore, in order to fulfill that $E_1 = E_2$, two independent conditions have to be satisfied:

$$H_{11} = H_{22};\ H_{12} = H_{21} = 0 \tag{2.2.23}$$

leading to the existence of at least two independent coordinates, $\boldsymbol{q_1}$ and $\boldsymbol{q_2}$.

In a diatomic molecule, H_{12} is always zero for states of different symmetry, thus only $H_{12} = H_{21}$ has to be satisfied. This is coherent with the existence of only one internal coordinate (i.e. the interatomic distance), being a necessary value to satisfy the condition. If the two states belong to the same symmetry, an intersection is therefore not possible.

In a polyatomic (three or more atoms) molecule, the increased number of degrees of freedom allows both conditions of (2.2.23) to be satisfied simultaneously (even for the same symmetry) for suitable values of $\boldsymbol{q_1}$ and $\boldsymbol{q_2}$. This means that a branching plane spanned by $\boldsymbol{q_1}$ and $\boldsymbol{q_2}$ vectors can be defined (with the origin at the point where both conditions of (2.2.23) are satisfied), where energy degeneracy is left. On the other hand, the *3N-8* hyperspace defined by all degrees of freedom but $\boldsymbol{q_1}$ and $\boldsymbol{q_2}$ determines the coordinates which can be varied remaining in the crossing region (i.e. energy degeneracy holds).

Imposing the conditions of (2.2.23) two eigenvalues are found, resulting in the equation of a double cone with vertex at the origin. This is why crossing points between electronic states are called conical intersections (CIs).

The crossing can be real or avoided: considering the two diabatic orthogonal states Φ_1 and Φ_2 which form the two adiabatic states Ψ_1 and Ψ_2 as depicted in (2.2.20), the crossing condition is fulfilled when Φ_1 and Φ_2 cross each other, meaning that $H_{12} = H_{21}$. At this point the energies of the adiabatic functions are $E_1 = H_{11} - H_{12}$ and $E_1 = H_{11} + H_{12}$. The energy gap is therefore $E_2 - E_1 = 2H_{12}$. If $H_{12} = 0$ the crossing is real (a CI), on the other hand if $H_{12} \neq 0$ the crossing is avoided, meaning that both PESs involved in the process become near in energy but do not cross and instead repel each other.

In the adiabatic basis, $\boldsymbol{q_1}$ and $\boldsymbol{q_2}$ are defined as follows:

$$\mathbf{q}_1 = \frac{\partial\left(E_1 - E_2\right)}{\partial \mathbf{q}} \tag{2.2.24}$$

$$\mathbf{q}_2 = \left\langle \Psi_1 \middle| \frac{\partial H}{\partial \mathbf{q}} \middle| \Psi_2 \right\rangle \tag{2.2.25}$$

$\mathbf{q}_1$ corresponds to the gradient difference (**GD**) vector, while $\mathbf{q}_2$ is parallel to the direction of the derivative coupling (**DC**) vector:

$$DC = \left\langle \Psi_1 \middle| \frac{\partial}{\partial \mathbf{q}} \Psi_2 \right\rangle \tag{2.2.26}$$

Apart from their mathematical description, **GD** and **DC** vectors have a physical meaning: the **GD** vector measures the distortion of the system leading to the largest variation of the energy difference between the two electronic states involved in the crossing. The **DC** vector measures the distortion of the system providing the maximum coupling between the two electronic states involved in the crossing.

2.3 Spectroscopic Properties

In electronic spectroscopy, two quantities are fundamental in order to reproduce absorption and emission spectra: the energy difference between distinct electronic states and the oscillator strength. Indeed, an experimental UV/visible spectrum is characterized by absorption or emission wavelengths (corresponding to the energies of the electronic transitions) and absorption or emission intensities (which depend on oscillator strengths and indicate the transition probabilities).

An electronic transition is intended from an initial state *i* to a final state *f*, being usually (but not necessarily) *i* the ground-state and *f* one of the excited-states for absorption, while *i* is one of the excited-states and the *f* the ground-state for emission. More in general $i < f$ for absorption, while $i > f$ for emission. The transition dipole moment couples the wavefunctions of initial and final states (Ψ_i and Ψ_f), resulting in a vector $\boldsymbol{\mu}_{if}$ which expresses the redistribution of electrons in the molecular system after the transition:

$$\mu_{if} = \left\langle \Psi_i(\mathrm{q}) \middle| \hat{\mu} \middle| \Psi_j(\mathrm{q}) \right\rangle \tag{2.3.1}$$

Being **q** the position vector. It may be shown that the square of μ_{if} module is, in case of emission:

$$\mu_{if}^{if} = A_{if} \frac{3\varepsilon_0 hc^3}{2\omega_{if}^3} \tag{2.3.2}$$

where ε_0 the dielectric constant is in vacuum, h the Planck's constant, *c* the speed of light, ω_{if} the resonance frequency of the transition and A_{if} is the Einstein coefficient to describe the total rate of spontaneous emission. The emission oscillator strength f_{if}^{em} can be then defined by the relation (Hilborn 1982):

$$f_{if}^{em} = -\frac{1}{3}\frac{A_{if}}{\gamma_{cl}} \tag{2.3.3}$$

$$\gamma_{cl} = \frac{e^2\omega_{if}^2}{6\pi\varepsilon_0 m_e c^3} \tag{2.3.4}$$

where *e* and m_e are charge and mass of the electron. γ_{cl} determines the classical radiative decay rate of the single electron oscillator at frequency ω_{if}.

The absorption oscillator strength f_{if}^{abs} is then defined by:

$$g_{down} f_{if}^{abs} \equiv -g_{up} f_{if}^{em} \equiv gf \tag{2.3.5}$$

where g_{down} and g_{up} are the degeneracy factors of the two electronic states (upper and lower energy). The *f* values have been defined like this: if *(i)* g_{down}=1 (i.e. the angular momentum of the lower state in energy J_{down}, *(ii)* g_{up}=3 (i.e. J_{up}=1) and *(iii)* $A_{if} = \gamma_{cl}$, then f_{if}^{abs}=1 and $f_{if}^{em} = -\frac{1}{3}$. Tables of *gf* values can be found in literature (Hilborn 1982).

The absorption oscillator strength can be finally related to A_{if}

$$f_{if}^{abs} = \frac{g_{up}}{g_{down}} \frac{2\pi\varepsilon_0 m_e c^3 A_{if}}{e^2 \omega_{if}^2} \tag{2.3.6}$$

As alternative procedure, f_{if}^{abs} can be determined by comparing the absorption cross section of a classical oscillator with the one determined by the Einstein B coefficients (which are defined in terms of transition rates for induced absorption and stimulated emission).

2.4 Interpolation Methods

2.4.1 Quadratic approximation

In order to construct the potential energy surfaces of a molecule in a given state we have to perform, as a first approximation, a quadratic expansion of the potential energy function in terms of internal coordinates:

$$E^{(n)}(\boldsymbol{q}) = E^{(n)}(\boldsymbol{q_0}) + (\boldsymbol{q}-\boldsymbol{q_0})^t \cdot \boldsymbol{g}_{\boldsymbol{q_0}}^{(n)} + \frac{1}{2}(\boldsymbol{q}-\boldsymbol{q_0})^t \boldsymbol{H}_{\boldsymbol{q_0}}^{(n)} (\boldsymbol{q}-\boldsymbol{q_0}) \tag{2.4.1}$$

Where **q** is a vector in internal coordinates denoting any configuration (i.e. molecular structure), $\mathbf{q_0}$ is also a vector in internal coordinates corresponding to the reference configuration for the expansion $\mathbf{g_{q0}}^{(n)}$ and $\mathbf{H_{q0}}^{(n)}$ are the energy gradient vector and hessian matrix of the (*n*) electronic state evaluated for the $\mathbf{q_0}$ geometry, both expressed in internal coordinates. From the approximate PES given in (1.1), the energy gradient vector obtained is

$$\nabla E^{(n)}(\boldsymbol{q}) = \boldsymbol{g}_{\boldsymbol{q_0}}^{(n)} + \boldsymbol{H}_{\boldsymbol{q_0}}^{(n)} (\boldsymbol{q}-\boldsymbol{q_0}) \tag{2.4.2}$$

The election of internal instead of cartesian coordinates for deriving the force field has some advantages, since the curvilinear coordinate system, if correctly chosen, preserves more accurately the quadratic approximation, making the spanned PES more precise as the displacement vector ($\mathbf{q-q_0}$) increases (Bakken and Helgaker 2002). Selecting a set of internal coordinates for the PES expansion with chemical meaning is necessary in order to predict accurately the energy of the extrapolated points. Since usually first and second derivatives are available in cartesian coordinates, it is necessary to transform the cartesian derivatives into internal derivatives. The relation between the derivatives of the energy with respect to internal and cartesian coordinates is described by

the Wilson B matrix which elements $B_{ij} = \frac{dq_i}{dx_j}$, are given by the derivatives of the internal coordinates with respect to de cartesian coordinates (Wilson 1955). Using this matrix the relation between the gradients are given by

$$\boldsymbol{B}_x^t \boldsymbol{g}_q^{(n)} = \boldsymbol{g}_x^{(n)} \tag{2.4.3}$$

$$\boldsymbol{g}_q^{(n)} = \boldsymbol{G}^{-1} \boldsymbol{B}_x \boldsymbol{g}_x^{(n)} \tag{2.4.4}$$

Where $\mathbf{g_x}^{(n)}$ is the energy gradient vector in cartesian coordinates, evaluated for an arbitrary **x** configuration, which is also expressed in cartesian coordinates. Since the **B** matrix is not square, its inversion requires to find the generalized inverse of a **G** matrix given by $\mathbf{G} = \mathbf{BUB}^t$ where **U** is a unitary matrix. In the case of using a set of redundant internal coordinates, the inversion of the **G** matrix required a previous diagonalization followed by the elimination of the zero eigenvalues resulting from the redundant internal coordinates, keeping only those eigenvectors corresponding with the 3N-6 degrees of vibrational freedom (Peng, et al. 1996). The relations between hessian matrices in both set of coordinates are obtained after differentiating equation (1.3) and (1.4)

$$\boldsymbol{B}_{\mathbf{x}_0}^t \boldsymbol{H}_{\mathbf{q}_0}^{(n)} \boldsymbol{B}_{\mathbf{x}_0} + \boldsymbol{B}_{\mathbf{x}_0}'^t \boldsymbol{g}_{\mathbf{q}_0}^{(n)} = \boldsymbol{H}_{\mathbf{x}_0}^{(n)} \tag{2.4.5}$$

$$\boldsymbol{H}_{\mathbf{q}_0}^{(n)} = \boldsymbol{G}_{\mathbf{x}_0}^{-1} \boldsymbol{B}_{\mathbf{x}_0} \boldsymbol{U} (\boldsymbol{H}_{\mathbf{x}_0}^{(n)} - \boldsymbol{B}_{\mathbf{x}_0}'^t \boldsymbol{g}_{\mathbf{q}_0}^{(n)}) \boldsymbol{U}^t \boldsymbol{B}_{\mathbf{x}_0}^t \boldsymbol{G}_{\mathbf{x}_0}^{-1} \tag{2.4.6}$$

where $\mathbf{H_{x0}}^{(n)}$ is the Hessian matrix in cartesian coordinates evaluated for the $\mathbf{X_0}$ configuration, and **B'** is a three dimensional array whose elements $B'_{ijk} = \partial^2 q_i / \partial x_j \partial x_k$ are the second derivatives of the i^{th} internal coordinates with respect to the j^{th} and k^{th} cartesian coordinate.

In order to obtain the numerical values of the gradient and Hessian matrix in internal coordinates, analytical expressions were obtained and implemented for the first and second derivatives of the internal coordinates with respect to the cartesian coordinates (i.e. B_{ij} and B'_{ijk} terms).

In order to calculate the forces in each integration step when this potential is applied to molecular dynamics, it is necessary to transform the gradient vector from internal to cartesian coordinates, using the relations given by Equations (1.3.3) and. (1.3.4).

2.5 Geometry Optimization

Central in theoretical quantum chemistry is the optimization of minima and transitions states. A big number of optimization algorithms have been developed using both internal and Cartesian coordinates, each one offering a set of advantages and drawbacks, for a comprehensive discussion see (Bakken and Helgaker 2002).

The Newton-Raphson method provides a very fast convergence algorithm, but is very expensive since it requires the calculation of the Hessian matrix. An approximation to bypass this shortcoming is the Broyden-Fletcher-Goldfarb-Shanno (BFGS) updating scheme (Fletcher 1987), in which an initial inexpensive hessian is updated in each optimization step, using the following equation:

$$\mathbf{H}_{k+1} = \mathbf{H}_k + \frac{\mathbf{g}_k \mathbf{g}_k^T}{\mathbf{g}_k^T \Delta \mathbf{R}_k} - \frac{\mathbf{H}_k \Delta \mathbf{R}_k \left(\mathbf{H}_k \Delta \mathbf{R}_k\right)^T}{\Delta \mathbf{R}_k^T \mathbf{H}_k \Delta \mathbf{R}_k} \tag{2.5.1}$$

Where

$$\mathbf{g}_k = \nabla f(\mathbf{X}_{k+1}) - \nabla f(\mathbf{X}_k) \tag{2.5.2}$$

$$\Delta \mathbf{R}_k = \mathbf{X}_{k+1} - \mathbf{X}_k \tag{2.5.3}$$

Using the previous procedure and changing the gradient for a new one that takes into account both an external and internal force, as Expressed in (2.5.4). It is then possible to optimize geometries subjected to an external stress.

$$\nabla f(\mathbf{X}_k)_{totalForce} = -\mathbf{F}_{ext} - \mathbf{F}_{\text{int}} \tag{2.5.4}$$

2.6 Programming Methods

Since the computational chemistry field directly address a set of common problem in scientific computing, there is a kind of folklore with respect to the design of scientific software. For an excellent review of this topics see (Wilson, et al. 2014). These guidelines includes: the automation of work, extensive use of heavily optimized libraries, planning the development of a software, documentation and code readability and, among others,

using the highest-level language possible. In this section we deeply discussed the programming language issue.

Mainstream languages like C, C++, Python, Java, FORTRAN etc. are classified as imperative languages in computer science. This means that a program in the imperative paradigm is a sequence of commands describing how things are done, i.e. these commands are execute in the preset order while changing the state of a set of variables. Although it is undeniable the impact of these languages in modern software application and particularly FORTRAN in the field of computational physics and chemistry, they (especially FORTRAN) still lack some properties as explained in Table 1.1.

	Explanation
Scalability	It is hard to parallelize and distribute the computations
Modularity	Programs tend to be large monolithic blocks, difficult to compose.
Refactoring	It is difficult to reuse functions.
Side Effects	There is no difference between input/output actions and pure mathematical functions. For a given function the same input is not always returning the same output. It is impossible to apply a broad set of optimization at compile time.
Mutable data	There is not a clear control of the program state, leading to obscure code.
Composition	There is no an easy way to compose functions or data structures.
Readable code	Programs tend to be hundreds of unintelligible lines.
Polymorphic and high level functions	It is quite hard (if possible at all) to implement functions that work on different kinds of data and that functions can return functions as answer.

Table 1.1. List of the main drawbacks of using FORTRAN.

On the other hand the functional programming languages as Haskell, Erlang, Ocaml, Scala, Lisp, etc. (Armstrong 2007, Marlow and Jones 2012), are focused on specifying what needs to be done instead of "how", generating functions which are composed in a primary function which is the actual program. The main advantages of this paradigm are that programs tend to be modular and easy to compose. This increases

readability and maintainability, since functions are pure in a mathematical sense and they can be tested isolated from the context. Immutable data does not lead to race conditions in concurrency. Polymorphism and higher order function enhance the reusability of code. The separation of input/output code from the pure mathematical functions enable the compiler to make aggressive transformations which results in more efficient code (O'Sullivan, et al. 2008). For a comprehensive discussion in the utility and advantages of functional programming see (Hughes 1990).

Even though the computational theory behind programming languages is beyond the scope of this thesis, we want to present in this section a brief description of Haskell. It is not the objective of this section to compare extensively the advantages of one languages with respect to others language, but to introduce some concepts regarding the functional paradigm. However, from time to time differences between the imperative and functional paradigms are pointed with pedagogical purposes.

2.6.1 A brief Haskell tour

Haskell is the result of an academic research project that begins in the early 1990's, which has been incorporating the result of the research to produce a programming language that has leading scientific ideas and production quality. The Glasgow Haskell Compiler (GHC) is the "de facto" implementation of Haskell, and because its fundaments are deeply rooted in the mathematics, it is spreading not only in academic environments by also in industrial production (see http://www.haskell.org/haskellwiki/Haskell).

The most outstanding feature of Haskell is its type system. Types are a ubiquitous concept in computer science, it can be thought as a mathematical object that represents some structural properties of a set of values. Another point of view is that a type is a value with only partial information, meaning that you can specify the intended context to use the value, but you cannot compute a specific value with a type. Types naturally arise from the fact that certain values can be meaningfully used only in certain contexts. Therefore all programming languages use some kind of *Type System* for reasoning about types (Turbak, et al. 2008). Another interesting way to look at types is through the *Curry-Howard isomorphism* (Thompson 1999), which in plain language is a formal proof that types can be regarded as propositions in a formal logical framework, while programs are "proofs" of those propositions, then a compiler can be regarded as a theorem checker.

Haskell type system enables to rule out spurious declarations, bypassing the use of extensive debugging protocols, providing an equational reasoning framework to deduce properties about the given implementation. equational reasoning refers to the fact of introduce any possible simplification using mathematical reasoning, replacing equal by equals, which as obvious as it seems is not always possible in common languages (Harper 2013).

Another startling feature of Haskell is that of having variables that do not vary, once defined they never change, they are immutable. The reason behind this behaviors is that in Haskell a variable is a name bound to some value, like an equation where expressions are named, for instance *y=5* and *x=3*, but it does not make sense that in the same equation *x=3* and *x=6*, are defined simultaneously. On the contrary, variables in imperative languages like C or FORTRAN are directions pointing to locations in a variable computer memory.

Since Haskell is a strong typed Language, meaning that every expression must have a type at compilation time, the compiler can provide the types of the expressions declared, but for documentation and clarity reason is customary to provide the signature of the function declared. The signature refers to the number of arguments takes by a function, known as *arity*, and the types of the arguments of the function, as is exemplify below:

$$\begin{aligned} &\mathit{MultiplyBy}5 :: \mathit{Int} \rightarrow \mathit{Int} \\ &\mathit{MultiplyBy}5\ \mathrm{x} = 5*\mathrm{x} \end{aligned} \tag{2.6.1}$$

The first line in the previous equation states that *MultiplyBy5* is a function which takes an integer as argument and returns another integer as result, while the second line declares the actual computation.

A more involving concept is the polymorphism. Polymorphism permits procedure declarations that are parameterized over the types of their inputs, meaning that a polymorphic function is a function that works for many different types. For instance the *times* function is given by:

$$(*) :: \mathit{Num}\ \mathrm{a} \Rightarrow a \rightarrow a \rightarrow a \tag{2.6.2}$$

The signature declares that the function takes two arguments (called parameters) which must belong to the Numerical type class (e.g. integers, floating points, etc.) and finally return a third number which also must belong to the Numerical type class. A class member in Haskell can be defined as a set of functions which are implemented depending on the kind of types on which those methods are applied. Therefore the *times* function belongs to the numerical type class have a different implementation if it is intended to be applied over integers or floating points.

A big difference between imperative language and Haskell is the way in which it takes the arguments in functions. Haskell use a mechanism called curryfication which means that only one argument is take into the function at a time, for instance the plus function operating over two integers is expressed as:

$$\begin{aligned} &plus :: Int \rightarrow Int \rightarrow Int \\ &plus\ \mathrm{x}\ \mathrm{y} = x + y \end{aligned} \tag{2.6.3}$$

If you supply only one number to the above function we obtain a new function, for example if we apply 4 to *plus* we get:

$$\begin{aligned} &plus4 :: Int \rightarrow Int \\ &plus4\ \mathrm{y} = 4 + y \end{aligned} \tag{2.6.4}$$

Functions are first order expressions, meaning that functions can be returned as the actual result of function application, as has been pointed in the previous equations. If you supply a function with less arguments that the total number of arguments that a function is waiting, you are returned with a new function which takes the missing arguments.

Imperative languages rely on explicit loops declaration (represented with keywords like *For*, *While*, etc.), functional languages lack any explicit loops declaration and all the iterative tasks are carried out by general polymorphic functions as map and folds see (O'Sullivan, et al. 2008). A map is a *polymorphic higher-order* function which applies a chosen function to every element of a list and returns a new list with the results. For example the following function multiplies every element by 3,

$$\mathrm{map}\ (*3)\ [1,2,3] = [3,6,9] \tag{2.6.5}$$

When using these functions some mathematical properties must be enforced, for instance the multiplication of all the elements of a list by 5, followed by the sum of 2 can be expressed as

$$\text{map (+2) (map (*5) [1,2,3]) = map ((+2) . (*5)) [1,2,3]} \qquad (2.6.6)$$

Where the dot operator (.) denotes functions composition, meaning that $(f.g)x = f(g(x))$. Even though mathematically equivalent, left and right hand side are from "the implementation point of view" not equally efficient, since the right hand function avoids the building and memory representation of the intermediate result, fusing (*5) and (+2) in only one function, eliminating an intermediate list. Fusion is an important property when many operations are applied to an array, for a detailed description see (Lippmeier, et al. 2012).

Haskell has a good deal of libraries which allows encapsulating and reutilizing computation patterns, making possible to recycle function, avoiding the usual plague of the identical functions performing slightly different task, allowing to easily recognize a pattern which can be made a general function. There is a Common tendency in computational chemistry of "reinventing the wheel", meaning that each software has its own non-standard way of tackle a common situation leading to confusion. Haskell libraries on the other side make a strong point providing standard tools for common computations.

In this Thesis we have used GHC and the Haskell platform for the algorithms implementation (Marlow and Jones 2012), making heavy use of the high performance library REPA (Lippmeier, et al. 2012).

2.6.2 Parallelism and concurrency

The free lunch is over (Sutter 2005). This sentence marked the end of an era and it is only the rephrasing that transistor miniaturization has reached the physical limits. The empirical fact that every 18 months the performance of integrated circuits double, called the Moore's law, was the driving force of the software development for the last 50 years, where increasing clock frequencies and symmetric multiprocessing tried to manage the ever increasing demands of computing power among science and even commonly used information systems. Having reached the physical limits of miniaturization, chips manufacturers have focused on producing devices with many cores and smaller CPU

frequencies, saving electric power. Some years ago you only needed to wait some months in order to improve the performance, but now the new challenge is software parallelization (Breshears 2009, Fayez 2011), meaning that sequential applications are doomed to disappear and be replace by parallel and concurrent software.

A concurrent program can be roughly defined as one that reacts properly to independent input sources dealing with every task independently; having multiple threads of control and non-deterministic behavior, and the quantity of cores that the program can handle only improves performance and responsiveness. Parallelism on the other hand, can be classified as a special case of concurrency since a parallel program solves a single problem and has a deterministic behavior (e.g. stream in data, makes calculation and output result), which takes advantages of multiplicity of hardware to improve the speed of a computation (Jones 2007).

Current efforts in mainstream languages (Java, C, C++ and FORTRAN in chemical physics simulations) do not directly address distributed concurrency; instead they focus on a shared memory models where locks and condition variables are in charge of updating the data. Since threads will be working together in shared memory, there may be times when two or more threads need to access the same memory location, phenomenon called race condition. If one or more of these threads is trying to update some memory location (e.g. one thread wants to evaluate $x = x+1$ and the other $x = x+2$), you will have a race for the resources. These issues have been traditionally tackled through the implementation of locks and semaphores, resulting in extremely complex and costly software. One example of such programs are most of the operating systems (Marlow 2013).

Concurrently software must cope with the scheduling of threads, which are managed by rather complex algorithms which depend on many factors (current load of the system, priority of the tasks, etc.), and therefore scheduling appears to be nondeterministic or asynchronous. And more import, it is the programmer responsibility to handle all these events simultaneously, in order to produce a correct program. Besides, the cost of moving data from one processor to another as you want to distribute calculations, becomes a dominant factor, because all the caches of the all the processors must be kept updated of all the changes in the shared variables and data, independently of the architecture, using high-performance buses for example (Vadja 2011).

The functional programing paradigm makes a strong point on having multiple entities which can shared or not memory managing to accomplish the computations by several mechanisms, being the message passing one of the most successful in handling hundreds or even millions of independent computations (Armstrong 2007)

2.7 Software in Quantum Chemistry

In his lecture of the Turing award the physician Edsger W. Dijkstra said that: "The sooner we can forget that Fortran has ever existed, the better, for as a vehicle of thought it is no longer adequate: it wastes our brainpower, is too risky and therefore too expensive to use. FORTRAN's tragic fate has been its wide acceptance, mentally chaining thousands and thousands of programmers to our past mistakes" (Dijkstra 1972). No longer after, John Backus, leader of the team which developed FORTRAN, in his Turing award Lecture deeply questioned the strategies of programming in vogue during that period, 40 years later these practices still pervades the chemical physical simulation branch.

For years the FORTRAN programming style has been sustained only by the steady increase in the velocity of the transistors, but once the future has opened to highly distributed architectures and highly parallelized software, maybe it is time to switch to more robust computation theories. If giants of computer performance such as Google make use of the functional paradigm why physical simulations cannot take advantages of it?

2.8 Electronic Structure Packages

- A development in the Molcas-7 quantum chemistry package was carried out in order to perform constant temperature "on the fly" molecular dynamics. Besides, the same package was used to perform CASSCF and CASPT2 calculations (Aquilante, et al. 2010).
- The Gaussian 09 software was used for the DFT and TD-DFT calculations (M. J. Frisch, et al. 2009).
- The Gromacs package was used to perform simulation of large scale systems as biomolecules (Hess 2008).
- Our own set of packages was tailored to carry molecular dynamics at constant temperature, external forces and surface hopping. Besides other set

of algorithm as constrained optimizations, data analysis and several miscellaneous tasks were also implemented (see appendixes).

2.9 Chapter Bibliography

Andersen, H. C., Molecular dynamics at constant pressure and/or temperature. *J. Chem. Phys.* **1980,** *72*, 2384–2393.

Andersson, K.; Malmqvist, P. A.; Roos, B. O.; Sadlej, A. J.; Wolinski, K., Second-order perturbation theory with a CASSCF reference function. *The Journal of Physical Chemistry* **1990,** *94*, 5483-5488.

Aquilante, F.; De Vico, L.; Ferré, N.; Ghigo, G.; Malmqvist, P.-å.; Neogrády, P.; Pedersen, T. B.; Pitoňák, M.; Reiher, M.; Roos, B. O.; Serrano-Andrés, L.; Urban, M.; Veryazov, V.; Lindh, R., MOLCAS 7: The Next Generation. *J. Comput. Chem.* **2010,** *31*, 224-247.

Armstrong, J., *Programming Erlang*. Pragmatic Bookshelf: Raleigh, North Carolina, 2007.

Bakken, V.; Helgaker, T., The efficient optimization of molecular geometries using redundant internal coordinates. *The Journal of Chemical Physics* **2002,** *117*, 9160-9174.

Ben-Nun, M.; Quenneville, J.; Martínez, T. J., Ab Initio Multiple Spawning: Photochemistry from First Principles Quantum Molecular Dynamics. *The Journal of Physical Chemistry A* **2000,** *104*, 5161-5175.

Berendsen, H. J. C., Molecular Dynamics Simulations: The Limits and Beyond. In *Computational Molecular Dynamics: Challenges, Methods, Ideas*, Deuflhard, P.; Hermans, J.; Leimkuhler, B.; Mark, A. E.; Reich, S.; skeel, R. D., Eds. Springer: Berlin, 1998.

Born, M.; Huang, K., Dynamical Theory of Crystal Lattices. Oxford University Press: New York, 1954.

Bowman, J. M.; Braams, B. J.; Carter, S.; Chen, C.; Czakó, G.; Fu, B.; Huang, X.; Kamarchik, E.; Sharma, A. R.; Shepler, B. C.; Wang, Y.; Xie, Z., Ab-Initio-Based Potential Energy Surfaces for Complex Molecules and Molecular Complexes. *Journal of Physical Chemistry Letters* **2010,** *1*, 1866-1874.

Breshears, C., *The Art of Concurrency*. O'Reilly: 2009.

Brooks, B. R.; Brooks III, C. L.; Mackerell, A. D.; Nilsson, L.; Petrella, R. J.; Roux, B.; Won, Y.; Archontis, G.; Bartels, C.; Boresch , S.; Caflisch, A.; Caves, L.; Cui, Q.; Dinner, A. R.; Feig, M.; Fischer, S.; Gao, J.; Hodoscek, M.; Im, W.; Kuczera, K.; Lazaridis, T.; Ma, J.; Ovchinnikov, V.; Paci, E.; Pastor, R. W.; Post, C. B.; Pu, J. Z.; Schaefer, M.; Tidor, B.; Venable, R. M.; Woodcock, H. L.; Wu, X.; Yang, W.; York, D. M.; arplus., M. K., CHARMM: The Biomolecular simulation Program. *J. Comput. Chem.* **2009,** *30*, 1545-1615.

Case, D. A.; Darden, T. A.; Cheatham, I. T. E.; Simmerling, C. L.; Wang, J. J.; Duke, R. E.; Luo, R.; Merz, K. M.; Pearlman, D. A.; Crowley, M.; Walker, R. C.; Zhang, W.; Wang, B.; Hayik, S.; Roitberg, A.; Seabra, G.; Wong, K. F.; Paesani, F.; Wu, X.; Brozell, S.; Tsui, V.; Gohlke, H.; Yang, L.; C., T.; Mongan, J.; Hornak, V.; Cui, G.; Beroza, P.; Mathews, D. H.; Schafmeister, C.; Ross, W. S.; Kollman, P. A. *AMBER 9*, University of California: San Francisco, 2006.

Clary, D. C., Quantum Dynamics of Chemical Reactions. *Science* **2008,** *321*, 789-791.

Cramer, C. J., *Essentials of Computational Chemistry. Theories and Models*. second ed.; John Wiley & Sons: 2004.

Cheatham, T. E.; Young, M. A., Molecular dynamics simulation of nucleic acids: Successes, limitations, and promise*. *Biopolymers* **2000,** *56*, 232-256.

Dijkstra, E. W., the humble programmer. *Communications of the ACM* **1972,** *15*, 859-866.

Espinosa-Garcia, J.; Monge-Palacios, M.; Corchado, J. C., Constructing Potential Energy Surfaces for Polyatomic Systems: Recent Progress and New Problems. *Advances in Physical Chemistry* **2012,** *2012*, 19.

Fayez, *Algorithms and Parallel Computing*. Wiley: 2011.

Ferré, N.; Ángyán, J. G., Approximate electrostatic interaction operator for QM/MM calculations. *Chem. Phys. Lett.* **2002,** *356*, 331-339.

Field, M. J., *A Practical Introduction to the Simulation of Molecular Systems*. Cambridge University Press: New York, 2007.

Fletcher, R., *Practical methods of optimization* second ed.; John Wiley & Sons: New York, 1987.

Frenkel, D.; Smit, B., *Understanding Molecular Simulation*. second ed.; Academic Press: San Diego, 2002; Vol. 1.

Granucci, G.; Persico, M., Critical appraisal of the fewest switches algorithm for surface hopping. *The Journal of Chemical Physics* **2007,** *126*, -.

Griebel, M.; Knapek, S.; Zumbusch, G., *Numerical Simulation in Molecular Dynamics*. Springer: Germany, 2007; Vol. 5.

Harper, R., Equational Reasoning In *Practical Foundations for Programming Languages* Cambridge University Press: New York, 2013; pp 495-547.

Hess, B., GROMACS 4: Algorithms for Highly Efficient, Load-Balanced, and Scalable Molecular Simulation. *Journal of Chemical Theory and Computation* **2008,** *4*, 435-447.

Hilborn, R. C., Einstein coefficients, cross sections, f values, dipole moments, and all that. *American Journal of Physics* **1982,** *50*, 982-986.

Ho, T.; Rabitz, H., A general method for constructing multidimensional molecular potential energy surfaces from ab initio calculations. *J. Chem. Phys.* **1996,** *104*, 2584-2597.

Hohenberg, P.; Kohn, W., Inhomogeneous Electron Gas. *Physical Review* **1964,** *136*, B864-B871.

Hollebeek, T.; Ho, T.-S.; Rabitz, H., Constructing Multidimensional Molecular Potential Energy Surfaces From ab Initio Data. *Annu. Rev. Phys. Chem.* **1999,** *50*, 537-570.

Hoover, W.; Hoover, C. G., Nonequilibrium molecular dynamics. *Condens. Matter Phys.* **2005,** *8*, 247-260.

Hughes, J., Why Functional Programming Matters. In *Research Topics in Functional Programming*, Turner, D., Ed. Addison-Wesley: 1990; pp 17-42

Ischtwan, J.; Collins, M. A., Molecular potential energy surfaces by interpolation. *The Journal of Chemical Physics* **1994,** *100*, 8080-8088.

Jaeger, H. M.; Fischer, S.; Prezhdo, O. V., Decoherence-induced surface hopping. *The Journal of Chemical Physics* **2012,** *137*, -.

Jones, S. P., Beautiful Concurrency. In *Beautiful Code*, Wilson, G., Ed. O'Reilly

2007.

Kaminski, G. A.; Friesner, R. A.; Tirado-Rives, J.; Jorgensen, W. L., Evaluation and Reparametrization of the OPLS-AA Force Field for Proteins via Comparison with Accurate Quantum Chemical Calculations on Peptides. *J. Phys. Chem. B* **2001,** *105*, 6474-6487.

Köuppel, H.; Domcke, W.; Cederbaum, L. S., Multimode Molecular Dynamics Beyond the Born-Oppenheimer Approximation. In *Adv. Chem. Phys.*, John Wiley & Sons, Inc.: 2007; pp 59-246.

Kuppermann, A.; Abrol, R., Quantum Reaction Dynamics for Multiple Electronic States. In *The Role of Degenerate States in Chemistry*, John Wiley & Sons, Inc.: 2003; pp 283-322.

Lin, H.; Truhlar, D., QM/MM: what have we learned, where are we, and where do we go from here? *Theor. Chem. Acc.* **2007,** *117*, 185-199.

Lippmeier, B.; Chakravarty, M. M. T.; Keller, G.; Jones, S. P., Guiding Parallel Array Fusion with Indexed Types. In *Proceedings of the 2012 symposium on Haskell symposium*, ACM: Copenhagen, Denmark, 2012; pp 25-36.

M. J. Frisch; G. W. Trucks; H. B. Schlegel; G. E. Scuseria; M. A. Robb; J. R. Cheeseman; G. Scalmani; V. Barone; B. Mennucci; G. A. Petersson; H. Nakatsuji; M. Caricato; X. Li; H. P. Hratchian; A. F. Izmaylov; J. Bloino; G. Zheng; J. L. Sonnenberg; M. Hada; M. Ehara; K. Toyota; Fukuda, R.; J. Hasegawa; M. Ishida; T. Nakajima; Y. Honda; O. Kitao; H. Nakai; T. Vreven; J. A. Montgomery; Jr., J. E. P.; F. Ogliaro; M. Bearpark; J. J. Heyd; E. Brothers; K. N. Kudin; V. N. Staroverov; R. Kobayashi; J. Normand; K. Raghavachari; Rendell, A.; Burant, J. C.; Iyengar, S. S.; Tomasi, J.; Cossi, M.; Rega, N.; Millam, J. M.; Klene, M.; Knox, J. E.; Cross, J. B.; Bakken, V.; Adamo, C.; Jaramillo, J.; Gomperts, R.; Stratmann, R. E.; Yazyev, O.; Austin, A. J.; Cammi, R.; Pomelli, C.; Ochterski, J. W.; Martin, R. L.; Morokuma, K.; Zakrzewski, V. G.; Voth, G. A.; Salvador, P.; Dannenberg, J. J.; Dapprich, S.; Daniels, A. D.; Farkas, Ö.; J. B. Foresman; Ortiz, J. V.; Cioslowski, J.; Fox, D. J. *Gaussian 09, Revision A.1*, Gaussian, Inc.: Wallingford CT, 2009.

Maisuradze, G. G.; Thompson, D. L.; Wagner, A. F.; Minkoff, M., Interpolating moving least-squares methods for fitting potential energy surfaces: Detailed analysis of one-dimensional applications. *The Journal of Chemical Physics* **2003,** *119*, 10002-10014.

Marlow, S., *Parallel and Concurrent Programming in Haskell*. O'reilly: 2013.

Marlow, S.; Jones, S. P., The Glasgow Haskell Compiler. Brown, A.; Wilson, G., Eds. Aosabokk: 2012.

Martyna, G. J.; Tuckerman, M. E.; Tobias, D. J.; Klein, M. L., Explicit reversible integrators for extended systems dynamics. *Mol. Phys.* **1996,** *87*, 1117-1157.

Marx, D.; Hutter, J., *Ab Initio Molecular Dynamics: Basis Theory and Advanced Methods*. Cambridge University Press: New York, United States of America, 2009.

Neumann, J. v.; wigner, E., Über merkwürdige diskrete eigenwerte. *Z. physik* **1929,** *30*, 465-467.

Norrby, P.-O.; Brandt, P., Deriving force field parameters for coordination complexes. *Coord. Chem. Rev.* **2001,** *212*, 79-109.

Nosé, S., A molecular dynamics method for simulation in the canonical ensemble. *Mol. Phys.* **1984,** *52*, 255-268.

O'Sullivan, B.; Goerzen, J.; Stewart, D. B., *Real World Haskell*. O'Reilly Media: 2008.

Peng, C.; Ayala, P. Y.; Schlegel, H. B.; Frisch, M. J., Using redundant internal coordinates to optimize equilibrium geometries and transition states. *J. Comput. Chem.* **1996,** *17*, 49-56.

Roos, B. O., The Complete Active Space Self-Consistent Field Method and its Applications in Electronic Structure Calculations. In *Adv. Chem. Phys.*, John Wiley & Sons, Inc.: 2007; pp 399-445.

Schelegel, H. B., Ab initio Methods in Quantum Chemistry. Lawley, K. P., Ed. John Wiley & Sons: New York, 1987; pp 249-286.

Sexton, J. C.; Weingarten, D. H., Hamiltonian evolution for the hybrid Monte Carlo algorithm. *Nucl. Phys. B* **1992,** *380*, 665-677.

Sutter, H. The free lunch is over: A fundamental turn toward concurrency in software *Dr. Dobb's Journal* [Online], 2005.

Swope, W. C.; Andersen, H. C.; Berens, P. H.; Wilson, K. R., A computer simulation method for the calculation of equilibrium constants for the formation of physical clusters of molecules: Application to small water clusters. *The Journal of Chemical Physics* **1982,** *76*, 637-649.

Szabo, A.; Ostlund, N. S., *Modern Quantum Chemistry*. Dover Publications: Toronto, Canada, 1996.

Teller, E., The Crossing of Potential Surfaces. *The Journal of Physical Chemistry* **1937,** *41*, 109-116.

Thompson, S., *Type Thoery & Functional Programming*. Addison Wesley: 1999.

Tuckerman, M.; Berne, B. J.; Martyna, G. J., Reversible multiple time scale molecular dynamics. *The Journal of Chemical Physics* **1992,** *97*, 1990-2001.

Tuckerman, M. E.; Liu, Y.; Ciccotti, G.; Martyna, G. J., Non-Hamiltonian molecular dynamics: Generalizing Hamiltonian phase space principles to non-Hamiltonian systems. *The Journal of Chemical Physics* **2001,** *115*, 1678-1702.

Tuckerman, M. E.; Martyna, G. J., Understanding Modern Molecular Dynamics: Techniques and Applications. *J. Phys. Chem. B* **2000,** *104*, 159-178.

Tully, J. C., Molecular dynamics with electronic transitions. *The Journal of Chemical Physics* **1990,** *93*, 1061-1071.

Turbak, F.; Gifford, D.; Sheldon, M. A., Simple Types. In *Design Concepts in Programming Languages*, MIT Press: Cambridge, Massachusetts, 2008.

Vadja, A., *Programming Many-Core Chips*. Springer: 2011.

Valentini, A.; Frutos, L. M., Tully's fewest switches algorithm with decoherence correction for the surface hop implemented in Molcas 7.6. 2012.

Wilson, E. B. J., *Molecular Vibrations: The Theory of Infrared and Raman Vibrational Spetra*. McGraw-Hill: New York, 1955.

Wilson, G.; Aruliah, D. A.; Brown, C. T.; Chue Hong, N. P.; Davis, M.; Guy, R. T.; Haddock, S. H. D.; Huff, K. D.; Mitchell, I. M.; Plumbley, M. D.; Waugh, B.; White, E. P.; Wilson, P., Best Practices for Scientific Computing. *PLoS Biol* **2014,** *12*, e1001745.

Witkoskie, J. B.; Doren, D. J., Neural Network Models of Potential Energy Surfaces: Prototypical Examples. *Journal of Chemical Theory and Computation* **2005,** *1*, 14-23.

Worth, G. A.; Cederbaum, L. S., BEYOND BORN-OPPENHEIMER : Molecular Dynamics Through a Conical Intersection. *Annu. Rev. Phys. Chem.* **2004,** *55*, 127-158.

Worth, G. A.; Robb, M. A., Applying Direct Molecular Dynamics to Non-Adiabatic Systems. In *The Role of Degenerate State in Chemistry*, Baer, M.; Billing, G. D., Eds. JOHN WILEY & SONS, INC.: 2002; Vol. 124.

Chapter 3: Aims

The Road Not Taken

Two roads diverged in a yellow wood,

and sorry I could not travel both

and be one traveller, long I stood

and looked down one as far as I could

to where it bent in the undergrowth;

Then took the other, as just as fair,

and having perhaps the better claim,

because it was grassy and wanted wear;

though as for that the passing there

had worn them really about the same,

and both that morning equally lay

in leaves no step had trodden black.

oh, I kept the first for another day!

yet knowing how way leads on to way,

I doubted if I should ever come back.

I shall be telling this with a sigh

somewhere ages and ages hence:

two roads diverged in a wood, and I—

I took the one less traveled by,

and that has made all the difference.

Mountain Interval. Robert Frost

The project presented in this Ph. D. Thesis concerns with the application and development of theoretical and computational methods to the description of the dynamical behaviour, photochemistry and photophysics of chemical and biologically relevant molecular systems.

The Following goals were achieved:

i) A definition of the reaction coordinate was developed for the triplet-triplet energy transfer process, based on the minimum energy principle for modulating the singlet-triplet energy gap.
ii) A generalized geometrical distortion parameter was developed to provide a quantitative measurement of the nonvertical character of a given donor or acceptor molecule in the triplet energy transfer process.
iii) A Nosé-Hoover chain of thermostat was implemented to carry out molecular dynamics at a constant temperature, which produces statistics belonging to the canonical ensemble. This methodology was applied to the study of different systems and phenomena as: triplet energy transfer, optomechanical tuning, excited state intramolecular proton transfer and chemiluminescence.
iv) "On the fly" molecular dynamics was used to simulate the behavior of the 1,2-dioxetane molecule, on the many-fold degeneration area which is central in the process of bioluminescence.
v) The QM/MM methodology was applied to the study of photofluorescent proteins, particularly to the fluorescent of the irisFP.
vi) The concept of structural substituent excitation energy effect aforementioned was applied to a wide series of S-nitrosothiols, in order to predict their ability to release nitric oxide. The final results suggest a clear tendency in favour of an absorption spectra modulation.
vii) The effects of the environment on a photoswitch were treated as external forces acting at two ends of the chromophore. In the case of azobenzene, cis and trans isomers show considerable photosensitivity to the applied forces, resulting in possible modulation of the maximum absorption wavelength.
viii) A theoretical methodology was proposed to build molecular motors and switches based on the protonated Schiff bases of the rhodopsin, using hydrogen bonds to produce unidirectional rotation.

ix) Most of the algorithms herein described were implemented using state of the art computational methodologies, with particular emphasis on readability, parallelization and performance.

Chapter 4: Triplet Energy Transfer

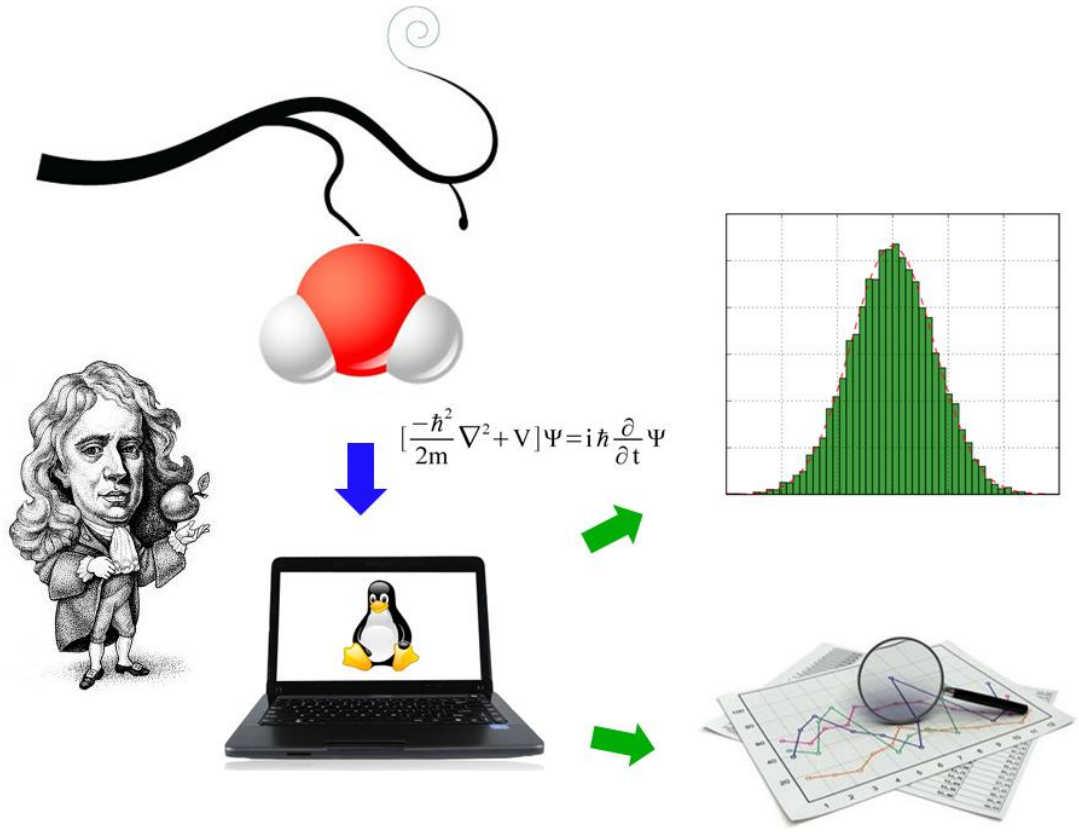

"We don't want to change. Every change is a menace to stability. That's another reason why we're so chary of applying new inventions. Every discovery in pure science is potentially subversive; even science must sometimes be treated as a possible enemy. Yes, even science."

Brave New World. Aldous Huxley

4.1 Introduction

Photophysical processes carry out a change in the electronic state of the system preserving its chemical identity. After excitation, the excess energy can be dissipated through emission or radiationless transitions. Such energy can also be transfer to other molecules through other processes, such as quenching or photosensitizing.

4.1.1 Energy Transfer Mechanisms

An energy transfer can take place between an electronically excited donor (D*) and a ground-state acceptor species (A) without the emission of a photon while transferring energy, where D and A can be two molecules (intermolecular process) or two parts of the same molecule (intramolecular process). The probability of intramolecular energy transfer between two moieties (i.e. a change in the electronic state) is inversely proportional to the energy gap ΔE, between the two states. The rate constant value for radiationless transitions decreases with the size of the energy gap between initial and final electronic states.

Energy transfer processes can be divided into two main classes, both of increasing importance in chemistry and biochemistry: Förster resonant energy transfer (FRET) and Dexter-type energy transfer. For some relevant applications see: (Langhals, et al. 2010, Muñoz-Losa, et al. 2009)(FRET) and (Monguzzi, et al. 2008, Reineke, et al. 2009)(Dexter-type). The Förster model is based on the idea that a Coulomb interaction stands between D* and A, by which the energy released by D* can simultaneously excite A, finally resulting in D and A* species. Exchange interaction takes place by the Dexter mechanism, that can be visualized as electron transfer where one electron moves from the excited donor highest occupied molecular orbital to the acceptor lowest unoccupied molecular orbital, while another electron moves from the acceptor highest occupied molecular orbital to the donor lowest unoccupied molecular orbital, therefore resulting in exchange energy transfer. The exchange resonance interaction of D* and A occurs via overlap of electron clouds and requires close contact between molecules. The transfer rate constant can be obtained through the golden rule formalism (Serpa, et al. 2003), which is expressed by:

$$k_e = \frac{2\pi}{\hbar} U^2 J \tag{4.1.1}$$

where U^2 represents the electron exchange coupling, depending only on the electronic configuration of the initial and final transfer states; J is a vibrational term that can be approached by the overlap integral between the normalized spectra of the donor phosphorescence ($^3D \rightarrow {}^1D$) and acceptor ground-state triplet absorption ($^3A \leftarrow {}^1A$) (Serpa, et al. 2003).

The electron exchange coupling term (U) for TET corresponds to the electronic exchange integral (Speiser 1996, You and Hsu 2010):

$$U = \langle \phi_{*_D}(1)\phi_A(2) | \frac{e^2}{r_{12}} | \phi_D(2)\phi_{*_A}(1) \rangle \qquad (4.1.2)$$

which mainly depends on the donor and acceptor molecular orbitals overlap (frequently HOMO and LUMO of donor and acceptor respectively), giving rise to an exponential decrease of the coupling as originally proposed by Dexter(Dexter 1953). Because of the non-vanishing coupling, adiabatic potential energy surfaces of both electronic states (i.e. before and after the transfer) do not present real crossings (i.e. conical intersections, see section 2.2.4), showing slightly avoided crossings in the intersection space defined by the diabatic states as a result of the weak coupling. Since triplet-triplet energy transfer (TET) is forbidden by the dipole-dipole energy transfer, the Dexter model is the only mechanism for TET. In Figure 4.1, it is shown a schematic diagram of the triplet energy transfer through the Dexter exchange mechanism.

In order to account for several crucial question regarding the nature of the TET, Frutos and Castaño proposed a methodology to identify the molecular coordinates that control the process of TET (Frutos and Castano 2005). Following this line of reasoning, in this Ph.D. Thesis, these initial studies have been is complemented and extended. In section 4.2.1, it is given a detailed account of the method developed to identify the main coordinates involved in the TET follow by further improvements of such algorithm.

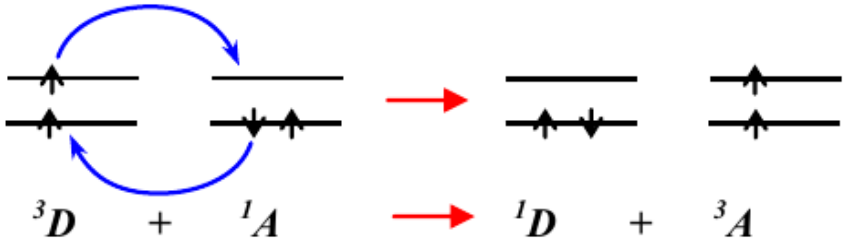

Figure 4.1. Electron and spin exchange between a triplet donor (D) and a singlet acceptor (A) in triplet-triplet energy transfer.

4.1.2 Energy Transfer Reaction Coordinate

It was early realized that in some highly endothermic TET reactions, the experimental value of the rate constant was much larger than that expected from the unfavorable energy balance, computed using singlet-triplet optical transition energies (Saltiel and Hammond 1963, Saltiel, et al. 1984). These anomalous cases had in common acceptor compounds with flexible molecular structure, like e.g. cis-stilbene, for which nonvertical $^3A \leftarrow\!\!- ^1A$ excitation processes were initially postulated (Saltiel, et al. 1984). It was later shown that excitation transitions in these cases do not depart from the classical vertical behavior, but the (unfortunate) nonvertical term became firmly established. These apparent deviations from classical TET are explained by postulating acceptor geometries for which the energy of the lowest triplet state is substantially lower than the optically recorded value and which are thermally accessible even at room temperature (Ramamurthy and Liu 1976). The overlap integral J in (4.1.1), for the kind of molecules discussed previously cannot be computed due to the absence of spectroscopic information on the electronic transitions of the thermally activated acceptor states. The geometrical distortions which are effective in lowering the triplet state energy of a flexible acceptor result from displacements along internal vibrational molecular coordinates, and provide the reaction path for the transfer process. There have been several attempts to identify experimentally these favorable molecular deformations, e.g. for the paradigmatic case of cis-stilbene but, unfortunately, the results were contradictory (Brennan, et al. 1994, Caldwell, et al. 1992, Lalevee, et al. 2005, Saltiel, et al. 2003). This ambiguity may be removed by theoretical modeling of the transfer step, and this also has been carried out at different levels of approximation (Catalán and Saltiel 2001).

In this Work it is addressed the aforementioned problem, being developed a formalism to characterize and quantify the contribution of each molecular coordinate to the reaction path for the TET, as well be detail in section 4.2.2.

4.1.3 Energy transfer Processes

TET process plays a fundamental role in several important applications as it is the photodynamic therapy (PDT), where a photosensitizer as porphyrin and its derivatives (Brasseur 2003), is administered to the patient in different ways. When the substance has its maximum accumulation in the target tissue, the affected area is irradiated at wavelength around 600-800 nm populating the singlet excited state S_n of the photosensitizer. After a vibrational decay to the S_1 state, the system carry out an intersystem crossing to T_1 which transfer the excitation energy to the $^3O_2$ molecule generating $^1O_2$ ($^1\Delta g$). The singlet oxygen has been appointed to be the cytotoxic agent (Ethirajan, et al. 2011, Redmond and Kochevar 2006). A schematic representation of the TET in the photodynamic therapy is shown in Figure 4.2.

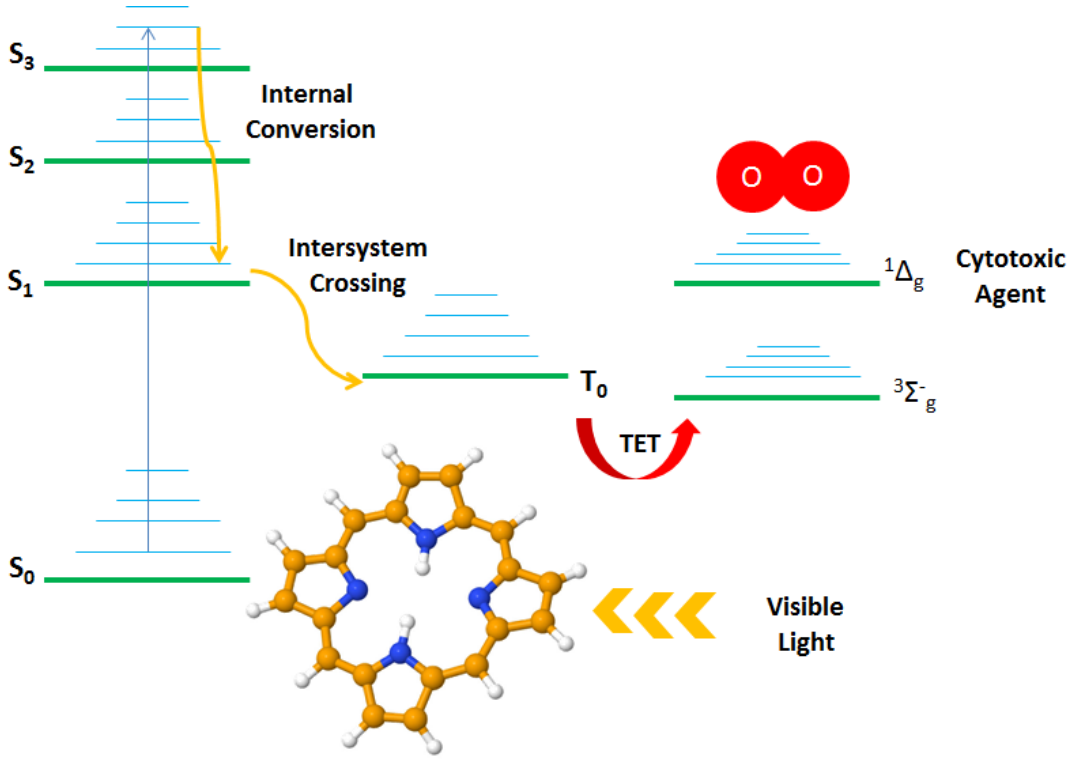

Figure 4.1. Pictorial representation of the photophysical process underlying the generation of the cytotoxic agents in the photodynamic therapy.

The key step in the TDP is the energy transfer from the donor to the molecular oxygen. Because this process happens in solution, as most of the TET applications, where a thermal equilibrium between the acceptor, donor and/or solvent is established, it is highly desirable to describe the geometrical and energetic changes at molecular level, which are relevant at a given temperature. Therefore In the section 4.2.3, we explored the dynamical behaviour of the system porphyrin-oxygen as a minimal model in the process of PDT, taking into account the temperature.

4.2 Results

4.2.1 Triplet energy transfer space

As has been discussed above, TET require that the singlet-triplet energy gap of both donor and acceptor becomes equal. For a given donor (or acceptor) there is associated a singlet-triplet energy gap, therefore the acceptor (or donor) moiety must carry out some geometrical distortions in order to modify its own singlet-triplet energy gap, maximizing the reaction efficiency.

4.2.1.1 TET-ACC algorithm

In order to calculate the set of geometrical configuration with a given singlet-triplet energy gap, which can be reached with the minimal energy distortion, it was initially developed an algorithm called triplet energy transfer–activated complex coordinate (TET-ACC) (Frutos and Castano 2005). In this development, the equilibrium geometry in S_0 belongs to the TET–ACC curve, therefore this point can be used as center of a hypersphere, containing at least two points on the surface, which fulfil that the gradient in both S_0 and T_1 states are parallel, one correspond to gradient vectors oriented in the same direction while the other case correspond to opposed directions. The TET-ACC localized both of these points and base on them, it is build a couple of new hyperspheres, where new points fulfilling the parallel condition are localized and the procedure continuous iteratively. This procedure is schematically represented in Figure 4.3.

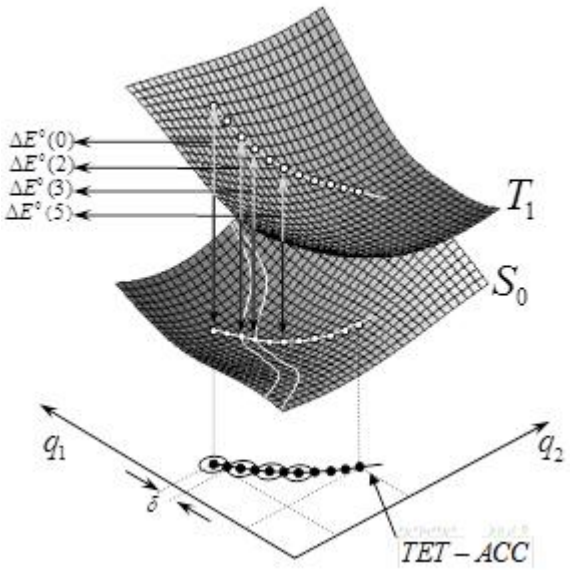

Figure 4.2 Beginning from the minimum energy point on the S_0 state, it is iteratively build a set of hyperspheres containing the optimized points which are the tangent point between the hyperspheres, creating a TET-ACC curve. Each point corresponds with a different singlet-triplet energy gap $\Delta E^0(i)$.

The optimization process on the hypersphere surface is based on the gradient difference (GD) or force difference vector $(\mathbf{\Delta F})$ between both electronic states (S_0 and T_1). $\mathbf{\Delta F}$ defines the direction which keeps constant the singlet-triplet energy gap, assuming that the singlet-triplet energy gap can be linearly approximated. The optimization is carried out taking a given displacement in the direction of the projection of S_0 force vector onto the subspace which is orthogonal to $\mathbf{\Delta F}$ and minimized S_0 while keeping constant the difference S_0-T_1, finally the displacement is projected onto the hypersphere surface, as shown on Figure 4.4. In the new optimized point it is again calculated the gradient vector both on S_0 and T_1, if both vectors are not parallel (optimization condition) the previous optimization algorithm is repeated until the convergence criteria are fulfilled.

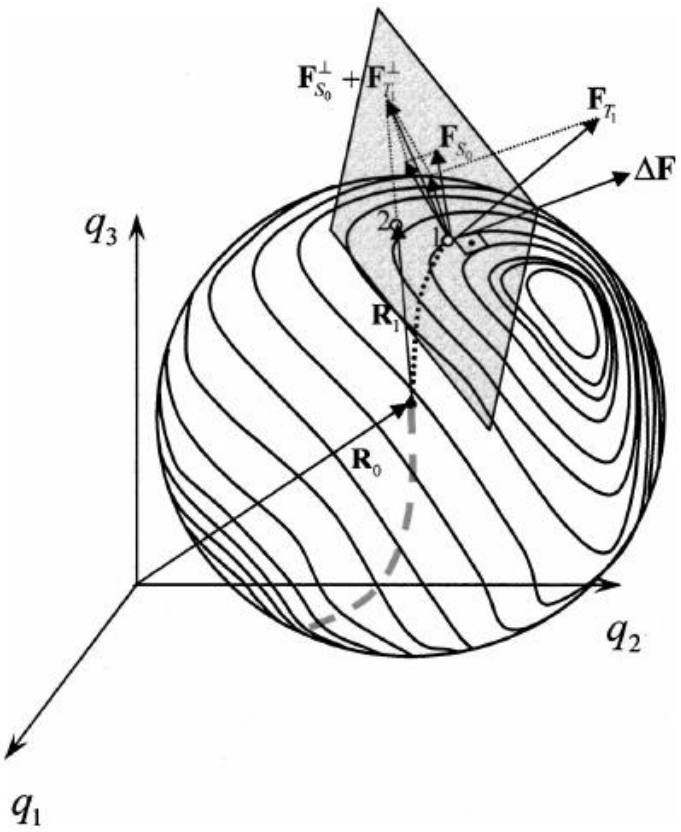

Figure 4.3. Schematic representation of the first step of the TET-ACC algorithm. The geometrical displacement from the point "1" to point "2" through the projection of the $\mathbf{F}_{S_0}^{\perp} + \mathbf{F}_{T_1}^{\perp}$ vector onto the hypersphere of center $\mathbf{R}_0$ and radius equal to $\|\mathbf{R}_1\|$ is represented. Likewise, the way that this vector is obtained as a sum of the projections of the force vectors on S_0 and T_1 ($\mathbf{F}_{S_0}$ and $\mathbf{F}_{T_1}$ vectors) onto the plane perpendicular to $\Delta\mathbf{F}$.

Even though the TET-ACC algorithm is accurate can be significantly inefficient, since it is on the energy gradients of both states, while the aim of the algorithm is to minimize (or maximize), the angle formed by these gradients, being most appropriate to analyse the gradient direction apart from its magnitude. Therefore it is important to include the Hessians for both states, improving the algorithm efficiency as will be described in the following section.

4.2.1.2 Quadratic approximation

Potential energy on both triplet and singlet states can be represented as a series expansion up to second order, allowing to follow the angular variation between the

energy gradient vectors as function of the internal coordinates. It is important to bear in mind, that this variation is unknown in the TET-ACC algorithm since the gradient difference vector is constant with the coordinates.

Quadratic energy expansions on both electronic states, can tackle the two main drawback of the TET-ACC algorithm which are: a) slow convergence b) breaking symmetry description (which is impossible in a linear approximation). Both problems are closely related to optimization methods based on the gradient, for which it is impossible to break the system symmetry to identify a more stable minimum. Besides, algorithms like steepest descent also suffer from a poor convergence nearby a stationary point.

The quadratic expansion for the energy in both singlet and triplet states are given by:

$$E_0(\Delta \boldsymbol{q}) = E_0(\boldsymbol{q_0}) + \Delta \boldsymbol{q}^t \boldsymbol{g}_0 + \frac{1}{2}\Delta \boldsymbol{q}^t \boldsymbol{H}_0 \Delta \boldsymbol{q} \tag{4.2.1}$$

$$E_1(\Delta \boldsymbol{q}) = E_1(\boldsymbol{q_0}) + \Delta \boldsymbol{q}^t \boldsymbol{g}_1 + \frac{1}{2}\Delta \boldsymbol{q}^t \boldsymbol{H}_1 \Delta \boldsymbol{q} \tag{4.2.2}$$

$$\Delta \boldsymbol{q} = \boldsymbol{q} - \boldsymbol{q_0} \tag{4.2.3}$$

where $\boldsymbol{q_0}$ is the Franck-Condon point around which the expansion is center, $\boldsymbol{q}$ a given configuration around the Franck-Condon point. $\boldsymbol{g}_n$ and $\boldsymbol{H}_n$ are the gradient and hessian computed at the expansion point, respectively. Accordingly the gradient at some point q for both states are:

$$\nabla E_0(\Delta \boldsymbol{q}) = \boldsymbol{g}_0 + \boldsymbol{H}_0 \Delta \boldsymbol{q} \tag{4.2.4}$$

$$\nabla E_1(\Delta \boldsymbol{q}) = \boldsymbol{g}_1 + \boldsymbol{H}_1 \Delta \boldsymbol{q} \tag{4.2.5}$$

Since we want to calculate the angle formed by the two gradient vectors, we can calculate firstly the dot product and use it to compute the angle between the two gradients as follows (omitting the $\boldsymbol{q_0}$ subscript):

$$\begin{aligned} &\left[\nabla E_0(\Delta \boldsymbol{q})\right]^t \nabla E_1(\Delta \boldsymbol{q}) = \left(\boldsymbol{g}_0 + \boldsymbol{H}_0\right)^t \left(\boldsymbol{g}_1 + \boldsymbol{H}_1\right) = \\ &\left(\boldsymbol{g}_0\right)^t \boldsymbol{g}_1 + \left(\boldsymbol{g}_1\right)^t \boldsymbol{H}_1 \Delta \boldsymbol{q} + \Delta \boldsymbol{q} \boldsymbol{g}_0 \boldsymbol{H}_1 + \Delta \boldsymbol{q} \boldsymbol{H}_0 \boldsymbol{H}_1 \Delta \boldsymbol{q} \end{aligned} \tag{4.2.6}$$

then

$$\cos\alpha\left(\Delta\boldsymbol{q}\right)=\frac{\left[\nabla E_0(\Delta\boldsymbol{q})\right]^t\nabla E_1(\Delta\boldsymbol{q})}{\left\{\left[\nabla E_0(\Delta\boldsymbol{q})\right]^t\nabla E_0(\Delta\boldsymbol{q})\right\}^{\frac{1}{2}}\left\{\left[\nabla E_1(\Delta\boldsymbol{q})\right]^t\nabla E_1(\Delta\boldsymbol{q})\right\}^{\frac{1}{2}}} \tag{4.2.7}$$

or equivalently

$$\begin{gathered}N_0N_1\cos\alpha\left(\Delta\boldsymbol{q}\right)=p\\ \textit{where } N_0=\left\{\left[\nabla E_0(\Delta\boldsymbol{q})\right]^t\nabla E_0(\Delta\boldsymbol{q})\right\}^{\frac{1}{2}},N_1=\left\{\left[\nabla E_1(\Delta\boldsymbol{q})\right]^t\nabla E_1(\Delta\boldsymbol{q})\right\}^{\frac{1}{2}}\\ \text{and } p=\left[\nabla E_0(\Delta\boldsymbol{q})\right]^t\nabla E_1(\Delta\boldsymbol{q})\end{gathered} \tag{4.2.8}$$

The angle variation as function of the coordinates is expressed as:

$$\begin{gathered}\nabla N_0\left[N_1\cos\alpha\left(\Delta\boldsymbol{q}\right)\right]+\nabla N_1\left[N_0\cos\alpha\left(\Delta\boldsymbol{q}\right)\right]+N_1N_2\nabla\cos\alpha\left(\Delta\boldsymbol{q}\right)=\\ \left(\boldsymbol{g}_0\right)^t\boldsymbol{H}_1+\boldsymbol{H}_0\boldsymbol{g}_1+2\boldsymbol{H}_0\boldsymbol{H}_1\Delta\boldsymbol{q}\end{gathered} \tag{4.2.9}$$

The gradients of $\nabla N0$ and $\nabla N1$ are given by:

$$\nabla N_0\left(\Delta\boldsymbol{q}\right)=\frac{\boldsymbol{H}_0\boldsymbol{g}_0+\boldsymbol{H}_0^2\Delta\boldsymbol{q}}{N_0} \tag{4.2.10}$$

$$\nabla N_0\left(\Delta\boldsymbol{q}\right)=\frac{\boldsymbol{H}_1\boldsymbol{g}_1+\boldsymbol{H}_1^2\Delta\boldsymbol{q}}{N_1} \tag{4.2.11}$$

Replacing (4.2.10) and (4.2.11) into (4.2.9) is obtained the rate of change of the angle between the gradients in both states as function of the molecular coordinates.

$$\begin{gathered}\nabla\cos\alpha\left(\Delta\boldsymbol{q}\right)=\frac{\left(\boldsymbol{g}_0\right)^t\boldsymbol{H}_1+\boldsymbol{H}_0\boldsymbol{g}_1+2\boldsymbol{H}_0\boldsymbol{H}_1\Delta\boldsymbol{q}}{N_0N_1}-\\ \cos\alpha\left[\frac{\boldsymbol{H}_0\boldsymbol{g}_0+\boldsymbol{H}_0\Delta\boldsymbol{q}}{N_0^2}+\frac{\boldsymbol{H}_1\boldsymbol{g}_1+\boldsymbol{H}_1^2\Delta\boldsymbol{q}}{N_1^2}\right]\end{gathered} \tag{4.2.12}$$

A first approximation to (4.2.12), is to evaluate it in the initial geometry $\left(\Delta\boldsymbol{q}=0\right)$, obtaining:

$$\nabla\cos\alpha\left(\Delta\boldsymbol{q}=\boldsymbol{0}\right)=\frac{\left(\boldsymbol{g}_0\right)^t\boldsymbol{H}_1+\boldsymbol{H}_0\boldsymbol{g}_1+2\boldsymbol{H}_0\boldsymbol{H}_1}{N_0N_1}-\cos\alpha\left[\frac{\boldsymbol{H}_0\boldsymbol{g}_0}{N_0^2}+\frac{\boldsymbol{H}_1\boldsymbol{g}_1}{N_1^2}\right] \tag{4.2.13}$$

The approximation (4.2.13) will be used in the improvement of the TET-ACC algorithm as is shown in the following section.

4.2.1.3 TET-ACC improvement

Since our primary objective is found those points for which the singlet and triplet energy gradients are parallel $\left(\cos\alpha = \pm 1 \text{ and } \nabla\cos\alpha = 0\right)$, equation (4.2.13) must fulfill that:

$$0 = \frac{\left(\boldsymbol{g}_0\right)^t \boldsymbol{H}_1 + \boldsymbol{H}_0\boldsymbol{g}_1 + 2\boldsymbol{H}_0\boldsymbol{H}_1\Delta\boldsymbol{q}}{N_0 N_1} - \cos\alpha\left[\frac{\boldsymbol{H}_0\boldsymbol{g}_0 + \boldsymbol{H}_0\Delta\boldsymbol{q}}{N_0^2} + \frac{\boldsymbol{H}_1\boldsymbol{g}_1 + \boldsymbol{H}_1^2\Delta\boldsymbol{q}}{N_1^2}\right] \quad (4.2.14)$$

And simultaneously:

$$\left\|\mathbf{q} - \mathbf{R}_0\right\| = \left\|\mathbf{q}_0\right\| \quad (4.2.15)$$

It was not found an analytical solution to the set of equation (4.2.14) and (4.2.15) for the $\left(\Delta\mathbf{q}_n\right)$ molecular position; therefore a numerical approximation was developed.

A schematic representation of the new optimization step is shown Figure 4.5. Beginning at new structure with coordinates $\left(\mathbf{R}_0 + \mathbf{q}_0\right)$ and imposing the optimization on the hypersphere surface of radius $\left\|\mathbf{q}_0\right\|$, it is calculated the vector $\nabla\mathbf{cos}\alpha$ evaluated at $\mathbf{q = 0}$, according to (4.2.13). Then, a displacement in the direction $\nabla\mathbf{cos}\alpha$ or $-\nabla\mathbf{cos}\alpha$ is carry out, depending if the aims is to minimize or maximize the singlet-triplet energy gap, restrained to a minimal activation energy. In this point it is newly calculated the gradient vector of the angle between both singlet and triplet states, if the convergence criteria is not achieved a new iteration is carry out until numerical convergence.

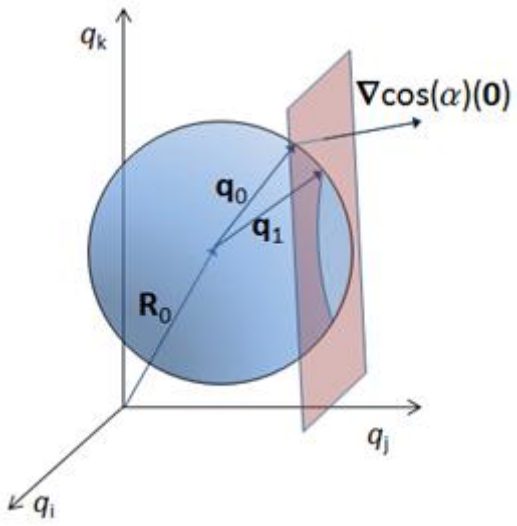

Figure 4.4. Schematic representation of an optimization step of the TET-ACC improved. Beginning at initial structure $\left(\mathbf{R}_0+\mathbf{q}_0\right)$ and calculating $\nabla\cos\alpha$ in that point it is determined the displacement which minimize or maximize $\cos\alpha$, obtaining a new structure $\left(\mathbf{R}_0+\mathbf{q}_1\right)$. Where q_i, q_j and q_k are internal coordinates of the system.

4.2.1.4 Convergence criteria and optimization parameters

There are several control parameters in the optimization process. The first of them is the hypersphere radius, which can be chosen only inside the boundaries of the quadratic approximation. Therefore, radiuses between 0.01-0.05 Angstroms were taken which are inside the quadratic approximation.

In order to avoid rotations of the pivot vector $\Delta\mathbf{q}_n$, it was imposed a maximum rotation of 0.5 degrees. This constrains results in an increased in the number of iterations per optimization step, but poses no computational cost, since the gradients and hessians energies are the always the same independently of the position vector $\Delta\mathbf{q}_n$.

A point is considered to be optimized when it fulfil that the module of $\nabla\cos\alpha$ is smaller than 10^{-3} radians/Bohr and simultaneously $\cos\alpha$ must be greater than 0.998. This last criterion guarantees that both gradient vectors in the singlet and triplet states are parallel.

4.2.2 Definition and determination of the triplet-triplet energy transfer reaction coordinate

Taking into account the weak electronic coupling limit, it is possible to uncouple both PESs for the donor and acceptor moieties involved in the process of TET. This partition, allows to describe separately in terms of geometrical distortion, the change that an acceptor (or donor) must undertake in order to favour the TET constrain to a minimal activation energy. Based on such approximation, it was developed a theoretical methodology to identify and quantify the contribution of each internal molecular coordinate to the TET reaction coordinate, through the definition of the so called *generalized geometrical distortion parameter* $\left(\gamma_q\right)$, which takes into account both the change in the singlet-triplet energy gap as the activation energy associated with the acceptor (or donor), formalized through the following expression,

$$\gamma_q^{RC} = \left\{ \frac{\left[\Delta E_T^A\left(\mathbf{q}^{RC}\right)\right]^2}{E_a\left(\mathbf{q}^{RC}\right)} \right\}^{\frac{1}{2}} \tag{4.2.16}$$

where $\Delta E_T^A\left(\mathbf{q}^{RC}\right) = E_T^A\left(\mathbf{q}^{RC}\right) - E_T^A$. Being $E_T^A\left(\mathbf{q}^{RC}\right)$ and E_T^A the singlet-triplet gap for the distorted molecule and equilibrium geometry, respectively. And $E_a\left(\mathbf{q}^{RC}\right)$ is the necessary energy to reach the distortion from the equilibrium geometry.

The geometrical distortions that the acceptor (or donor) should carry out in order to modified the singlet-triplet energy gap, must be reachable with a limited quantity of kinetic energy. Because of the limited supply of thermal energy, the TET reaction coordinate is defined as the set of internal coordinates which efficiently increase or decrease the singlet-triplet energy gap, with the minimal activation energy. These coordinates are characterized by having different force constants in both singlet and triplet states (under a quadratic approximation of the PES). Resulting in the possibility to modulate the singlet-triplet energy gap since changes in one electronic molecular state due to geometrical distortions are not mirror by the other electronic state, resulting in a deviation from the vertical singlet-triplet energy gap.

On the other hand, expression (4.2.16) gives us an idea of the nonvertical behaviour of a particular acceptor (or donor), since big values indicates that small

distortions of the molecular geometry result in big changes in the singlet-triplet energy gap. While in the opposite case, the molecule behaves as in a classical transfer, since the activation energy necessary to perform a given distortion is thermally inaccessible.

We can have a further inside into the weight of each internal coordinate to the overall reaction coordinate, if we define the *generalized geometrical distortion parameter* for each internal coordinate $\left(\gamma_{q_i}\right)$ which under a quadratic approximation of the PES is given by the following expression,

$$\gamma_{q_i}^{RC} = \left\{ \frac{\left[\left(\mathbf{q}_i^{RC}\right)^T \boldsymbol{g}_1 + \frac{1}{2}\left(\mathbf{q}_i^{RC}\right)^T \left(\boldsymbol{H}_1 - \boldsymbol{H}_0\right)\left(\mathbf{q}_i^{RC}\right) \right]^2}{\frac{1}{2}\left(\mathbf{q}^{RC}\right)^T \boldsymbol{H}_0 \left(\mathbf{q}_i^{RC}\right)} \right\}^{\frac{1}{2}} \tag{4.2.17}$$

where is a vector which entries are zero but the ith. $\boldsymbol{g}$ and $\boldsymbol{H}$ are the gradients and Hessian matrices, respectively.

It was also found that the *generalized geometrical distortion parameter* $\left(\gamma_q\right)$, can be related to λ parameter in the Marcus theory for electron transfer (Marcus 1964), through the expression

$$\left(\gamma_q^{RC}\right)^2 = 4\lambda \tag{4.2.18}$$

Because γ_q^{RC} is defined as the relation between the singlet-triplet energy gap and the required energy to achieve the distortion that result in the specific energy gap, which involves only the acceptor (or donor) coordinates, ignoring the solvent. Therefore, λ is the contribution of the acceptor (or donor) to the total reorganization energy, equivalent to the inner sphere reorganization energy in Marcus ET theory.

The preceding methodology was applied to the paradigmatic cis-stilbene nonvertical-behaving molecule. The behaviour of this molecule has been in much debate since its characterization (Saltiel and Hammond 1963), being still under discussion the nature of the geometrical distortion causing the nonvertical behaviour.

The mentioned methodology has shown that the central C=C bond stretching vibration, together with the phenyl-vinyl torsions are the main coordinate that modulate the singlet-triplet energy gap in the region of energy deficit (acceptor energy > donor energy), while the central dihedral angle (PhC-C-Ph) only plays an important role in the region of extremely energy deficit (acceptor energy - donor energy ~30kcal/mol). It is noteworthy that this result is in disagreement with previous hypothesis (Catalán and Saltiel 2001).

Definition and determination of the triplet-triplet energy transfer reaction coordinate

Felipe Zapata,[1] Marco Marazzi,[1] Obis Castaño,[1] A. Ulises Acuña,[2] and Luis Manuel Frutos[1,a)]
[1]*Departamento de Química Física, Universidad de Alcalá, 28871 Alcalá de Henares, Madrid, Spain*
[2]*Instituto de Química Física "Rocasolano", C.S.I.C., Serrano 119, 28006 Madrid, Spain*

(Received 28 August 2013; accepted 25 December 2013; published online 15 January 2014)

A definition of the triplet-triplet energy transfer reaction coordinate within the very weak electronic coupling limit is proposed, and a novel theoretical formalism is developed for its quantitative determination in terms of internal coordinates The present formalism permits (i) the separation of donor and acceptor contributions to the reaction coordinate, (ii) the identification of the intrinsic role of donor and acceptor in the triplet energy transfer process, and (iii) the quantification of the effect of every internal coordinate on the transfer process. This formalism is general and can be applied to classical as well as to nonvertical triplet energy transfer processes. The utility of the novel formalism is demonstrated here by its application to the paradigm of nonvertical triplet-triplet energy transfer involving *cis*-stilbene as acceptor molecule. In this way the effect of each internal molecular coordinate in promoting the transfer rate, from triplet donors in the low and high-energy limit, could be analyzed in detail. © *2014 AIP Publishing LLC*. [http://dx.doi.org/10.1063/1.4861560]

I. INTRODUCTION

Triplet-triplet energy transfer (TET) is an elementary radiationless process[1] taking place in natural photochemical reactions (e.g., photosynthesis) and in photosensitized processes.[2–4] TET is also a key step in many photocatalitic and photoinduced charge separation processes.[5,6]

In the case of intermolecular TET, donor molecules excited to the lowest electronic triplet state (^{3}D) exchange energy and spin[7–9] with ground-state singlet acceptor molecules (^{1}A), to yield triplet-excited acceptor molecules (^{3}A). In solution at room temperature TET is usually slower than vibrational relaxation and takes place from donor molecules which are in a vibrationless state, denoted here as the equilibrium geometry. The energy balance of the transfer process can be expressed from the respective singlet-triplet energies as $\Delta E_T = {E_T}^D - {E_T}^A$, where ${E_T}^D = E(^3\mathrm{D} \rightarrow {}^1\mathrm{D})$ and ${E_T}^A = E(^3\mathrm{A} \leftarrow {}^1\mathrm{A})$ are the vertical (Franck-Condon) transition energies from ^{3}D and ^{1}A equilibrium geometries to ^{1}D and ^{3}A states, respectively. These energies correspond to frequencies in the optical absorption (emission) spectrum of the triplet acceptor (donor). When the donor triplet energy is greater than that of the acceptor (the so-called exothermic case, $\Delta E_T \geq 0$) the transfer efficiency is nearly diffusion-controlled, indicating that close approach of donor and acceptor molecules (<1 nm) is required.[1] On the other hand, in biological systems is frequently observed that exothermic TET is limited by donor-acceptor separation and relative spatial orientation. If the donor triplet-energy is 2–3 kcal mol^{-1} less than that of the acceptor (endothermic case, $\Delta E_T \leq 0$), energy transfer still occurs but at much lower rate, because the difference in electronic energy must be compensated by vibrational excitation of the donor. In that case, TET becomes an Arrhenius-type thermally activated process in which the transfer efficiency decreases exponentially with the energy deficit.[10]

Intermolecular TET in solution can be modelled as a bimolecular rate process where (i) diffusive (rate constants k_d, k_{-d}) and energy transfer (k_e, k_{-e}) steps are separable,[11] and (ii) the transfer process takes place within an encounter complex [D · · · A], a kind of "supermolecule" in which donor and acceptor molecules are at collision distance. Energy transfer within the super molecule is assumed to take place by a Dexter two-electron exchange[7–9] mechanism (Scheme 1) by overlapping donor and acceptor molecular orbitals.[11] The total spin of reactant [^{3}D · · · ^{1}A] and product [^{1}D · · · ^{3}A] pairs is conserved.

There have been interesting attempts to derive theoretically a TET rate constant (see Ref. 12 for a brief review). For our purposes here we follow essentially the golden rule formalism discussed in great detail by Serpa *et al.*,[13] from which the transfer rate constant is expressed by

$$k_e = \frac{2\pi}{\hbar} U^2 J, \tag{1}$$

where U is the electron exchange coupling term due to the electrostatic interaction between D/A electron clouds, which

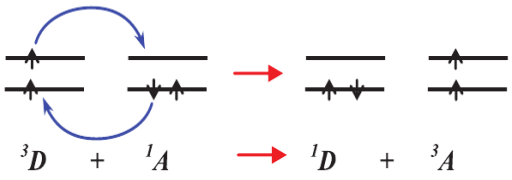

SCHEME 1. Electron and spin exchange between a triplet donor (^{3}D) and a singlet acceptor (^{1}A) in triplet-triplet energy transfer.

a)Author to whom correspondence should be addressed. Electronic mail: luisma.frutos@uah.es

depends only on the electronic configuration of the initial and final states; J is a vibrational term measuring the density of interacting initial and final states, that can be approached[13] by the overlap integral between the normalized spectra of the donor phosphorescence ($^3D \rightarrow {}^1D$) and acceptor ground-state triplet absorption ($^3A \leftarrow {}^1A$).

Absolute values of U turn to be rather small, usually in the 0.1–10 cm^{-1} range consistent with a very weak coupling case.[1,9] However, the electron exchange coupling term is crucial to interpret the TET mechanism.[14] For two electrons separated by a distance r_{12} within the supermolecule the coupling term U can be represented by the electronic exchange integral:[14]

$$U = \langle \phi_{*D}(1)\,\phi_A(2)|\,\frac{e^2}{r_{12}}\,|\phi_D(2)\,\phi_{*A}(1)\rangle\,, \qquad (2)$$

in which ϕ_D and ϕ_A are the spatial part of the electronic wavefunction for D and A within the Born-Oppenheimer approach, denoting the asterisk label the excited electronic state. The value of the integral depends essentially on the overlap between donor and acceptor molecular orbitals, frequently the donor HOMO and acceptor LUMO, and decreases exponentially with the donor-acceptor distance.[7] Because of the small value of this interaction energy, the adiabatic potential energy surfaces (PESs) of the two intervening electronic states (i.e., before and after the transfer) do not intersect each other, showing instead slightly avoided crossings in the intersection space defined by the diabatic states.

The vibrational overlap integral J contains the energy conservation condition, since J depends on the density of states fulfilling the resonance condition. In those cases in which spectroscopic data are available, Eq. (1) yields values in reasonable agreement with experimental TET rate constants,[13] as well as with the observed dependence of the transfer rate constant k_e with ΔE_T for endothermic transfer reactions.

It was early realized that in some highly endothermic TET reactions (5–20 kcal mol^{-1}), the experimental value of the rate constant was much larger than that expected from the negative energy balance,[15,16] as computed using singlet-triplet optical transition energies. These anomalous endothermic cases had in common an acceptor compound with flexible molecular structure, like, e.g., *cis*-stilbene, and for this reason *nonvertical* $^3A \leftarrow {}^1A$ excitation processes (non-Franck-Condon) were initially postulated (see Refs. 15 and 16 for a brief review). It was later shown that electronic excitation transitions in these cases do not depart from the "classical" vertical Frank-Condon scheme (Refs. 1 and 11), but the (unfortunate) *nonvertical* term became firmly established. These apparent deviations from classical TET are currently interpreted by postulating that thermal activation of the ground-state flexible acceptor gives rise to a distorted nuclear geometry, in which the energy of the first excited triplet state is substantially lower than the optically recorded value.[17] The geometrical distortions which are effective in lowering the triplet state energy result from displacements along internal vibrational molecular coordinates (e.g., bond stretchings and torsions), and eventually provide the reaction path for the transfer process. There have been several attempts to identify experimentally these favourable molecular deformations, for example, the paradigmatic case of *cis*-stilbene[18–20] but, unfortunately, the results have been contradictory. Additional insight at the molecular level may be attained by theoretical modelling of the transfer step, and this also has been carried out at different levels of approximation.[20,21] We presented before a formalism[12,22] for the specific case of *nonvertical* TET processes between a series of rigid donors and a flexible acceptor, based on local expansion of the PESs of singlet ground-state and triplet excited-state of the acceptor molecule. In this way, we derived an expression for the energy transfer rate constant (k_e) within the non-adiabatic formulation of transition-state theory. This expression contains a factor associated with the exchange electron coupling interaction U, an exponential term with a quadratic dependence on ΔE_T and a novel *geometrical distortion parameter* (γ) of the acceptor molecule that depends on two specific properties of its singlet and triplet PES: the energy gradient in the triplet state and a combination of different vibrational force constants of the singlet ground state. This approximation explained correctly the dependence of the TET rate constant to cyclooctatetraene (COT) from a series of rigid donor compounds with variable excitation energy, an extreme example of *nonvertical* transfer.[12,23] In addition, the model allowed the identification of the COT structural changes responsible for the decrease of the triplet-state energy.

We present here a method permitting the determination of the reaction coordinate for triplet-triplet excitation transfer in both the classical and *nonvertical* cases for any donor/acceptor pair, based on similar principles as those used previously.[12,22] From this reaction coordinate it can be assigned a numerical value to the *nonvertical* character of the transfer process and to the contribution of each internal coordinate of donor or acceptor molecules to the energy transfer process. As a practical example, this theory is applied to the much debated *nonvertical* TET process to *cis*-stilbene, providing for the first time a very detailed description of the relevant internal coordinates involved in the process, as well as its quantitative determination. The formalism developed here is completely general, and can be extended to any donor/acceptor interaction within the very weak electronic coupling limit.

II. RESULTS AND DISCUSSION

A. Potential energy surfaces in triplet energy transfer

As mentioned above, the transfer process in condensed phase can be analyzed as proceeding from a reactant supermolecule [$^3D\cdots{}^1A$] to the product one [$^1D\cdots{}^3A$].

In Figure 1, top panel, the PESs of two model supermolecules [$^3D\cdots{}^1A$] and [$^1D\cdots{}^3A$] involved in a TET process are illustrated, as a function of internal coordinates $\mathbf{q}_A$ and $\mathbf{q}_D$ defining the molecular structure of the acceptor and donor, respectively. Since the absolute value of the electronic coupling interaction is very low compared with other energies involved in the transfer step, the intersecting space becomes slightly avoided, as shown in the top left inset of Figure 1. The energy of the two model supermolecules at

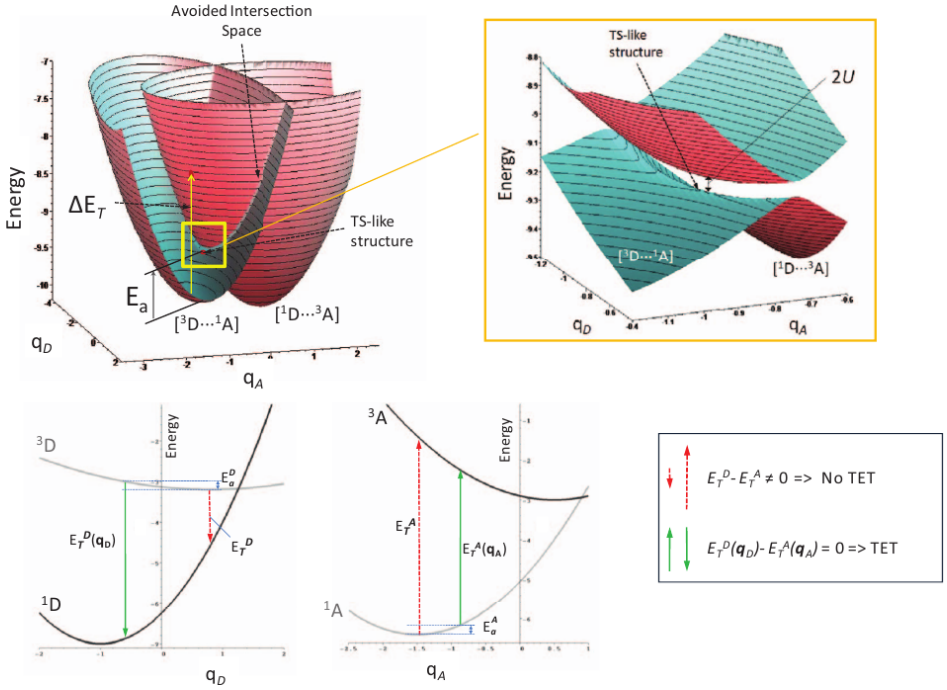

FIG. 1. Top panel: Complete potential energy surfaces of the model supermolecules [^{3}D · · · ^{1}A] and [^{1}D · · · ^{3}A] in a TET process as a function of A/D internal coordinates $\mathbf{q}_A$ and $\mathbf{q}_D$. Each point of the intersecting space corresponds to A/D nuclear configurations for which E[^{3}D · · · ^{1}A] = E[^{1}D · · · ^{3}A]. In fact, both surfaces never intersect, due to the weak 2U interaction energy. The inset shows expanded the avoided crossing between both surfaces for the minimum-energy, transition-state like configuration (TS) of the supermolecule. Lower panel: The TET process represented by the simultaneous individual singlet-triplet transitions of donor and acceptor molecules. Red arrows correspond to the energy of donor deactivation, E_T^D (^{3}D → ^{1}D *transition*), and acceptor excitation, E_T^A (^{3}A ← ^{1}A *transition*), for the respective equilibrium vibrationally relaxed conformation. These values yield a highly endothermic energy balance (right box) and therefore TET would not be possible. However, D-A energy resonance can be attained by simultaneous small geometrical changes of donor and acceptor molecules (shown as green arrows) requiring modest activation energies E_a^{D} and E_a^{A}, respectively. Numerical scales serve as visual aids only.

the equilibrium geometry is different, i.e., two different minima define the equilibrium structure. Nevertheless, the system can achieve energy resonance by thermal activation and attaining in this way a point of the PESs intersecting space. In addition, considering the negligible value of electronic coupling (compared to the activation energy necessary to reach the intersection space), the PES of the supermolecule can be separated in two uncoupled PESs for the donor and acceptor partners. Therefore, the resonance condition E[^{3}D · · · ^{1}A] = E[^{1}D · · · ^{3}A] in the energy transfer process can be properly discussed in terms of the individual transitions ^{3}D → ^{1}D and ^{3}A ← ^{1}A.

The potential energy curves corresponding to these individual singlet-triplet transitions are depicted in Figure 1, lower panel, as a function of internal coordinates $\mathbf{q}_A$ or $\mathbf{q}_D$. In this example there is a large difference between the ground- and excited-state geometry of donor and acceptor molecules. It is evident that TET is not possible if both transitions ^{3}D → ^{1}D and ^{3}A ← ^{1}A take place from each equilibrium configuration. This is because the energy available from the donor deactivation transition ^{3}D → ^{1}D at the zero-point equilibrium conformation ($E_T{}^D$, pictured as a red arrow in Figure 1, left lower panel) is much lower than that required for excitation of the acceptor from its equilibrium conformation ($E_T{}^A$, corresponding to ^{3}A ← ^{1}A transition, red arrow in Figure 1, right lower panel). However, small changes in the conformation of both partners along coordinates $\boldsymbol{q}_A$ for the acceptor and $\boldsymbol{q}_D$ for the donor give rise to singlet-triplet transition energies very different from those corresponding to the equilibrium conformation (represented by green arrows in Figure 1). In this way energy resonance is achieved, i.e., $E_T{}^D(\boldsymbol{q}_D) - E_T{}^A(\boldsymbol{q}_A) \approx 0$, and efficient transfer could take place for these specific donor and acceptor geometries, which correspond to the (avoided) intersecting space represented in Figure 1, top panel. Nevertheless, among all the points fulfilling the resonance condition within the avoided intersection space, only a single structure corresponds to the point of minimum energy, and therefore to a transition-state like configuration (see Figure 1, upper panel). This privileged D · · · A geometry yields the structure with lowest activation energy that fulfils the resonance condition. Thermal energy is, of course, the source of these molecular geometry changes, which would take place at room temperature depending on the value of the corresponding activation energies $E_a{}^{\mathrm{D}}$ and $E_a{}^{\mathrm{A}}$. In summary, TET would be most efficient for D/A pairs in which the resonance condition $E_T{}^D(\boldsymbol{q}_D) - E_T{}^A(\boldsymbol{q}_A) \approx 0$ can be reached by changes in molecular geometry ($\boldsymbol{q}_A$ and $\boldsymbol{q}_{\mathbf{D}}$) that are very efficient in altering (tuning) the singlet-triplet gap with the lowest possible activation energy. In general, every geometrical distortion may influence to a different extent the singlet-triplet energy gap of donor or acceptor, and it is very likely that some displacements along specific internal coordinates would leave

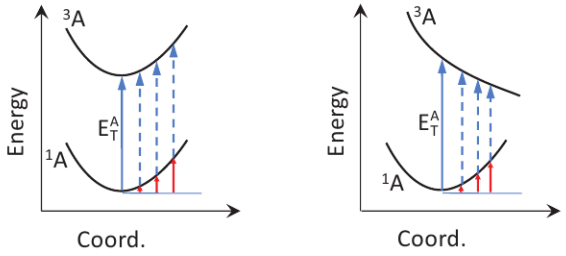

SCHEME 2. Energy profiles for singlet ^{1}A and triplet ^{3}A states of an acceptor molecule. Left: Vibrational excitation of *inactive* coordinates (blue arrows) does not modify the ^{1}A-^{3}A zero-point equilibrium energy gap (E_T^A). Right: In the case of *active* coordinates, these changes modulate efficiently (decrease here) the singlet-triplet energy gap. All these geometrical changes require an activation energy E_a^A indicated by red arrows.

unchanged the energy of this transition. This is illustrated in the simplified potential energy curves of Scheme 2 for an ideal acceptor molecule. On the other hand, the conformational changes which are very efficient in modifying the singlet-triplet energy gap of donor or acceptor molecules would be likely a combination of multiple internal coordinates characterized by low values of activation energy, as noted above.

Therefore, a complete description of the TET reaction coordinate requires the simultaneous analysis of (i) the change in the value of the acceptor S-T and donor T-S energy gaps along all internal coordinates, and (ii) the activation energy associated to the geometrical change that takes place along each coordinate.

B. Triplet energy transfer reaction coordinate (TET-RC)

The **TET-RC** is expressed in terms of the properties of the individual acceptor (or donor) molecule as the minimum energy configuration on the PES fulfilling a given resonance condition imposed by the energy of the donor (acceptor), which is taken as a parameter for the definition of the energy transfer coordinate. Therefore, the reaction coordinate of a given acceptor $\mathbf{q}_A^{RC}$ is a function of the singlet-triplet excitation energy surface $E_A^T(\mathbf{q}_A)$ and depends parametrically on the triplet energy of the donor (E_D^T), i.e., $\mathbf{q}_A^{RC}(E_A^T(\mathbf{q}_A); E_D^T)$. In a similar way, the reaction coordinate of a given donor $\mathbf{q}_D^{RC}$ would depend on $E_D^T(\mathbf{q}_D)$ and E_A^T. All of the internal coordinates that may modulate the singlet-triplet energy gap would be contained in the reaction coordinate, but with a relative weight that would be higher for those that are more efficient in decreasing the activation energy of the initial state (^{1}A in the case of acceptor and ^{3}D in the case of donor). Therefore, the TET-RC would include those coordinates providing a maximum variation of singlet-triplet energy with a minimum energy of activation. Moreover, the analysis of the TET process in terms of separated donor and acceptor transitions, as discussed above, allows the definition of a reaction coordinate TET-RC for each individual process, that is, a TET-RC of the donor deactivation (^{3}D $\rightarrow$ ^{1}D) and a TET-RC for acceptor excitation (^{3}A $\leftarrow$ ^{1}A). Each TET-RC would be composed by the collection of minimum energy configurations providing a given set of singlet-triplet energy gaps. Thus, the singlet-triplet energy becomes the parameter for determining the reaction coordinate, since the reaction coordinate depends parametrically on this energy. This definition is consistent with a minimum energy principle: the energy transfer reaction will take place with the lowest possible activation energy.

In summary, the construction of the TET-RC entails the identification of those molecular distortions that change the singlet-triplet energy gap in the donor and acceptor molecules with the lowest energy demand. Two reaction coordinates are necessary to fully characterize the system if both donor and acceptor molecules are likely to present these molecular distortions: donor TET-RC and acceptor TET-RC. However, a single TET-RC would be enough if only one of the transfer partners may contain active coordinates. Since the most frequent experimental situation corresponds to transfer from rigid donors to flexible acceptors (*v. infra*), we discuss next the TET-RC for a generic acceptor molecule which is promoted to the triplet state ^{3}A $\leftarrow$ ^{1}A as a result of the transfer, although the same reasoning is applicable to donor triplet quenching. Accordingly, the energy transfer reaction coordinate for this acceptor molecule is determined by the set of ground-state minimum-energy structures that present a given singlet-triplet energy gap, i.e., among all the points of the PES characterized by a given singlet-triplet energy gap, only that point of minimum energy in the ground state is a point of the reaction coordinate. This situation is illustrated in Figure 2: the PESs of the singlet (S_0) and triplet (T_1) states of the generic acceptor molecule have been pictured (left) as a function of nuclear displacements described by internal nuclear coordinates q_1 and q_2. A series of nuclear configurations for which the singlet-triplet energy gap is constant are shown here by combining pairs of the blue curves drawn on the T_1 and S_0 surfaces, for energy values of 2, 5, and 7 relative units. For example, all the configurations defined by the pair of blue curves joined by the red arrow correspond to a singlet-triplet energy gap of 7 relative units. Thus, it can be seen that there are many different ways of changing the acceptor zero-point equilibrium geometry to get a reduction of the singlet-triplet excitation energy, as was proposed before.[20] However, among all these possible molecular configurations yielding a given reduction of the singlet-triplet gap, only a single structure corresponds to a minimum energy point in the initial state, S_0 in this example. The TET reaction coordinate is defined by joining all these points on the PES.

The minimum-energy configurations in S_0 in the case of an acceptor molecule (or in T_1 for a donor) with a given singlet-triplet energy can be located by constraining the energy gradient vectors on both singlet and triplet states to be parallel.[12,22] Therefore, if $E_{S_0}(\mathbf{q})$ and $E_{T_1}(\mathbf{q})$ represent the S_0 and T_1 potential energy surfaces as a function of nuclear internal coordinates $\mathbf{q}$, a molecular geometry corresponding to a minimum activation energy in the initial state (S_0 in the case of an acceptor molecule or T_1 for a donor) must satisfy the following condition:

$$\frac{(\nabla \mathrm{E}_{T_1}(\mathbf{q}^{RC}))^T \bullet \nabla \mathrm{E}_{S_0}(\mathbf{q}^{RC})}{\|\nabla \mathrm{E}_{T_1}(\mathbf{q}^{RC})\| \|\nabla \mathrm{E}_{S_0}(\mathbf{q}^{RC})\|} = \pm 1, \tag{3}$$

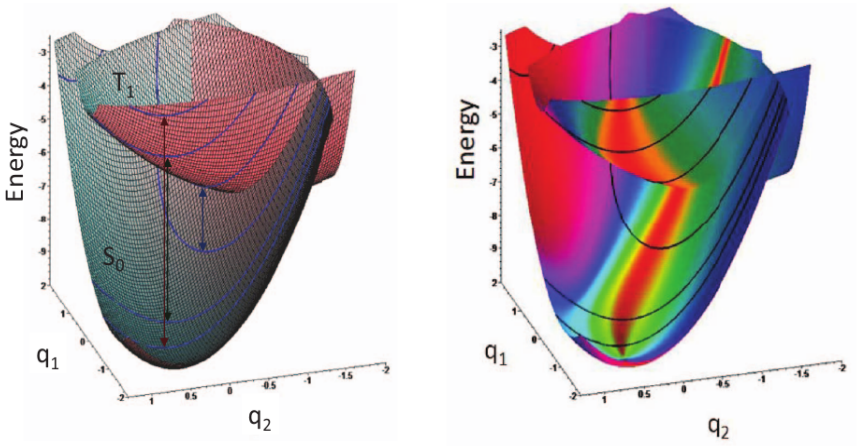

FIG. 2. Schematic representation of the PES of singlet S_0 and triplet T_1 electronic states of a generic acceptor molecule as a function of internal nuclear coordinates q_1 and q_2. Left: The arrows joining pairs of the blue curves highlighted over each surface, mark sets of configurations with a constant S_0-T_1 energy gap; three different gap values have been represented for three different energy values: 2, 5, and 7 relative units. Right: the same PESs color-mapped to show the value of cosine of the angle between S_0 and T_1 energy gradient vectors. Red color corresponds to cosine values $\approx \pm 1$, i.e., parallel gradient vectors.

where ∇E is the first derivative of the energy for the indicated electronic state, that is the energy gradient. The reaction coordinate for triplet energy transfer ($\mathbf{q}^{\mathrm{RC}}$) is defined by the set of geometries which are solutions of Eq. (3), in mass-weighted Cartesian coordinates. In Figure 2 (right) the PESs of the generic acceptor have been mapped with a color scale representing the value of the cosine of the angle formed by the two gradient vectors ∇E_{S_0} and ∇E_{T_1}, where red color corresponds to absolute values of the cosine close to unit. The molecular configurations of S_0 that satisfy this condition define the triplet energy transfer coordinate for this specific acceptor.

Since the TET-RC is defined in terms of local properties of S_0 and T_1 potential energy surfaces, $\mathbf{q}^{\mathrm{RC}}$ will be, in general, a complex combination of internal coordinates. Therefore, it would be unlikely to find a TET-RC determined only by a single molecular deformation, e.g., a bond torsion or a stretching.

C. A quantitative determination of *nonvertical* transfer properties

In flexible acceptor molecules giving rise to *nonvertical* endothermic energy transfer, a large reduction of the equilibrium singlet-triplet energy gap E_T^A takes place due to distortions of the acceptor molecular geometry which require low activation energy E_a^A. These two factors are correlated along the TET-RC: maximum variation of the singlet-triplet energy gap with minimum activation energy on the ground state. Therefore, the TET-RC makes it possible to assign a quantitative meaning to *nonvertical* deviation from classical transfer for a given acceptor/donor pair. As noted above, we derived[12] a *geometrical distortion parameter* (γ) which is a function of the ratio of the above two factors: the reduced singlet-triplet energy gap of the acceptor and the corresponding activation energy, both of them depending on the acceptor internal coordinates ($\mathbf{q}_{\mathrm{A}}$). This parameter was originally derived from local quadratic expansion of acceptor singlet and triplet PES, but its definition is completely general and can be computed for any molecular configuration along the TET-RC without any approximation in the PES. The γ value measures the extent to which geometrical changes in the acceptor molecule modulate its singlet-triplet gap: large γ values correspond to large changes in singlet-triplet energy gap with low activation energy (*nonvertical* transfer), while low γ values correspond to the opposite situation in which the S-T energy gap is not affected by vibrational activation (classical transfer). Since this applies also to donor molecules it is possible to compute a γ value for each individual point of the reaction coordinate ($\mathbf{q}^{\mathrm{RC}}$). We obtain in this way the *generalized geometrical distortion parameter*, which is defined for a specific donor or acceptor molecule as

$$\gamma_{q^{RC}} = \left\{ \frac{[\Delta E_T^A(\mathbf{q}^{RC})]^2}{E_a(\mathbf{q}^{RC})} \right\}^{\frac{1}{2}}, \tag{4}$$

where $\Delta E_T^A(\mathbf{q}^{RC}) = E_T^A(\mathbf{q}^{RC}) - E_T^A$, that is, the difference between the singlet-triplet energy of the distorted molecule $E_T^A(\mathbf{q}^{RC})$ (green arrow in Figure 1) and that of the molecule at the zero-point equilibrium geometry $\mathrm{E_T^A}$ (corresponding red arrow in Figure 1), for a specific point of the reaction coordinate $\mathbf{q}^{RC}$; $\mathrm{E_a}(\mathbf{q}^{\mathrm{RC}})$ is the corresponding activation energy of this molecular distortion. Note that, for a given acceptor molecule, *nonvertical* deviation from classical transfer should be also a function of the donor triplet energy, because the extent of the geometrical changes that would take place in the acceptor molecule to approach energy resonance $E_T^D(\mathbf{q}^{RC}) - E_T^A(\mathbf{q}^{RC}) = 0$ depends on the available donor triplet energy.

D. Determination of the relative weight of the internal coordinates in TET

As shown above for the case of an acceptor molecule, the optimal molecular structure to match a given triplet excitation energy is defined by the reaction coordinate ($\mathbf{q}^{\mathrm{RC}}$),

corresponding to a collection of molecular structures showing a complex combination of internal coordinates. Nevertheless, the extent (i.e., magnitude) of the internal coordinate variations along the reaction coordinate is not strictly related to the weight of the specific coordinate in the reaction coordinate ($\mathbf{q}^{\mathrm{RC}}$) definition. This is due to the following factors: (i) the eventual coupling between efficient and inefficient vibrational displacements provoking large changes along the inefficient coordinate which do not modify the TET-RC, and (ii) the possible presence of large amplitude ground-state low-frequency vibrational modes which do not contribute efficiently to the energy gap variation, in spite that may result in large geometrical distortions. Concluding, the amplitude of variation of an internal coordinate along the TET-RC is not a direct measurement of their relevance in enabling the energy transfer.

The weight of a specific internal coordinate (e.g., bond torsion) for a given point of the TET-RC depends on its contribution to the variation of the singlet-triplet energy gap, as well as on the value of the associated activation energy. According to that, a coordinate with a large weight in the TET process (e.g., bond torsion) should provide a large variation of the S-T energy gap with low activation energy. It is possible to determine weight along the TET-RC according to these conditions. Specifically, within a second order approximation for the PES, the variation of the singlet-triplet energy gap for an acceptor (donor), $\Delta E_T^{A(D)}$, and the corresponding activation energy in the initial state, $E_a^{A(D)}$, for a transition between two electronic states (denoted as initial "0" and final "1" states) are given by

$$\Delta E_T^A(\mathbf{q}^{RC}) = E_T^A(\mathbf{q}^{RC}) - E_T^A = (\mathbf{q}^{RC})^T \mathbf{g}_1 + \frac{1}{2}(\mathbf{q}^{RC})^T(\mathbf{H_1} - \mathbf{H_0})(\mathbf{q}^{RC}) \quad (5)$$

and

$$E_a^A(\mathbf{q}^{RC}) = \frac{1}{2}(\mathbf{q}^{RC})^T \mathbf{H_0} \mathbf{q}^{RC}, \quad (6)$$

where $\mathbf{q}^{\mathrm{RC}}$ represent the change in molecular internal coordinates relative to the minimum energy structure of the initial state, $\mathbf{g}_1$ is the energy gradient vector in the final state for the same geometry, $\mathbf{H}_0$ and $\mathbf{H}_1$ are the Hessian matrices for the initial and final state, respectively, determined also at the equilibrium structure of the initial state. Each coordinate contributes to the singlet-triplet energy gap difference $\Delta E_T^{A(D)}$ linearly in the energy gradient term and quadratically through the Hessian matrices. Therefore, for a given internal coordinate $\mathbf{q}_i^{RC}$, Eqs. (5) and (6) can be formulated in terms of the "*N*" internal coordinates of the molecule:

$$\Delta E_T^{A(D)}(\mathbf{q}^{RC}) = \sum_{i=1}^{N} \left\{ q_i^{RC}(\mathbf{g_1})_i + \frac{1}{2} \sum_{j=1}^{N} q_i^{RC} q_j^{RC} (\mathbf{H_1} - \mathbf{H_0})_{ij} \right\} \quad (7)$$

and

$$E_a^{A(D)}(\mathbf{q}^{RC}) = \sum_{i=1}^{N} \left\{ \frac{1}{2} \sum_{j=1}^{N} q_i^{RC} q_j^{RC} (\mathbf{H_0})_{ij} \right\}, \quad (8)$$

where the expressions in brackets are the individual contribution of each component q_{i} to the global singlet-triplet energy difference (Eq. (7)) and activation energy (Eq. (8)).

The definition of the *generalized geometrical distortion parameter* discussed above (Eq. (4)) allows the computation of a γ value for each individual coordinate, determining its weight in the overall reaction coordinate. Accordingly, the value of the γ parameter for each internal coordinate of the donor (or acceptor) molecule would be given by

$$\gamma_{\mathbf{q}_i^{RC}} = \left\{ \frac{\left[\left(\mathbf{q}_i^{RC}\right)^T \mathbf{g}_1 + \frac{1}{2}(\mathbf{q}^{RC})^T (\mathbf{H_1} - \mathbf{H_0})\left(\mathbf{q}_i^{RC}\right) \right]^2}{\frac{1}{2}(\mathbf{q}^{RC})^T \mathbf{H_0} \mathbf{q}_i^{RC}} \right\}^{\frac{1}{2}}, \quad (9)$$

where $\mathbf{q}_i^{RC} = (0, 0, \ldots, q_i^{RC}, \ldots, 0, 0)$ is a vector in which all the terms are zero except the "*i*" term, that is equal to the value of the coordinate "*i*" in the specific point of the TET-RC, $\mathbf{q}_i^{RC}$. Each $\gamma_{\mathbf{q}_i}^{RC}$ parameter yields the contribution of every $\mathbf{q}_i$ internal coordinate to *nonvertical* transfer, permitting to express the role of each coordinate in the TET process in terms of relative energies.

Interestingly, it is possible to establish a relation between the *generalized geometrical distortion parameter* and the λ parameter in the Marcus theory for electron transfer,[24] which yields the energy barrier due to reorganization of reactants and solvent shell. It can be easily shown that

$$\gamma^2{}_{\mathbf{q}^{RC}} = 4\lambda. \quad (10)$$

Since the γ parameter was defined (Eqs. (4) and (9)) as the change in the acceptor (or donor) singlet-triplet energy relative to the vibrational activation energy required to produce that change, this parameter contains terms (coordinates) pertaining only to acceptor (or donor) molecules, excluding the solvent. In consequence, the λ parameter in Eq. (10) yields the contribution of donor/acceptor molecules to the total reorganization energy, and in that regard is equivalent to the inner sphere reorganization energy in Marcus ET theory. Moreover, since the donor and acceptor transitions can be treated separately within the very weak electronic coupling limit, the λ parameter can also be expressed by the donor and acceptor contribution to the total reorganization energy for each internal coordinate:

$$\gamma^2{}_{\mathbf{q}_A^{RC}} + \gamma^2{}_{\mathbf{q}_D^{RC}} = 4\lambda. \quad (11)$$

In this way it is now possible to interpret the reorganization energy in terms of internal coordinates, when Marcus ET theory is applied to triplet energy transfer processes.[25]

E. *Nonvertical* TET in *cis*-stilbene

Hammond and Saltiel introduced the *nonvertical* TET concept while studying *cis*-stilbene (*c*-Stb) as triplet-energy acceptor.[15,26] This outstanding work ignited a great interest on the process and gave rise to a substantial amount of related investigations (see Refs. 16, 20, and 21 for reviews). However, in spite of the elapsed 50 years from the initial discovery, there is not yet consensus on the nature of *c*-Stb structural changes responsible for the *nonvertical* effect, as is also the case for other *nonvertical* acceptors. In this regard, a description of the

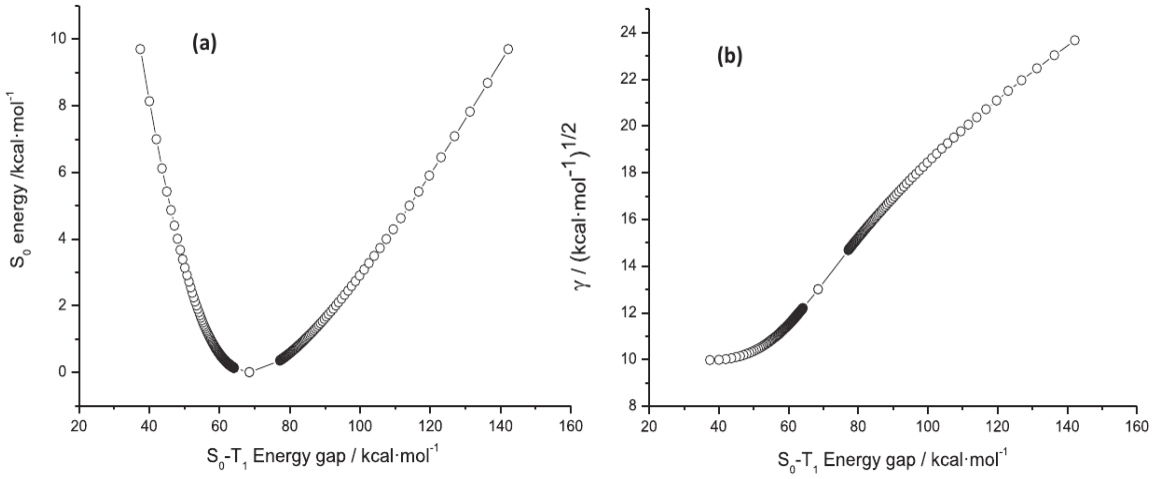

FIG. 3. (a) The relation between E_a^{S0} and the S_0-T_1 energy gap, the excess thermal activation energy required to change the equilibrium geometry of ground-state *c*-stilbene, and the S_0-T_1 energy gap of that distorted geometry. $E_a^{S0} = 0$ corresponds to the S-T energy gap of the vibrationless equilibrium geometry (67 kcal mol^{-1}). (b) The relation between the *geometrical distortion parameter* γ and the S_0-T_1 energy gap, for the same triplet energy transfer reaction coordinate.

reaction coordinate for the triplet energy transfer in this prototype acceptor that incorporates the ideas discussed above may provide a well-founded interpretation of the molecular changes that make possible triplet excitation. Therefore, we present below the TET-RC for the process in which *c*-Stb is the acceptor compound being excited to its triplet state by a series of undefined rigid triplet-donor molecules. In this particular case the system is completely defined by the TET-RC for acceptor activation only, since there are no active coordinates in the donor molecules.

The TET-RC was constructed by computing molecular and electronic structure properties of *c*-Stb with density functional theory, using an hybrid B3LYP functional with a 6-31+G* basis set, as implemented in Gaussian 03.[27] In addition, a novel algorithm detailed in Ref. 22 was applied using mass-weighted Cartesian coordinates and including a second-order local expansion of the PES. Figure 3(a) shows the reduction in *c*-Stb singlet-triplet energy gap along the TET-RC for different values of the relative energy required to produce geometrical changes in the molecule ground-state (E_a^{S0}), computed following the condition expressed by Eq. (3). It can be seen that modest changes in ground-state energy give rise to a large reduction in the S_0-T_1 energy gap and, consequently, in the required triplet excitation energy. Thus, for example, thermal activation by only ca. 4 kcal mol^{-1} of the ground-state conformation gives rise to the reduction of ca. 20 kcal mol^{-1} in the S_0-T_1 energy gap. This allows low-energy donors to transfer very efficiently the excitation energy to that fraction of thermally activated *c*-Stb molecules and is, of course, the origin of the *nonvertical* TET. Figure 3(a) also shows that variations in *c*-Stb ground-state energy may produce instead a large *increase* of the singlet-triplet energy gap; for instance, the same 4 kcal mol^{-1} change in S_0 energy gives rise to an increase of more than 40 kcal mol^{-1} in the S_0-T_1 energy gap. Therefore, vibrational (i.e., thermal) activation of *c*-Stb singlet ground-state can convert the molecule in a good acceptor for either low- or high-energy triplet donors. Indeed, *c*-Stb presents an even more pronounced *nonvertical* transfer character when considering high-energy triplet donors.

As mentioned above, the *generalized geometrical distortion parameter* γ as defined in Eq. (4) permits a quantitative description of the *nonvertical* transfer. Thus, Figure 3(b) shows the relationship between γ and the S_0-T_1 energy gap for *c*-Stb, along the TET-RC. The γ parameter takes a value of $\sim$13 (kcal mol^{-1})$^{1/2}$ for the S_0-T_1 energy gap corresponding to ground-state equilibrium geometry ($E_0^A \sim 67$ kcal mol^{-1}),[28] decreasing slowly for lower values of the energy gap, and increasing rapidly for augmented singlet-triplet energy gaps.

The key internal coordinates controlling the *nonvertical* character of TET to *c*-Stb, as well as their relative weight in diminishing the triplet excitation energy, have been obtained by computing the respective γ_{qi} values. The *c*-Stb equilibrium geometry, together with the relevant internal coordinates, $\mathbf{r_i}$ (bond stretching) and $\mathbf{d_i}$ (bond torsion) are presented in Scheme 3, while Figure 4 shows the weight of each internal coordinate in tuning the singlet-triplet energy gap, expressed by its γ_{qi} value. As discussed above, a large γ_{qi} value

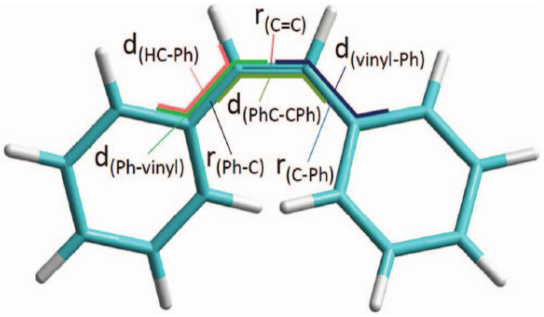

SCHEME 3. Ground-state equilibrium geometry of *cis*-stilbene and internal coordinates $\mathbf{r_i}$ (bond stretching) and $\mathbf{d_i}$ (bond torsion). Ph = phenyl ring.

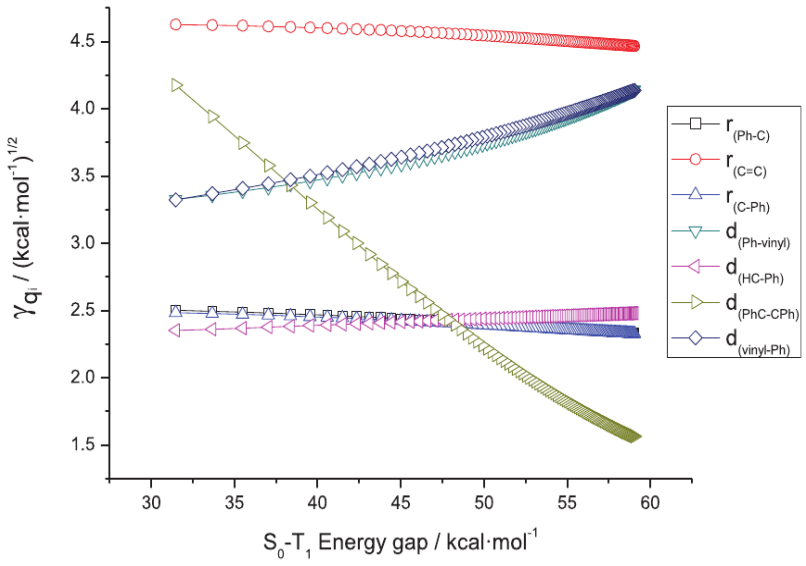

FIG. 4. The γ_{qi} values computed for each effective internal coordinate of *cis*-stilbene, for triplet energies in the 30–60 kcal mol^{-1} range along the TET-RC. Since the singlet-triplet excitation energy of this compound for the S_0 equilibrium configuration is ca. 67 kcal mol^{-1}, efficient TET from lower energy triplet donors would be only possible if the energy mismatch (ΔE_T) is cancelled by thermally activated geometrical distortions of the polyene. Large γ_{qi} values correspond to geometrical distortions that are very effective in attaining energy resonance ($\Delta E_T \approx 0$) for the indicated singlet-triplet energy exchange.

indicates that this q_i specific internal coordinate is very effective in matching (decreasing) the *c*-Stb singlet-triplet excitation energy to that available from the donor. In this regard, the central double-bond *stretching* vibration $r_{(C=C)}$ appears as the most important geometrical change in minimizing the singlet-triplet excitation energy of the acceptor, with a large weight value virtually independent on the energy deficit. This observation is in disagreement with many of previously proposed ideas regarding the origin of *nonvertical* transfer in this compound.[18–21] The other group of stretching vibrations localized along the two carbon-phenyl bonds $r_{(Ph-C)}$ and $r_{(C-Ph)}$ produce a much lower effect (low γ_{qi} values) in altering the triplet energy gap. Single and double-bond torsion modes are of high interest due to the discrepancies regarding their relative effect in minimizing S-T excitation energy.[18–21] The computed γ_{qi} values indicate that the contribution of the two phenyl-vinyl single-bond torsions $d_{(Ph-vinyl)}$ and $d_{(vinyl-Ph)}$ should be very important for a small triplet energy deficit, but become less effective when the energy mismatch increases. In contrast, the central double-bond torsion $d_{(PhC-CPh)}$ shows a very low contribution in the triplet energy range close to resonance (donor triplet energies close to 67 kcal mol^{-1}), but rapidly becomes much more important for large values of energy mismatch (Figure 4). Finally, the single-bond torsion including the vinyl hydrogen atom $d_{(HC-Ph)}$ shows a modest effect, similar to that of the carbon-phenyl stretching. The effects of the different internal motions shown above were determined by considering all the degrees of freedom of the *c*-Stb molecule. Nevertheless, if restrictions are introduced in any of them, as in the case of the *stiff*-stilbenes,[19] the final effect and the relative contribution of each nuclear motion would be different.

III. CONCLUSIONS

The TET-RC is defined here for individual acceptor (or donor) molecules as the minimum energy configuration on the PES fulfilling the resonance condition imposed by the energy of the donor (acceptor). This definition applies to energy transfer reactions in the very weak electronic coupling limit (Dexter electron exchange), which allows the process to be analyzed in terms of the two intervening individual electronic transitions: donor deactivation $^3D \rightarrow {}^1D$ and acceptor excitation $^3A \leftarrow {}^1A$. In this way a reaction coordinate ($\mathbf{q}^{RC}$) for each individual transition was defined according to a constrained optimization by imposing the condition of parallel energy gradient vectors for both electronic states for a given molecule (i.e., singlet and triplet states). Based on this definition, a *generalized geometrical distortion parameter* (γ_q^{RC}) was developed, that provides a quantitative assignment of the *nonvertical* character of a given donor or acceptor molecule in the TET process. In addition to that, a novel formalism was elaborated to determine the contribution of each individual internal coordinate to the TET-RC and, in this way, to identify the key coordinates in the excitation transfer process.

The practical application of the new formalism was illustrated by analyzing the TET-RC for the conflicting case of endothermic triplet energy transfer to *c*-stilbene as an acceptor compound. It is shown that the important internal coordinates in explaining the unexpected large transfer efficiency are geometrical distortions of the flexible polyene due to the central C=C bond stretching vibration and phenyl-vinyl torsions. Thermal activation of these vibrations gives rise to a large decrease of the S-T energy gap of ground-state *c*is-stilbene, facilitating the transfer. In contrast, the central double bond

torsion shows a variable effect, being very important for large donor-acceptor energy discrepancies but of lesser relevance near energy resonance conditions.

Since the TET-RC formulation developed here is completely general, this approximation may be helpful for the detailed characterization of the TET process involving a wide range of donor and acceptor molecular partners, as well as to any transfer process taking place within the very weak coupling limit.

ACKNOWLEDGMENTS

This work was supported by projects CTQ 2010-16457 and CTQ-2012-36966 of the Spanish Secretaría de Estado de Investigación Desarrollo e Innovación, and UAH2011/EXP-041 and CCG2013/EXP-089 of the University of Alcalá (UAH). F.Z. and M.M. acknowledge receipt of doctoral fellowships from the Spanish MICINN and UAH, respectively. We thank the anonymous reviewer for providing helpful comments, especially regarding the comparison with Marcus theory.

[1] A. A. Lamola, in *Energy Transfer and Organic Photochemistry*, edited by P. A. Leemakers and A. Weissberger (Interscience, N.Y., 1969), pp. 117–126; N. J. Turro, *Modern Molecular Photochemistry* (University Science Books, Sausalito, California, 1991); B. Valeur and M. N. Berberán-Santos, *Molecular Fluorescence*, 2nd ed. (Wiley-VCH Verlag, Weinheim, Germany, 2012).

[2] A. L. Moore, A. Joy, R. Tom, D. Gust, T. A. Moore, R. V. Bensasson, and E. J. Land, Science **216**, 982 (1982); D. Gust and T. A. Moore, *ibid.* **244**, 35 (1989); D. Gust, T. A. Moore, and A. L. Moore, Acc. Chem. Res. **42**, 1890 (2009); J. Vura-Weis, S. H. Abdelwahed, R. Shukla, R. Rathore, M. A. Ratner, and M. R. Wasielewski, Science **328**, 1547 (2010).

[3] M. M. Nicholson, in *Phthalocyanine: Properties and Applications*, edited by A. B. P. Lever and C. C. Leznoff (VCH, New York, 1993), Vol. 3, p. 71.

[4] P. Altoè, N. Haraszkiewicz, F. G. Gatti, P. G. Wiering, C. Frochot, A. M. Brouwer, G. Balkowski, D. Shaw, S. Woutersen, W. Jan Buma, F. Zerbetto, G. Orlandi, D. A. Leigh, and M. Garavelli, J. Am. Chem. Soc. **131**, 104 (2009); L. M. Frutos, U. Sancho, and O. Castaño, Org. Lett. **6**, 1229 (2004); J. Phys. Chem. A **109**, 2993 (2005).

[5] A. Fujishima, X. T. Zhang, and D. A. Tryk, Surf. Sci. Rep. **63**, 515 (2008); S. Ardo and G. Meyer, J. Chem. Soc. Rev. **38**, 115 (2009); H. Chen, C. E. Nanayakkara and V. H. Grassian, Chem. Rev. **112**, 5919 (2012); M. A. Henderson, and I. Lyubinetsky, *ibid.* **113**, 4428 (2013).

[6] S. Ardo and G. J. Meyer, J. Am. Chem. Soc. **133**, 15384 (2011); A. Kubacka, M. Fernández-García, and G. Colón, Chem. Rev. **112**, 1555 (2012); G. Bottari, G. de la Torre, D. M. Guldi, and T. Torres, *ibid.* **110**, 6768 (2010).

[7] D. L. Dexter, J. Chem. Phys. **21**, 836 (1953).

[8] K. R. Naqvi and C. Steel, Chem. Phys. Lett. **6**, 29 (1970).

[9] T. Förster, in *Modern Quantum Chemistry*, edited by O. Sinanoglu (Academic Press, New York, 1965), p. 93.

[10] K. Sandros, Acta Chem. Scand. **18**, 2355 (1964).

[11] J. Saltiel, P. T. Shannon, O. C. Zafiriou, and A. K. Uriarte, J. Am. Chem. Soc. **102**, 6799 (1980); J. Saltiel and B. W. Atwater, in *Advances in Photochemistry* (John Wiley & Sons, Inc., 2007), p. 1.

[12] L. M. Frutos, O. Castaño, J. L. Andrés, M. Merchán, and A. U. Acuña, J. Chem. Phys. **120**, 1208 (2004).

[13] C. Serpa, L. G. Arnaut, S. J. Formosinho, and K. R. Naqvi, Photochem. Photobiol. Sci. **2**, 616 (2003).

[14] S.-T. Levy and S. Speiser, J. Chem. Phys. **96**, 3585 (1992); S. Speiser, Chem. Rev. **96**, 1953 (1996); Z.-Q. You, C.-P. Hsu, and G. R. Fleming, J. Chem. Phys. **124**, 044506 (2006); J. Phys. Chem. A **115**, 4092 (2011).

[15] J. Saltiel and G. S. Hammond, J. Am. Chem. Soc. **85**, 2515 (1963).

[16] J. Saltiel, G. R. Marchand, E. Kirkor-Kaminska, W. K. Smothers, W. B. Mueller, and J. L. Charlton, J. Am. Chem. Soc. **106**, 3144 (1984); P. J. Forward, A. A. Gorman, and I. Hamblett, J. Chem. Soc., Chem. Commun. 250 (1993).

[17] V. Ramamurthy and R. S. H. Liu, J. Am. Chem. Soc. **98**, 2935 (1976).

[18] R. A. Caldwell, S. J. Riley, A. A. Gorman, S. P. Mcneeney, and D. J. Unett, J. Am. Chem. Soc. **114**, 4424 (1992); C. M. Brennan, R. A. Caldwell, J. E. Elbert, and D. J. Unett, *ibid.* **116**, 3460 (1994).

[19] J. Saltiel, J. E. Mace, L. P. Watkins, D. A. Gormin, R. J. Clark, and O. Dmitrenko, J. Am. Chem. Soc. **125**, 16158 (2003).

[20] J. Lalevee, X. Allonas, and J. P. Fouassier, Chem. Phys. Lett. **401**, 483 (2005).

[21] J. Catalán and J. Saltiel, J. Phys. Chem. A **105**, 6273 (2001).

[22] L. M. Frutos and O. Castaño, J. Chem. Phys. **123**, 104108 (2005).

[23] L. M. Frutos, O. Castaño, and M. Merchán, J. Phys. Chem. A **107**, 5472 (2003).

[24] R. A. Marcus, in *Advances in Chemical Physics* (John Wiley & Sons, Inc., NY, 1999) Vol. 107, Part 1, and references therein.

[25] G. L. Closs, M. D. Johnson, J. R. Miller, and P. Piotrowiak, J. Am. Chem. Soc. **111**, 3751 (1989).

[26] G. S. Hammond, J. Saltiel, A. A. Lamola, N. J. Turro, J. S. Bradshaw, D. O. Cowan, R. C. Counsell, V. Vogt, and C. Dalton, J. Am. Chem. Soc. **86**, 3197 (1964).

[27] M. J. Frisch, G. W. Trucks, H. B. Schlegel, *et al.*, Gaussian 03, Gaussian, Inc., Wallingford, CT, 2009.

[28] The *c*-Stb triplet energy in solution is ~ 58 kcal mol^{-1}, estimated from the onset of the optical $T_1 \leftarrow S_0$ absorption by oxygen perturbation techniques (D. F. Evans, J. Chem. Soc. 1351 (1957); A. Bylina, and Z. R. Grabowski, Trans. Faraday Soc. **65**, 458 (1969); T. Ni, R. A. Caldwell, and L. A. Melton, J. Am. Chem. Soc. **111**, 457 (1989); A. A. Gorman, R. L. Beddoes, S. P. Hamblet, S. P. McNeeney, A. L. Prescott, and D. J. Unett, J. Chem. Soc., Chem. Commun. 963 (1991). Since the main properties of the c-Stb TET reaction coordinate do not depend on the absolute value of this energy, we used here the value computed by density functional theory techniques (67 kcal mol^{-1}) for internal consistency.

4.2.3 A Dynamical approach to the triplet-triplet energy transfer reaction coordinate

Even though the geometrical distortion parameter can effectively characterize the relevant coordinates of the TET process, it does not tell us how the system behaves in condensed phase where there is a significant amount of energy constantly interchange between the solute and the solvent. Besides, there is a physical limit of the available thermal energy that can be used to module the singlet-triplet energy gap. Therefore in this section a dynamical approach is presented, taking the system porphyrin-oxygen (PH_2-O_2) as model for the simulations.

As has been stated in the foregoing sections the process of TET can be divided in terms of the independent geometrical distortions suffered by both the acceptor and donor. Therefore a dynamical approach to the TET can be approached trough independent dynamic simulation of both donor and acceptor. In order to simulate the TET between porphyrin and O_2, it was firstly optimized the PH_2 minimum in the first triplet state (i.e. the initial triplet state T_1) at DFT/ CC-pVDZ theory level, which report a value for the singlet-triplet energy gap of 31.1 kcal/mol, while the reported experimental value is 36.4 kcal/mol (Gouterman and Khalil 1974). On the other hand, we found that our chosen level of theory poorly reproduce the experimental value of triplet-singlet energy gap in molecular oxygen (22.5Kcal/mol); therefore we worked with the experimental value in the following discussion.

Given that the singlet-triplet energy gap for both donor and acceptor must be the same for the TET to take place, the donor (PH_2) can use the available thermal energy to overcome the energy deficit of 8.6 kcal/mol, since oxygen capacity of modulation singlet-triplet energy gap is very limited due to the similar bond force constants on the ground (S_0) an triplet (T_1) states and similar minimum energy structures on both states.

Our aims are then to identify trough dynamic simulation the internal coordinates involved in the geometrical disruption of the PH_2, which lead to the reduction of the singlet-triplet gap. As well as to make a statistical interpretation of the MD simulation, which relates the population density with a given singlet-triplet energy gap allowing the energy transfer.

Accordingly, it was used the methodology described in section 2.4 to build analytical gradients for the dynamical simulations, using a quadratic interpolation as a cheap alternative to "on the fly" molecular dynamics. Besides, the Nose-Hoover chain of thermostat was applied to introduce the effect of the temperature as described in section 2.1.4. Using this methodology, it was carried out dynamical simulation of the porphyrin at 300, 200, 100 and 50 Kelvin, during 1 ns integrating each 0.1 fs, sampling around 10^7 points of the phase space (i.e. position and velocity).

The sampled points were firstly used to calculate the *generalized geometrical distortion parameter* $\left(\gamma_q\right)$ for each internal coordinate in each step of integration, following the methodology described in the previous section (Zapata, et al. 2014). The mean values of γ_{q_i}, obtained after the simulation shown that the main coordinates involved in the process of modulation are the valence angle between the pyrrolic ring and the carbon bridge that join them, together with the bonds liking the bridge and the pyrrolic ring.

Subsequently, the statistical interpretation of the sampled points is based on the assumption that up to a constant, the rate of TET is proportional to the density of configuration of both PH_2 and O_2 which reach the same singlet-triplet energy gap, for a given temperature. Therefore, using the predicted population density determined in the surrounding of the vertical $T_1 \rightarrow S_0$ transition for the oxygen at (22.5 kcal/mol) it was possible to calculate the population overlap between PH_2 and O_2. It was found that the TET rate increase exponentially with temperature, as is predicted by assuming a Boltzmann distribution of the initial states of donor and acceptor and using the transition state theory.

Triplet Energy Transfer Reaction Coordinate Determined from Molecular Dynamics Simulations

Felipe Zapata[1], Raúl Palmeiro[1], Obis Castaño[1], Luis Manuel Frutos[1,a)]

[1]Physical Chemistry Unit, Universidad de Alcalá, 28871 Alcalá de Henares (Madrid), Spain.

Molecular dynamics simulations provide fundamental knowledge on the reaction mechanism of a given simulated molecular process. Nevertheless, other methodologies based on the "static" exploration of potential energy surfaces are usually employed to firmly provide the reaction coordinate directly related to the reaction mechanism, as is the case of *intrinsic reaction coordinates* for thermally activated reactions. Photoinduced processes in molecular systems can also be studied with these two strategies, as is the case of the triplet energy transfer process. Triplet energy transfer is a fundamental photophysical process in photochemistry and photobiology, being for instance a fundamental step in the generation or removal of the highly oxidant singlet oxygen from porphyrin and derivatives in two very different processes as is the case of photosynthesis and photodynamics therapy in the treatment of different kind of skin diseases. Here we study triplet energy transfer process between triplet porphyrin and triplet oxygen by means of nanoseconds time-scale molecular dynamics simulations, and the results obtained are compared to the "statical" determination of the reaction coordinate for such a process. The molecular distortions leading to an effective energy transfer are determined by both "statical" and dynamical methods. Moreover, the already existing definition of the triplet energy transfer reaction coordinate, which is based on an accurate description of the potential energy surfaces involved in the process, is compared to the dynamical results. A clear relation between both descriptions supports the possibility of defining from molecular dynamics simulation the reaction coordinate of the triplet energy transfer process.

a) Author to whom correspondence should be addressed. Electronic email: luisma.frutos@uah.es

I. INTRODUCTION

Molecular dynamics is a fundamental tool for shedding light on many processes ranging from biological to chemical systems. In spite of ignoring quantum effects, classical dynamics within Born-Oppenheimer approximation provides faithful results for many systems and conditions.[1,2] The reliability of the result of the classical dynamics depends on the accuracy of the potential for describing interactions among the particles of the system,[3,4] therefore is of central importance the use of accurate potential energy surfaces (PES), providing molecular forces which describe accurately the interactions in the molecular systems in an affordable computational time. There have been different approximations for determining forces in molecular dynamics; the first procedure consists in approximating molecular potential energy surfaces as a contribution of different interactions (usually bonding and non-bonding) obtained from experimental data of quantum-mechanical calculations, permitting the generation of force fields capable of reproducing many properties of the systems.[5,6] In these cases, there exists different force fields for different kind of systems, and usually they are limited to describe conformational changes rather than chemical processes. Among the existing force fields, it can be remarked AMBER for biological systems,[7] CHARMM for different chemical systems,[8] OPLS for liquid simulations,[9] and many others for a large variety of problems. On the other hand, a second approximation implies the calculation of the molecular forces in every step of the dynamics simulation (i.e. "on the fly" dynamics) by using some ab-initio or any other electronic structure method, avoiding any analytical or numerical representation of the PES and describing only local properties of the PES.[10,11] There is a third possibility, which is actually a set of algorithms, to obtain an approximated PES through a interpolation or fitting of a set of points calculated at high level of theory adjusted to minimize the error. The most outstanding interpolation methods are the reproducing Kernal Hilbert space,[12] the neural networks,[13] interpolating moving least squares [14] and the modified Shepard interpolation.[15]

The disadvantage of the first strategy, i.e. force fields, is that its accuracy is in most cases limited to a qualitative description of the simulated processes and also unable to describe chemical reactions or predict excited state properties,[1,16] meanwhile in the second strategy, i.e. on the fly molecular dynamics, the computational cost of molecular forces calculations using a high level of theory is unaffordable in many cases, especially for medium to large size systems and large time simulations (over nanosecond time-scale).[1] Moreover, in the case of the third strategy, the construction of a grid for the determination of PESs involves a very large

set of parameters which are usually limited to few coordinates in small molecular systems, Being the accuracy of the fitted PES constrained by the quality of the fitting procedure.[17] It is also relevant that usually molecular dynamics involving electronic excited states are performed using "on the fly" dynamics and no force fields are developed for this kind of processes.[11]

Nevertheless, an alternative to these methodologies, which has been followed in this work, is the construction of analytical PES. It is possible to construct these analytical functions by spanning the potential energy surface as an extrapolation from some key configurations like minima and the Frank-Condon (FC) points. The advantages of this methodology is the fast evaluation of the molecular forces for every structure in the dynamics (i.e. large simulation times) without losing accuracy in the force prediction as long as the expansion is correct in the configuration space covered by the dynamics simulation. This approximation can be especially useful for fast determination of electronic excited states force fields used in the determination of different molecular properties involving these kinds of states (e.g. simulation of absorption spectra). The simplest way to construct the analytical PES from local approximations (i.e. energy derivatives) is to use second-order energy derivatives expansion for all the electronic states under study. This kind of simple approach can be extremely useful when the molecular system presents a well-define minimum energy molecular structure in the electronic state of simulation (e.g. the ground state) and the excited states under study are well represented by up to second-order approach.

Many different photophysical processes involve several electronic states, and therefore capable of being studied by the above mentioned methodology. Among them, the energy transfer is a fundamental photophysical process involving usually two different electronic states of a donor and an acceptor molecule. Significantly, the triplet energy transfer between triplet porphyrin (^{3}Por) and triplet molecular oxygen $^3O_2$ ($X^3\Sigma^-_g$) to generate singlet oxygen is a model system for the study of the basic photoinduced processes taking place in the singlet oxygen generation in photodynamic therapy treatments.[18]

The general mechanism underlying the TET process involves a triplet donor (^{3}D) and a singlet (^{1}A) or triplet acceptor (^{3}A), that when reach close contact (significant electronic clouds overlap), can fulfill the energy transfer. The contact between both molecules permits interchanging their total spin momentum by an electron exchange mechanism, being the electronic spin multiplicity of the whole system (donor and acceptor) conserved, and making the process spin-allowed.[19,20] As has been discussed elsewhere the TET rate constant in condensed phase

depends mainly on three factors: the diffusion rate constant of donor and acceptor in the solvent, the efficient overlap of the electronic clouds of both molecules, and the triplet energy difference between donor (E_T^D) and acceptor (E_T^A) molecules.[21-25] Nevertheless TET can also take place as an intramolecular process where contact between donor and acceptor moieties of the molecule is mediated by spacers.[26,27]

The maximum TET efficiency is reached when the triplet energy of donor equals that of the acceptor (i.e. $E_T^D = E_T^A$). As the triplet energy difference, defined as $\Delta E_T = E_T^D - E_T^A$, becomes negative (i.e. the available triplet energy from the donor is lower that the triplet excitation energy of the acceptor), the rate constant of the process decays exponentially.[24] And its contribution is significant until ΔE_T is bigger than 3-4 kcal/mol. In the case of exothermic reactions, i.e. $E_T^D > E_T^A$, the rate constant of the energy transfer in condensed phase match the rate constant of encounter donor-acceptor and there is not experimental evidence of decreasing in quenching efficient as the reactions becomes more exothermic.[28] The modulation of the triplet energy of donor(acceptor) can be determined as a function of the activation energy (i.e. the thermal energy necessary to achieve a given variation of the triplet energy referred to the vertical transition) providing a reaction coordinate for the process.[29] This reaction coordinate provides the relation between activation energy and triplet energy for a given donor (acceptor) molecule.

For the chosen system, porphyrin/oxygen, the experimental values of the triplet energy are 36.4 kcal/mol for the porphyrin and 22.5 kcal/mol for the molecular oxygen where the transference is between the states $X^3\Sigma^-_g$ and $^1\Delta g$,[18,30] therefore the TET process is exothermic.

The TET process is the base for the photodynamic therapy (PDT), where a photosensitizer as porphyrin and its derivatives,[31] is administered to the patient in different ways, being the intravenous injection one of the most common, and when the substance has its maximum accumulation in the target tissue, the affected area is irradiated at wavelength around 600-800 nm populating the singlet excited state S_n of the photosensitizer, which after vibrational relaxing decayed to the S_1 state, that in turn can carry out an Intersystem crossing to the T_1 state. Finally the T_1 triplet state transfers the excitation energy to the $^3O_2$ molecule generating $^1O_2$ ($^1\Delta g$), specie that had been appointed to be the cytotoxic agent.[32,33]

At room temperature the molecular system has enough energy for populating areas of the phase space corresponding with the surroundings around the bottom of the potential well and as it has been appointed in a theoretical work,[21,22] for a given distance acceptor-donor the electronic energy difference between the state of the donor and state of the acceptor are modulated through the thermal

activation of some specific molecular coordinates of the reagents, leaving that both electronic energies become equal, allowing the process of energy transfer to take place. Therefore the developed methodology can help to establish through a dynamical approach, a correlation between the configuration changes in the geometry of the molecular oxygen and the porphyrin which favors or delays the TET process.

II. COMPUTATIONAL DETAILS

The minimum energy structures of porphyrin in the lowest singlet and triplet states where determined by using the hybrid functional B3LYP with a CC-pVDZ basis set. First and second derivatives of the energy in cartesian coordinates were determined for the optimized structures in both electronic states. All the calculations were performed with Gaussian09 software package.[34]

The complete molecular dynamics simulations within the microcanonical and canonical ensembles (see point 3.1 for details) were performed using our own code.[35]

The reaction coordinate has been obtained by using the algorithm and definition described elsewhere,[22,29] using analytical gradients determined with the electronic methods described above.

III. RESULTS AND DISCUSSIONS

TET involves two different states of a donor-acceptor complex, the state before the energy transfer [*D···A] and after the transfer [D···*A], where the asterisk denotes the excitation. It has been proposed elsewhere that TET process can be separated in terms of single transitions $^{*}D \rightarrow D$ and $A \rightarrow {}^{*}A$ in the very weak coupling limit,[22] as usually occurs in solution. Following this approach, in order determine the excitation transfer rate it is necessary to know the energy of each electronic transition and study whether the resonance condition (i.e. same electronic transition energy for both molecules) can be fulfilled. Even if the energy of the vertical transitions for $^{*}D \rightarrow D$ and $A \rightarrow {}^{*}A$ does not match; the resonance condition can be reached by thermal activation. Imposing that energy resonance is fulfilled following a minimum energy principle, the activation energy for a given pair of donor-acceptor can be determined.[22] On the other hand, for the study of the TET from a dynamical description of the system, it is necessary to use accurate force fields for both molecules in ground and excited states.

In the following we describe the procedure for setting up the force field for both molecules in the two possible electronic states. Then, the developed molecular dynamics methodology using analytical PES is described, and subsequently applied to the porphyrin/oxygen case. The obtained results from

molecular dynamics simulations are finally compared with those resulting from the study of the reaction coordinate, and the contribution of the internal degrees of freedom of donor and acceptor is examined and compared to the dynamics results.

A. Construction of Analytical Potential Energy Surfaces in Internal Coordinates

The description of the TET process implies the description of singlet and triplet potential energy surfaces for both molecules (donor and acceptor). In order to construct the potential energy surfaces of a molecule in a given state we have perform a quadratic expansion of the potential energy function in terms of internal coordinates:

$$E^{(n)}(\boldsymbol{q}) = E^{(n)}(\boldsymbol{q}_0) + (\boldsymbol{q}-\boldsymbol{q}_0)^t \cdot \boldsymbol{g}^{(n)}_{q_0} + \frac{1}{2}(\boldsymbol{q}-\boldsymbol{q}_0)^t \boldsymbol{H}^{(n)}_{q_0}(\boldsymbol{q}-\boldsymbol{q}_0) \quad (1)$$

where $\mathbf{q}$ is a vector in internal coordinates denoting any configuration (i.e. molecular structure), $\mathbf{q_0}$ is also a vector in internal coordinates corresponding to the reference configuration for the expansion. $\mathbf{g}^{(n)}_{q_0}$ and $\mathbf{H}^{(n)}_{q_0}$ are the energy gradient vector and hessian matrix of the (n) electronic state evaluated for the $\mathbf{q_0}$ geometry, both expressed in internal coordinates. From the approximate PES given in (1), the energy gradient vector obtained is

$$\nabla E^{(n)}(\boldsymbol{q}) = \boldsymbol{g}^{(n)}_{q_0} + \boldsymbol{H}^{(n)}_{q_0}(\boldsymbol{q}-\boldsymbol{q}_0)\,. \quad (2)$$

The election of internal instead of cartesian coordinates for deriving the force field has some advantages, since the curvilinear coordinate system, if correctly chosen, preserves more accurately the quadratic approximation, making the spanned PES more precise as the displacement vector $(\mathbf{q}-\mathbf{q_0})$ increases.[36]

Selecting a set of internal coordinates for the PES expansion with chemical meaning is necessary in order to predict accurately the energy of the extrapolated points. Since usually first and second derivatives are available in cartesian coordinates, it is necessary to transform the cartesian derivatives into internal derivatives. The relation between the derivatives of the energy with respect to internal and cartesian coordinates is described by the Wilson B matrix which elements $B_{ij} = \dfrac{\partial q_j}{\partial x_j}$, are given by the derivatives of the internal coordinates with respect to de cartesian coordinates. [37] Using this matrix the relation between the gradient are given by

$$\boldsymbol{B}^t_x \boldsymbol{g}^{(n)}_q = \boldsymbol{g}^{(n)}_x \quad (3)$$

and

$$\boldsymbol{g}^{(n)}_q = \boldsymbol{G}^{-1}\boldsymbol{B}_x \boldsymbol{g}^{(n)}_x \quad (4)$$

where $\mathbf{g}^{(n)}_X$ is the energy gradient vector in cartesian coordinates evaluated for an arbitrary $\mathbf{X}$ configuration, which is also expressed in cartesian coordinates. Since the $\mathbf{B}$ matrix is not square, its inversion requires to find the generalized inverse of a $\mathbf{G}$ matrix given by $\mathbf{G} = \mathbf{BUB}^t$ where $\mathbf{U}$ is a unitary matrix. In the case of using a set of redundant

internal coordinates, the inversion of the **G** matrix required a previous diagonalization follow by the elimination of the zero eigenvalues resulting from the redundant internal coordinates, keeping only those eigenvectors corresponding with the 3N-6 degrees of vibrational freedom.[38] The relation between the hessian matrices in both set of coordinates are obtained after differentiating (3) and (4)

$$\boldsymbol{B}_{\mathbf{x}_0}^{t}\boldsymbol{H}_{\mathbf{q}_0}^{(n)}\boldsymbol{B}_{\mathbf{x}_0}+\boldsymbol{B}_{\mathbf{x}_0}''^{t}\boldsymbol{g}_{\mathbf{q}_0}^{(n)}=\boldsymbol{H}_{\mathbf{x}_0}^{(n)} \qquad (5)$$

and

$$\boldsymbol{H}_{\mathbf{q}_0}^{(n)}=\boldsymbol{G}_{\mathbf{x}_0}^{-1}\boldsymbol{B}_{\mathbf{x}_0}\boldsymbol{U}(\boldsymbol{H}_{\mathbf{x}_0}^{(n)}-\boldsymbol{B}_{\mathbf{x}_0}''^{t}\boldsymbol{g}_{\mathbf{q}_0}^{(n)})\boldsymbol{U}^{t}\boldsymbol{B}_{\mathbf{x}_0}^{t}\boldsymbol{G}_{\mathbf{x}_0}^{-1} \quad (6)$$

Where $\mathbf{H}_{\mathbf{x}_0}^{(n)}$ is the Hessian matrix in cartesian coordinates evaluated for the $\mathbf{X_0}$ configuration, and **B'** is a three dimensional array whose elements $B'_{ijk}=\dfrac{\partial^2 q_i}{\partial x_j \partial x_k}$ are the second derivatives of the i^{th} internal coordinates with respect to the j^{th} and k^{th} cartesian coordinate.

In order to obtain the numerical values of the gradient and Hessian matrix in internal coordinates, it was obtained and implemented analytical expressions for the first and second derivatives of the internal coordinates with respect to cartesian coordinates (i.e. B_{ij} and B'_{ijk} terms).

B. Molecular Dynamics Methodology

The integration of the equations of motion has been done for the case of microcanonical ensemble using the velocity-Verlet algorithm as was describe by implemented using the two-steps procedure described elsewhere.[39] The first step advances the positions and semi advances the velocities and then the force is calculated using the new positions. Finally, in the second step the velocity is semi advanced with the calculated forces. Because of the potential of the system is an analytical function of the internal coordinates, in order to calculate the forces in each step of integration it is necessary the transformation of the gradient vector from internal to cartesian coordinates, using the relation given by (2) and (3). These two equations are the heart of the present methodology for the molecular dynamic simulations.

For the simulation of the molecular systems at constant temperature it was used the Nosé-Hoover chain thermostat and the equations resulting from the extended-Lagrangian method which generates non-Hamiltonian dynamics.[40] The equations of motion were integrated using a time reversible integrator, using the Liouville approach through the Trotter factorization. [41] As it has been shown, a chain of thermostats can drive the variables of the harmonic oscillator to a canonical distribution,[42] and since the potential developed in this work is given by a collection of harmonic oscillator, the Nosé-Hoover chain thermostat seems a sensible election for the system, for a more detail description of the thermostat lookup the supporting information.

Similarly to the constant energy simulation, the potential calculation use (2) and (3).

In order to achieve the desired temperature, the initial conditions for the constant energy simulations were obtained by scaling the velocity randomly and periodically, in such a way that the system increases its energy in small quantities followed by a relaxation period, until the system acquire the total required energy. On the other hand, the initial conditions for simulating the canonical ensemble are prepared getting random velocities of the Maxwell-Boltzmann distribution, assuming that every component of the velocity of each atom can be considered as an independent Gaussian random variable.[6] In order to avoid misinterpretation and numerical drifting in the temperature, the motion and rotation of the center of mass is removed at every step of integration in both ensembles.

The constant temperature dynamic simulations were carried out in the gas phase at 300K, 200K, 100K and 50K. The simulation time was 1.0 ns using an integration step of 0.1 fs.

The conservation of the total energy was checked for the simulations at constant energy while in constant temperature simulation it was check the variance in the temperature. The variation in the temperature for a simulation at constant temperature is greater than for constant energy simulations. This behavior is expected according to (8) and (9) that provide the variance of the temperature for microcanonical and canonical ensemble respectively, where N is the number of atoms and Cv is the constant-volume heat capacity. [3,43]

$$\sigma_T^2 = \frac{2 < T^2 >_{NVE}}{3N}(1 - \frac{3}{2C_v}) \qquad (7)$$

$$\sigma_T^2 = \frac{2 < T^2 >_{NVT}}{3N} \qquad (8)$$

Accordingly with the foregoing, a molecular system simulated at constant temperature can reach conformations that are out of range for a simulation at constant energy at the same temperature. It was also checked that the molecular velocities for the simulated trajectories, belong to the Maxwell-Boltzmann distribution.

C. Dynamics of the Triplet Porphyrin Sensitization of Triplet Oxygen

Using the methodology described above we have studied the dynamic behavior of porphyrin in the triplet (T_1) state and the evolution of the T_1-S_0 energy gap along the simulation.

Dynamics simulation provides among other information the probability distribution for the configuration space, permitting to identify the frequency (or probability density) of a given range of coordinate values in a given electronic state in a certain conditions (e.g. temperature). Different electronic properties depending also on the configuration of the system can be also determined

and expressed in terms of probability density. This is the case of the energy gap between two electronic states. For the study of TET, it is necessary to measure the T_1-S_0 energy gap of porphyrin along the trajectory, obtaining from a large simulation times a distribution function of the T_1-S_0 energy gap. This distribution can be directly related to the T_1-S_0 emission spectrum of porphyrin. For the T_1 minimum energy structure the energy of the T_1-S_0 transition is 31 kcal·mol^{-1}. This value corresponds with activation energy equal to zero, according with the definition given in Section 3.1. On the contrary, the S_0-T_1 energy gap for triplet equilibrium structure of molecular oxygen is 22.5 kcal·mol^{-1}. The distribution functions of the T_1-S_0 energy gap in porphyrin and S_0-T_1 for triplet oxygen obtained from molecular dynamics simulations provides the normalized spectra for both transitions. Normalized spectra permits to obtain by integration the spectral overlap, which is related to the triplet energy transfer rate constant through the Fermi golden rule.[44]

The probability distribution obtained in the simulations at constant energy is qualitatively equal to the constant temperature simulations, being the difference the energy storage in the normal modes due to smaller fluctuations of the kinetics energy in the constant energy simulations.

From a chemical point of view, there is not an easy way to predict how every internal coordinate can stabilize or destabilize both the triplet and the singlet ground state in order to modulate the triplet energy. But the simulation at constant temperature provide realistic geometries that besides the definition of the triplet energy transfer reaction coordinate, help on the identification of those coordinates having a greater statistical weight in the process of TET.

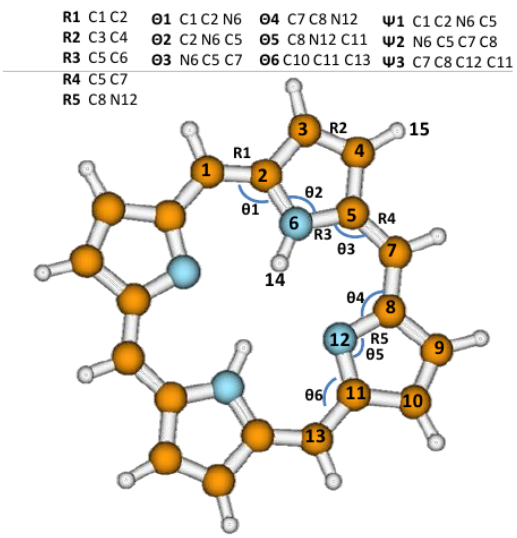

Figure 2. Internal coordinates for two of four pyrrolic rings that modulate more efficiently the TET process.

Therefore, there were calculated the values of geometrical distortion parameter γi for every internal redundant coordinate for every geometry obtained in each integration step, for simulations at constant energy and temperature. In Figure 2 are represented the internal coordinates that have the greatest influence in the TET process between porphyrin and oxygen, for constant temperature simulation at 300K.

Coordinate	γi (kcal/mol)	Coordinate	γi (kcal/mol)
R1	2.8	Θ3	10.9
R2	2.0	Θ4	10.6
R3	1.6	Θ5	3.6
R4	3.5	Θ6	5.3
R5	1.9	Ψ1	0.8
Θ1	4.2	Ψ2	2.0
Θ2	5.3	Ψ3	1.0

Table 1. Values for the individual geometrical distortion parameters of the most relevant internal coordinates of porphyrin.

In Table 1 are reported the values of γ_i for the set of internal coordinates shown in Figure 2 in the range of triplet energy between 23-38 kcal/mol. According of these values the contractions and expansions of the porphyrin cycle are the most import movements for changing the triplet energy and even though out of plane torsion are the most notorious geometrical distortions at room temperature, bonds and valence angle changes, have the greatest influence in the modulation of the triplet energy. This is due to the fact that dihedral force constants are in general smaller than those of bonds and valence angles, allowing the molecular amplitude of the vibrational modes that imply rotation being in a bigger scale than vibrational stretching and bending but small changes in bond distances and angles could account for a significant chance in the triplet energy.

a. **Triplet Energy Transfer reaction Coordinate for porphyrin/Oxygen system**

Singlet oxygen generation by triplet porphyrin takes place according to:

$$^3\text{Por} + {}^3\text{O}_2 \rightarrow {}^1\text{Por} + {}^1\text{O}_2$$

where both transitions $^3O_2 \leftarrow {}^1O_2$ and $^3\text{Por} \rightarrow {}^1\text{Por}$ are spin forbidden. Nevertheless, as has been discussed above the whole process involving both electronic transitions is spin allowed.[45] On the other hand, both transitions must fulfill the energy resonance condition, which ensures the balance between the transferred and the accepted energy. But the triplet energy of the $^1\text{Por} \leftarrow {}^3\text{Por}$ transition defined as vertical excitation from ^{3}Por relaxed structure (i.e. phosphorescence maximum) is ca. 31 kcal·mol^{-1}, being the $^3O_2 \leftarrow {}^1O_2$ transition is, following the same definition, ca. 22.5 kcal·mol^{-1},[30] which implies that some changes must take place on both molecules in order to reach the resonance condition.[29] In the case of weak coupling limit, Since the absolute value of the electronic coupling term is very low compared with other energies involved in the transfer step, the

PES of the complex Por…O_2 can be separated in two uncoupled PESs for the donor and acceptor partners,[22] and therefore the role of the internal coordinates of each molecule in reaching the energy resonance can be analyzed independently.

If the resonance condition is assumed to take place with minimum activation energy, the triplet energy transfer reaction coordinate can be determined as described elsewhere.[29] We have investigated $^3O_2 \leftarrow {}^1O_2$ and $^1Por \leftarrow {}^3Por$ transitions as well as the coordinates modulating the singlet-triplet energy gap in Por permitting the energy transfer.

In Figure 3, the variation of the $^3O_2 \leftarrow {}^1O_2$ and $^1Por \leftarrow {}^3Por$ transition energies are displayed as a function of the activation energies. The energy resonance condition for both transitions is fullfilled for a porphyrin structure where stretching modes and out-of-plane distortions contributes significantly in lowering $^1Por \leftarrow {}^3Por$ energy to equal the oxygen energy as shown in Figure 3. Triplet oxygen has a very small capacity of modulation of the singlet-triplet energy gap because of the single stretching mode of the molecule, therefore its triplet energy can be consider as constant.

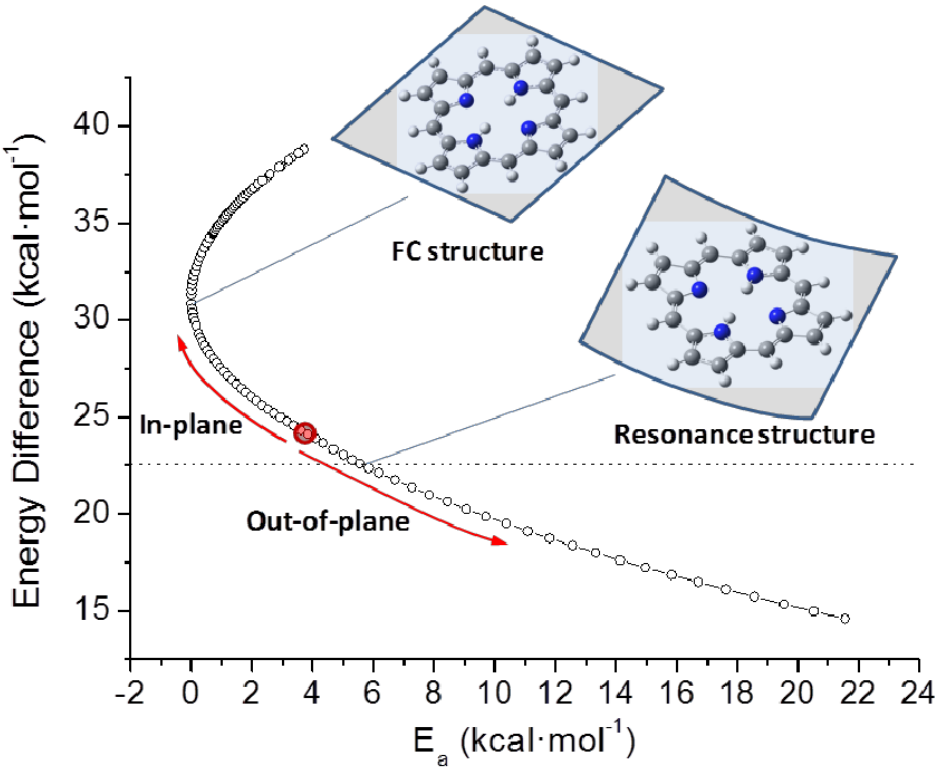

Figure 3. T_1-S_0 energy gap as a function of activation energy on T_1 obtained from the determination of the triplet energy transfer reaction coordinate for triplet porphyrin ($S_0 \leftarrow T_1$ transfer). Out of plane distortion is reached at. 24 kcal·mol^{-1}. The singlet oxygen energy ($a^1\Delta g \leftarrow X^3\Sigma g$- transition) at 22.5 kcal·mol-1 is also indicated with a dotted line. The porphyrin structure for the triplet excitation transfer is displayed.

Nevertheless, porphyrin shows a significant ability to modulate the ^{1}Por←^{3}Por energy gap by thermal activation with relatively small activation energies. In fact, in order to decrease the energy gap, the optimal molecular distortions corresponds to in-plane distortions (i.e. stretching modes) for the initial ca. 7 kcal·mol^{-1} (i.e. from energy gap from 31 to 24 kcal·mol^{-1}), while further reduction of this gap is efficiently reached by out-of-plane distortions (sheet bend like distortion, see Figure 3) which provides the optimal distortion in order to reach the ca. 22.5 kcal·mol^{-1} necessary to achieve the resonance with the singlet oxygen energy ($a^1\Delta g \leftarrow X^3\Sigma g^-$ transition).

b. Comparison of the reaction coordinate and dynamics simulations

Molecular dynamics of the triplet state porphyrin provides useful information for understanding the triplet energy transfer reaction coordinate. By analyzing the 10^6 points obtained from the different constant temperature simulations (T= 50K, 100K, 200K and 300K) a population density as a function of activation energy and triplet energy variation can be obtained (see Figure 4). It has to be noted that activation energy differs from the energy in the triplet state referred to the minimum, since the latter includes 3N-6 coordinates, while activation energy is referred to a single reaction coordinate. Therefore, in Figure 4 the potential energy corresponding to 3N-7 internal degrees of freedom has been subtracted in order to make the population density to correspond to the activation energy associated to a single coordinate. As can be seen from the population density results, the porphyrin tends to explore regions with larger variation of the triplet energy as the thermal energy increases (i.e. permitting the system to reach higher activation energies). In any case, the density distribution is always located in the region defined by the "static" definition of the reaction coordinate. In fact, it is possible to define the reaction coordinate from MD results by taking the lowest activation energy structure for a given interval of triplet energy. In this way it is possible to get a functional dependence of the activation energy on the initial state (T_1) with the triplet energy variation.

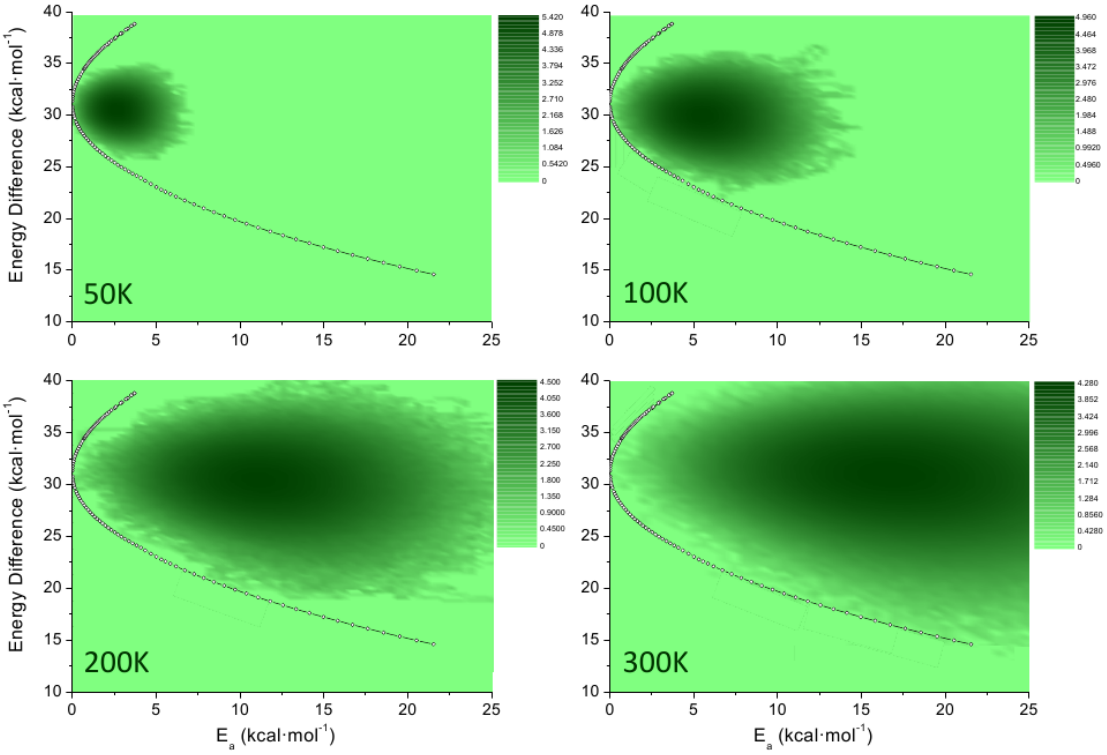

Figure 4. Porphyrin population density obtained from 1ns MD simulations at different temperatures (50K, 100K, 200K, and 300K) represented as a function of T_1-S_0 energy difference vs. T_1 vibrational energy (density populations are given in a logarithmic scale).

Moreover, from the MD results it is also possible to estimate the fraction of porphyrin molecules that along the time reach the resonance condition with the oxygen. This fraction, which is a function of the temperature, can be computed as the overlap between the oxygen density population for the triplet to singlet transition, and the corresponding triplet to singlet transition in porphyrin. By computing such a population overlaps it is found that energy transfer rate constant increases exponentially with temperature, as is predicted by assuming a Boltzmann distribution of the initial states of donor and acceptor and using the transition state theory.[21]

D. CONCLUSIONS

It was developed and implemented a methodology for building analytical PES in function of the first and second derivatives of the energy with respect to the internal coordinates. These analytical PES were used for molecular dynamics simulation at constant temperature for the simulation of the triplet energy transfer process between triplet porphyrin and triplet molecular oxygen. The obtained results indicate that the out of plane motion and in plane stretching are the coordinates enabling the process, being these coordinates the bonds and angles between the bridges and the pyrollic rings and the out of plane

distortion between the pyrrolic rings. This structural deformation permits the prophyrin to accommodate its triplet energy to that of molecular oxygen. The molecular dynamics simulations are in agreement with the reaction, where out of plane motion predicted is found in the dynamics simulations. Moreover, the triplet energy variation with the activation energy in the triplet state for porphyrin matches correctly with the predictions made on the basis of reaction coordinate determination. Consequently, the reaction coordinate can be determined via analysis of molecular dynamics simulations. The coordinates enabling the process are equally determined by both dynamics and reaction coordinate.

ACKNOWLEDGEMENT

This research has been supported by the projects CTQ2009-07120 and CTQ2012-36966 of the Spanish MICINN, and CCG2013EXP-089 of UAH/CAM. F. Z. acknowledges the Spanish Ministry of Science and Innovation for the doctoral fellowship.

REFERENCES

1 H. J. C. Berendsen, in *Computational Molecular Dynamics: Challenges, Methods, Ideas*, edited by P. Deuflhard *et al.* (Springer, Berlin, 1998).

2 M. E. Tuckerman, and G. J. Martyna, J. Phys. Chem. B **104**, 159 (2000).

3 D. Frenkel, and B. smit, *Understanding Molecular Simulation* (Academic Press, San Diego, 2002), second edn., Vol. 1, Computational Science Series.

4 M. Griebel, S. Knapek, and G. Zumbusch, *Numerical Simulation in Molecular Dynamics* (Springer, Germany, 2007), Vol. 5, Texts in Computational Science and Engineering.

5 P.-O. Norrby, and P. Brandt, Coord. Chem. Rev. **212**, 79 (2001).

6 M. J. Field, *A Practical Introduction to the Simulation of Molecular Systems* (Cambridge University Press, New York, 2007).

7 D. A. Case, T. A. Darden, I. T. E. Cheatham, C. L. Simmerling *et al.*, (University of California, San Francisco, 2006).

8 B. R. Brooks, C. L. Brooks III, A. D. Mackerell, L. Nilsson *et al.*, J. Comput. Chem. **30**, 1545 (2009).

9 G. A. Kaminski, R. A. Friesner, J. Tirado-Rives, and W. L. Jorgensen, J. Phys. Chem. B **105**, 6474 (2001).

10 J. M. Bowman, B. J. Braams, S. Carter, C. Chen *et al.*, Journal of Physical Chemistry Letters **1**, 1866 (2010).

11 D. Marx, and J. Hutter, *Ab Initio Molecular Dynamics: Basis Theory and Advanced Methods* (Cambridge University Press, New York, United States of America, 2009).

12 T. Ho, and H. Rabitz, J. Chem. Phys. **104**, 2584 (1996).

13 J. B. Witkoskie, and D. J. Doren, Journal of Chemical Theory and Computation **1**, 14 (2005).

14 G. G. Maisuradze, D. L. Thompson, A. F. Wagner, and M. Minkoff, The Journal of Chemical Physics **119**, 10002 (2003).

15 J. Ischtwan, and M. A. Collins, The Journal of Chemical Physics **100**, 8080 (1994).

16 T. E. Cheatham, and M. A. Young, Biopolymers **56**, 232 (2000).

17 J. Espinosa-Garcia, M. Monge-Palacios, and J. C. Corchado, Advances in Physical Chemistry **2012**, 19 (2012).

18 M. C. DeRosa, and R. J. Crutchley, Coord. Chem. Rev. **233-234**, 351 (2002).

19 A. Monguzzi, J. Mezyk, F. Scotognella, R. Tubino *et al.*, Physical Review B **78**, 195112(1) (2008).

20 S. Reineke, F. Lindner, G. Schwartz, N. Seidler *et al.*, Nature **459**, 234 (2009).

21 L. M. Frutos, O. Castano, J. L. Andrés, M. Merchán *et al.*, J. Chem. Phys. **120**, 1208 (2004).

22 L. M. Frutos, and O. Castano, J. Chem. Phys. **123**, 104108 (2005).

23 J. Saltiel, and B. W. Atwater, in *Advances in Photochemistry* (John Wiley & Sons, Inc., 2007), pp. 1.

24 K. Sandros, Acta Chem. Scand. **27**, 3015 (1973).

25 A. A. Lamola, and N. J. Turro, in *Technique of Organic Chemistry* (Wiley, New York, 1969).

26 L. M. Frutos, U. Sancho, and O. Castaño, Org. Lett. **6**, 1229 (2004).

27 L. M. Frutos, U. Sancho, and O. Castano, J. Phys. Chem. A **109**, 2993 (2005).

28 N. J. Turro, *Modern Molecular Photochemistry* (University Science Books, Sausalito, California, 1991).

29 F. Zapata, M. Marazzi, O. Castaño, A. U. Acuña *et al.*, The Journal of Chemical Physics **140**2014).

30 M. Gouterman, and G.-E. Khalil, J. Mol. Spectrosc. **53**, 88 (1974).

31 N. Brasseur, in *Photodynamics Therapy*, edited by D.-P. Häder, and G. Jori (Royal Society of Chemistry, Cambridge, UK, 2003).

32 M. Ethirajan, Y. Chen, P. Joshi, and R. K. Pandey, Chem. Soc. Rev. **40**, 340 (2011).

33 R. W. Redmond, and I. E. Kochevar, Photochem. Photobiol. **82**, 1178 (2006).

34 M. J. Frisch, G. W. Trucks, H. B. Schlegel, G. E. Scuseria *et al.*, (Gaussian, Inc., Wallingford CT, 2009).

35 B. O'Sullivan, J. Goerzen, and D. B. Stewart, *Real World Haskell* (O'Reilly Media, 2008).

36 V. Bakken, and T. Helgaker, The Journal of Chemical Physics **117**, 9160 (2002).

37 E. B. J. Wilson, *Molecular Vibrations: The Theory of Infrared and Raman Vibrational Spetra* (McGraw-Hill, New York, 1955).

38 C. Peng, P. Y. Ayala, H. B. Schlegel, and M. J. Frisch, J. Comput. Chem. **17**, 49 (1996).

39 W. C. Swope, H. C. Andersen, P. H. Berens, and K. R. Wilson, The Journal of Chemical Physics **76**, 637 (1982).

40 M. E. Tuckerman, Y. Liu, G. Ciccotti, and G. J. Martyna, The Journal of Chemical Physics **115**, 1678 (2001).

41 G. J. Martyna, M. E. Tuckerman, D. J. Tobias, and M. L. Klein, Mol. Phys. **87**, 1117 (1996).

42 G. J. Martyna, M. L. Klein, and M. Tuckerman, The Journal of Chemical Physics **97**, 2635 (1992).

43 J. L. Lebowitz, J. K. Percus, and L. Verlet, Physical Review **153**, 250 (1967).

44 C. Serpa, L. G. Arnaut, S. J. Formosinho, and K. R. Naqvi, Photochemical & Photobiological Sciences **2**, 616 (2003).

45 C. Peng, P. Y. Ayala, H. B. Schlegel, and M. Frisch, J. Comput. Chem. **17**, 49 (1996).

4.3 Chapter Bibliography

Brasseur, N., Sensitizers for PDT: phthalocyanines. In *Photodynamics Therapy*, Häder, D.-P.; Jori, G., Eds. Royal Society of Chemistry: Cambridge, UK, 2003.

Brennan, C. M.; Caldwell, R. A.; Elbert, J. E.; Unett, D. J., Nonvertical Triplet Excitation Transfer to Arylalkene Acceptors: Further Evidence That Double Bond Torsion Is Unimportant. *J. Am. Chem. Soc.* **1994,** *116*, 3460-3464.

Caldwell, R. A.; Riley, S. J.; Gorman, A. A.; McNeeney, S. P.; Unett, D. J., Relaxed triplet energies of phenylnorbornenes. The role of phenyl-vinyl torsions. Origin of nonvertical triplet excitation transfer. *J. Am. Chem. Soc.* **1992,** *114*, 4424-4426.

Catalán, J.; Saltiel, J., On the Origin of Nonvertical Triplet Excitation Transfer: The Relative Role of Double-Bond and Phenyl-Vinyl Torsions in the Stilbenes. *The Journal of Physical Chemistry A* **2001,** *105*, 6273-6276.

Dexter, D. L., A Theory of Sensitized Luminescence in Solids. *The Journal of Chemical Physics* **1953,** *21*, 836-850.

Ethirajan, M.; Chen, Y.; Joshi, P.; Pandey, R. K., The role of porphyrin chemistry in tumor imaging and photodynamic therapy. *Chem. Soc. Rev.* **2011,** *40*, 340-362.

Frutos, L. M.; Castano, O., A new algorithm for predicting triplet-triplet energy-transfer activated complex coordinate in terms of accurate potential-energy surfaces *J. Chem. Phys.* **2005,** *123*, 104108-104111.

Gouterman, M.; Khalil, G.-E., Porphyrin free base phosphorescence. *J. Mol. Spectrosc.* **1974,** *53*, 88-100.

Lalevee, J.; Allonas, X.; Fouassier, J. P., Triplet–triplet energy transfer reaction to cis-stilbene: a dual thermal bond activation mechanism. *Chem. Phys. Lett.* **2005,** *401*, 483-486.

Langhals, H.; Esterbauer, A. J.; Walter, A.; Riedle, E.; Pugliesi, I., Foerster Resonant Energy Transfer in Orthogonally Arranged Chromophores. *J. Am. Chem. Soc.* **2010,** *132*, 16777-16782.

Marcus, R. A., Chemical and Electrochemical Electron-Transfer Theory. *Annu. Rev. Phys. Chem.* **1964,** *15*, 155-196.

Monguzzi, A.; Mezyk, J.; Scotognella, F.; Tubino, R.; Meinardi, F., Upconversion-induced fluorescence in multicomponent systems: Steady-state excitation power threshold. *Physical Review B* **2008,** *78*, 195112(1)– 195112(5).

Muñoz-Losa, A.; Curutchet, C.; Krueger, B. P.; Hartsell, L. R.; Mennucci, B., Fretting about FRET: failure of the ideal dipole approximation." Biophys. J. 96: 8. *Biophys. J.* **2009,** *96*, 4779-4788.

Ramamurthy, V.; Liu, R. S. H., Photochemistry of polyenes. IX. Excitation, relaxation, and deactivation of dienes, trienes, and higher polyenes in the vitamin A series in the sensitized isomerization reaction. *J. Am. Chem. Soc.* **1976,** *98*, 2935-2942.

Redmond, R. W.; Kochevar, I. E., Symposium-in-Print: Singlet Oxygen Invited Review. *Photochem. Photobiol.* **2006,** *82*, 1178-1186.

Reineke, S.; Lindner, F.; Schwartz, G.; Seidler, N.; Walzer, K.; Luessem, B.; Leo, K., White organic light-emitting diodes with fluorescent tube efficiency. *Nature* **2009,** *459*, 234-238.

Saltiel, J.; Hammond, G. S., Mechanisms of Photochemical Reactions in Solution. XVII. cis-trans Isomerization of the Stilbenes by Excitation Transfer from Low Energy Sensitizers. *J. Am. Chem. Soc.* **1963,** *85*, 2515-2516.

Saltiel, J.; Mace, J. E.; Watkins, L. P.; Gormin, D. A.; Clark, R. J.; Dmitrenko, O., Biindanylidenes: Role of Central Bond Torsion in Nonvertical Triplet Excitation Transfer to the Stilbenes. *J. Am. Chem. Soc.* **2003,** *125*, 16158-16159.

Saltiel, J.; Marchand, G. R.; Kirkor-Kaminska, E.; Smothers, W. K.; Mueller, W. B.; Charlton, J. L., Nonvertical triplet excitation transfer to cis- and trans-stilbene. *J. Am. Chem. Soc.* **1984,** *106*, 3144-3151.

Serpa, C.; Arnaut, L. G.; Formosinho, S. J.; Naqvi, K. R., Calculation of triplet-triplet energy transfer rates from emission and absorption spectra. The quenching of hemicarcerated triplet biacetyl by aromatic hydrocarbons. *Photochemical & Photobiological Sciences* **2003,** *2*, 616-623.

Speiser, S., Photophysics and Mechanisms of Intramolecular Electronic Energy Transfer in Bichromophoric Molecular Systems: Solution and Supersonic Jet Studies. *Chem. Rev.* **1996,** *96*, 1953-1976.

You, Z.-Q.; Hsu, C.-P., The fragment spin difference scheme for triplet-triplet energy transfer coupling. *The Journal of Chemical Physics* **2010,** *133*, 074105.

Zapata, F.; Marazzi, M.; Castaño, O.; Acuña, A. U.; Frutos, L. M., Definition and determination of the triplet-triplet energy transfer reaction coordinate. *The Journal of Chemical Physics* **2014,** *140*, -.

Chapter 5: Mechanism and Dynamics on Photoinduced Processes in Biological Systems

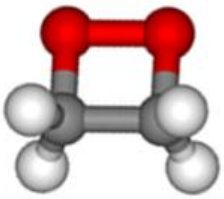

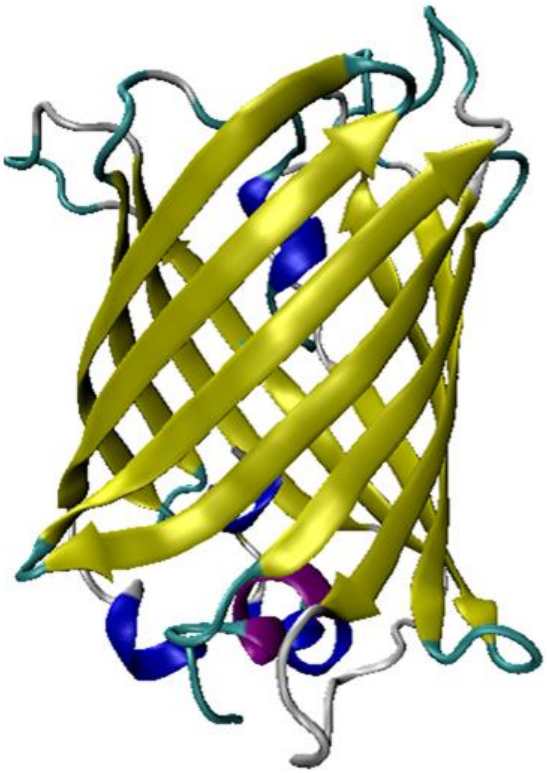

"Because today we live in a society in which spurious realities are manufactured by the media, by governments, by big corporations, by religious groups, political groups... So I ask, in my writing, What is real? Because unceasingly we are bombarded with pseudo-realities manufactured by very sophisticated people using very sophisticated electronic mechanisms. I do not distrust their motives; I distrust their power. They have a lot of it. And it is an astonishing power: that of creating whole universes, universes of the mind. I ought to know. I do the same thing."

Philip K. Dick

5.1 Introduction

In this section we have approach two phenomena directly linked with biological related application: chemiluminescence and fluorescent proteins. Both of which offer many technological application, beside their great academic interest.

5.1.1 Chemiluminescence

Chemiluminescence refers to the phenomenon of light emission by an excited product resulting from a chemical reaction. When the same phenomenon is produced in living beings is called bioluminescence. The exoergic reaction induces the promotion of an electron from its ground state to an excited electronic state, usually through a transition from a p bonding to a p* anti-bonding orbital (p→p*) or from a non-bonding to an anti-bonding orbital (n→p*) in organic molecules. Both chemiluminescence and bioluminescence phenomena, have attracted considerable attention not only because its role in nature (Fraga 2008, Zimmer 2009) as well as theoretical interest(Carpenter 2006), but also because is application in analytical chemistry (Lippert, et al. 2011, Paley and Prescher 2014, Razgulin, et al. 2011).

In general quantum efficiencies are greater in case of bioluminescence than chemiluminescence in solution. The high quantum yield and the presence of oxygen has suggested that that the family 1,2-dioxetanes are key intermediates for the highly efficient bioluminescent phenomena in nature (Matsumoto 2004).

In order to account for several unanswered experimental question about bioluminescence, in section 5.2.1, we have focused on the study of a molecular model using the multi-reference perturbation theory CASPT2 and CASSCF “on the fly” molecular dynamics, to give a deeper insight in such phenomena.

5.1.2 Modulation of Excited-State Properties of Fluorescent Proteins

In the past years, fluorescent proteins (FPs) derived from the green fluorescent protein (GFP) family were successfully applied as biological markers, allowing the visualization of a wide type of processes, ranging from gene expression to cell development and protein movements within live cells (Konstantin, et al. 2005, Shaner, et al. 2007, Wiedenmann and Nienhaus 2006). Moreover, other technological areas as

optical microscopy and photonics took advantage of the particular characteristics offered by FPs, leading to the development of optical nanoscopy (Betzig, et al. 2006, Hess, et al. 2006) and promising advances in data-storage devices (Sauer 2005).

These achievements were possible because of the high spatial and time resolution offered by FPs, which multiple variants can emit different colors and intensities, depending on the wavelength required for irradiation. Indeed, starting from the original green fluorescence, blue (higher energy) and red (lower energy) shifted emission FPs are nowadays available (Kredel, et al. 2008, Merzlyak, et al. 2007, Shaner, et al. 2004)

Experimental studies are pointing towards genetic engineering (through site-directed mutagenesis) and structural characterization (through spectroscopic and X-ray crystallographic techniques), which are powerful tools to investigate systematically the effect of amino acid replacement on the stability of the protein itself and on the absorption and emission energy shifts, compared to their predecessor FPs. Nevertheless, most of the attempts revealed the difficulty of guessing which specific mutation can lead to a certain change in biophysical properties, being the chromophore pocket highly sensitive to the chemical environment (hydrogen bonding, proton transfer, π-π stacking). In some cases a single amino acid replacement is enough to observe the expected spectroscopic variation, as the introduction of the Asn143Ser substitution into d2eqFP611 to generate d2RFP630, and the additional Ser158Cys mutation to generate RFP639, involving the weakening of hydrogen bonding interactions between side chains and the chromophore (Nienhaus, et al. 2008). In other cases amino acids replacements lead to unexpected nearly complete loss of fluorescence, which could be recovered after completion of several rounds of random mutagenesis and multi-site directed mutagenesis, as is the case of mRuby which required altogether 28 amino acid replacements, compared to wild-type eqFP611 (Kredel, et al. 2009).

On the other hand, theoretical and computational studies were performed to elucidate the underlying mechanisms suggested or indicated by experiments, by which we can currently divide FPs in three groups:

a) Reversibly photoswitchable FPs, characterized by a fluorescent on state and a non-fluorescent off state, connected by cis-trans photoisomerization (Ando, et al. 2004);

b) Irreversibly photoconvertible FPs, leading to transformation from a non-fluorescent state to a fluorescent state (Patterson and Lippincott-Schwartz 2002), or between differently emitting states, involving extension of the conjugate π system by rupture of a covalent bond (Tsutsui, et al. 2005);

c) FPs showing both irreversible photoconversion and reversible photoswitching of the two photoconvertible states, resulting in a four-states FP (Fuchs, et al. 2010).

Computational studies are focusing on understanding how photoinduced isomerization and protonation are coupled, being the first ultrafast steps which the chromophore undergoes. This constitutes a topic still under debate, also considering the variety of possible chromophores, post-translationally formed by autocatalytic cyclization and oxidation. As an example, we should mention the results obtained on asFP595 (a prototype for photoswitchable proteins) by quantum mechanics-coupled-molecular mechanics (QM/MM) techniques, by which different processes were suggested or validated (Schäfer, et al. 2007).

Nevertheless, the task to obtain a FP variant absorbing in the red region (630-750 nm) remains difficult, being currently far-red PSmOrange-like the only monomeric form with a near-red excitation wavelength (636) (Subach, et al. 2011). Moreover, the excitation maximum of most of the other available FPs is set in the range 400-588 nm (Kredel, et al. 2009), therefore requiring costly lasers to be used for photoactivation, while above 640 nm a common laser pointer could be employed, determining important budget reduction, always desired especially for technological applications. Nevertheless a rational design of the fluorescence properties of FPs was still not attempted.

Therefore in section 5.2.2, we present our first approach to the study of the relation between environment and spectroscopical properties trough the QM/MM methodology.

5.2 Results

5.2.1 Revisiting the Non-Adiabatic process in 1,2-dioexetane

There has been much discussion regarding the mechanism of decomposition of the 1,2-dioxetanes (De Vico, et al. 2007), being three the mechanism proposed: the biradical, concerted and merged mechanism. The biradical mechanism is characterized by the initial formation of a biradical after the O-O bonds cleavage through a transition state, follows by breaking of the C-C bond, which bring the system to the excited stated responsible for the light emission. On the other hand the merged mechanism implies the starting of the cleavage of the C-C bond, before the O-O bond is completed broken. Finally the concerted mechanism, involves the simultaneous cleave of both C-C and O-O bonds.

Even though there is experimental and theoretical evidence which support the biradical mechanism, there is not an agreement about the nature of the mechanism. Besides, some other facts as the large ratio phosphorescence/fluorescence of the chemiluminescence emission are still unanswered. In this section we presented a work which provides further inside into the biradical mechanism of the decomposition of the 1,2-dioxetane, and simultaneously address the phosphorescence/fluorescence ratio problem. The methodology employed to explore the aforementioned problematic, was multistate multiconfigurational reference second-order perturbation theory (MS-CASPT2) calculations and "on the fly" molecular dynamics.

It was previously reported that a entropic trap region plays a crucial role in the dynamics of the decomposition of the 1,2-dioxdetane (De Vico, et al. 2007). The entropic trap is the situation when the entire four singlet and four triplet states manifold becomes degenerate, when the molecule is in the vicinity of the transition state corresponding to the O-O bond rupture. This situation becomes more complicated because in order to properly describe the interaction between the states is important to introduce the spin coupling of the two radical electrons. A First dynamical approach to this entropic trap is to consider only the singlet states and carrying out molecular dynamics without taking into account the spin coupling.

Of special interest in this thesis is the used of the so called "on the fly" molecular dynamics using CASSCF/ANO-RCC-VDZP theory Level. The idea is to provide a

statistical relevant sampling which account for time spent in the entropic trap by the molecule on the ground state. On the other hand, because the phosphorescence process requires a population transfer from the ground state S_0 to the triplet state T_1, a preliminary dynamics can describes the kind of geometrical configurations available for a future intersystem crossing study.

The dynamic simulation where carried out begging from the transition state of the O-O breaking. It was then run 300 trajectories, using initial velocities taken from a Maxwell-Boltzmann distribution as explained in section 2.1.4. These trajectories provide an exponential decay model for the time spent in the entropic trap, with a half-time of 613fs.

JCTC Journal of Chemical Theory and Computation
Article
pubs.acs.org/JCTC

Revisiting the Nonadiabatic Process in 1,2-Dioxetane

Pooria Farahani,[†] Daniel Roca-Sanjuán,*[,‡] Felipe Zapata,[§] and Roland Lindh*[,†]

[†]Department of Chemistry, Ångström, Uppsala University, P.O. Box 518, SE-751 20 Uppsala, Sweden
[‡]Instituto de Ciencia Molecular, Universitat de València, P.O. Box 22085, ES-46071 València, Spain
[§]Departamento de Quimica Fisica, Universidad de Alcalá, E-28871, Alcalá de Henares, Madrid, Spain

Supporting Information

ABSTRACT: Determining the ground and excited-state decomposition mechanisms of 1,2-dioxetane is essential to understand the chemiluminescence and bioluminescence phenomena. Several experimental and theoretical studies has been performed in the past without reaching a converged description. The reason is in part associated with the complex nonadiabatic process taking place along the reaction. The present study is an extension of a previous work (De Vico, L.; Liu, Y.-J.; Krogh, J. W.; Lindh, R. *J. Phys. Chem. A* **2007**, *111*, 8013−8019) in which a two-step mechanism was established for the chemiluminescence involving asynchronous O−O′ and C−C′ bond dissociations. New high-level multistate multi configurational reference second-order perturbation theory calculations and *ab initio* molecular dynamics simulations at constant temperature are performed in the present study, which provide further details on the mechanisms and allow to rationalize further experimental observations. In particular, the new results explain the high ratio of triplet to singlet dissociation products.

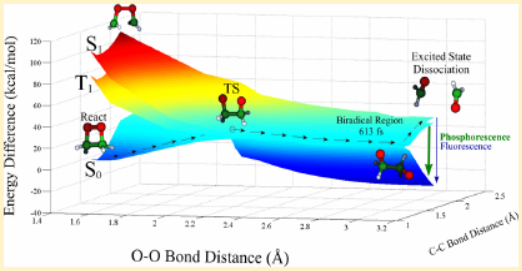

1. INTRODUCTION

The phenomenon that a chemical reaction generates a light emitting product is called chemiluminescence, the same phenomenon observed in living organisms is referred to as bioluminescence. The phenomenon is used as a practical tool in medicine and chemistry. This is easily seen in the large amount of biotechnological applications, for example, as a research tool in genetic engineering with the use of reporter genes,[1] or as a noninvasive study of biochemical processes in living small laboratory animals through bioluminescence imaging.[2] Nature provides us with plenty of examples of such phenomena, of which the firefly beetle is the most well-known. The bioluminescence is in principle a catalyzed version of chemiluminescence involving a substrate, luciferin, and an enzyme, luciferase, which will catalyze the chemical reaction. Oxidation of luciferins, yields a peroxy compound, called 1,2-dioxetane. This four-membered ring peroxide has been shown to be a common functional group in chemi- and bioluminescent systems. Accordingly, the thermal decomposition of isolated 1,2-dioxetane is the most simple example of the chemi- and bioluminescence reaction. A detailed description of the process in this system at the molecular level is key to an unified understanding of the chemistry of bioluminescence. During the last 20 years, significant theoretical and experimental efforts have been performed to understand the mechanism of the thermally activated chemi- and bioluminescence. According to these efforts, three different mechanisms have been proposed for the thermal dissociation of 1,2-dioxetane; the biradical, concerted, and merged mechanisms (see Figure 1). The biradical mechanism is a two-step reaction in which the C−C′ bond breaking occurs after the complete breakage of the O−O′ bond—the intermediate product has a biradical character. The concerted reaction is a single-step process in which the O−O′ and C−C′ bond breakage occur simultaneously. Finally, the merged mechanism implies that the C−C′ cleavage starts before the O−O′ bond breaking is fully completed. It is also well-known that three channels compete in the decomposition of 1,2-dioxetane giving rise to two formaldehyde fragments (see Figure 1). A small fraction of the formaldehyde molecules is generated in an excited state, from which the system returns to the ground state by emitting light. Both singlet and triplet paths are possible, thus producing fluorescence and phosphorescence emission, respectively. The remaining fraction of formaldehyde products is formed without emission of radiation.

Luminescence in thermal decomposition of 1,2-dioxetane systems, in particular, 3,3,4-trimethyl-1,2-dioxetane, was early (in 1968) observed by Kopecky and Mumford.[3] In this study, an emission of light associated with an activation energy of 25 kcal/mol was interpreted to be due to a singlet excited state in a concerted reaction. Next, in 1970, O'Neal and Richardson[4] hypothesized that 1,2-dioxetane decomposition should proceed similarly to analogous saturated four-membered ring systems, such as cyclobutane, whose thermochemical data clearly showed a two-step biradical mechanism. The authors demonstrated that the observed experimental kinetic data and

Received: September 3, 2013

dx.doi.org/10.1021/ct4007844 | J. Chem. Theory Comput. XXXX, XXX, XXX−XXX

Journal of Chemical Theory and Computation Article

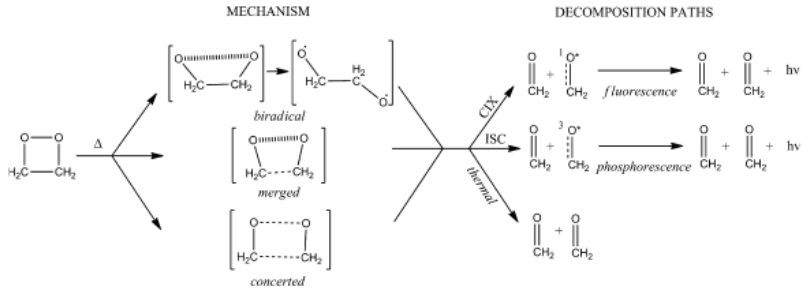

Figure 1. Mechanisms proposed in the literature and dissociation channels for the chemiluminescent reaction of 1,2-dioxetane.

the thermochemical calculations were consistent with such a mechanism.[4] A series of works appeared later introducing and giving support to the merged (or asynchronous concerted) mechanism on the basis of the highly efficient chemiexcitation found in methyl-substituted 1,2-dioxetanes, arguing that a biradical mechanism would result in the formation of basically only ground state products.[5,6] Adam and Baader[6] also reported in some of these studies that the thermal dissociation and chemiluminescence have the same activation energy and that phosphorescence in 1,2-dioxetane is favorable over fluorescence by a factor of 1000. In the 1990s, Olivucci, Robb, and co-workers[7,8] performed *ab initio* theoretical studies employing the complete active space self-consistent field (CASSCF) method with Möller−Plesset second-order perturbation theory (MP2) corrections to explore the potential energy surfaces (PESs) of the ground state and lowest-lying triplet excited state. The authors characterized the singlet−triplet crossing (ISC) regions that mediate the chemiexcitation process. A biradical region was also determined in the triplet energy surface between the transition states (TSs) related to O−O′ and C−C′ bond cleavage. These TS structures were found at similar energies, therefore supporting previous experimental findings from Adam and Baader[6] and other measurements for tetramethyldioxetane[9] and *cis*-diethoxy-1,2-dioxetane.[10] Nevertheless, Wilsey et al.[8] computed a value of 16 kcal/mol for the activation energy for the ring-opening of 1,2-dioxetane, which was clearly lower than the experimental observed value (22 kcal/mol).[6] In 2007, De Vico et al.[11] employed a higher level of theory using the multistate complete active space second-order perturbation theory (MS-CASPT2) method to study the dissociation process, finding a more accurate value for the activation energy of the thermal dissociation in agreement with the experiment.[6] De Vico et al. also studied the lowest-lying triplet excited states and considered in addition the lowest-lying singlet excited state which give rise to fluorescence. Conical intersections (CIX) and singlet−triplet ISC crossings were identified, and an entropic trapping of biradical character was obtained similarly to Wilsey et al.[8] The activation barriers for the O−O′ cleavage were obtained, however, at higher energies with respect to those related to the C−C′ bond breaking on the singlet and triplet excited states. Most recently, a direct dynamics simulation of the dissociation at the unrestricted density functional theory level of approximation has been carried out by Sun et al.[12] who have found on the ground state that some trajectories proceeded with an almost simultaneous O−O′ and C−C′ bond dissociations after the formation of 1,2-dioxetane.[12] They also found that the kinetics showed a strong non-RRKM behavior. To conclude, experimental and theoretical investigations are not conclusive with respect to the nature of the reaction mechanism, although there are evidence in support of biradical characteristics. While theory and experiment finally agree on the activation energy of the ground state dissociation process, details on the ratio of the phosphorescence and fluorescence emissions and the activation energy of the chemiluminescence are not correctly taken into account.

The aim of the present study is to clarify the qualitative concept and complete our previous quantitative study with additional results, which allow us to rationalize most of the experimental observations. In particular, we put some efforts in understanding the large ratio phosphorescence/fluorescence of the chemiluminescence emission, which was not explained on the basis of the results obtained from the previous study.[11] Electronic structure calculations using the CASSCF and MS-CASPT2 methods have been carried out in association with *ab initio* molecular dynamics (AIMD) at constant temperature (the canonical ensemble). The present study is subsequently structured as follows, a section with the computational details with regard to the electronic structure and *ab initio* molecular dynamics simulations, a section of presentation and discussion of the results, and finally some conclusions.

2. COMPUTATIONAL DETAILS

Details about the electronic structure and the AIMD computations are given below.

2.1. Electronic Structure. The CASSCF[13,14] and CASPT2[15−17] methods were employed for the geometry optimizations of the stationary points in conjunction with the atomic natural orbital (ANO-RCC)[18] basis set contracted to O,C[4s3p2d1f]/H[3s2p1d] (hereafter ANO-RCC-VTZP). Additional CASPT2 energy computations were performed at the CASSCF and CASPT2 geometries improving the basis set from triple-ζ to quadruple-ζ quality, in particular, using the ANO-RCC[18] basis set contracted to O,C[5s4p3d2f1g]/H[4s3p2d1f] (hereafter ANO-RCC-VQZP). The same active space as the one employed in the previous study was used, that is, 12 electrons distributed in 10 orbitals.[11] It corresponds to the C−C′, C−O, C′−O′, and O−O′ σ bonding and σ^* antibonding orbitals plus the two oxygen lone-pair orbitals (n_O). To account for all the degenerate combinations of the electrons in the oxygen (n_O) orbitals in the biradical region of the chemiluminescence mechanism (see Figure 2), four equally weighted roots were employed in the state averaged (SA) CASSCF procedure for all the CASSCF computations. Energies of the lowest-lying four singlet (S_0, S_1, S_2, and S_3) and four triplet (T_1, T_2, T_3, and T_4) states were calculated. Zero-point vibrational energy (ZPVE) corrections were computed numerically at the SA(4)-CASSCF/ANO-RCC-VQZP level through the second-order derivatives of the energy using the harmonic

dx.doi.org/10.1021/ct4007844 | J. Chem. Theory Comput. XXXX, XXX, XXX−XXX

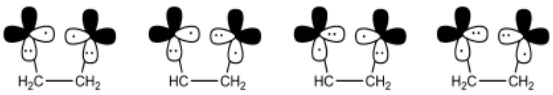

Figure 2. Electron occupation of the oxygen lone-pair orbitals at the biradical region of the chemiluminescence and thermal mechanisms of 1,2-dioxetane.

approximation. The multistate (MS) approach[19] of the CASPT2 method was used throughout to keep the consistency with the previous work.[11] Unless stated otherwise, the CASPT2 results shown in this paper are MS-CASPT2 results. The state specific (SS) CASPT2 and MS-CASPT2 methods give rise to energy values with deviations lower than 1 kcal/mol (see Supporting Information Table S2). The MS and SS approaches were compared along the extended region of state crossing, verifying that the out-of-diagonal elements of the effective Hamiltonian defined in the MS approach are in all the cases lower than 2−3 kcal/mol, which point to an accurate characterization of the mechanism with the MS-CASPT2 method.[20] As for the previous work,[11] core orbitals of non-hydrogen atoms were frozen in all the MS-CASPT2 calculations and the standard ionization potential electron affinity (IPEA) modification of the zeroth-order Hamiltonian with a value of 0.25 was employed.[21]

The energy profiles relevant for the chemiluminescence mechanism of 1,2-dioxetane were mapped at the MS-CASPT2//CASSCF(12in10)/ANO-RCC-VTZP level by means of the constrained optimization technique, using the C−C′ and O−O′ bond distances as constraints.[22] In each calculation, these bond distances were kept fixed and all the other internal coordinates were optimized. The range of values for the C−C′ and O−O′ bond lengths are 1.42−2.02 and 1.48−3.08 Å, respectively, with a step size of 0.1 Å. Other possibilities were also considered for the constraints. In particular, the C−C′ bond distance plus the O−C−C′−O′ dihedral angle. In this case, the former internal coordinate ranges also 1.42−2.02 Å, with a step size of 0.1 Å, and the values for the dihedral angle are between 0° and 180°, with different step sizes.

Spin−orbit coupling (SOC) terms between singlet and triplet states were computed within the AMFI and CASSI frameworks,[23,24] as implemented in the MOLCAS-7 quantum-chemistry program.[25] A CASSCF(12in10)/ANO-RCC-VQZP wave function averaged over four singlet and four triplet states was used.

2.2. *Ab Initio* Molecular Dynamics. The standard formulation of the molecular dynamics results in trajectories belonging to the microcanonical (NVE) ensemble. In this ensemble, the number of particles, volume, and total energy of the system is preserved. Nevertheless, most of the chemical experiments are carried out at constant temperature, the statistical behavior of which is described by the canonical (NVT) ensemble. An approach to take into account the temperature is the Nosé-Hoover chain of thermostats, in which the molecular system is coupled to a heat bath, generating the correct canonical ensemble.[26]

Therefore, improvements to the MOLCAS package were introduced to facilitate molecular dynamics simulations in the canonical ensemble, through the Nosé-Hoover method, which permits to include in the Hamiltonian the required degrees of freedom to simulate a thermostat.[27] The resulting motion equations were integrated by a time reversible integrator, applying the Liouville approach through the Trotter factorization.[28] The chosen initial conditions assumed that the particles velocities obey the Maxwell−Boltzmann distribution, therefore every component of the velocity can be considered as an independent Gaussian random variable for a given temperature.[29]

The methodology of the molecular dynamics at a constant temperature of 300 K was applied to the 1,2-dioxetane molecule for simulating the dynamical behavior in the so-called entropic trapping volume of the phase space. "On-the-fly" molecular dynamics were performed on S_0, starting from the TS of the thermal decomposition (TS_{S0}). By initiating the dynamics trajectories at the TS, the efficiency of the dynamics simulations is enhanced since the proper vibrational modes are enforced. Previous studies have also employed this approach,[12,30,31] showing that TS sampling gives dynamics results in agreement with experiments under the transition state theory (TST) approximation.[30,31] A set of 300 trajectories were run with an integration step of 1 fs and a maximum simulation time of 4 ps. The molecule was considered out of the biradical region when the distance between the carbon atoms of the two formaldehyde moieties was larger than 2.3 Å.

To perform the dynamics simulations, we tested in advance less time-demanding CASSCF/CASPT2 approaches than those mentioned in the previous section. The basis set and active space that maximize the ratio accuracy/time are the double-ζ quality ANO-RCC basis set contracted to O,C[3s2p1d]/H[2s1p] (hereafter, ANO-RCC-VDZP) and 8 electrons distributed in 6 orbitals, respectively. Since the C−O and C′−O′ bonds do not break in the chemiluminescence mechanism, the occupation numbers of the σ and σ^* orbitals of the C−O and C′−O′ orbitals are very close to two and zero, respectively. Hence, the results are still accurate enough when these four orbitals are removed from the active space. The MS-CASPT2 energies of the lowest-lying four singlet and four triplet states were computed at each integration step. These values were also employed together with the C−C′ distance to evaluate the departure of the molecule from the entropic-trapping region.

A development version of the MOLCAS-7 quantum-chemistry package suite was used in all electronic structure and molecular dynamics simulations of this study.[25]

3. RESULTS AND DISCUSSION

The findings obtained for the chemiluminescence mechanism of 1,2-dioxetane are presented in three sections. First, the analysis of the geometries and energies is presented for the stationary points obtained with the different CASSCF/CASPT2 approaches. Next, the details of the mechanism are explained using a two-dimensional model of the PESs for the lowest-lying four singlet and four triplet states. Finally, a few dynamical properties of the dissociation reaction are discussed.

3.1. Stationary Points of the Thermal and Chemiluminescence Mechanism. Several structures were found in the previous work by De Vico et al.,[11] which are relevant for the mechanism of thermally activated light emission of the 1,2-dioxetane molecule: the starting geometry (Reactant), the TS involving O−O′ bond breaking (TS_{S0}), the singlet and triplet biradical minima with O−C−C′−O′ dihedral angles of 70° ($Min_{S1(70)}$ and $Min_{T1(70)}$) and 180° ($Min_{S1(180)}$ and $Min_{T1(180)}$), the singlet and triplet TS involving C−C′ bond breaking with dihedral angle 70° ($TS_{S1(70)}$ and $TS_{T1(70)}$) and 180° ($TS_{S1(180)}$ and $TS_{T1(180)}$), and the products on the excited singlet [OCH_2

+ $^1(OCH_2)$] and triplet states [OCH_2 + $^3(OCH_2)$]. Note that in this work we have used a slightly different notation, the type A and B TSs of De Vico et al.[11] are those that we denote 70 and 180, respectively, although the actual angles are not exactly 70 and 180°. Note also that the TSs at the dihedral angle of 70° have a symmetry partner at −70°.

In this work, CASSCF(12in10)/ANO-RCC-VTZP geometries from De Vico et al.[11] were reoptimized, and subsequently, MS-CASPT2 geometry optimizations with the same active space and basis set were carried out. Table 1 compiles the computed C−C′ and O−O′ bond distances and the O−C−C′−O′ dihedral angle (see Cartesian coordinates in Table S1). The CASSCF and MS-CASPT2 results show small differences for all the internal coordinates of the bound structures, with average deviations of 0.05 Å, 0.06 Å, and 2° for the O−O′ and C−C′ bonds and the O−C−C′−O′ dihedral angle, respectively. As expected from the lower accuracy of the CASSCF method to describe noncovalent interactions, the largest deviations appear for the complex formed between the two formaldehyde molecules once the O−O′ and C−C′ bond dissociations take place. Overall, the CASSCF method is accurate enough for the geometry optimization of the 1,2-dioxetane and all the intermediates in the chemiluminescence mechanism. However, energy values are dramatically affected by the dynamical correlation. This fact is observed, for example, at the TS_{S0} structure, in which the CASSCF method underestimates the activation energy for O−O′ bond breaking by 14.0 kcal/mol (see Table 2). Much lower deviations occur in the comparison of the MS-CASPT2/ANO-RCC-VTZP energies obtained at the CASSCF/ANO-RCC-VTZP or MS-CASPT2/ANO-RCC-VTZP geometries, with an average difference of 1.8 kcal/mol.

Table 1. Main Geometrical Parameters of 1,2-Dioxetane Optimized at the CASSCF/ANO-RCC-VTZP (left) and MS-CASPT2/ANO-RCC-VTZP (right) Levels of Theory[a]

	C−C′	O−O′	O−C−C′−O′
react	1.51/1.49	1.58/1.51	17/19
TS_{S0}	1.54/1.49	2.26/2.28	37/44
$Min_{T1(70)}$	1.55/1.51	3.11/3.02	77/77
$Min_{S1(70)}$	1.53/1.53	2.98/2.92	66/75
$Min_{T1(180)}$	1.55/1.51	3.68/3.60	180/179
$Min_{S1(180)}$	1.55/1.54	3.70/3.54	180/179
$TS_{T1(70)}$	2.02/2.07	3.27/3.25	79/83
$TS_{S1(70)}$	2.09/2.21	3.27/3.25	76/76
$TS_{T1(180)}$	2.02/2.08	3.76/3.73	180/180
$TS_{S1(180)}$	2.08/2.19	3.81/3.82	180/180
$Prod_{T1}$	4.47/3.45	4.63/3.61	156/179
$Prod_{S1}$	4.15/3.41	4.06/3.57	136/180

[a]Bond lengths in Å and dihedral angles in degree.

Next, in order to analyze the basis set effect on the energies, we performed calculations with the ANO-RCC-VQZP basis set at the CASSCF/ANO-RCC-VTZP and MS-CASPT2/ANO-RCC-VTZP optimized geometries. Large discrepancies appear in the case of the vertical excitation energies between the four singlet and four triplet states computed (see Supporting Information Table S2). Conversely, the relative energies between the stationary structures are much less affected, showing average deviations of 1.3 and 2.8 kcal/mol at the CASSCF/ANO-RCC-VTZP and MS-CASPT2/ANO-RCC-VTZP geometries, respectively (cf. Table 2). In all the points along the mechanism, the ANO-RCC-VQZP basis set gives rise to larger energy values relative to the reactant, being the $TS_{(180)}$ structures the most sensitive. It is worth noting that almost no differences are found with the larger basis set between the energies obtained at the CASSCF and MS-CASPT2 geometries (average deviation of 0.3 kcal/mol, always lower than 1.4 kcal/mol).

Table 2. Relative Energies (in kcal/mol) of the Main Stationary Structures of 1,2-Dioxetane in the Chemiluminescence Mechanism Computed with Different CASSCF/CASPT2 Approaches[a]

	CASSCF/TZ	MS-CASPT2//CASSCF/TZ	MS-CASPT2/TZ	MS-CASPT2/QZ//CASSCF/TZ	MS-CASPT2/QZ//MS-CASPT2/TZ
react	0.0	0.0	0.0	0.0	0.0
TS_{S0}	9.7	23.7	23.4	24.9	25.5
$Min_{T1(70)}$	7.7	18.4	17.8	19.6	20.0
$Min_{S1(70)}$	9.0	18.4	17.2	19.6	19.4
$Min_{T1(180)}$	7.1	17.9	18.5	19.1	19.9
$Min_{S1(180)}$	8.8	18.1	16.6	19.2	18.7
$TS_{T1(70)}$	22.2	30.0	28.4	31.7	31.2
$TS_{S1(70)}$	26.5	35.0	33.7	36.6	36.3
$TS_{T1(180)}$	21.1	29.0	24.2	30.6	30.4
$TS_{S1(180)}$	25.7	34.3	29.4	35.9	35.6
$Prod_{T1}$	7.2	25.3	22.1	27.0	25.5
$Prod_{S1}$	13.2	32.4	29.5	34.1	32.7

[a]Vertical excitation energies for the other singlet and triplet states at these geometries are compiled in Table S2.

Further improvements to the mechanism come from the inclusion of ZPVE corrections (see Table 3). Since the presence of four roots in the SA procedure within the CASSCF method is needed to describe properly the geometries and energetics in the biradical region, the second-order derivatives of the energy were computed numerically at the CASSCF(12in10)/ANO-RCC-VTZP level. The entropic factor was also estimated by means of these calculations. The ZPVE results show a clear pattern: each bond dissociation implies a decrease of around 2 kcal/mol in the values of the corresponding TS. Thus, taking into account the ZPVE corrections, the TS_{S0}

Table 3. Zero-Point Vibrational Energy Corrections and Gibbs Energies (in kcal/mol) at 300 K of the Main Stationary Structures of 1,2-Dioxetane in the Chemiluminescence Mechanism Computed at the CASSCF/ANO-RCC-VTZP Level of Theory

	ZPVE	Gibbs energy
react	40.2	23.9
TS_{S0}	38.4	21.8
$Min_{T1(70)}$	38.1	21.2
$Min_{S1(70)}$	37.0	20.2
$Min_{T1(180)}$	38.2	21.3
$Min_{S1(180)}$	37.5	20.6
$TS_{T1(70)}$	35.0	17.6
$TS_{S1(70)}$	36.0	18.5
$TS_{T1(180)}$	35.9	18.7
$TS_{S1(180)}$	35.5	18.1
$Prod_{T1}$	33.7	14.0
$Prod_{S1}$	34.0	13.1

dx.doi.org/10.1021/ct4007844 | J. Chem. Theory Comput. XXXX, XXX, XXX−XXX

structure is stabilized by 1.8 kcal/mol with respect to the reactant, and the energies of the $TS_{(70)}$ and $TS_{(180)}$ on the singlet and triplet manifolds decrease an average of 4.8 and 4.5 kcal/mol, respectively, also with respect to the close-ring dioxetane. Bond dissociation also changes the entropy of the molecule along the mechanism, stabilizing further the opened structures. Our results show a decrease of 2.1 kcal/mol for the TS_{S0} structure and an average decrease of 5.9 and 5.5 kcal/mol for the Gibbs energies of the $TS_{(70)}$ and $TS_{(180)}$ points, respectively, estimated at 300 K.

Figure 3 shows the steps performed to improve the description of the energy profile for the chemiluminescence

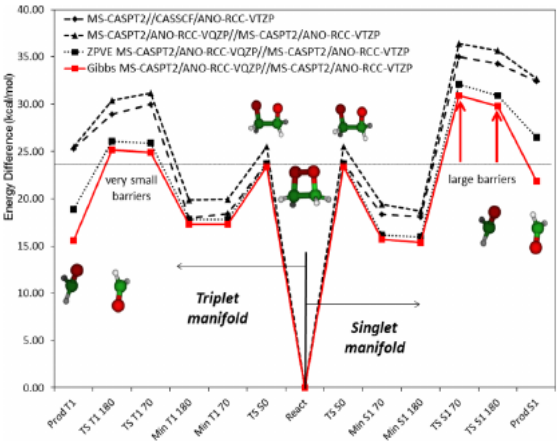

Figure 3. Relative energies of the stationary points obtained at different levels along the singlet and triplet manifolds. The energy barrier heights for the TS of the C−C bond dissociations ($TS_{S1(70)}$, $TS_{S1(180)}$, $TS_{T1(70)}$, and $TS_{T1(180)}$) are highlighted relative to the TS of the O−O bond breaking (TS_{S0}).

of 1,2-dioxetane with respect to the previous paper.[11] Whereas the improvements in the electronic energies, by means of the inclusion of dynamical correlation in the method for geometry optimization and the enlargement of the basis set, imply in general relatively small deviations, ZPVE corrections and the entropic factor change some aspects of the mechanism for chemiluminescence. The former results show TSs for the C−C′ bond cleavage higher in energy with respect to the TS related to the O−O′ bond breaking. This is true for both the singlet and triplet states and for the TSs with O−C−C′−O′ dihedral angles of 70° and 180°. Conversely, a more accurate description (including ZPVE and entropy corrections) brings the $TS_{T1(70)}$ and $TS_{T1(180)}$ structures close to the energy of the TS_{S0} point. In addition, taking into account the symmetry of the molecule, a total amount of two and six TS structures exist on the PESs related to the O−O′ and C−C′ bond dissociations, respectively, which will effectively reduce the activation barrier of the later process. This translates to that at 300 K the effective activation energies are 23.0, 23.9, and 29.2 kcal/mol for the O−O′ breakage on the S_0 surface, the C−C′ breakage on the T_1 surface, and the C−C′ breakage on the S_1 surface, respectively. Therefore, the rate-determining step for the phosphorescence emission is basically the O−O′ cleavage, and not the second C−C′ bond breaking as it is the case on the basis of the electronic energies.[11] The total energy needed to rupture the O−O′ bond seems to be enough to access the triplet TS and the emissive formaldehyde T_1 state. Fluorescence, on the other hand, still needs a significant amount of extra energy with respect to the level of the TS_{S0}, which makes the C−C′ bond dissociation more difficult and the emissive S_1 state less accessible. The phosphorescence process requires a population transfer from the ground state S_0 to the triplet state T_1. This is possible through the wide region of ISC crossing that exists between the TS_{S0} and the $TS_{T1(70)}$ or $TS_{T1(180)}$. The ISC is also probable because computations of the SOC give values as high as 49 cm^{-1} for the biradical structures (degeneracy region) of 1,2-dioxetane. A strict quantitative analysis of the ratio phosphorescence to fluorescence is subject to careful simulations including both internal conversion and interstate crossing. However, a preliminary rough estimation of the ratio based on the Arrhenius equation gives a value of $7903 \times (A_T/A_S)$, where A_T and A_S are the Arrhenius frequency factors for the triplet and single excited state dissociations. Considering that the second term (A_T/A_S) is smaller than unity, due to the fact that the single-triplet transition is forbidden to first order, the estimated ratio $(7903 \times (A_T/A_S))$ demonstrates that the presented activation energies of the triplet and singlet excited products are consistent with the observed ratio of phosphorescence to fluorescence. Also, the experimental threshold of 22.7 ± 0.8 kcal/mol[6] for chemiluminescence in 1,2-dioxetane is now rationalized by the fact that the triplet TSs related to the C−C′ cleavage are close in terms of energy to the TS_{S0}, in contrast to the previous study by De Vico et al.[11] This would make the activation of the ground state dissociation and the chemiluminescence from the phosphorescent triplet state literarily indistinguishable based on a study of the activation energy of the processes. This conclusion is in agreement with measurements for tetramethyldioxetane[9] and *cis*-diethoxy-1,2-dioxetane[10] and previous computed data with the CASSCF/MP2 method for the ground and lowest-lying triplet states.[8]

3.2. Two-Dimensional Model of the Decomposition Reaction. As explained in the Introduction, three types of mechanisms have been proposed for the chemiluminescence of 1,2-dioxetane: (1) concerted O−O′ and C−C′ bond dissociation, (2) two-step process involving a •O−CH_2−C′H_2−O• biradical intermediate, and (3) merged mechanism. The findings obtained by De Vico et al.[11] and the results from the previous section point to a biradical mechanism. In order to further verify it, we explore here the surroundings of the stationary points by means of the MS-CASPT2//CASSCF-(12in10)/ANO-RCC-VTZP method and a constraint geometry optimization procedure.

Even in such a small molecule as 1,2-dioxetane, the PES characterization by means of constraint optimizations must be performed with caution, comparing with additional data from strategies which provide accurate paths, such as MEPs and intrinsic reaction paths. In fact, our first attempt, selecting the C−C′ bond length and the O−C−C′−O′ dihedral angle as constraints, failed. From the reactant, the structure becomes "twisted" (see Figure 4) and does not connect it with the TS_{S0} structure as the MEP computations do (cf. De Vico et al.[11]). An

Figure 4. 1,2-Dioxetane structures obtained as TS in the constraint optimizations by two different sets of constraints: C−C′ bond length and O−C−C′−O′ dihedral angle (left) and C−C′ and O−O′ bond lengths (right).

Journal of Chemical Theory and Computation Article

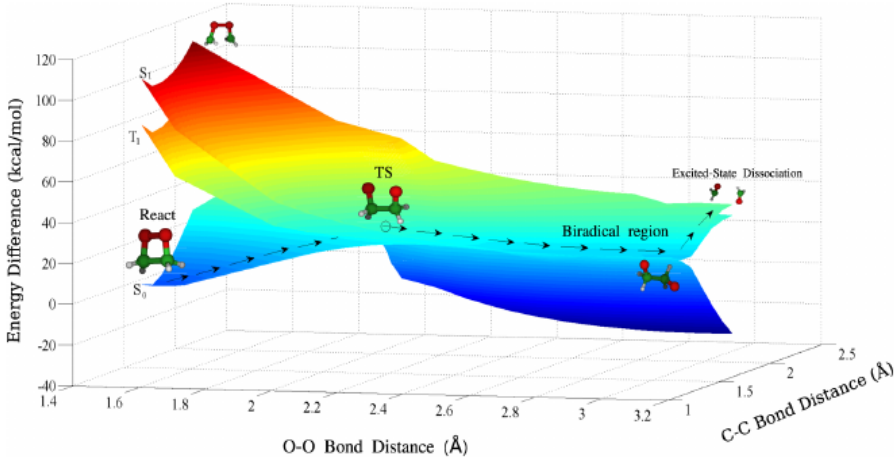

Figure 5. MS-CASPT2/ANO-RCC-VTZP energies (in kcal/mol) of the lowest-lying singlet and triplet excited states of 1,2-dioxetane vs the C−C′ and O−O′ bond lengths (in Å) for the CASSCF/ANO-RCC-VTZP constraint optimization of the singlet ground state, S_0.

appropriate set of constraints are the C−C′ and O−O′ bond distances, which reproduce the stationary points and MEPs. Figure 5 shows the two-dimensional PESs obtained in this manner for the singlet and triplet states. Taking into account the large barriers to reach the excited state and the absence of degeneracy in the C−C′ axis or the diagonal starting from the Reactant point in the PES, the concerted mechanism can be discarded. The most accessible path to the excited formaldehyde is clearly the initial formation of the biradical structure, which eventually must surmount the second barrier following a perpendicular direction to the one involved in the first process. Hence, these results also discard the merge mechanism in favor of the two-step biradical mechanism.

3.3. Lower-Bound Estimation for the Lifetime of the Biradical Intermediate. The formation of a •O−CH_2−C′H_2−O′• intermediate and the presence of an entropic trapping region in which the molecule can split the population among the lowest four singlet and four triplet states was proposed in the previous theoretical study by De Vico et al.[11] Our interest here is to estimate how fast can be the pass through the intermediate region before thermal decomposition by means of AIMD. We performed the trajectories on the S_0 PES without considering the transfer of population to the other states. This approximation will give us a lower-bound estimation, since the effect of CIX and ISC crossings among the degenerate states is expected to increase the time spent in this region.

A total amount of 300 trajectories were run at a constant T of 300 K from the TS_{S0} and using the CASSCF(6in6)/ANO-RCC-VDZP gradients of the ground state. All the dynamics computations give rise to the C−C′ dissociation within the limit time of 1 ps (see distribution of dissociation times in Figure 6). In agreement with the previous results obtained from the static modeling of the reaction, the dynamics simulations shows a torsion of the O−C−C′−O′ dihedral angle in the biradical region. MS-CASPT2(6in6)/ANO-RCC-VDZP calculations along the trajectories verify the degeneracy of the lowest four singlet and four triplet states, which disappears when the C−C′ bond breaks. The half-life time obtained as lower-bound for the entropic trap is 613 fs (to be compared with the oscillation time of a C−C′ single bond of about 30 fs). If the molecule has not on average transferred the population to the

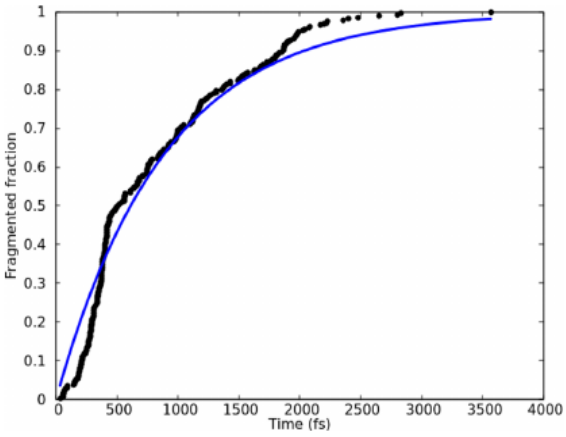

Figure 6. Fragmented fraction of the 300 trajectories (black dots) as a function of time in the ab initio molecular dynamics simulation in the canonical ensemble at 300 K. The blue line corresponds to an exponential decay with a half-life time of 613 fs. The simulation is conducted on the S_0 surface of 1,2-dioxetane after the TS_{S0} ignoring internal conversions and interstate crossings. The molecule is considered to be dissociated at a C−C′ bond distance larger than 2.3 Å.

excited singlet or triplet states after that time, it will decompose in the ground state without emission of light. According to the experimental data, the latter process, that is, the thermal dissociation, is the most probable process occurring in 1,2-dioxetane.[6] In order to produce fluorescence and phosphorescence, the system must reach the excited singlet and triplet states, respectively, along the biradical region. Crossings and recrossings among the four singlet and four triplet degenerate states, which are not considered in the current dynamics simulations, are expected to increase the lifetime of the entropic trap, thus explaining the luminescence properties. Further AIMD simulations considering nonadiabatic crossings between singlet states (CIX) and between singlet and triplet states (ISC) shall be performed in future works in order to provide quantitative quantum yields for the thermal dissociation,

dx.doi.org/10.1021/ct4007844 | J. Chem. Theory Comput. XXXX, XXX, XXX−XXX

fluorescence, and phosphorescence processes, to be directly compared with the experimental data.

We would like to point out that the dynamics presented here are in line with a non-RRKM behavior as demonstrated by Sun et al.[12] However, their study did not demonstrate an effect due to the entropic trapping and the formation of a biradical intermediate, rather the C−C′ bond rupture occurred at about 20 fs after the initial O−O′ bond rupture. This would correspond to the behavior of the few trajectories in this study which dissociate before 100 fs (see Figure 6). This difference between the results of the dynamics is possibly associated with (a) the underlying level of theory to describe the PES and (b) the starting structures of the respective molecular dynamics simulations. First, while we use MS-CASPT2 theory, Sun et al.[12] use unrestricted density functional theory; the latter puts the second TS at about 10 kcal/mol below the first TS, the former does not predict a clear TS at the C−C′ bond rupture but predicts a shoulder at around 2−3 kcal/mol below the first TS.[11] Effectively, the larger energy difference between the two TSs in the study by Sun et al. would amount to that no biradical intermediates are formed. Second, the simulations by Sun et al.[12] starts at a TS associated with the formation of dioxetane from molecular oxygen and ethene. This TS is about 45 kcal/mol above the energy of the dioxetane in its equilibrium structure. Hence, the molecule will, on the path toward the fragmentation to formaldehyde, reach the O−O′ bond rupture TS with an excess energy of about 20 kcal/mol. In this respect, a strong non-RRKM behavior is expected and the super hot species will not form a biradical intermediate.

4. CONCLUSIONS

The chemiluminescence reaction of 1,2-dioxetane is revisited in the present contribution. High-level CASSCF/CASPT2 calculations and AIMD simulations at T equal 300 K have been carried out in order to further understand the thermal dissociation and chemiluminescence processes of the molecule and to interpret some experimental observations which were still not accounted for, in particular, the high ratio of triplet to singlet dissociation products.

The findings confirm a stepwise mechanism for the chemiluminescence reaction, which can be described as follows. First, the O−O′ bond is broken and the molecule enters in an extended region of biradical character, in which four singlet and four triplet states are degenerated. Here, a biradical intermediate if formed which, in absence of internal conversion to the S_1 state and interstate crossing to the T_1 state, thermally dissociated wth a half-life time of 613 fs. The nonadiabatic process is possible in singlet as well as triplet states. A high probability for the spin-forbidden triplet population is predicted in this region, according to the SOC calculations. In order to produce chemiluminescence, a second energy barrier must be surmounted in the manifolds of the lowest-lying singlet or triplet excited states related to the C−C′ bond dissociation. This activation energy is lower in the triplet manifold, presenting a TS basically degenerated with the first TS on the ground state related to the O−O′ bond breaking, while the TS on the singlet excited state surface is about 6−7 kcal/mol higher in energy. Hence, in contrast to the fluorescence emission of light, the phosphorescence requires the same energy as the activation energy for the thermal dissociation (around 23−24 kcal/mol). These results are in agreement with the experiments and allow to rationalize the observed larger quantum yield of phosphorescence as compared to fluorescence.

■ ASSOCIATED CONTENT

Supporting Information

Cartesian coordinates and energies of the low-lying singlet and triplet states. This material is available free of charge via the Internet at http://pubs.acs.org.

■ AUTHOR INFORMATION

Corresponding Authors

*E-mail: Daniel.Roca@uv.es.
*E-mail: Roland.Lindh@kemi.uu.se.

Notes

The authors declare no competing financial interest.

■ ACKNOWLEDGMENTS

D.R.-S. thanks the Spanish MINECO source through project CTQ2010-14892. P.F. and R.L. acknowledge financial support from Behrouz Nik Ind and the Swedish Research Council (VR), respectively. The computations were performed on resources provided by SNIC through Uppsala Multidisciplinary Center for Advanced Computational Science (UPPMAX) under Project s00112-19.

■ REFERENCES

(1) Contag, C.; Bachmann, M. Advances in in vivo bioluminescence imaging of gene expression. *Annu. Rev. Biomed. Eng.* **2002**, *4*, 235.
(2) Jenkins, D.; Oei, Y.; Hornig, Y.; Yu, S.; Dusich, J.; Purchio, T.; Contag, P. Bioluminescence imaging (BLI) to improve and refine traditional murine models of tumor growth and metastasis. *Clin. Exp. Metastasis* **2003**, *20*, 733.
(3) Kopecky, K. R.; Mumford, C. Luminescence in the thermal decomposition of 3,3,4-trimethyl-1,2-dioxetane. *Can. J. Chem.* **1969**, *47*, 709−711.
(4) O'Neal, H. E.; Richardson, W. H. Thermochemistry of 1,2-dioxetane and its methylated derivatives. Estimate of activation parameters. *J. Am. Chem. Soc.* **1970**, *92*, 6553−6557.
(5) Turro, N. J.; Lechtken, P. Molecular photochemistry. LXII. Thermal generation of organic molecules in electronically excited states. Evidence for a spin forbidden, diabatic pericyclic reaction. *J. Am. Chem. Soc.* **1973**, *95*, 264−266.
(6) Adam, W.; Baader, W. J. Effects of methylation on the thermal stability and chemiluminescence properties of 1,2-dioxetanes. *J. Am. Chem. Soc.* **1985**, *107*, 410−416.
(7) Reguero, M.; Bernardi, F.; Bottoni, A.; Olivucci, M.; Robb, M. A. Chemiluminescent decomposition of 1,2-dioxetanes: an MC-SCF/MP2 study with VB analysis. *J. Am. Chem. Soc.* **1991**, *113*, 1566−1572.
(8) Wilsey, S.; Bernardi, F.; Olivucci, M.; Robb, M. A.; Murphy, S.; Adam, W. The thermal decomposition of 1,2-dioxetane revisited. *J. Phys. Chem. A* **1999**, *103*, 1669−1677.
(9) Steinmetzer, H.; Yekta, A.; Turro, N. J. Chemiluminescence of tetramethyl-1,2-dioxetane. Measurement of activation parameters and rates of exceedingly slow reactions by a simple and nondestructive method. Demonstration of indistinguishable activation energies for generation of acetone singlets and triplets. *J. Am. Chem. Soc.* **1974**, *96*, 282.
(10) Wilson, T.; Schaap, P. Chemiluminescence from cis-diethoxy-1,2-dioxetane. Unexpected effect of oxygen. *J. Am. Chem. Soc.* **1971**, *93*, 4126.
(11) De Vico, L.; Liu, Y.-J.; Krogh, J. W.; Lindh, R. Chemiluminescence of 1,2-dioxetane. reaction mechanism uncovered. *J. Phys. Chem. A* **2007**, *111*, 8013−8019.
(12) Sun, R.; Park, K.; de Jong, W.; Lischka, H.; Windus, T.; Hase, W. Direct dynamics simulation of the dioxetane formation and

decomposition via the singlet .O-O-CH2-CH2. biradical: Non-RRKM dynamics. *J. Chem. Phys.* **2012**, *137*, 044305.
(13) Roos, B. O.; Taylor, P. R.; Siegbahn, P. E. M. A complete active space SCF method (CASSCF) using a density matrix formulated super-CI approach. *Chem. Phys.* **1980**, *48*, 157−173.
(14) Roos, B. O. The complete active space SCF method in a Fock-matrix-based super-CI formulation. *Int. J. Quantum Chem.* **1980**, *S14*, 175−189.
(15) Andersson, K.; Malmqvist, P.-Å.; Roos, B. O.; Sadlej, A. J.; Wolinski, K. Second-order perturbation theory with a CASSCF reference function. *J. Phys. Chem.* **1990**, *94*, 5483−5488.
(16) Andersson, K.; Malmqvist, P.-Å.; Roos, B. O. Second-order perturbation theory with a complete active space self-consistent field reference function. *J. Chem. Phys.* **1992**, *96*, 1218−1226.
(17) Roca-Sanjuán, D.; Aquilante, F.; Lindh, R. Multiconfiguration second-order perturbation theory approach to strong electron correlation in chemistry and photochemistry. *Wiley Interdisciplinary Reviews: Computational Molecular Science* **2012**, *2*, 585−603.
(18) Roos, B. O.; Lindh, R.; Malmqvist, P.-Å.; Veryazov, V.; Widmark, P.-O. Main group atoms and dimers studied with a new relativistic ANO basis set. *J. Phys. Chem. A* **2004**, *108*, 2851−2858.
(19) Finley, J.; Malmqvist, P.-Å.; Roos, B.; Serrano-Andrés, L. The multi-state CASPT2 method. *Chem. Phys. Lett.* **1998**, *288*, 299−306.
(20) Serrano-Andrés, L.; Merchán, M.; Lindh, R. Computation of conical intersections by using perturbation techniques. *J. Chem. Phys.* **2005**, *122*, 104107.
(21) Ghigo, G.; Roos, B. O.; Malmqvist, P.-Å A modified definition of the zeroth-order Hamiltonian in multiconfigurational perturbation theory (CASPT2). *Chem. Phys. Lett.* **2004**, *396*, 142−149.
(22) De Vico, L.; Olivucci, M.; Lindh, R. New general tools for constrained geometry optimizations. *J. Chem. Theor. Comput.* **2005**, *1*, 1029−1037.
(23) Rubio-Pons, Ò.; Serrano-Andrés, L.; Merchán, M. A theoretical insight into the photophysics of acridine. *J. Phys. Chem. A* **2001**, *105*, 9664−9673.
(24) Strickler, S. J.; Berg, R. A. Relationship between absorption intensity and fluorescence lifetime of molecules. *J. Chem. Phys.* **1962**, *37*, 814.
(25) Aquilante, F.; De Vico, L.; Ferré, N.; Ghigo, G.; Malmqvist, P.-Å.; Neogrady, P.; Pedersen, T. B.; Pitonak, M.; Reiher, M.; Roos, B. O.; Serrano-Andrés, L.; Urban, M.; Veryazov, V.; Lindh, R. Software news and update MOLCAS 7: The next generation. *J. Comput. Chem.* **2010**, *31*, 224−247.
(26) Frenkel D., S. B. *Understanding Molecular Simulation*; Academic Press: San Diego, 2002.
(27) Tuckerman, M. E.; Martyna, G. J. Understanding modern molecular dynamics: Techniques and applications. *J. Phys. Chem. B* **2001**, *105*, 7598−7598.
(28) Martyna, G. J.; Tuckerman, M. E.; Tobias, D. J.; Klein, M. L. Explicit reversible integrators for extended systems dynamics. *Mol. Phys.* **1996**, *87*, 1117−1157.
(29) Field, M. *A Practical Introduction to the Simulation of Molecular Systems*; Cambridge University Press: New York, 2007; pp 1−344.
(30) Lourderaj, U.; Park, K.; Hase, W. L. Classical trajectory simulations of post-transition state dynamics. *Int. Rev. Phys. Chem.* **2008**, *27*, 361.
(31) Sun, L.; Park, K.; Song, K.; Setser, D. W.; Hase, W. L. Use of a single trajectory to study product energy partitioning in unimolecular dissociation: Mass effects for halogenated alkanes. *J. Chem. Phys.* **2006**, *124*, 064313.

5.2.2 QM/MM Simulations of IrisFP

In this Thesis we focus on the IrisFP which presents both a reversible photoswitching between fluorescent and nonfluorescent states, and irreversible photoconversion (Adam, et al. 2008). In Figure 5.1, it is presented a scheme showing the possible states of the IrisFP chromophore and its comparison with the well-studied Dronpa fluorescent protein (Andresen, et al. 2007). In this Ph.D. Thesis we primarily focused on the anionic green chromophore, which maximum peak of absorption is centered at 488nm.

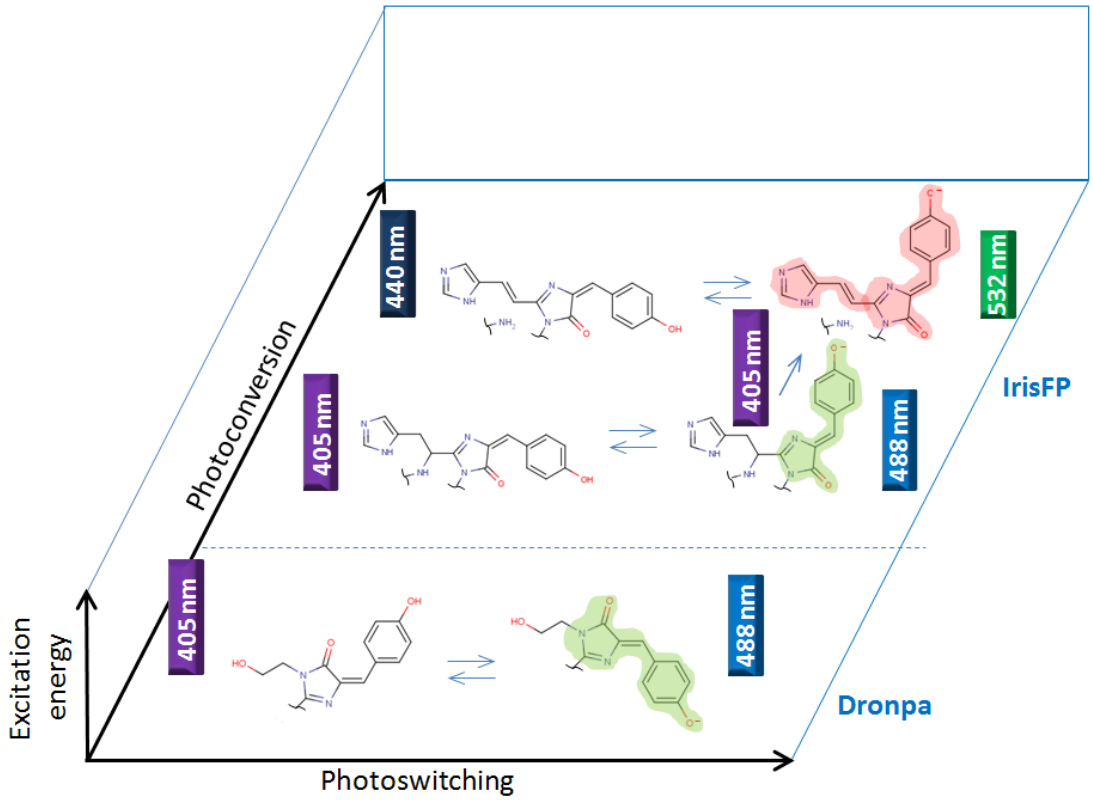

Figure 5.1. (Top) β-barrel overall structure of fluorescent proteins, with chromophore location and main dimensions (related to nano-technological applications) highlighted. (Bottom) Two examples of photoactivatable FPs: photoswitchable Dronpa, interconverting trans-dim and cis-green state, by irradiating with violet and blue light; photoswitchable and photoconvertible IrisFP, interconverting trans-dim and cis-green/red states, by multiple irradiation channels.

Previous reported calculations (Martin, et al. 2004), have shown that the PES of the green fluorescent protein chromophore in vacuum (green shaded structure in Figure 6), presents an ultra-fast deactivation due to the lack of some minimum on S_1 (i.e.

fluorescence emission is negligible), being then presumed that the protein pocket stabilized the charged chromophore, in such a way that the chromophore is driven towards a minimum, where the fluorescent emission can occur.

Firstly, in collaboration with the group of Professor Marcus Elstner at the Karlsruhe Institute of Technology (Germany) and the nano-bio spectroscopy group of the University of the Basque Country (Spain), the DFTB/MM dynamics methodology (Han, et al. 2000) was applied to the IrisFP system surrounded by water solvent, in order to corroborate the protonation state of the cromophore pocket. Also, the DFTB/MM methodology was used to optimize the minimal energy structure on the ground electronic state (S_0), which is used as the initial structure for the excited state (S_1) optimization.

In order to correctly describe the excited state, the QM/MM methodology using the Molcas/Tinker interface (Aquilante, et al. 2010), was applied to the whole protein, (using the CASSCF/6-31G* theory level for the QM region) to calculate the S_1 topology and dynamics. Also, in the case of the molecular dynamic simulation it was applied the Nosé-Hoover chain of thermostat method, as explained in section 2.1.4.

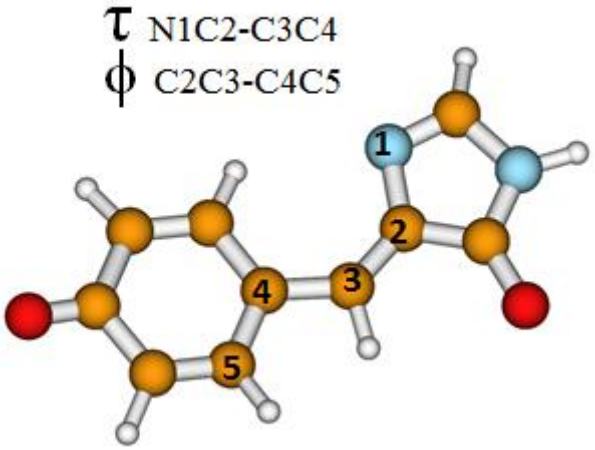

Figura 5.2. Schematic representation of the τ and ϕ dihedral angles in the IrisFP chromophore.

Also, as first approximation it was considered that oscillator strength is constant for all the values of the electronic energy gap recorded during the dynamic simulations (i.e. it does not change within the phase space sampled at a given temperature), assuming then that oscillator strength is equal to that of the optimized S_1 geometry. Also, it is considered that both PESs at CASSCF and CASPT2 theory level are parallel. Therefore both energies and oscillator strength were corrected using the optimized S_1 geometry at theory level CASSCF/CASPT2. Besides, the initial positions used in the dynamical simulations, are the optimized geometries in the protein environment. On the other hand, the initial velocities were chosen accordingly to the Maxwell-Boltzmann distribution at 300K.

Using the aforementioned methodology, it was obtained the minimum energy geometry on S_1, which ($S_1 \rightarrow S_0$) energetic gap and oscillator strength after CASPT2 correction are 490.5 nm and 0.95, respectively. As has been mentioned before, such minimum does not exist for the chromophore in vacuum. On the other hand, the experimental results reported in the literature from *In crystallo* spectroscopy, reveal a fluorescence peak which maximum is centered at 516 nm for the anionic chromophore at 100K (Adam, et al. 2008). Given that the minimum energy geometries for both ground S_0 and first excited state S_1 are almost identical as can be seen in Figures 5.3 and 5.4, the vertical absorption ($S_0 \rightarrow S_1$) is almost equal to emission ($S_1 \rightarrow S_0$) and therefore our model underpredict significantly the wavelength emitted and the fluorescence spectrum.

Subsequently, it was firstly explored the region around the S_1 minimum energy geometry and the S_1/S_0 intersection spaces. For doing so, it was chosen two particular molecular coordinates, which are deeply discussed in the literature: the τ and φ dihedral angles. In Figure 5.2 it is presented a schematic representation of both angles, which numerical values are approximately zero in the S_1 minimum energy geometry.

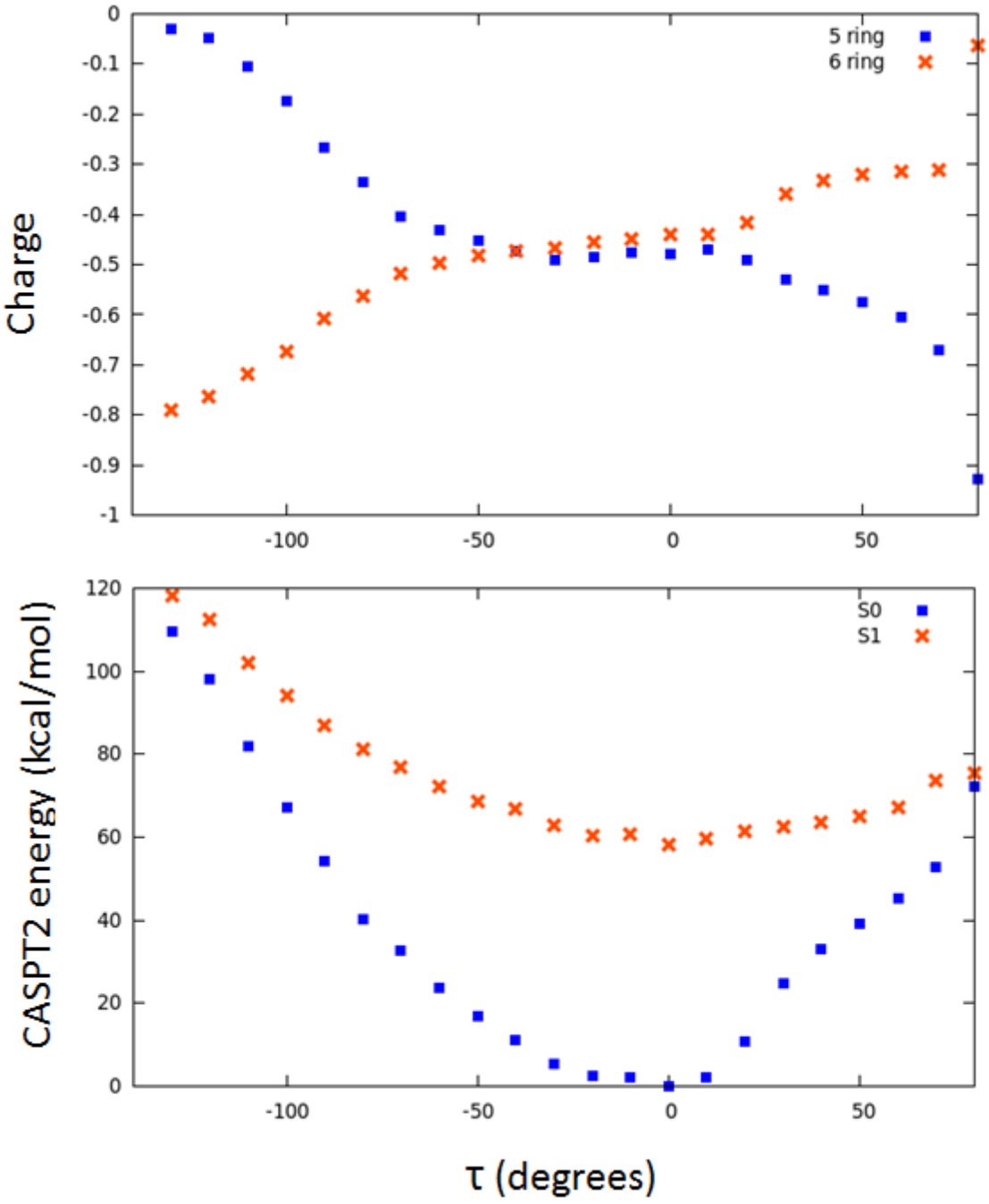

Figure 5.3. (Top) charge variation profile as function of the torsional angle τ. (Bottom) CASPT2/CASSCF energy profile as function of the torsion angle τ.

On the other hand, in Figure 5.3 can be seen that at the equilibrium geometry the charge is delocalized between the five and sixth membered rings, but at negative values of τ, the charge is mainly localized at the sixth member ring. While at positive values of τ, the charge is localized at the five membered ring. On the other hand, in Figure 5.4 it is

shown that the charge is mainly localized on the five membered ring, for almost all values of the φ angle.

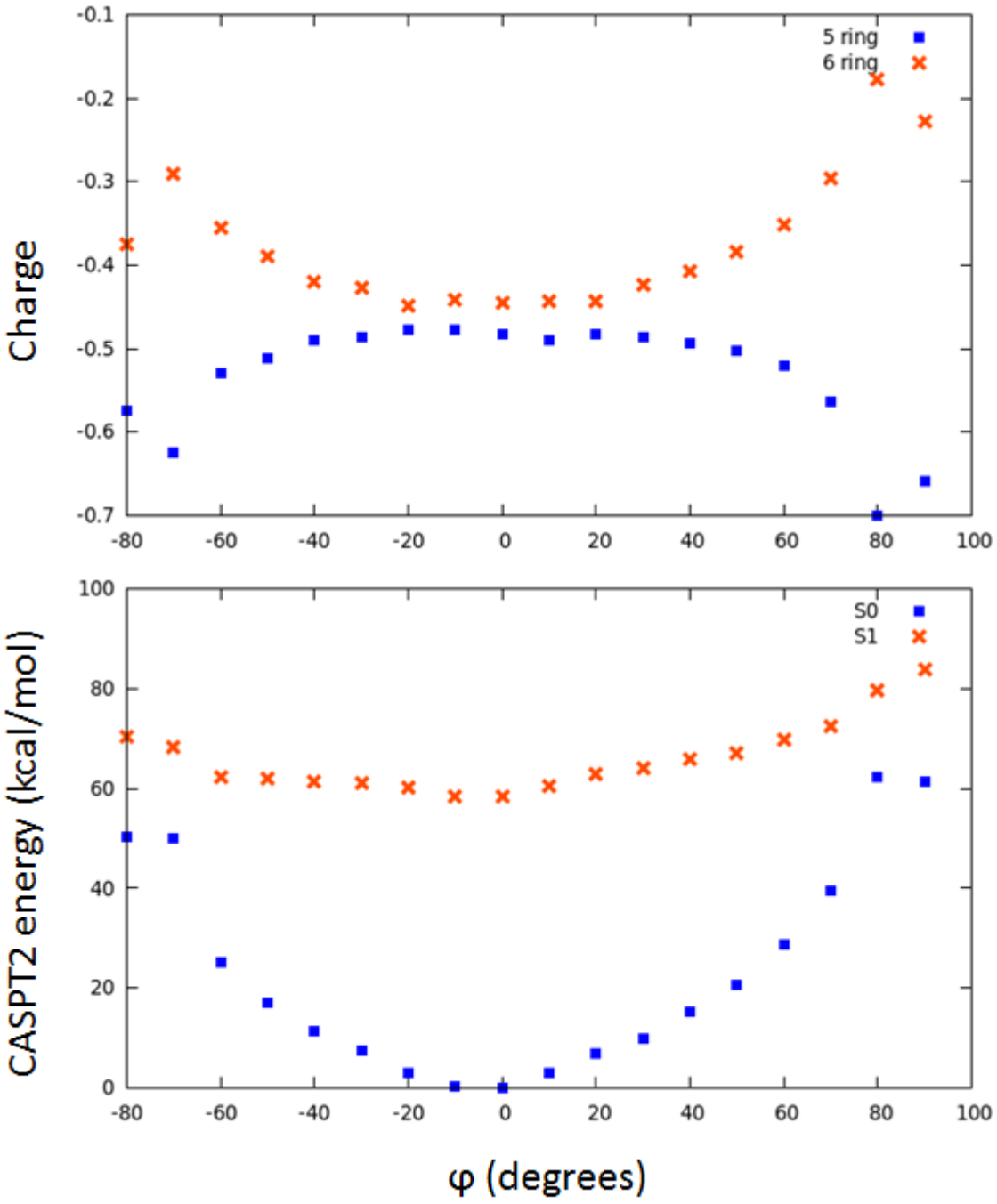

Figure 5.4. .(Top) charge variation profile as function of the torsional angle φ. (Bottom) CASPT2/CASSCF energy profile as function of the torsion angle φ.

Finally, in order to evaluate the dynamical effect of the environment in the spectroscopical properties of the chromophore, it was simulated the fluorescence spectrum for the chromophore in the protein environment (QM/MM). To simulate the spectrum it was carried out a set of molecular dynamics in the first excited state (S_1), where it was recorded the energy in both ground and excited state in each integration step. With these data it was created a histogram for all the QM/MM simulations, each histogram containing the probability of finding the system in a configuration with a given energy gap (i.e. S_1-S_0). The simulated spectrum is finally obtained by multiplying such probabilities for the corresponding oscillator strength.

A total of 70 trajectories were run for up to100 fs, to obtain the simulated spectrum at 300K through the histogram method, as presented in Figure5.5. The resulting simulated spectra is considerable blue-shifted compared to the experimental spectrum, which emission maximum peaks at 516 nm, indicating that the chosen MM model to not reproduce realistically the protein environment.

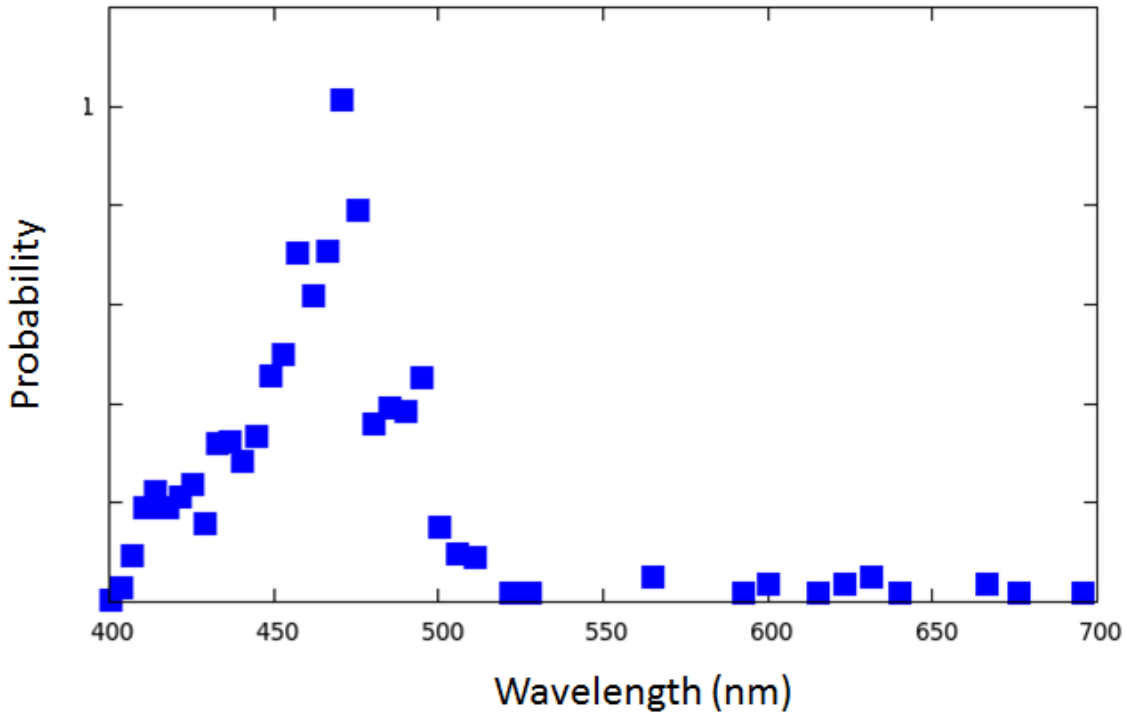

Figure 5.5. Simulated spectrum calculated as a histogram using the $S_1 \rightarrow S_0$ energy gaps calculated using QM/MM molecular dynamics and corrected at CASSCF/CASPT2 theory level.

Taking into account the given results, it is firstly required an improvement of our QM/MM model that account for the observed experimental fluorescence spectrum. And after we establish a reliable QM/MM model, our next goal will be to carry out systematic modifications in the protein neighbourhood surrounding the chromophore, in order to identify the chemical interactions together with the geometrical modifications that modules efficiently the absorption and emission spectra.

5.3 Chapter Bibliography

Adam, V.; Lelimousin, M.; Boehme, S.; Desfonds, G.; Nienhaus, K.; Field, M. J.; Wiedenmann, J.; McSweeney, S.; Nienhaus, G. U.; Bourgeois, D., Structural characterization of IrisFP, an optical highlighter undergoing multiple photo-induced transformations. *Proceedings of the National Academy of Sciences* **2008,** *105*, 18343-18348.

Ando, R.; Mizuno, H.; Miyawaki, A., Regulated Fast Nucleocytoplasmic Shuttling Observed by Reversible Protein Highlighting. *Science* **2004,** *306*, 1370-1373.

Andresen, M.; Stiel, A. C.; Trowitzsch, S.; Weber, G.; Eggeling, C.; Wahl, M. C.; Hell, S. W.; Jakobs, S., Structural basis for reversible photoswitching in Dronpa. *Proceedings of the National Academy of Sciences* **2007,** *104*, 13005-13009.

Aquilante, F.; De Vico, L.; Ferré, N.; Ghigo, G.; Malmqvist, P.-å.; Neogrády, P.; Pedersen, T. B.; Pitoňák, M.; Reiher, M.; Roos, B. O.; Serrano-Andrés, L.; Urban, M.; Veryazov, V.; Lindh, R., MOLCAS 7: The Next Generation. *J. Comput. Chem.* **2010,** *31*, 224-247.

Betzig, E.; Patterson, G. H.; Sougrat, R.; Lindwasser, O. W.; Olenych, S.; Bonifacino, J. S.; Davidson, M. W.; Lippincott-Schwartz, J.; Hess, H. F., Imaging Intracellular Fluorescent Proteins at Nanometer Resolution. *Science* **2006,** *313*, 1642-1645.

Carpenter, B. K., Electronically nonadiabatic thermal reactions of organic molecules. *Chem. Soc. Rev.* **2006,** *35*, 736-747.

De Vico, L.; Liu, Y.-J.; Krogh, J. W.; Lindh, R., Chemiluminescence of 1,2-Dioxetane. Reaction Mechanism Uncovered. *The Journal of Physical Chemistry A* **2007,** *111*, 8013-8019.

Fraga, H., Firefly luminescence: A historical perspective and recent developments. *Photochemical & Photobiological Sciences* **2008,** *7*, 146-158.

Fuchs, J.; Bohme, S.; Oswald, F.; Hedde, P. N.; Krause, M.; Wiedenmann, J.; Nienhaus, G. U., A photoactivatable marker protein for pulse-chase imaging with superresolution. *Nat Meth* **2010,** *7*, 627-630.

Han, W.-G.; Elstner, M.; Jalkanen, K. J.; Frauenheim, T.; Suhai, S., Hybrid SCC-DFTB/molecular mechanical studies of H-bonded systems and of N-acetyl-(L-Ala)nN′-methylamide helices in water solution. *Int. J. Quantum Chem* **2000,** *78*, 459-479.

Hess, S. T.; Girirajan, T. P. K.; Mason, M. D., Ultra-High Resolution Imaging by Fluorescence Photoactivation Localization Microscopy. *Biophys. J.* **2006,** *91*, 4258-4272.

Konstantin, A.; Lukyanov, D. M.; Chudakov, S. L.; Verkhusha, V. V., Photoactivatable fluorescent proteins. *Nature Reviews Molecular Cell Biology* **2005,** *6*, 885.

Kredel, S.; Nienhaus, K.; Oswald, F.; Wolff, M.; Ivanchenko, S.; Cymer, F.; Jeromin, A.; Michel, F. J.; Spindler, K.-D.; Heilker, R.; Nienhaus, G. U.; Wiedenmann, J., Optimized and Far-Red-Emitting Variants of Fluorescent Protein eqFP611. *Chemistry & biology* **2008,** *15*, 224-233.

Kredel, S.; Oswald, F.; Nienhaus, K.; Deuschle, K.; Röcker, C.; Wolff, M.; Heilker, R.; Nienhaus, G. U.; Wiedenmann, J., mRuby, a Bright Monomeric Red Fluorescent Protein for Labeling of Subcellular Structures. *PLoS ONE* **2009,** *4*, e4391.

Lippert, A. R.; Van de Bittner, G. C.; Chang, C. J., Boronate Oxidation as a Bioorthogonal Reaction Approach for Studying the Chemistry of Hydrogen Peroxide in Living Systems. *Acc. Chem. Res.* **2011,** *44*, 793-804.

Martin, M. E.; Negri, F.; Olivucci, M., Origin, Nature, and Fate of the Fluorescent State of the Green Fluorescent Protein Chromophore at the CASPT2//CASSCF Resolution. *J. Am. Chem. Soc.* **2004,** *126*, 5452-5464.

Matsumoto, M., Advanced chemistry of dioxetane-based chemiluminescent substrates originating from bioluminescence. *Journal of Photochemistry and Photobiology C: Photochemistry Reviews* **2004,** *5*, 27-53.

Merzlyak, E. M.; Goedhart, J.; Shcherbo, D.; Bulina, M. E.; Shcheglov, A. S.; Fradkov, A. F.; Gaintzeva, A.; Lukyanov, K. A.; Lukyanov, S.; Gadella, T. W. J.; Chudakov, D. M., Bright monomeric red fluorescent protein with an extended fluorescence lifetime. *Nat Meth* **2007,** *4*, 555-557.

Nienhaus, K.; Nar, H.; Heilker, R.; Wiedenmann, J. r.; Nienhaus, G. U., Trans−Cis Isomerization is Responsible for the Red-Shifted Fluorescence in Variants of the Red Fluorescent Protein eqFP611. *J. Am. Chem. Soc.* **2008,** *130*, 12578-12579.

Paley, M. A.; Prescher, J. A., Bioluminescence: a versatile technique for imaging cellular and molecular features. *MedChemComm* **2014**.

Patterson, G. H.; Lippincott-Schwartz, J., A Photoactivatable GFP for Selective Photolabeling of Proteins and Cells. *Science* **2002,** *297*, 1873-1877.

Razgulin, A.; Ma, N.; Rao, J., Strategies for in vivo imaging of enzyme activity: an overview and recent advances. *Chem. Soc. Rev.* **2011,** *40*, 4186-4216.

Sauer, M., Reversible molecular photoswitches: A key technology for nanoscience and fluorescence imaging. *Proceedings of the National Academy of Sciences of the United States of America* **2005,** *102*, 9433-9434.

Schäfer, L. V.; Groenhof, G.; Klingen, A. R.; Ullmann, G. M.; Boggio-Pasqua, M.; Robb, M. A.; Grubmüller, H., Photoswitching of the Fluorescent Protein asFP595: Mechanism, Proton Pathways, and Absorption Spectra. *Angew. Chem. Int. Ed.* **2007,** *46*, 530-536.

Shaner, N. C.; Campbell, R. E.; Steinbach, P. A.; Giepmans, B. N. G.; Palmer, A. E.; Tsien, R. Y., Improved monomeric red, orange and yellow fluorescent proteins derived from Discosoma sp. red fluorescent protein. *Nat Biotech* **2004,** *22*, 1567-1572.

Shaner, N. C.; Patterson, G. H.; Davidson, M. W., Advances in fluorescent protein technology. *J. Cell Sci.* **2007,** *120*, 4247-4260.

Subach, F. V.; Piatkevich, K. D.; Verkhusha, V. V., Directed molecular evolution to design advanced red fluorescent proteins. *Nat Meth* **2011,** *8*, 1019-1026.

Tsutsui, H.; Karasawa, S.; Shimizu, H.; Nukina, N.; Miyawaki, A., Semi-rational engineering of a coral fluorescent protein into an efficient highlighter. *EMBO Rep* **2005,** *6*, 233-238.

Wiedenmann, J.; Nienhaus, G. U., Live-cell imaging with EosFP and other photoactivatable marker proteins of the GFP family. *Expert Review of Proteomics* **2006,** *3*, 361-374.

Zimmer, M., GFP: from jellyfish to the Nobel prize and beyond. *Chem. Soc. Rev.* **2009,** *38*, 2823-2832.

Chapter 6: Photochemical response to external forces

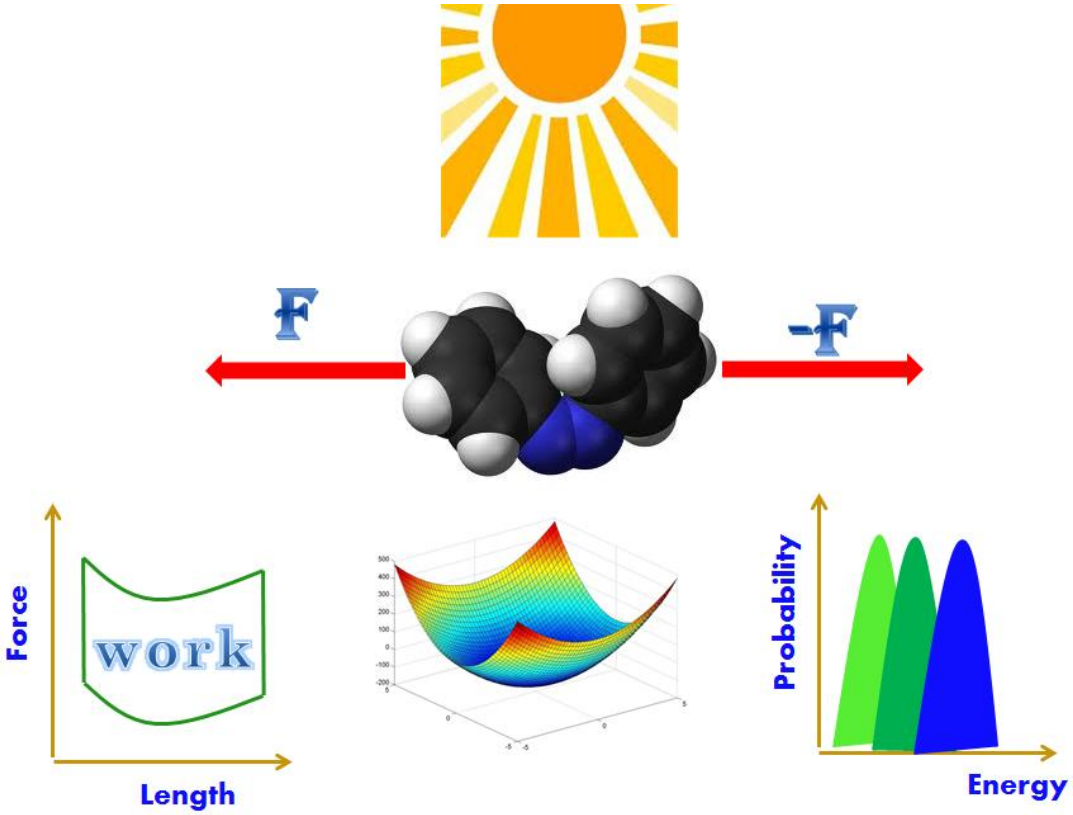

…There was little work left of a routine, mechanical nature. Men's minds were too valuable to waste on tasks that a few thousand transistors, some photoelectric cells, and a cubic metre of printed circuits could perform. There were factories that ran for weeks without being visited by a single human being. Men were needed for trouble-shooting, for making decisions, for planning new enterprises. The robots did the rest.
The existence of so much leisure would have created tremendous problems a century before. Education had overcome most of these, for a well-stocked mind is safe from boredom. The general standard of culture was at a level which would once have seemed fantastic. There was no evidence that the intelligence of the human race had improved, but for the first time everyone was given the fullest opportunity of using what brains they had.

Childhood's End. Arthur Clarke

6.1 Introduction

The modulation of spectroscopical properties can be accomplished based on different approaches, which seek to induce a bathochromic or hypsochromic shift in the spectra. Some of those experimental methods are: chemical modification of the chromophore, application of an external force in the chromophore, change of solvent, adjustment in the pH conditions or mutation in the gen which expressed a protein in the proper case, changing the chemical surrounding. Nevertheless, since those modifications, in general does not follow a well-defined methodology, but rather are random modifications of countless possibilities it will be desirable to establish a procedure in order to accurately determine which kind of modifications produces the desired effect.

In this Ph.D. thesis we have focused on developed a set of methodologies which provides guidelines on the prediction and if possible, the modulation of wavelength absorbed for a general chromophore under the effect of an external force. Firstly, in section 6.2.1 we have tackled the problem of the influence of a substituent on the excitation energy of a chromophore and subsequently in section 6.2.2 we have engaged in a dynamical study of the application of a mechanical external force to a chromophore.

6.1.1 Mechanochemistry

Even though the application of external mechanical forces has been linked to chemistry since its beginning as science (e.g. maceration and grinding of raw materials), it has been only in the last years that it has received attention as a possibility to induce chemical reactions or change physical chemistry properties. Since the introduction of the surface force apparatus in the early 1970's, a new and proliferous experimental field in the researching of the interaction of external forces with molecular systems has bloom. The capacity to measure not only the macroscopic properties of some bulk material under stress, but the ability to follow the breaking of a covalent bond into single molecules, has endowed us with chemical information that was not possible to obtain before, clearing the way to design new simulations. For an extended discussion of the state of the art in Mechanochemistry see: (Balaz, et al. 2013, Beyer and Clausen-Schaumann 2005).

Experimental Methodologies as single-molecule force spectroscopy (SMFS) and scanning tunneling microscopy (STM) alongside with theoretical methodologies have

allowed us to follow different phenomena in a very atomistic detail as: polymeric properties (Caruso, et al. 2009, Holland, et al. 2003, Wiggins, et al. 2012) , optomechanics (Bléger, et al. 2011), peptides conformation (Blanco-Lomas, et al. 2012), bond stability (Helgaker, et al. 2000), switchable conductivity (Wang, et al. 2009) among others.

In this thesis the simulation of applied mechanical forces in molecules is used on the modulation of the energetic gap between the fundamental and the optical brilliant states of some relevant molecules. Of special interest in this thesis is the work generated by molecular motors under the influence of mechanical forces (Hugel, et al. 2002, McCullagh, et al. 2011). Specially we focus on the control of the spectroscopical properties once the molecular switch is subject to external forces transmitted through the linker (*e.g.* covalently bound to a protein or peptide (Blanco-Lomas, et al. 2012, Schierling, et al. 2010), or introduced in the main chain of a polymer systems (Ercole, et al. 2010, Sapich, et al. 2005). More generally, in this thesis we present a new and efficient method to simulate single molecule force spectroscopy of whatever chromophore.

6.2 Results

6.2.1 Structural Substituent Effect

The relation between structure and reactivity which has been in vogue for many years in chemistry since the initial Linear Free Energy Relationship (LFER) of Hammett (Hammett 1937) to the series of improvements and modification to interpret the mechanism of organic reaction in the ground state (Swain and Lupton 1968, Taft 1952) , has been extensively studied and successfully applied to the study of mechanism and catalysis. On the other hand, the substituent effect on the excited states was attempted to rationalize by the Woodward's rules which relates empirically the wavelength of the absorption maximum in UV spectra and the extent of carbon-carbon double bond substitution in conjugated systems (Woodward 1941), but still there is not a clear methodology to predict the excitation energy of substituted chromophores. Therefore, in this Ph.D. thesis it is presented a methodology which predicts the excitation energy of a substituted chromophore based on the structural modifications induces by the substituent on the reference chromophore.

In the case of an organic chomophores, if the substituent does not play an important role in the nature of the excitation state, meaning that the substituent does not have a lone pair of electrons or π orbitals which can resonate with the chromophore, it is possible to analyse the effect substituent on the alteration of the energy absorbed by the chromophore, regarding the substituent as an external force which disrupts the equilibrium of an unsubstituted molecule.

In the work presented in this section, it is shown how the excitation energy can be expressed as function of the some intrinsic parameters of the unsubstituted chromophore, assuming that a quadratic interpolation spanned around the equilibrium geometry of the unsubstituted chromophore can accurately described the structural modifications induces by the substituent. It is then shown that the excitation energy is given by the following expression,

$$E_{exc}^{R} = E_{ES}\left(\boldsymbol{q}_c^{eq}\right) - E_{GS}\left(\boldsymbol{q}_c^{eq}\right) + \left(\Delta\boldsymbol{q}^{R}\right)^{T}\boldsymbol{g}_{ES} + \frac{1}{2}\left(\Delta\boldsymbol{q}^{R}\right)^{T}\left(\boldsymbol{H}_{ES} - \boldsymbol{H}_{GS}\right)\Delta\boldsymbol{q}^{R} \quad (4.2.19)$$

Where *R* stands for properties of the substituted chromophore, $\boldsymbol{q}_c^{eq}$ is the equilibrium structure of the unsubstituted chromophore, $\Delta\boldsymbol{q}^{R}$ is the structural distortion caused by the substituent, $\boldsymbol{g}_{ES}$ is the gradient of the unsubstituted chromophore in the excited state, $\boldsymbol{H}_{GS}$ and $\boldsymbol{H}_{ES}$ are the Hessian matrices for the unsubstituted chromophore for the gradient and excited state, respectively.

According to equation (4.2.19) the change in the excitation energy resulting from the modification of the equilibrium geometry caused by the disruption of the substituent, can be divided in two factors: the distortion along the gradient and perpendicular to it. Subsequently is developed a method to identify the most relevant internal coordinates, being associated directly to the gradient or perpendicular to it.

Afterwards, the method is tested on the family of S-nitrosothiols RSNO which has been shown to store, transport and release nitric oxide (NO) within the mammalian body (Stamler, et al. 1997). Considering the previous results of the mechanism of the photocleavage of the family of S-nitrosothiols, calculated at the CASPT2 level of theory (Marazzi, et al. 2012), it was obtained accurate geometrical structures which together with the methyl nitrosothiol as reference structure , were used to tested the foregoing

methodology. Obtaining both excitation energies and the set of internal coordinates most relevant in the modulation of the absorption wavelength. Finally, it is shown the comparison of the results given by the presented method with respect to *ab initio* calculations, showing the accuracy of the method and the interpretation of the error.

JCTC Journal of Chemical Theory and Computation
Article
pubs.acs.org/JCTC

Structural Substituent Effect in the Excitation Energy of a Chromophore: Quantitative Determination and Application to S-Nitrosothiols

Miguel Ángel Fernández-González, Marco Marazzi, Alberto López-Delgado, Felipe Zapata, Cristina García-Iriepa, Daniel Rivero, Obis Castaño, Manuel Temprado,* and Luis Manuel Frutos*

Departamento de Química Física, Universidad de Alcalá, E-28871 Alcalá de Henares (Madrid), Spain

ABSTRACT: A methodology for the prediction of excitation energies for substituted chromophores on the basis of ground state structures has been developed. The formalism introduces the concept of "*structural substituent excitation energy effect*" for the rational prediction and quantification of the substituent effect in the excitation energy of a chromophore to an excited electronic state. This effect quantifies exclusively the excitation energy variation due to the structural changes of the chromophore induced by the substituent. Therefore, excitation bathochromic and hypsochromic shifts of substituted chromophores can be predicted on the basis of known ground and excited potential energy surfaces of a reference unsubstituted chromophore, together with the ground state minimum energy structure of the substituted chromophore. This formalism can be applied if the chemical substitution does not affect the nature of the electronic excitation, where the substituent effect can be understood as a force acting on the chromophore and provoking a structural change on it. The developed formalism provides a useful tool for quantitative and qualitative determination of the excitation energy of substituted chromophores and also for the analysis and determination of the structural changes affecting this energy. The proposed methodology has been applied to the prediction of the excitation energy to the first bright state of several S-nitrosothiols using the potential energy surfaces of methyl-S-nitrosothiol as a reference unsubstituted chromophore.

I. INTRODUCTION

The substituent effect has become one of the major research topics in physical organic chemistry during the past decades. This fact is due to the need of setting a systematic description of the influence of chemical substitution on physical and chemical molecular properties. In this sense, great strides have been made to explain the effect of different substituents in the description of synthetic, mechanistic, and catalytic properties; in the prediction of chemical reactions and equilibria; and even in the control of agonist/antagonist properties in hormone receptor modulators.[1,2]

In order to make this possible, different relationships between substituent groups and chemical properties have been developed to date. Among them, those providing a quantitative description of these relations are useful tools for predicting and interpreting chemical properties. As a consequence, much emphasis was given to quantitative structure−activity relationships (QSAR) and linear free energy relationships (LFER).

The first empirical quantitative relationship was observed by Hammett (eq 1) in 1937,[3] where a relation between substituted (k) and unsubstituted (k_0) aryl reaction rate constants is proposed to be proportional to the product of a term (ρ) depending on the specific reaction and a term (σ) depending on the specific substituent.

$$\log \frac{k}{k_0} = \rho\sigma \tag{1}$$

He introduced the idea that for any two reactions with two aromatic reactants only differing in the type of substituent (*meta* or *para* positions), the change in Gibbs activation energy is proportional to the change in Gibbs energy. This LFER allowed elucidation of the reaction mechanism concerning the ionization of substituted benzoic acids. Subsequent modifications of the Hammett equation were proposed. The Swain−Lupton equation[4] emerged from the idea of Swain and Lupton that two variables are enough (taking into account resonance effects and field effects) to describe the effects of any substituent, therefore redefining the Hammett's substituent parameter, σ. Other modifications to the Hammett equation are the Taft equation,[5−7] which describes the steric effects of a substituent apart from field, inductive, and resonance effects, and the Yukawa−Tsuno equation,[8] which introduces a new term to the original Hammett relationship that reflects the extent of resonance stabilization for a reactive structure that enhances the transition state's charge. These LFERs were found to be useful tools in interpreting and predicting organic reactions and their mechanisms in the ground state.

Moreover, the substituent effect has important consequences in processes involving excited states, such as the variation of the maximum absorption wavelength of a given chromophore. The prediction of this spectroscopical property, and its eventual modulation, is of special interest in the development of photochromic compounds used as photoresponsive materials,[9] materials with nonlinear optical properties,[10] organic light-emitting diodes,[11,12] etc. In some cases, the Hammett equation has successfully correlated the rates of some reactions in the excited state for a series of molecules differently substituted

Received: July 13, 2012
Published: August 21, 2012

dx.doi.org/10.1021/ct300597u | J. Chem. Theory Comput. 2012, 8, 3293−3302

with the Hammett constants of the same substituents derived for reactions proceeding in the ground state. Instead, in other cases, it has been observed that the influence of the substituent on the photochemical reaction is different from that found in the ground state,[13] and subsequently $\sigma^{h\nu}$,[14] $\sigma_{ex,}$[15,16] σ^{*},[17,18] $\sigma^{\bullet h\nu}$,[19] and σ_{cc}^{ex20} parameters were introduced as an attempt to describe photochemical substituent effects. As an additional attempt, the Hammett equation has been reformulated in order to correlate the substituent effect with the absorption frequency,[21] in any case leaving the application of the Hammett equation to the description of excited state properties as a non-prominent *trial and error* methodology.

Nevertheless, different empirical rules were developed in order to rationalize substituent effects in chromophores: the Woodward rules are among the most outstanding empirical rules in the study of chemical reactivity in organic chemistry. Woodward demonstrated that the wavelength of the absorption maximum in the UV spectra is strictly correlated with the extent of the carbon−carbon double bond substitution in conjugated systems, including carbonyl compounds, mono/disubstituted benzene derivates, and benzoyl derivatives.[22] These rules have been extensively applied, broadly studied, and expanded by Fieser et al.[23] and Scott[24] by adding a considerable amount of experimental data. Another empirical rule to calculate the absorption band maxima and extinction coefficients of conjugated molecules, especially polyenes, is the Fieser−Kuhn rule,[25] which complements Woodward−Fieser rules that are applicable only to molecules with one to four conjugated double bonds.

Here, we present a general methodology for the prediction of absorption energies in substituted chromophores, focusing on the structural modifications that the substituent causes, with respect to the unsubstituted chromophore. After defining the substituent structural effect with respect to the vertical excitation energy, the methodology is formally developed, realizing how the substituent effect can be used to properly tune the absorption spectra of a molecule and determining which internal coordinates control the excitation energy modulation.

The developed methodology is applied to S-nitrosothiols (RSNOs), a family of compounds of biological and medical relevance for their capability to release nitric oxide (NO) when irradiated in the visible and UV regions,[26−29] therefore making the study of the S−N photocleavage attractive for possible use in phototherapy.[30,31] We recently studied the absorption energy required to initiate photocleavage in a wide variety of RSNOs, showing the possibility of NO release modulation as a function of the substituent.[32]

II. DEVELOPED METHODOLOGY

Substituent Structural Effect and Excitation Energy. Chemical substitution of a given chromophore can alter different physical and chemical properties of the chromophore. Among these properties, the molecular structure is usually affected by substituent groups. These structural changes can affect, in general, all the internal coordinates of the chromophore and can induce modifications on the relative stability of some electronic excited states regarding the ground state. Moreover, if the substituent does not participate in the excitation (i.e., the promoted electrons do not involve orbitals with significant contribution of the substituent), it is expected that the nature of the considered excited electronic state will not change. This situation is quite common, for example when the excited state of a chromophore has a given nature (e.g., π,π^*), and the substituent does not present electrons participating in the excitation, (e.g., no conjugated π electrons). This concept is also present in the widely used multiconfigurational method CASSCF (Complete-Active-Space Self-Consistent-Field),[33] where the selected active space must include those occupied molecular orbitals participating in the electronic excitations, and therefore defining the nature of the excited state to be studied.

In this work, we focus on this situation, where the substituent has no significant effect on the nature of the studied excited state and also does not participate in the excitation itself. Within this premise, which defines the applicability limits of the developed methodology, it is possible to analyze the effect of the structural changes due to chemical substitution, and their effect on the excitation energy.

It is possible to formally divide the molecular entity (chromophore-substituent) into two fragments, being the electronic energy of the system in the ground state (E_{GS}) equal to

$$E_{GS} = E_{GS}^{chrom} + E_{GS}^{subs} + E_{GS}^{chrom/subs} \quad (2)$$

where E_{GS}^{chrom} is the electronic energy of the chromophore, E_{GS}^{subs} is the corresponding energy of the substituent, and $E_{GS}^{chrom/subs}$ is the energy of interaction between both parts of the molecule with all terms referred to the ground state.

Likewise, the energy of the excited state is given by

$$E_{ES} = E_{ES}^{chrom} + E_{GS}^{subs} + E_{GS}^{chrom/subs} \quad (3)$$

Note that the excitation is "localized" in the chromophore (as we assume that the substituent is not participating), and therefore the substituent term is the one corresponding to the ground-state since the energy stabilization/destabilization caused by the substituent is essentially identical for both ground and excited states (i.e., we assume that $E_{GS}^{subs} = E_{ES}^{subs}$). Furthermore, as discussed above, considering only substituents not affecting the excitation significantly, the chromophore-substituent energy term has to be essentially equal for both states ($E_{ES}^{chrom/subs} = E_{GS}^{chrom/subs}$). The larger the extent of validity of this equality, the higher the accuracy of the obtained results from the present formalism.

The excitation energy (E_{exc}) can be easily obtained by subtracting eq 2 from eq 3:

$$E_{exc} = E_{ES} - E_{GS} = E_{ES}^{chrom} - E_{GS}^{chrom} \quad (4)$$

This expression indicates that if the substituent does not contribute differentially to the relative stabilization/destabilization of the ground and excited states, the excitation energy will be governed by the intrinsic properties of the chromophore moiety. Nevertheless, it has to be noted that even if the excitation energy is correctly described by the intrinsic properties of the chromophore, the absolute energy of each state is not. Thus, the ground state of the molecule is affected by the presence of the substituent; specifically it will have an effect on the ground state structure of the molecule. Taking into account the Born−Oppenheimer approximation, every energy term in eq 2 and eq 3 will depend on the molecular coordinates of the chromophore ($\mathbf{q}_c$), substituent ($\mathbf{q}_s$), or both ($\mathbf{q}_c;\mathbf{q}_s$). Therefore, if we take the first derivatives of the energy for the ground electronic state (eq 2), we obtain

Journal of Chemical Theory and Computation Article

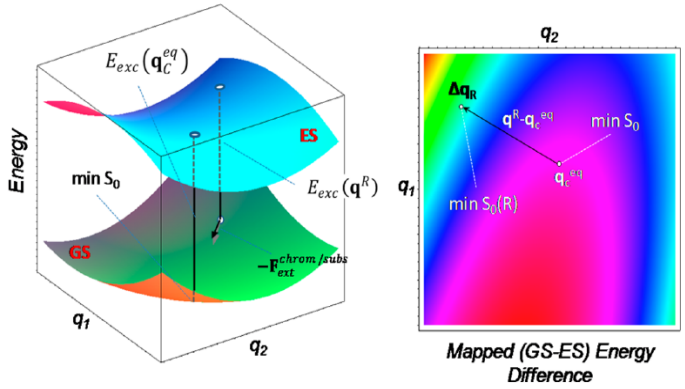

Figure 1. Left: Schematic potential energy surfaces for the ground state (GS) and excited state (ES) of an unsubstituted chromophore as a function of two of its coordinates (q_1, q_2). The substituent provokes a change of the molecular structure from $\mathbf{q}_C^{eq}$ to $\mathbf{q}^R$, which can be explained in terms of the effect of an external force ($\mathbf{F}_{ext}^{chrom/subs}$) acting on the chromophore due to the presence of the substituent. This structural change in the chromophore provokes a shift of the excitation energy from $E_{exc}(\mathbf{q}_C^{eq})$ to $E_{exc}(\mathbf{q}^R)$. Right: Color-mapped excitation energy for the chromophore as a function of the same two coordinates (q_1, q_2). The excitation energy changes due to the substituent effect on the structure of the chromophore, from the unsubstituted chromophore geometry ($\mathbf{q}_C^{eq}$) to the "R" substituted structure ($\mathbf{q}^R$) corresponding to a change of the ground state equilibrium structure from min S_0 to min S_0(R).

$$\nabla E_{GS}(\mathbf{q}_c;\mathbf{q}_s) = \nabla E_{GS}^{chrom}(\mathbf{q}_c) + \nabla E_{GS}^{subs}(\mathbf{q}_s) + \nabla E_{GS}^{chrom/subs}(\mathbf{q}_c;\mathbf{q}_s) \quad (5)$$

The equilibrium geometry of the ground state must fulfill $\nabla E_{GS}(\mathbf{q}_c;\mathbf{q}_s) = 0$. Since we are only interested in the chromophore structure (as the excitation energy only depends on the chromophore), it is straightforward to obtain eq 6 for the equilibrium structure of the molecule.

$$\nabla E_{GS}^{chrom}(\mathbf{q}_c) - \mathbf{F}_{ext}^{chrom/subs} = \mathbf{0} \quad (6)$$

where the term $\mathbf{F}_{ext}^{chrom/subs}$ is interpreted as an external force provoked by the effect of the substituent ($\nabla E_{GS}^{chrom/subs}(\mathbf{q}_c;\mathbf{q}_s)$ term). This external force induced by the substituent is characteristic of the specific chromophore/substituent couple and provokes the displacement of the equilibrium structure of the substituted chromophore regarding the unsubstituted chromophore. The new ground state equilibrium structure of the chromophore is determined by the $\mathbf{F}_{ext}^{chrom/subs}$ force, which exerts a displacement of the energy minimum to a new configuration where $\nabla E_{GS}^{chrom}(\mathbf{q}_c)$ equals $\mathbf{F}_{ext}^{chrom/subs}$ (Figure 1), consequently altering the potential energy surface shape by displacing the minimum. The solution to eq 6 provides the chromophore structure with the attached substituent (R). Finally, by knowing the structure of the substituted chromophore, it is straightforward to predict the excitation shift by using eq 4, which will depend only on the new coordinates of the chromophore under the substituent effect. This procedure is explained in Figure 1.

Substituent Absorption Tuning from Chromophore Potential Energy Surfaces (PESs). As discussed above, if the effect of the substituent in the chromophore is limited to provoke some structural changes but does not affect the nature of the electronic excitation, the electronic transition energy depends only on the new equilibrium structure of the substituted chromophore. Under this assumption, it is possible to predict, avoiding direct *ab initio* calculation, the excitation energy of the substituted chromophore just by correct knowledge of the following information: (i) the ground state structure of the substituted chromophore and (ii) to some extent the PESs (ground and excited) of the unsubstituted chromophore. Usually, the former can be easily obtained with *ab initio* calculations in the ground state; nevertheless, different approaches can be employed in order to have the ground and excited PESs of the unsubstituted chromophore. In the current work, we have used a quadratic approximation of the PESs involved in the excitation to describe the topology of the surfaces.

By using this approximation, the energy of the ground and excited states of the unsubstituted chromophore species can be expanded taking the ground state equilibrium geometry ($\mathbf{q}_C^{eq}$) as the origin according to eq 7 and eq 8.

$$E_{GS}(\Delta\mathbf{q}) = E_{GS}(\mathbf{q}_C^{eq}) + \frac{1}{2}\Delta\mathbf{q}^T\mathbf{H}_{GS}\Delta\mathbf{q} \quad (7)$$

$$E_{ES}(\Delta\mathbf{q}) = E_{ES}(\mathbf{q}_C^{eq}) + \Delta\mathbf{q}^T\mathbf{g}_{ES} + \frac{1}{2}\Delta\mathbf{q}^T\mathbf{H}_{ES}\Delta\mathbf{q} \quad (8)$$

where $\Delta\mathbf{q} = \mathbf{q} - \mathbf{q}_C^{eq}$ is the displacement coordinate vector regarding the ground state equilibrium geometry ($\mathbf{q}_C^{eq}$) for the unsubstituted chromophore, $\mathbf{H}_{GS}$ and $\mathbf{H}_{ES}$ are the Hessian matrices for both states calculated for this geometry, and $\mathbf{g}_{ES}$ is the energy gradient vector in the excited state, also evaluated for the same geometry.

Therefore, according to eqs 7 and 8, the excitation energy for any configuration of the chromophore $E_{exc}(\Delta\mathbf{q})$ is given by eq 9.

$$\begin{aligned} E_{exc}(\Delta\mathbf{q}) &= E_{ES}(\Delta\mathbf{q}) - E_{GS}(\Delta\mathbf{q}) \\ &= E_{ES}(\mathbf{q}_C^{eq}) - E_{GS}(\mathbf{q}_C^{eq}) + \Delta\mathbf{q}^T\mathbf{g}_{ES} \\ &\quad + \frac{1}{2}\Delta\mathbf{q}^T(\mathbf{H}_{ES} - \mathbf{H}_{GS})\Delta\mathbf{q} \end{aligned} \quad (9)$$

Finally, knowing all the parameters in eq 9 ($E_{ES}(\mathbf{q}_C^{eq})$, $E_{GS}(\mathbf{q}_C^{eq})$, $\mathbf{g}_{ES}$, $\mathbf{H}_{ES}$, and $\mathbf{H}_{GS}$), the ground state equilibrium structure for the "−R" substituted chromophore ($\mathbf{q}^R$), and therefore the structural displacement $\Delta\mathbf{q}^R = \mathbf{q}^R - \mathbf{q}_C^{eq}$, it is possible to predict the excitation energy of the "−R" substituted chromophore (E_{exc}^R) according to eq 10.

dx.doi.org/10.1021/ct300597u | J. Chem. Theory Comput. 2012, 8, 3293−3302

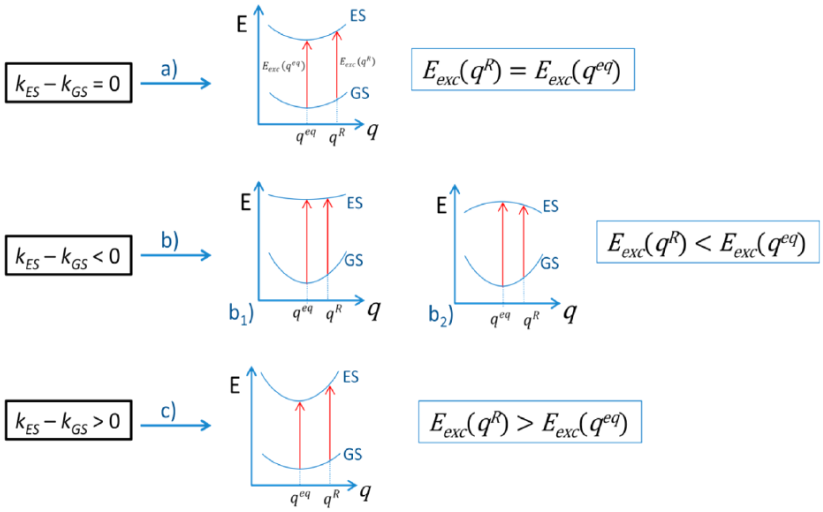

Figure 2. The possible energy difference (excited-ground) force constants (k). Three different cases are possible when distorting the equilibrium structure ($\mathbf{q}^{eq}$) along the corresponding eigenvector ($\mathbf{q}$) to reach the equilibrium geometry for the substituted chromophore ($\mathbf{q}^{R}$): the excitation energy (E_{exc}) does not change significantly (case a); reduction of the excitation energy with positive and negative excited state curvature (cases b_1 and b_2, respectively); increase of the excitation energy (case c).

$$E_{exc}^{R} = E_{ES}(\mathbf{q}_C^{eq}) - E_{GS}(\mathbf{q}_C^{eq}) + (\Delta\mathbf{q}^{R})^T\mathbf{g}_{ES} + \frac{1}{2}(\Delta\mathbf{q}^{R})^T(\mathbf{H}_{ES} - \mathbf{H}_{GS})\Delta\mathbf{q}^{R} \quad (10)$$

Therefore, by using high-level *ab initio* derived PESs and computing ground state structures of substituted chromophores with an affordable method, it is possible to predict (applying eq 10) the excitation energy of a series of substituted chromophore derivatives.

Determination of the Coordinates Controlling the Excitation Energy. According to the discussed methodology, it is possible to have a computationally saving estimation of the excitation energy of a given substituted chromophore on the basis of quadratic ground and excited state PESs of the unsubstituted chromophore—calculation made only once for a given chromophore—and the ground state equilibrium geometry of a substituted chromophore—one calculation in the ground state for each substituent. Moreover, we can take advantage of this situation to analyze the role of each molecular coordinate by predicting their efficiency in modulating the energy gap. According to eq 10, the first order variation of the excitation energy gap is given by the excited state gradient vector ($\mathbf{g}_{ES}$), which will be predominant for small displacements of the substituted chromophore structure. Nevertheless, the second order term in the excitation energy variation (last term in eq 10) can be also relevant, especially when the substituent induces distortions in the ground state that are orthogonal to the energy gradient vector, or when the gradient vector itself ($\mathbf{g}_{ES}$) tends to vanish.

In order to analyze this effect, it is useful to separate the coordinates into two subsets, one corresponding to the energy gradient vector and the rest of coordinates orthogonal to it. The energy gradient vector coordinate provides the first-order correction to the energy difference along $\mathbf{g}_{ES}$, while those orthogonal to $\mathbf{g}_{ES}$ provide the second-order energy gap variation through a projected Hessian difference matrix ($\mathbf{H} \equiv \mathbf{H}_{ES} - \mathbf{H}_{GS}$) which can be obtained by using a projection operator as shown in eq 11.

$$\mathbf{H}^{P} = \mathbf{PHP} \quad (11)$$

where $\mathbf{P}$ is the projector operator defined by

$$\mathbf{P} = \mathbf{I} - \mathbf{g}_{ES}^{N}(\mathbf{g}_{ES}^{N})^T \quad (12)$$

where $\mathbf{I}$ is the identity matrix with $N - 1$ elements, N being the number of molecular coordinates, and $\mathbf{g}_{ES}^{N}$ is the normalized excited state gradient vector . The eigenvalues of the projected Hessian difference ($\mathbf{H}^{P}$) provide the set of force constants difference between ground and excited states ($k_{ES} - k_{GS}$). Close to zero eigenvalues denote that distortions along the corresponding eigenvectors do not provide significant change of the excitation energy (Figure 2, case a). However, negative eigenvalues are related to reduction of the excitation energy (Figure 2, cases b1 and b2) while positive eigenvalues are related to an increase of the energy gap (Figure 2, case c) when structural changes take place along the corresponding eigenvectors. With this information, it is possible to rationalize the influence of the different internal coordinates of a chromophore in tuning the excitation energy.

Electronic-Structure Methods. The implementation of the methodology discussed above has been tested for the prediction of the excitation energy of a wide family of S-nitrosothiol derivatives. All S-nitrosothiol structures, except S-nitrosoglutathione, have been taken from ref 32, all of them being optimized on the ground state at the B3P86 level (Becke's three-parameter hybrid exchange along with Perdew's nonlocal correlation functionals) and calculating the excitation energy by time dependent treatment of the same functional (TD-DFT), as implemented in the Gaussian09 suite of programs.[34] In all cases, a 6-311+G(2df) basis set was applied. This method has been proven to predict excitation energies in good agreement with high-level multiconfigurational methods as Complete Active Space Perturbation Theory to Second Order (CASPT2).[35,36] The analytical PESs for the ground and excited states of *syn*- and *anti*-methyl-S-nitrosothiol have been constructed from energy gradients and Hessians determined at the ground state minima. Numerical Hessians have been

computed in the case of excited state, while analytical Hessians have been determined for the ground state.

III. APPLICATION TO S-NITROSOTHIOL DERIVATIVES

S-nitrosothiols are a family of compounds where the chromophore corresponds to the −SNO terminal fragment (see Figure 3). The partial double bond character of the S−N bond, caused by delocalization of the sulfur lone pairs in the nitroso group, makes possible the existence of two different RSNO ground state conformers: *syn* and *anti*.[37] In spite of their usual instability at room temperature, the main interest about RSNOs concerns their ability to release nitric oxide (NO), a molecule of fundamental importance in medicine and biology.[38−48] Especially, the generation of NO as a stable radical by irradiating RSNOs at a specific wavelength (i.e., photochemical rupture of the S−N bond) is of potential interest in phototherapy.[29]

Figure 3. *Anti* (left) and *syn* (right) methyl-S-nitrosothiol ground state equilibrium structures at the B3P86/6-311+G(2df) level of theory. The main geometrical parameters are shown.

One of the simplest members of this family of molecules is methyl-S-nitrosothiol (CH_3SNO, see Figure 3), which was studied theoretically but not experimentally, because of the intrinsic instability shown by the compound.[37,49−51] We have taken this compound as the representative model chromophore for building up the reference PESs (ground and excited state). As already described by the authors, after irradiation of CH_3SNO to the bright state (S_2 corresponding to a $^1(\pi,\pi^*)$ state), the minimum energy paths lead to a barrierless photocleavage process resulting in the formation of $CH_3S^\bullet$ and $^\bullet NO$ radicals. This implies that an ultrafast process is expected, making possible a modulation of the NO release only by modulation of the vertical excitation energy required to initiate photocleavage.[32]

In the following, the construction of the PESs for ground and excited electronic states is described, and the coordinates modulating the energy gap are identified. Finally, a series of S-nitrosothiols are studied, determining the excitation energy predicted on the basis of CH_3SNO PESs and ultimately compared with the excitation energy directly computed by the above-described TD-DFT methodology.

The PESs of Methyl-S-nitrosothiol. CH_3SNO has two conformations in the ground state, *syn* and *anti* conformers (see Figure 3), where the most relevant structural difference is related to the CSNO dihedral angle (∼0° and ∼180° for *syn* and *anti* isomers respectively). The absorption spectra for *syn* and *anti* CH_3SNO were previously reported by the authors at the MS-CASPT2/ANO-L level of theory.[32] For both conformers, the two lowest-energy vertical excitations ($S_0 \rightarrow S_1$ and $S_0 \rightarrow S_2$) correspond to optically dark $^1(n,\pi^*)$ and bright $^1(\pi,\pi^*)$ transitions, respectively. More in detail, the absorption spectrum of *syn* CH_3SNO is characterized by a $S_0 \rightarrow S_1$ transition at 530 nm and a $S_0 \rightarrow S_2$ transition at 330 nm, while a red shift in *anti* CH_3SNO sets the $S_0 \rightarrow S_1$ transition at 600 nm and the $S_0 \rightarrow S_2$ transition at 342 nm. For both conformers, the $S_0 \rightarrow S_2$ transition is associated with a much higher oscillator strength than for $S_0 \rightarrow S_1$ (higher by a factor 33 and 28 for *syn* and *anti* CH_3SNO, respectively). The present study is focused

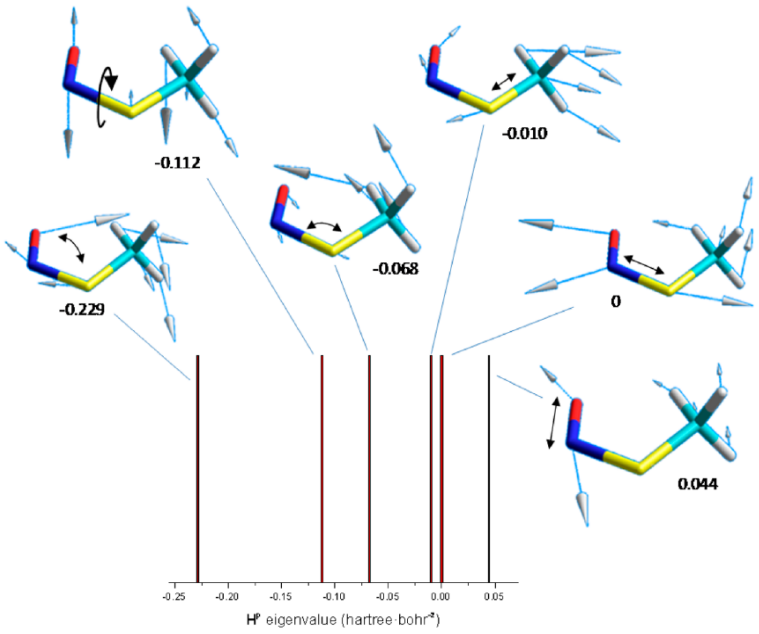

Figure 4. *Syn*-methyl-S-nitrosothiol projected Hessian difference ($\mathbf{H}^P$) eigenvectors and eigenvalues in hartree·bohr^{-2}. The eigenvalue spectrum is displayed with vertical bars, where the $\mathbf{H}^P$ eigenvalue (x axis) indicates the different ability to modify the energy gap (positive for hypsochromic shift and negative for bathochromic shift). The main coordinates associated with each eigenvector are shown with black arrows.

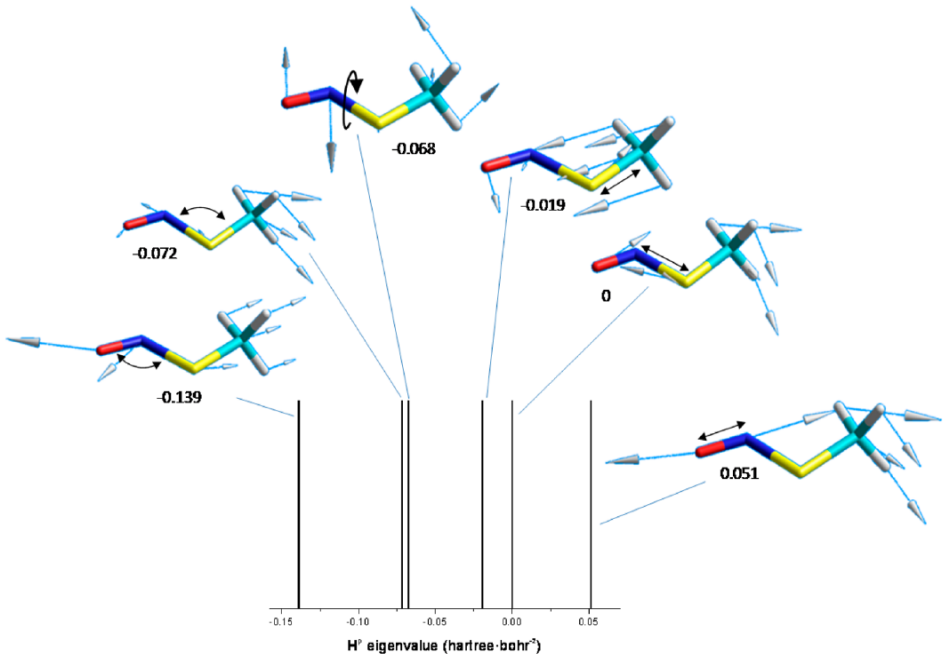

Figure 5. *Anti*-methyl-S-nitrosothiol projected Hessian difference ($\mathbf{H}^P$) eigenvectors and eigenvalues in hartree·bohr^{-2}. The eigenvalue spectrum is displayed with vertical bars, where the $\mathbf{H}^P$ eigenvalue (x axis) indicates the different ability to modify the energy gap (positive for hypsochromic shift and negative for bathochromic shift). The main coordinates associated with each eigenvector are shown with black arrows.

on the prediction of the lowest-energy bright $^1(\pi,\pi^*)$ transition of a series of differently substituted RSNOs.

In order to explore the role of the internal coordinates controlling the $S_0 \rightarrow S_2$ excitation energy, we have determined the second order approximated PESs of both conformers: the excitation energies, the energy gradient vectors, and the projected Hessian difference, $\mathbf{H}^P$ (see eq 11), as well as its eigenvalues and eigenvectors. The later magnitudes provide the directions orthogonal to the excited state gradient vector modulating the $S_0 \rightarrow S_2$ energy gap, while the corresponding eigenvalues quantify the extent of the energy gap variation. Negative eigenvalues of the projected Hessian difference (note that the Hessian difference matrix is defined as $\mathbf{H} \equiv \mathbf{H}_{S_2} - \mathbf{H}_{S_0}$, where ES stands for S_2 and GS for S_0 in Figure 2) are related to distortions where the force constant in S_0 is larger than that of S_2, and consequently, displacements along the corresponding eigenvectors reduce the $S_0 \rightarrow S_2$ excitation energy. On the other hand, positive eigenvalues are related to eigenvectors providing an increase of the energy gap.

Using a minimal set of internal coordinates for the chromophore, the *syn*-methyl-S-nitrosothiol $\mathbf{H}^P$ matrix shows eigenvalues raging from −0.229 to 0.044 hartree·[bohr(rad)]$^{-2}$, indicating that an energy gap increase and decrease can be achieved not only by distortions along the excited state energy gradient vector but also along different coordinates (see Figure 4). On one hand, the excited state energy gradient vector is mainly associated with S−N stretching (corresponding to an eigenvector of the projected Hessian difference with zero eigenvalue). On the other hand, the eigenvectors of $\mathbf{H}^P$ can be associated, to a large extent, with single internal coordinates. The highest eigenvalues (0.044, 0.0, and −0.01) are related to stretching coordinates (N−O, S−N, and C−S, respectively) while the lowest eigenvalues (−0.068, −0.112, and −0.229) correspond to eigenvectors that are mostly related to CSN bending, CSNO torsion, and SNO bending, respectively. With these results, a clear picture of the energy gap variation can be obtained: lowering the $S_0 \rightarrow S_2$ energy gap can be reached by increasing the S−N distance (gradient contribution) and by changing (decrease or increase) the N−O distance (second order contribution). However, an increase of the energy gap is possible by decreasing the S−N distance (gradient contribution) and mainly by varying bendings (CSN and SNO) and torsion (CSNO) and, to a lesser extent, by changing the C−S bond distance.

Similar behavior is observed for the *anti* isomer (see Figure 5). The energy gradient vector is also dominated by the S−N stretching, and the ordering of the corresponding eigenvalues of the projected Hessian difference is equivalent: bendings, torsions, and stretchings in ascending order of the corresponding eigenvalue. Therefore, in order to increase the excitation energy, the coordinates that are able to modulate the energy are the energy gradient vector, mainly described by S−N stretching (by decreasing the S−N distance), while N−O distance variation (increase or decrease) also permits the $S_0 \rightarrow S_2$ energy gap increase. On the other hand, in order to reduce the energy gap, different coordinates can contribute: the increase of the S−N distance (gradient contribution) and the variation of SNO and CSN bendings as well as CSNO torsion and C−S stretching. Of course, the eigenvalues of the diagonal $\mathbf{H}^P$ matrix provide just the excitation energy modulation efficiency of each coordinate per unit displacement. Nevertheless, in order to understand the specific effect of a given substituent, the amplitude of the distortion induced by this substituent has to be taken into account explicitly, obtaining the concrete energy gap variation due to each coordinate.

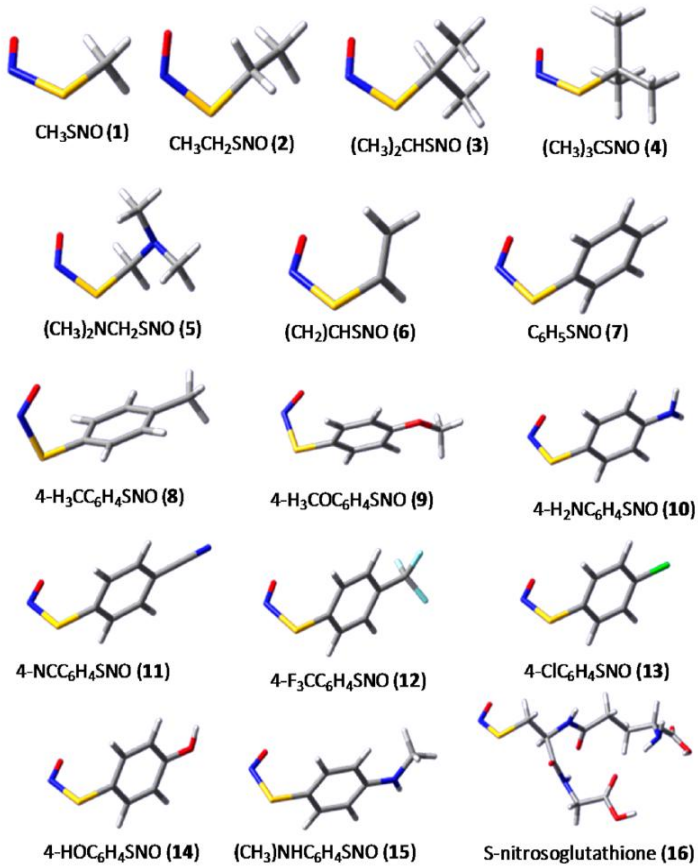

Figure 6. *syn*-S-nitrosothiol derivatives studied (same derivatives for *anti* conformers).

It is therefore concluded that the energy gradient has the same nature for both conformers and is described mainly by C−S stretching. The variation of this coordinate provides a first-order variation of the energy gap, making possible to decrease (or increase) this gap by shortening (enlarging) the C−S distance. Analyzing the second order energy variation, bendings are effective in decreasing the $S_0 \rightarrow S_2$ excitation energy, as well as torsion and, to a lesser extent, the C−S distance. However, the N−O distance variation provokes an increase of the energy gap for both isomers. Finally, the *syn* conformer shows a higher capacity to decrease the energy gap by structural distortions in comparison to the *anti* conformer (as is evident from the higher negative eigenvalues of $\Delta \mathbf{H}^{p}$ for the *syn* conformation) while the *anti* conformers show a slightly higher capacity to increase the energy gap.

Excitation Energy Prediction for Substituted S-Nitrosothiols. In order to study the substituent effect on the $S_0 \rightarrow S_2$ energy gap for S-nitrosothiols, we have previously determined the excitation energy for a wide variety of substituted RSNOs: primary, secondary, and tertiary substituted (i.e., alkyl); vinyl; and aryl RSNOs.[32] In Figure 6, the ground state minima (B3P86/6-311+G(2df) level of theory) of different S-nitrosothiols are shown. All kinds of substitution do not affect the nature of the excitation, therefore making it possible to use the developed formalism to study the excitation energy tuning on the basis of structural distortions of the chromophore. Moreover, it was previously shown that aryl substituents do not expand the π-conjugation of the −SNO chromophore, since the aryl group and the −SNO moiety always form a dihedral angle between them ranging from 50 to 90°.[32] Nevertheless, in order to minimize the aryl π-conjugation and being able to measure the structural effect of the substituent, we have restrained to 90° the torsion of those derivatives which are not completely orthogonal. Therefore, these minimum energy conformations completely out of planarity keep the −SNO fragment as the unique chromophore, ranging the absorption maxima for the different substituted derivatives from 350 to 290 nm.[32]

The optimized structures on the ground state have been compared with the reference chromophore (CH_3SNO) and the corresponding structural changes interpreted in terms of the coordinates controlling the excitation energy variation. Finally, on the basis of the ground state optimized structures for the different derivatives, the excitation energies are predicted by using the information of the CH_3SNO PESs.

Before doing the analysis of the structural effect on the excitation energy, the second order approximation made for ground and excited states of the CH_3SNO reference compound has been tested. In this regard, the ground state equilibrium structure coordinates of each derivative have been transferred to CH_3SNO PESs, resulting in a differently distorted CH_3SNO structure for each RSNO. The excitation energy of each "distorted" CH_3SNO was calculated and compared to that obtained from analytical PESs according to the procedure developed in this work (see Figure 7). The correlation between

both magnitudes is quantitative, showing the predictive quality of the second order approximation of the PESs employed.

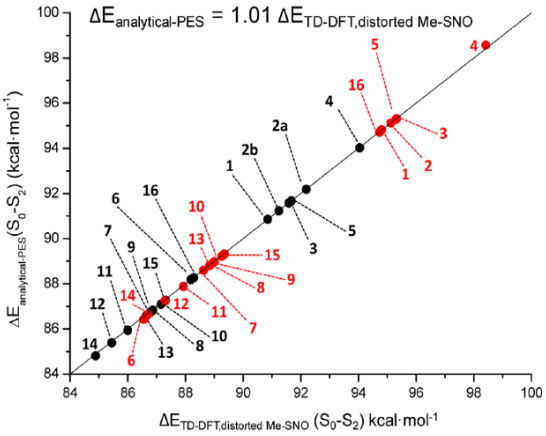

Figure 7. TD-DFT excitation energies of the different distorted Me-SNO (**1**) structures (fitting the corresponding optimized RSNO structures), versus the predicted excitation energies obtained from analytical PESs (black dots, *anti* derivatives; red dots, *syn* derivatives). The correlation shows quantitative agreement in the predictions made on the basis of analytical PESs for Me-SNO (see Figure 6 for numbering).

Finally, the excitation energies of the R-SNO derivatives have been predicted by using the corresponding optimized structures in the ground-state, applying the developed formalism, and then compared with those directly determined with TD-DFT calculations. The excitation energies obtained from analytical PES render exclusively the structural effect of the substituent (i.e., the chromophore structural change induced by the substituent) in the excitation energy. Therefore, the comparison of this energy with that obtained from TD-DFT calculations provides the quantification of the structural role of the substituent in tuning the excitation energy. The correlation between both energies is remarkable, indicating the principal role of the structural substituent effect in tuning S-nitrosothiol excitation energy. In fact, linear regression of these data (see Figure 8) gives a suitable correlation between predicted and TD-DFT computed excitation energies. Since both correlation lines cross the CH_3SNO reference, the slope of the correlation can be easily interpreted as the contribution of the structural substituent effect to the excitation energy variation. In this way, for *syn* derivatives the linear regression provides a slope equal to 0.82, indicating that, on average, 82% of the excitation energy variation is due to the effect of the substituent in the structure of the CSNO chromophore. In the case of *anti* derivatives, this effect rises to 89%.

As previously described, the developed methodology is useful not only to predict the role of the structural effect of a substituent on the excitation energy but also to identify and quantify the role of each coordinate of the chromophore in tuning the transition energy. In this regard, from methyl-S-nitrosothiol PESs analysis, we have obtained the potential role of each internal coordinate of the chromophore in tuning the $S_0 \rightarrow S_2$ excitation energy (*vide supra*). It has to be noted that, at second order, all the coordinates except one (N−O stretching) provide a reduction of the energy gap. Therefore, it is not odd to find that most of the derivatives reduce the energy gap.

We have analyzed the role of each internal coordinate of the chromophore in controlling the excitation energy for all the substituted S-nitrosothiols. The energy gradient component, related mainly to the S−N stretching, is the most important coordinate in tuning the energy gap of S-nitrosothiols (see Figure 9), representing 86% to 99% of the total excitation energy variation, second order contributions being less important (see Figure 10).

The energy gap variation due to the energy gradient ranges from ca. −6 to 3 kcal·mol^{-1} in the case of *anti*-S-nitrosothiols, and from ca. −8 to 4 kcal·mol^{-1} in the case of *syn*-S-nitrosothiols. Moreover, only alkyl derivatives show an energy gap increase, while for vinyl and aryl derivatives the excitation energy is reduced as compared to that of methyl-S-nitrosothiol. Interestingly, for *anti*-S-nitrosoglutathione, which should be more similar to alkyl-derivatives, the energy gap is significantly reduced, indicating an increase of the S−N distance.

Although second order terms in eq 10 are significantly lower than first order contributions, it can be realized that the N−O bond length is the only coordinate able to increase the energy gap (see Figure 10) in both *syn*- and *anti*-S-nitrosothiols, the

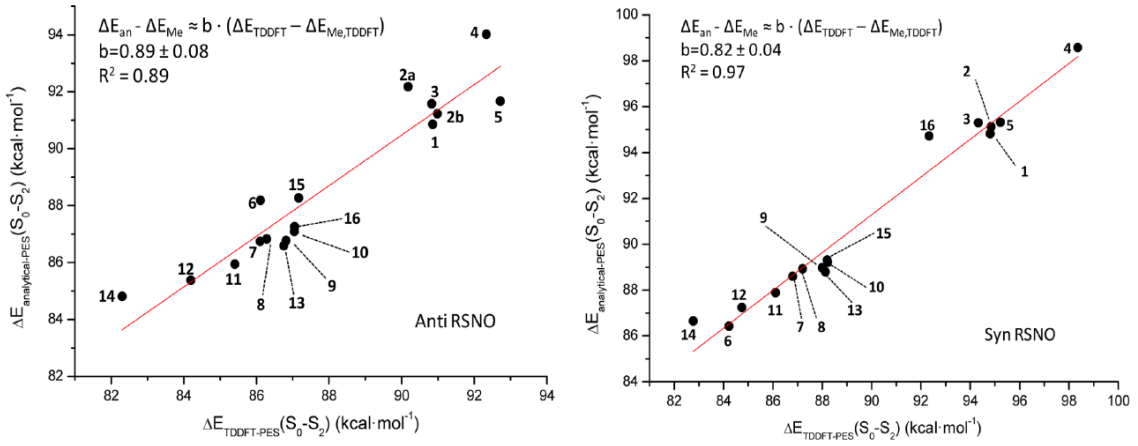

Figure 8. *Anti* (left) and *syn* (right) S-nitrosothiol excitation ($S_0 \rightarrow S_2$) energies obtained from analytical PESs of CH_3SNO versus the computed excitation energies of each S-nitrosothiol derivative (see Figure 6 for numbering).

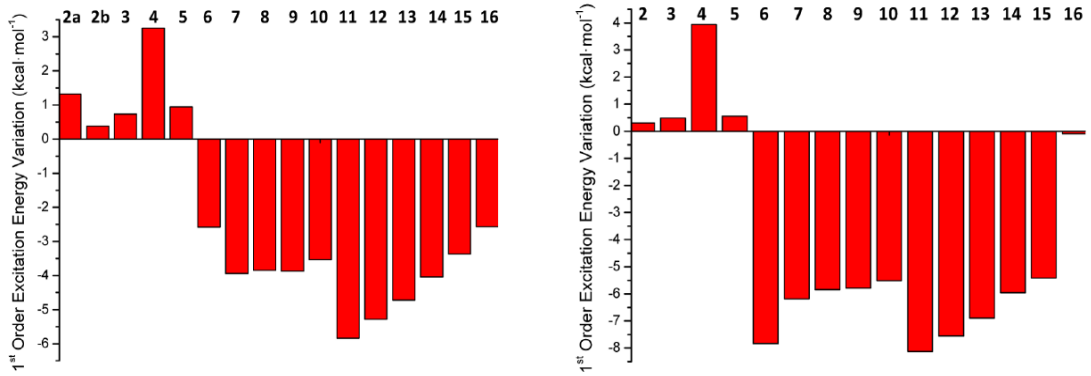

Figure 9. *Anti* (left) and *syn* (right) S-nitrosothiol excitation energy variation with respect to CH_3SNO due to first order (energy gradient component) contribution.

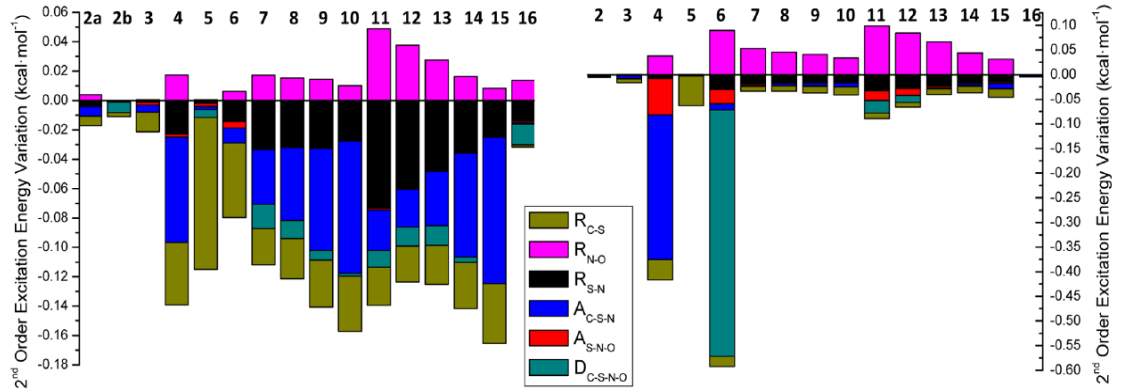

Figure 10. *Anti* (left) and *syn* (right) S-nitrosothiol excitation energy variations due to the second order terms. The individual contribution of each eigenvector of the projected energy Hessian difference ($\mathbf{H}^P$) is shown (the eigenvectors are confidently assigned to distances "R" C−S, N−O, and S−N; to bond angles "A" C−S−N and S−N−O; and to the dihedral angle "D" C−S−N−O).

effect of this coordinate being minimal for alkyl-S-nitrosothiols and small but similar for the rest of substituents. On the other hand, *syn* derivatives show a slightly lower capacity of energy gap reduction in comparison to *anti* derivatives. This is the general rule, except in the case of the *tert*-butyl substituent (compound **4**) where the steric hindrance should be responsible for the large participation of the C−S−N bond angle. Also, compound **6** (vinyl substituent, see Figure 6) exhibits a large participation of the C−S−N−O dihedral angle in energy gap modulation of the *syn* conformer. This contribution highlights the different effects of substituents in the chromophore structure, where a vinyl moiety activates the C−S−N−O dihedral angle while aryl derivatives do not provoke such a change in this coordinate. However, *anti* derivatives show an opposite behavior regarding this coordinate (aryl derivatives are C−S−N bond angle sensitive while vinyl derivative is not). For *anti* isomers, N−O, C−S, and S−N bond lengths contribute in a similar way, taking into account that the former coordinate increases the gap and the rest decrease it. Again, alkyl-S-nitrosothiols are the most energy-gap-insensitive derivatives. The most important coordinate for the decrease of the energy gap is the C−S−N bond angle, showing more pronounced response than *syn* derivates to this coordinate.

IV. CONCLUSIONS

Here, we present a methodology to easily predict the excitation energy shift (bathochromic or hypsonchromic) of substituted chromophores. The formalism is valid for substituted chromophores when the substituent fulfills the following conditions: (i) It does not change the excitation character of the electronic excited state under consideration. (ii) It does not participate directly in the excitation (no molecular orbitals with a significant contribution of the substituent are involved in the excitation process). This methodology only permits one to take into account the structural effect of the substituent in the chromophore excitation energy; therefore, no explicit through-space interaction is considered.

We show that from second-order term PESs for both ground and excited electronic states, it is possible to analyze the role of each molecular coordinate in the excitation energy tuning of the chromophore, being able to identify the ability of each coordinate in the modulation of the gap. The analysis is made on the basis of first- and second-order contributions.

This formalism has been applied to the prediction of excitation energy in a large family of substituted S-nitrosothiols. For these derivatives, 80% to 90% of the total excitation energy shift is due to structural effects induced by the substituent in the chromophore, the gradient vector being the main coordinate controlling the excitation energy variation.

This methodology offers a simple and fast procedure to obtain information regarding the substituent effect in the excitation of a chromophore, permitting the determination of the capability of the chromophore in the excitation energy tuning as well as the identification of the coordinates responsible for such a behavior, which eventually would permit the rational design of substituted derivatives with desired batho- or hypsochromic shifts. Moreover, once the ground and excited PESs (e.g., up to second order) of a chromophore are characterized, only ground-state calculations are needed in order to predict the excitation energy of a substituted derivative, being also possible to use different levels of theory for the prediction of the ground-state structures. Therefore, this methodology could be used for high-level *ab initio* excitation energy prediction where the excited-state calculations are in general computationally expensive, eventually permitting the fast prediction of excitation energies for a large number of substituted chromophores with simple ground state optimizations. Furthermore, the reference compound can be chosen as the simplest possible chromophore, in order to save computational time in the construction of the analytical PESs.

AUTHOR INFORMATION

Corresponding Author

*E-mail: luisma.frutos@uah.es; manuel.temprado@uah.es.

Notes

The authors declare no competing financial interest.

ACKNOWLEDGMENTS

This research was supported by the Spanish MICINN grant CTQ2009-07120 and UAH2011/EXP-041 of the University of Alcalá. M.A.F.-G., M.M., and C.G.-I. are grateful to the UAH and F.Z. to the Spanish MEC for a doctoral fellowship. D.R. acknowledges the University of Alcalá for a research grant. L.M.F. acknowledges receipt of a "Ramon y Cajal" contract from MEC.

REFERENCES

(1) Nguyen, N.-H.; Apriletti, J. W.; Baxter, J. D.; Scanlan, T. S. *J. Am. Chem. Soc.* **2005**, *127*, 4599.
(2) Schultz, D.; Nitschke, J. R. *J. Am. Chem. Soc.* **2006**, *128*, 9887.
(3) Hammett, L. P. *J. Am. Chem. Soc.* **1937**, *59*, 96.
(4) Swain, C. G.; Lupton, E. C., Jr. *J. Am. Chem. Soc.* **1968**, *90*, 4328.
(5) Taft, R. W., Jr. *J. Am. Chem. Soc.* **1952**, *74*, 3120.
(6) Taft, R. W., Jr. *J. Am. Chem. Soc.* **1952**, *74*, 2729.
(7) Taft, R. W., Jr. *J. Am. Chem. Soc.* **1953**, *75*, 4538.
(8) Yukawa, Y.; Tsuno, Y. *Bull. Chem. Soc. Jpn.* **1959**, *32*, 965.
(9) Dong, H.; Zhu, H.; Meng, Q.; Gong, X.; Hu, W. *Chem. Soc. Rev.* **2012**, *41*, 1754.
(10) Khoo, I. C. *J. Nonlinear Opt. Phys. Mater.* **1999**, *8*, 305.
(11) Bruetting, W.; Frischeisen, J.; Scholz, B. J.; Schmidt, T. D. *Europhys. News* **2011**, *42*, 20.
(12) Thejo, K. N.; Dhoble, S. J. *Renewable Sustainable Energy Rev.* **2012**, *16*, 2696.
(13) Sadlej-Sosnowska, N.; Kijak, M. *Struct. Chem.* **2012**, *23*, 359.
(14) McEwen, J.; Yates, K. *J. Phys. Org. Chem.* **1991**, *4*, 193.
(15) Wehry, E. L.; Rogers, L. B. *J. Am. Chem. Soc.* **1965**, *87*, 4234.
(16) Baldry, P. J. *J. Chem. Soc., Perkin Trans. 2* **1979**, 951.
(17) Shim, S. C.; Park, J. W.; Ham, H. S. *Bull. Korean Chem. Soc.* **1982**, *3*, 13.
(18) Shim, S. C.; Park, J. W.; Ham, H. S.; Chung, J. S. *Bull. Korean Chem. Soc.* **1983**, *4*, 45.
(19) Fleming, S. A.; Jensen, A. W. *J. Org. Chem.* **1996**, *61*, 7040.
(20) Cao, C.; Chen, G.; Yin, Z. *J. Phys. Org. Chem.* **2008**, *21*, 808.
(21) Charton, M. *Prog. Phys. Org. Chem.* **1981**, *13*, 119.
(22) Woodward, R. B. *J. Am. Chem. Soc.* **1941**, *63*, 1123.
(23) Fieser, L. F.; Fieser, M.; Rajagopalan, S. *J. Org. Chem.* **1948**, *13*, 800.
(24) Scott, A. I. *The Interpretation of Ultraviolet Spectra of Natural Products*; Pergamon Press: Elmsford, NY, 1962.
(25) Kuhn, H. *J. Chem. Phys.* **1948**, *16*, 840.
(26) Sexton, D. J.; Muruganandam, A.; McKenney, D. J.; Mutus, B. *Photochem. Photobiol.* **1994**, *59*, 463.
(27) Singh, R. J.; Hogg, N.; Joseph, J.; Kalyanaraman, B. *J. Biol. Chem.* **1996**, *271*, 18596.
(28) Singh, S. P.; Wishnok, J. S.; Keshive, M.; Deen, W. M.; Tannenbaum, S. R. *Proc. Natl. Acad. Sci. U. S. A.* **1996**, *93*, 14428.
(29) Wood, P. D.; Mutus, B.; Redmond, R. W. *Photochem. Photobiol.* **1996**, *64*, 518.
(30) Bartberger, M. D.; Houk, K. N.; Powell, S. C.; Mannion, J. D.; Lo, K. Y.; Stamler, J. S.; Toone, E. J. *J. Am. Chem. Soc.* **2000**, *122*, 5889.
(31) Bharatam, P. V.; Amita. *Tetrahedron Lett.* **2002**, *43*, 8289.
(32) Marazzi, M.; Lopez-Delgado, A.; Fernandez-Gonzalez, M. A.; Castano, O.; Frutos, L. M.; Temprado, M. *J. Phys. Chem. A* **2012**, *116*, 7039.
(33) Roos, B. O.; Taylor, P. R.; Siegbahn, E. M. *Chem. Phys.* **1980**, *48*, 157.
(34) Frisch, M. J.; Trucks, G. W.; Schlegel, H. B.; Scuseria, G. E.; Robb, M. A.; Cheeseman; J. R.; Scalmani; G.; Barone; V.; Mennucci; B.; Petersson, G. A.; Nakatsuji, H.; Caricato, M.; Li, X.; Hratchian, H. P.; Izmaylov, A. F.; Bloino, J.; Zheng, G.; Sonnenberg, J. L.; Hada, M.; Ehara, M.; Toyota, K.; Fukuda, R.; Hasegawa, J.; Ishida, M. N.; Honda, Y.; Kitao, O.; Nakai, H.; Vreven, T.; Montgomery, J. A., Jr.; Peralta, J. E.; Ogliaro, F.; Bearpark, M.; Heyd, J. J.; Brothers, E.; Kudin, K. N.; Staroverov, V. N.; Kobayashi, R.; Normand, J.; Raghavachari, K.; Rendell, A.; Burant, J. C.; Iyengar, S. S.; Tomasi, J.; Cossi, M.; Rega, N.; Millam, J. M.; Klene, M.; Knox, J. E.; Cross, J. B.; Bakken, V.; Adamo, C.; Jaramillo, J.; Gomperts, R.; Stratmann, R. E.; Yazyev, O.; Austin, A. J.; Cammi, R.; Pomelli, C.; Ochterski, J. W.; Martin, R. L.; Morokuma, K.; Zakrzewski, V. G.; Voth, G. A.; Salvador, P.; Dannenberg, J. J.; Dapprich, S.; Daniels, A. D.; Farkas, O.; Foresman, J. B.; Ortiz, J. V.; Cioslowski, J.; Fox, D. J. *Gaussian 09*, revision B.01; Gaussian, Inc.: Wallingford, CT, 2009.
(35) Andersson, K.; Malmqvist, P.-A.; Roos, B. O.; Sadlej, A. J.; Wolinski, K. *J. Phys. Chem.* **1990**, *94*, 5483.
(36) Finley, J.; Malmqvist, P.-A.; Roos, B. O.; Serrano-Andres, L. *Chem. Phys. Lett.* **1998**, *288*, 299.
(37) Bartberger, M. D.; Mannion, J. D.; Powell, S. C.; Stamler, J. S.; Houk, K. N.; Toone, E. J. *J. Am. Chem. Soc.* **2001**, *123*, 8868.
(38) Garthwaite, J. *Trends Neurosci.* **1991**, *14*, 60.
(39) Hibbs, J. B., Jr. *Res. Immunol.* **1991**, *142*, 565.
(40) Ignarro, L. J. *Pharm. Res.* **1989**, *6*, 651.
(41) Ignarro, L. J. *Nitric Oxide* **1996**, 111.
(42) Ignarro, L. J.; Byrns, R. E.; Buga, G. M.; Wood, K. S. *Circ. Res.* **1987**, *61*, 866.
(43) Moncada, S.; Palmer, R. M. J.; Gryglewski, R. J. *Proc. Natl. Acad. Sci. U. S. A.* **1986**, *83*, 9164.
(44) Mowbray, M.; McLintock, S.; Weerakoon, R.; Lomatschinsky, N.; Jones, S.; Rossi, A. G.; Weller, R. B. *J. Invest. Dermatol.* **2009**, *129*, 834.
(45) Palmer, R. M. J.; Ferrige, A. G.; Moncada, S. *Nature (London)* **1987**, *327*, 524.
(46) Scatena, R.; Bottoni, P.; Pontoglio, A.; Giardina, B. *Curr. Med. Chem.* **2010**, *17*, 61.
(47) Stamler, J. S.; Jia, L.; Eu, J. P.; McMahon, T. J.; Demchenko, I. T.; Bonaventura, J.; Gernert, K.; Piantadosi, C. A. *Science (Washington, DC, U. S.)* **1997**, *276*, 2034.
(48) Tennyson, A. G.; Lippard, S. J. *Chem. Biol.* **2011**, *18*, 1211.
(49) de Oliveira, M. G.; Shishido, S. M.; Seabra, A. B.; Morgon, N. H. *J. Phys. Chem. A* **2002**, *106*, 8963.
(50) Grossi, L.; Montevecchi, P. C. *Chem.—Eur. J.* **2002**, *8*, 380.
(51) Lü, J. M.; Wittbrodt, J. M.; Wang, K.; Wen, Z.; Schlegel, H. B.; Wang, P. G.; Cheng, J. P. *J. Am. Chem. Soc.* **2001**, *123*, 2903.

6.2.2 Towards an Optomechanical Control of Photoswitches by Tuning the Spectroscopical Properties

As has been discussed in the foregoing section it is important to notice, that an external force can be regarded as an agent which can induce structural changes in the conformation of the molecule, being it a substituent or a direct applied mechanical force. Once we have tackled the "structural substituent excitation energy effect" we focus on a dynamical and static approach to the tuning of Spectroscopical properties.

Therefore in the contribution presented in this section, we have chosen a well study system regarding application of external mechanical forces as it is the azobenzene, in order to have an experimental framework for comparison. Then a careful study of the ground state topology was carried out, aiming to identify the mechanical limits of molecule and set the maximum external force which can be applied.

Subsequently using the methodology described on section 2.4, we carried out molecular dynamics at constant temperature on both minima for the cis and trans conformation of the azobenzene, using a quadratic interpolation around the both cis and trans minima. The external forces is represented as pair of forces (same magnitude and oppose direction) applied in the para position of both phenyl substituents. Using also a quadratic interpolation it was possible to obtain an analytical PES representation for the S_1 and S_2 excited states around the Franck-Condon point with respect to the ground states, being possible to compute in each step of the molecular dynamics the energy gap, for the lowest energy transitions $S_0 \rightarrow S_1$ and $S_0 \rightarrow S_2$, which correspond to optically dark (n,π^*) and bright (n,π^*) transitions, respectively. Allowing to simulate the absorption spectra for different magnitudes of external forces, for both the cis and trans configurations.

The simulated spectrum is obtained as an histogram which consist of a collection of evenly distributed deltas of excitation energy, where it is counted how many conformations of the (cis or trans) azobenzene sampled during the molecular dynamic simulation, have excitation energy inside one of those deltas, which after normalization provides the probability to have a given excitation energy. But in order to calculate the spectrum it is necessary to multiple those probabilities for the oscillator strength. With regard to the oscillator strength for the given range of excitation energies, it was calculated the oscillator strength using an electronic structure package, for a set of 100 random geometries taken from the trajectories of the molecular dynamics. If there is no

correlation between the excitation energy and the oscillator strength, the oscillator strength is given as the mean arithmetic value. Otherwise, an adjusted function is used to described the correlation, being finally possible to obtain spectra for both cis and trans conformation, for both excitations ($S_0 \rightarrow S_1$ or $S_0 \rightarrow S_2$) using different magnitudes of external forces.

It was found that compression forces for both cis and trans conformations barely affects the absorption spectra, while stretching forces alter significantly the spectral shape as well as the wavelength absorbed. The shifting in the absorption spectra was rationalized in terms of the differences between the forces constants on the ground and excited states, identifying the most import internal coordinates in the modulation of the energy gap. Also it was proposed a set of force-pairs on different positions which can promote the red or blue shifting depending on the desired functionality.

Finally, based on given results, it was proposed a linear polymeric photoswitch device, which operates in two possible kinds of four steps cycles. The first operation mode consist in the application of an external force at para position to the trans conformation, follow by irradiation to allow the trans-cis isomerization then the external force is disengage of the cis isomer and finally a photoinduced cis-trans isomerization results in the original molecule. The other cycle involves the same steps, but swapping the cis and trans isomers. It is proposed the amount of work generated by both cycles and also it is analyse the feasible work as function of the polymerization degree.

JCTC Journal of Chemical Theory and Computation
Article
pubs.acs.org/JCTC

Toward an Optomechanical Control of Photoswitches by Tuning Their Spectroscopical Properties: Structural and Dynamical Insights into Azobenzene

Felipe Zapata, Miguel Ángel Fernández-González, Daniel Rivero, Ángel Álvarez, Marco Marazzi,*,† and Luis Manuel Frutos*

Departamento de Química Analítica, Química Física e Ingeniería Química, Universidad de Alcalá, E-28871 Alcalá de Henares, Madrid, Spain

Supporting Information

ABSTRACT: A new methodology to calculate efficiently the absorption spectrum of a single molecule when subjected to mechanical stress is presented. As example, the developed methodology was applied to *cis*- and *trans*-azobenzene, commonly used as photoswitch in a wide variety of applications. The results show that both $^1(n,\pi^*)$ and $^1(\pi,\pi^*)$ optical transitions can be efficiently modulated by applying an external force. A structural analysis was performed to evaluate the role of each internal coordinate in the excitation process, taking into account the application of external forces at different positions of azobenzene. Moreover, stress−strain curves were calculated in order to determine the maximum applicable forces within the elastic region, highlighting notable differences between the mechanical properties of *cis*- and *trans*-azobenzene conformers. The optomechanical work obtained by elongation and compression steps is calculated for a single azobenzene molecule and compared to available experimental data. Finally, the implications derived from the application of azobenzene as main chain component of a linear polymer acting as a photoinduced motor are discussed.

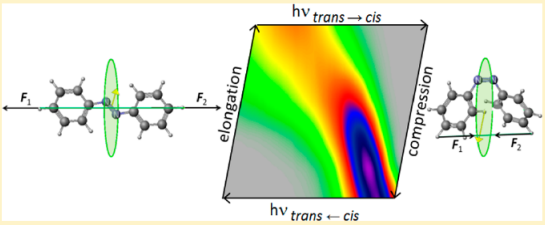

INTRODUCTION

Optomechanics is a modern multidisciplinary field of science in which fundamental aspects have been discovered in the past decade, outlying important challenges and perspectives for the future. Optomechanical materials are based on direct conversion of light (applied as input) into macroscopic motion. This behavior, in turn, depends on the molecular structure of the material itself. Especially, soft organic materials were successfully designed as optomechanical responsive systems (e.g., oligomers and polymers) where the presence of one or more chromophore units is essential to ensure light absorption, which constitutes the first necessary event to promote the subsequent conformational and/or chemical modification underlying mechanical motion.[1,2]

Photoswitches are bistable (state A and B) chromophores of special interest in the design and fabrication of optomechanical devices, since the absorption of light at a certain wavelength by state A is usually followed by a large structural change, which makes it possible to reach state B. Then a second pulse of light (or thermal relaxation step), commonly at a different wavelength, reverses the process defining a pathway from state B back to state A.[3,4] Specifically, switches based on photoisomerization are commonly applied to solve a variety of scientific and engineering problems, ranging from protein conformation control to photocatalysis, from molecular data storage to foldamers. In all these cases, photoisomerization provides an efficient (i.e., ultrafast time scale) way to switch a process ON and OFF.[5]

Moreover, we can take advantage of the photoswitching property of a chromophore by generating optomechanical work in a single molecule device, operating switching cycles in a periodic mode, and therefore leading to the eventual design and fabrication of optomechanical motors.[6−10]

Here, we focus on the photophysical step of the cycle (i.e., absorption of light) aiming to control spectroscopical properties once the switch is subject to external forces in an applied environment (e.g., covalently bound to a protein or peptide,[11,12] or introduced in the main chain of liquid crystal polymer systems[13,14]). More generally, in this study, we present a new and efficient method to simulate single molecule force spectroscopy of whatever chromophore. We show its application to (*cis* and *trans*) azobenzene, being one of the most studied and applied photoisomerizable switch.[15−20]

The paper is organized as follows: first, the proposed theoretical methods are presented, especially the ground state molecular optimization and dynamics schemes, necessary for the simulation of the absorption spectra, the structural analysis required to determine which internal coordinates are more involved in the modulation of the excitation energy (including

Received: August 29, 2013
Published: December 19, 2013

dx.doi.org/10.1021/ct4007629 | J. Chem. Theory Comput. 2014, 10, 312−323

the application of different sets of external forces), the simulation of single molecule stress−strain curves and the calculation of optomechanical work and power. This is followed by a description of the results obtained when applying the proposed methods to azobenzene. Therefore, azobenzene ground state topology is studied first, followed by an evaluation of its mechanical properties. This allows us to estimate the maximum applicable force to both *cis* and *trans* conformers, within the elastic region. The spectra recorded when applying a different set of forces are shown, indicating a relevant force induced modulation of spectroscopical properties (shift of the maximum absorption wavelength, broadening of the peak, change of absorption intensity), which can be useful in designing new optomechanical tools at a low computational cost. The main coordinates involved in the observed bathochromic and hypsochromic shifts are found, and the application of external forces at different positions of azobenzene is proposed. Finally, we discuss the possible implications derived from the introduction of azobenzene as main chain component of a linear polymer,[21−24] especially focusing on maximizing the optomechanical work and power, which could be obtained by applying the highest possible deforming force compatible with the mechanical tests performed.

THEORETICAL METHODS

Force-Induced Ground State Molecular Optimization and Dynamics. Recently, a growing interest was shown by the theoretical chemistry and physics communities in order to describe adequately the behavior of molecules when an external force is applied to selected pairs of nuclei. Especially, we should mention the work of Martinez and co-workers, who explained relevant mechanochemical processes (e.g., force induced rupture of covalent bonds) through "on the fly" *ab initio* steered molecular dynamics (AI-SMD) simulations.[25−27] Almost at the same time, Wolinski et al. proposed a method for geometry optimization in presence of external forces.[28,29]

In this study, we propose an alternative approach by which extensive dynamics simulations can be performed, since energy and forces are not evaluated at each step of the simulation (as for the "on the fly" approach), being classical molecular dynamics performed on a previously constructed analytical potential energy surface (PES). Among the different possible approaches for building an analytical PES, we opted for a simple quadratic expansion centered on the minimum energy structure of *cis* (and *trans*) azobenzene (see for details the section Azobenzene Topology and Supporting Information), which can be calculated as follows:

$$E_{GS}(\mathbf{q}) = E_{GS}(\mathbf{q}^{eq}) + \frac{1}{2}(\mathbf{q} - \mathbf{q}^{eq})^{T}\mathbf{H}_{GS}(\mathbf{q} - \mathbf{q}^{eq}) \quad (1)$$

where E_{GS} is the energy in the ground state (GS) as a function of the molecular configuration in internal coordinates $\mathbf{q}$, being $\mathbf{q}^{eq}$ the vector corresponding to the minimum energy (i.e., equilibrium) structure in the GS. Whatever displacement from $\mathbf{q}^{eq}$ corresponds to energy increase, as indicated by the second term on the right-hand side of eq 1, being $\mathbf{H}_{GS}$ the ground state Hessian matrix numerically calculated for the equilibrium geometry (the energy gradient is a null vector).

Classical molecular dynamics simulations were computed on the constructed ground state PES, applying the following methodology: a canonical ensemble was reproduced by expanding the current Hamiltonian through the Nosé−Hoover method, which permits to include in the Hamiltonian the required degrees of freedom to simulate a thermostat.[30] This results in a canonical distribution of the molecular system. The Newtonian equations of motion were integrated by a time reversible integrator, applying the Liouville approach through the Trotter factorization.[31] External forces are included by adding to the force vector determined from the analytical PES at each step of the dynamics, constant force vectors applied to selected pairs of nuclei. In our case, the pair of external force vectors was applied to the two hydrogen atoms of the benzene rings in *para* position with respect to the N=N moiety, in order to simulate the usual environment of azobenzene as a photoswitch in peptides and as main chain component of linear polymers. The direction of the external force is therefore the line connecting the two selected atoms, having both force vectors the same modulus. This leads to two possible mechanical stresses: elongation and compression. Both were considered as acting stresses over azobenzene (see Figure 5). In order to test the results obtained by the dynamical treatment, and as an additional method to estimate azobenzene structure under a static stress, force constrained optimizations were performed applying a quasi Newton−Raphson modified method, where at each step the external force is introduced by updating the calculated energy gradient (see Supporting Information for details).

Simulation of the Absorption Spectra. The same approach used to construct the ground state PES can be applied to build an electronic excited state PES:

$$E_{ES}(\mathbf{q}) = E_{ES}(\mathbf{q}^{eq}) + (\mathbf{q} - \mathbf{q}^{eq})^{T}\mathbf{g}_{ES} + \frac{1}{2}(\mathbf{q} - \mathbf{q}^{eq})^{T}\mathbf{H}_{ES}(\mathbf{q} - \mathbf{q}^{eq}) \quad (2)$$

where E_{ES} is the energy, $\mathbf{g}_{ES}$ the energy gradient vector, and $\mathbf{H}_{ES}$ the Hessian matrix, numerically calculated for the excited state (ES). The quadratic expansion in eq 2 is therefore centered on the same ground state equilibrium geometry ($\mathbf{q}^{eq}$, i.e. the Franck−Condon geometry) as in eq 1.

Following this approximation for the ES PES, the excitation energy can be determined at each step of a molecular dynamics simulation performed on the GS PES; that is, each step of the trajectory corresponds to a ground state and an excited state energy value, which difference is a vertical excitation energy: $E_{ES}(\mathbf{q}) - E_{GS}(\mathbf{q})$ (see Figure 1). Therefore, if the dynamics run

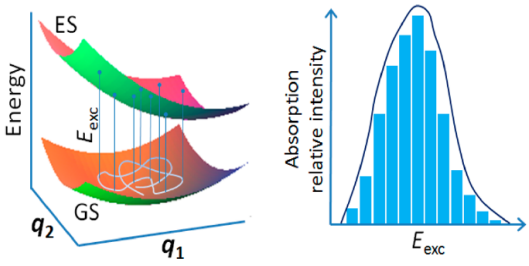

Figure 1. Left: schematic potential energy surfaces of the electronic ground state (GS) and excited state (ES) for a chromophore, as a function of two of its coordinate (q_1, q_2); a ground state trajectory is depicted, with some of the corresponding vertical excitation energies (E_{exc}). Right: absorption spectrum, calculated as a histogram of relative intensity as a function of E_{exc}, resulting from each geometry of the ground state trajectory.

dx.doi.org/10.1021/ct4007629 | J. Chem. Theory Comput. 2014, 10, 312−323

Journal of Chemical Theory and Computation Article

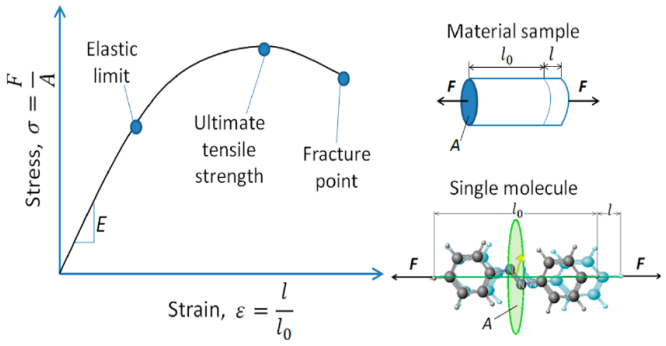

Figure 2. Example of a stress−strain curve, showing typical magnitudes of interest (left). A comparison between macroscopic and proposed microscopic samples is given (right).

is long enough to sample correctly the ground state PES at a given temperature, and if the quadratic approximation can be considered valid for both ground and excited states, the absorption spectrum corresponding to the GS → ES electronic transition is simulated. More in detail, the following procedure was adopted for calculating the absorption spectrum: as first, the lowest and the highest vertical excitation energies recorded during the dynamics determine the width of the spectrum. Such width is then divided into equal intervals of energy, defining the sensitivity of the spectrum. Finally, each vertical excitation energy computed during the trajectory is assigned to the corresponding energy interval. Therefore, the absorption spectrum results in a histogram of relative intensity as a function of the excitation energy, where the relative absorption intensity of a given interval is proportional to the oscillator strength (i.e., to the transition dipole moment) and to the number of structures of the trajectory presenting an excitation energy falling in this interval (see Supporting Information for details).

The proposed methodology permits to perform dynamics simulations in the picosecond-time-scale in few hours of computation, correctly sampling the phase-space and providing a consistent prediction of the absorption spectrum at a determined constant temperature.

Structural Analysis. A rational modulation of the shift in absorption energy under external stress was considered, based on the development of an algorithm to minimize or maximize the energy gap between ground and selected excited states. Especially, the following question can be answered: provided only the magnitude of the applied external force, which is the specific force vector (i.e., the components for each nucleus) that causes the highest (bathochromic and hypsochromic) shift in the absorption energy? Alternatively, an equivalent question is the following: provided a given shift of the excitation energy, which is the external force vector with the lowest magnitude yielding such a shift? To answer this question, a restrained optimization has to be performed, where the Lagrangian function is defined as:

$$L = |\nabla E_{GS}|^2 + \lambda(\Delta E_{exc} - k) \quad (3)$$

where the function to be optimized is the squared energy gradient vector of the ground state PES subject to the condition that the excitation energy is equal to a given value: $\Delta E_{exc} = k$, and where λ is the corresponding Lagrange multiplier. The coordinates of the shifted structure can be found by optimizing the Lagrange function:

$$\nabla L = 2\mathbf{H}_{GS}^2\mathbf{q}_{opt} + \lambda[\mathbf{g}_{ES} + (\mathbf{H}_{ES} - \mathbf{H}_{GS})\mathbf{q}_{opt}] = 0 \quad (4)$$

which can be rearranged in the form:

$$\left(\frac{2}{\lambda}\mathbf{H}_{GS}^2 - \mathbf{H}_{GS} + \mathbf{H}_{ES}\right)\mathbf{q}_{opt} = -\mathbf{g}_{ES} \quad (5)$$

If $\boldsymbol{A} = 2/\lambda\ \mathbf{H}_{GS}^2 - \mathbf{H}_{GS} + \mathbf{H}_{ES}$ and $\boldsymbol{b} = -\mathbf{g}_{ES}$, it follows that $\boldsymbol{q}_{opt} = \boldsymbol{A}^{-1}\boldsymbol{b}$. The optimized structure $\boldsymbol{q}_{opt}$ corresponds to the molecular configuration resulting from the application of a minimal external force giving rise to the desired excitation energy shift. Obviously, the optimal external force vector is known, since it equals the energy gradient of the ground state ∇E_{GS} (it should be taken into account that the external force is opposite to the internal force for the equilibrium configuration).

How could such an optimal external force be reproduced by a simple force pair applied in two atoms? In order to answer this question, a set of external force pairs can be systematically considered by a set of vectors, and projected onto the optimal external force vector, realizing which force pair corresponds to the highest projection.

Molecular Stress−Strain Curve. In order to determine quantitatively what is the range of external forces which can be applied to a certain molecular system (avoiding bond breaking or high interatomic repulsion), single molecule mechanical tests were simulated as follows: considering $\boldsymbol{q}^{eq}$ as starting structure, the geometry was optimized while constrained at increasingly compressed or elongated interatomic distances (by steps of 0.2 Å), where the pair of atoms selected is the same at which external forces are applied during the dynamics study described above. Nevertheless, contrary to the developed dynamics method, the mechanical properties were calculated by using the true PES, instead of a quadratic expansion around the equilibrium geometries at different external forces. The overall force is then calculated for each optimized structure, having now all elements to obtain a "single molecule stress−strain curve": the stress σ is defined as force divided by the projection area perpendicular to the applied force vector, based on the van der Waals radius of the molecule;[32] the strain corresponds to the deformation of the molecule along the direction of the external force, relative to the initial interatomic length, $\varepsilon = l/l_0$ (Figure 2).

In materials science, the relationship between stress and strain is a typical form to characterize macroscopic properties, being unique for each material. In this study, we aimed to characterize microscopic properties of single molecules by a

dx.doi.org/10.1021/ct4007629 | J. Chem. Theory Comput. 2014, 10, 312−323

similar approach, in order to evaluate (as well as in real materials) the Young's modulus E and therefore set the elastic limit, that is, up to which extent the proposed deformation is nonpermanent and hence recoverable, being a necessary information to design molecules with defined optomechanical properties. Moreover, depending on the actual stress−strain curve, plastic region and tensile strength can be estimated (see Figure 2).

Optomechanical Work and Power. The possibility to generate optomechanical work was considered by theorizing a periodic cycle for a photoisomerizable switch involving four consecutive steps, two mechanical and two photoinduced steps: (1) elongation of the molecule initially at state A equilibrium structure due to an external force; (2) electronic excitation of the stretched molecule followed by photoisomerization to state B; (3) recovery of state B equilibrium structure, by removing the elongation force applied in step 1; (4) electronic excitation of state B equilibrium structure to allow photoisomerization back to state A equilibrium structure, therefore closing the cycle. The optomechanical work is straightforward calculated as the area generated by drawing these four steps (linearly approximated) in a graph of force as function of deformation length (Figure 3).

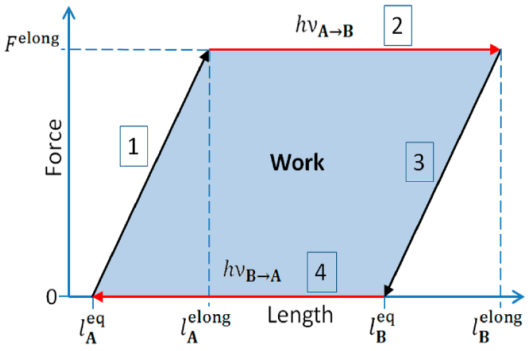

Figure 3. Optomechanical cycle to generate work. Two mechanical steps (1 and 3) and two photoinduced steps (2 and 4) are required, implying application/release of an external elongation force and photoswitching between A and B states, respectively.

The mechanical steps (1 and 3) can be accomplished only if the force applied is within the elastic regime previously calculated by stress−strain curves, otherwise full interconversion between state A and B cannot be ensured, and the periodicity of the optomechanical cycle is not fulfilled.

About the photoinduced steps, while step 4 does not involve any external force, step 2 implies irradiation of the previously stretched molecule, and it is therefore crucial to perform force spectroscopy in order to maximize the absorption and the overall efficiency of the optomechanical cycle.

Once the work is calculated, the optomechanical power can be estimated considering a determined constant frequency, that is, time per cycle accomplished. Especially, the work calculated for a single molecule can be readily amplified if, for example, such a molecule is introduced in the main chain of a polymer (as was already proposed to achieve photoresponsive materials),[7] hence being of potential interest for design of optomechanical devices.

RESULTS AND DISCUSSION

Azobenzene Topology. The methods described were applied to azobenzene, which is stable in two isomeric forms: *cis* and *trans* (Figure 4). The *trans* isomer is basically planar, being ca. 0.6 eV more stable than the *cis* isomer, due to twisting of the benzene rings around the C−N bond to avoid steric hindrance.[33]

The photophysics and photochemistry of this system have been extensively studied: with both (nonpolar) *n*-hexane and (polar) ethanol as solvents, the absorption spectrum shows a $^1(n,\pi^*)$ electronic transition at ca. 430 nm (440 nm) for the *trans* (*cis*) isomer, and a $^1(\pi,\pi^*)$ transition at ca. 320 nm (260 nm) for the *trans* (*cis*) isomer,[34−38] corresponding to visible and near-UV regions of the spectrum. Concerning the absorption relative intensity, the $^1(\pi,\pi^*)$ transition of *cis*-azobenzene is weaker, but the $^1(n,\pi^*)$ transition is stronger than *trans*-azobenzene[38] (see Figure 7). About the photochemistry, isomerization was found to be an ultrafast process for both *cis*-to-*trans* (170 fs) and *trans*-to-*cis* (320 fs) conformational changes.[17,39] In spite of a large number of experimental and theoretical studies which clarified azobenzene photoisomerization mechanisms and dynamics upon vertical excitation to $^1(n,\pi^*)$ and $^1(\pi,\pi^*)$ states,[16−20,39−46] few attempts were made to determine accurately the ground state topology.

In a recent work by Klug and Burcl,[47] the rotational barriers in azobenzene are calculated by Density Functional Theory (DFT) methods, connecting transition states and minima by constrained optimization, starting from a geometry slightly displaced from the transition state geometry along the vibrational eigenvector corresponding to the imaginary frequency. Here, this approach was improved by calculating the reaction path (i.e., by integrating the intrinsic reaction coordinate), hence leading to a minimum energy path description of all rotational barriers. The azobenzene ground state PES is schematically shown by energy levels in Figure 4. It was calculated at the CAM-B3LYP level of theory (i.e., the long-range corrected version of the Becke's three-parameter hybrid exchange functional[48] with the Lee−Yang−Parr correlation functional,[49] using the Coulomb-attenuating method[50]), as implemented in *Gaussian 09* suite of programs.[51] The 6-311+G(d,p) basis was adopted. Indeed, the CAM-B3LYP functional was shown to correctly describe $^1(n,\pi^*)$ and $^1(\pi,\pi^*)$ states[50] (see Table 1S in the Supporting Information).

In accordance with previous studies, a transition state structure (TS_{tc}) was found to be responsible for *cis*-to-*trans* thermal isomerization, being characterized by an almost linear N═N−C_1 angle and the phenyl ring containing C_1 perpendicular to the rest of the molecule. By calculating the reaction paths from TS_{tc}, we found two previously unreported inflection points (SP_t and SP_c). These structures are characterized, with respect to TS_{tc}, by a sort of translation of the perpendicular phenyl ring upward (SP_t) or downward (SP_c) of the N═N bond, starting to define which will be the final isomer. The numerical energy gradient vector was calculated for SP_t and SP_c with different step sizes for differentiation (0.01 Å, 0.02 Å, 0.03 Å), in order to map the sign change of the PES curvature in the proximity of the inflection point: we were able to define only one reaction path for each of the two SP structures, pointing lower in energy and connecting to a transition state that establishes the rotational barrier between the two iso-conformers (TS_t for *trans* and TS_c for *cis*). Actually, a second transition state was found at slightly lower energy (*ca.*

dx.doi.org/10.1021/ct4007629 | J. Chem. Theory Comput. 2014, 10, 312−323

Journal of Chemical Theory and Computation Article

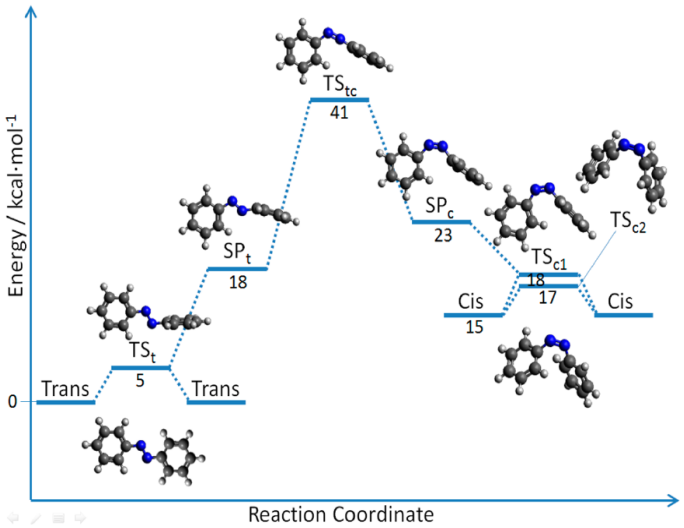

Figure 4. Schematic view of azobenzene ground state potential energy surface.

1 kcal·mol^{-1}) for the *cis* isomer (TS$_{c2}$), implying a simultaneous rotation of both phenyl rings from the stable (equilibrium) *cis* conformation, in order to reach a symmetric transition state with respect to the N═N bond. As a result, only 5 kcal·mol^{-1} (2 or 3 kcal·mol^{-1}) is required to overcome rotational barriers for the *trans* (*cis*) form, while a considerable energy of 41 kcal·mol^{-1} (26 kcal·mol^{-1}) is needed to undergo a *trans*-to-*cis* (*cis*-to-*trans*) isomerization on the ground state.

An exhaustive study of the ground state topology was considered fundamental in order to evaluate which is the maximum external force which can be applied before a bond is broken, van der Waals contact distance is reached, or, eventually, a mechanically driven isomerization is enforced.

As mentioned in the Methods section, in this study the external force was applied to the two hydrogen atoms of the benzene rings in *para* position with respect to the N═N moiety. In Figure 5 the effect of elongation and compression on the energy of the ground state is schematically represented: on the one hand elongation of the *cis* isomer or compression of the *trans* isomer will determine the minimum force required for mechanical isomerization; on the other hand, elongation of the *trans* isomer or compression of the *cis* isomer will result in a constant increase of energy, leading to the maximum force which can be applied before bond breaking or high interatomic repulsion is detected.

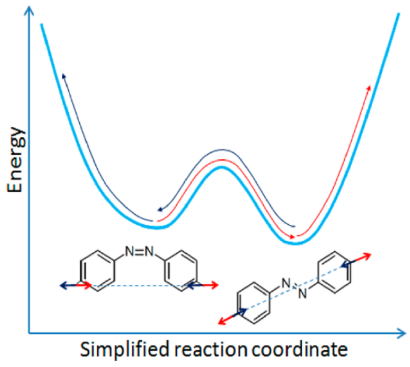

Figure 5. Scheme of compression (blue arrows) and elongation (red arrows) forces applied to azobenzene, with consequent response on a simplified ground state potential energy surface.

Azobenzene Mechanical Properties. The stress−strain curves for elongation and compression tests are shown in Figure 6. The projection area perpendicular to the applied force vector (see Figure 2) is 24.31 Å^2 for *trans* and 36.74 Å^2 for *cis* isomers. It results that the minimum force is 5.41 nN for *cis*-to-*trans* and 2.69 nN for *trans*-to-*cis* mechanical isomerization, corresponding to the highest stress recorded for *cis* elongation and *trans* compression curves, respectively. The former result qualitatively agrees with the value found by Shao et al. using the electron-radiation-ion dynamics method, that points toward elongation forces higher than 1.25 nN to produce a pure *cis*-to-*trans* mechanical isomerization (B3LYP/6-31G level of theory).[8] The maximum force that can be applied before reaching the van der Waals contact distance within the *cis* isomer is 19.50 nN (highest *cis* compression stress), and 6.84 nN before bond breaking of the *trans* isomer (highest *trans* elongation stress).

Among the information that is possible to get from stress−strain curves, we are particularly interested in the Young's modulus, since an optomechanical cycle can be accomplished only if both *cis* and *trans* isomer deformations are within the elastic limit. Interestingly, *E* was found to be much higher for the *trans* isomer (196.9 GPa for elongation, 310.2 GPa for compression) than for the *cis* isomer (8.7 GPa for elongation, 4.4 GPa for compression). We also notice that, even though the overall shape of all the calculated stress−strain curves are typical of thermoplastic materials, the two isomers show distinct features: the *cis* isomer behaves as a semicrystalline thermoplastic, while the *trans* isomer behaves as a glassy (i.e., amorphous) thermoplastic. Indeed, amorphous thermoplastics are usually stiff and brittle, therefore reaching the ultimate tensile strength point at relatively low deformations, following a plateau "rubbery" region at larger deformations (Figure 6, left), while semicrystalline thermoplastics are commonly characterized by larger deformations than amorphous thermoplastics, reaching the ultimate strength point without showing any

dx.doi.org/10.1021/ct4007629 | J. Chem. Theory Comput. 2014, 10, 312−323

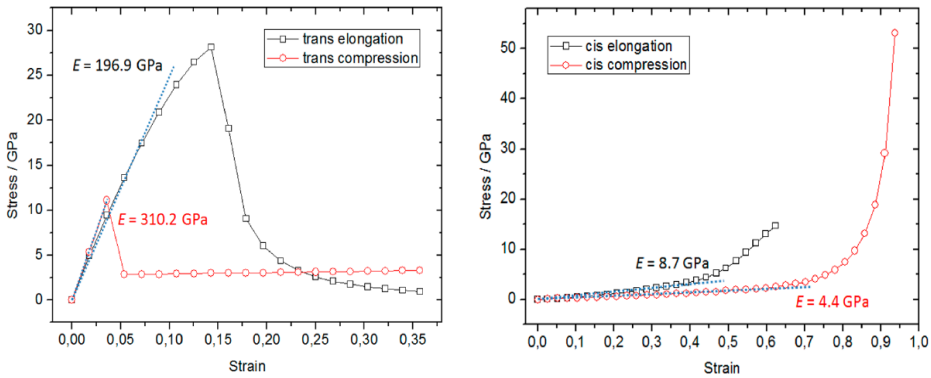

Figure 6. Stress−strain curves for *trans* (left) and *cis* (right) azobenzene isomers. Elongation tests (black) and compression tests (red) with the respective Young's modulus (E) calculated for each elastic region (dashed line) are shown.

"rubbery" region (Figure 6, right).[52] This could be of interest for the design of photoactive materials, especially photoactive polymers, since physical and engineering properties of thermoplastics (molding performance, behavior of the polymer during processing) mainly depend on their molecular structure.

Azobenzene Force Spectroscopy. The absorption spectra resulting from 1 ns ground state simulations (for a total of 10^7 integration steps) at a temperature of 300 K, obtained when not applying external forces or including a set of different elongation forces, are shown in Figure 7 and Figure 8,

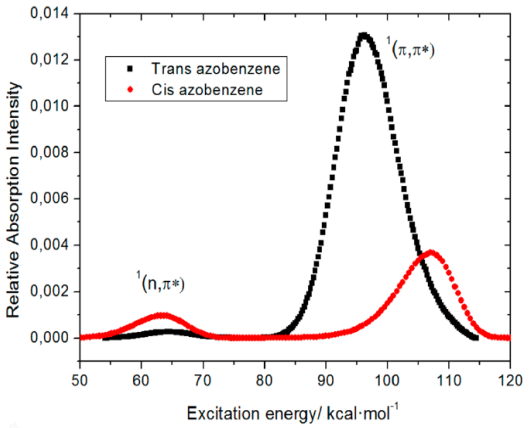

Figure 7. Simulated spectra when not applying external forces (0 nN), for both *cis* (red line) and *trans* (black line) azobenzene. The region of the spectrum assigned to $^1(n,\pi^*)$ or $^1(\pi,\pi^*)$ electronic transitions is shown.

respectively. As expected, the relative absorption is higher for $S_0 \rightarrow S_2$ vertical excitation, corresponding to an optically bright $^1(\pi,\pi^*)$ transition − than for $S_0 \rightarrow S_1$, corresponding to an optically dark $^1(n,\pi^*)$ transition. Moreover, the differences between *cis* and *trans* relative absorption intensities found by experiment (0 nN) are well represented by the simulation.[38]

In all cases, the applied elongation forces produce a shift of the whole spectrum, with significant differences between the two isomers: the amplitude of the excitation energy shift is considerably larger for *cis*-azobenzene (27−30 kcal·mol^{-1}) than for the *trans* isomer (5−8 kcal·mol^{-1}), allowing a more efficient modulation in the former case. Nevertheless, the *cis*-azobenzene series of spectra also shows a larger broadening of the peak, especially at forces larger than 2 nN. Moreover, we do observe in all cases a higher relative absorption intensity when applying forces between 1 and 2 nN. This can be explained by the fact that, when compared to 0 nN values, the oscillator strength is higher and, at the same time, the external force is still not large enough to produce a broadening of the peak.

Considering that the applied methodology implies molecular dynamics simulations on an analytical PES built by quadratic expansion (see eqs 1 and 2), a quantitative analysis of the calculated trajectories—within the limits of the method—can be performed by examining ground and excited state Hessian matrices ($\mathbf{H}_{GS}$, $\mathbf{H}_{ES}$) and the energy gradient vector ($\mathbf{g}_{ES}$). Also, a description of negative (imaginary) frequencies is given. The energy difference along $\mathbf{g}_{ES}$ provides the first-order correction to E_{exc}, while second-order corrections (orthogonal to $\mathbf{g}_{ES}$) are given by a projected Hessian difference matrix ($\mathbf{H}_{ES} - \mathbf{H}_{GS}$).[53] This allows us to fully understand which internal coordinates are responsible for the excitation energy shift observed.

Looking at $S_0 \rightarrow S_1$ force spectroscopy results (Figure 8 − a, c), a bathochromic shift for both isomers is observed. A single negative frequency is found in S_1, indicating torsion around the N═N bond (*trans*, −38 cm^{-1}; *cis*, −257 cm^{-1}). When analyzing the projected Hessian difference matrix ($\mathbf{H}_{S1} - \mathbf{H}_{S0}$), the eigenvalues with highest absolute value indicate that C—N═N and N═N—C angles are the most involved internal coordinates. In spite of a similar behavior, the higher frequency found for the *cis* isomer demonstrates that the S_1 PES curvature is larger than for the *trans* isomer, therefore explaining the higher amplitude of the excitation energy shift.

When examining $S_0 \rightarrow S_2$ force spectroscopy results (Figure 8b, d), the most evident difference between the two isomers is about the type of E_{exc} shift: the application of an elongation force provokes a bathochromic shift within *cis*-azobenzene, while a hypsochromic shift was found for *trans*-azobenzene. This can be explained considering S_2 frequencies: two negative frequencies are found for the *trans* isomer, being assigned to torsions around the N═N bond (−244 cm^{-1}) and around both N—C bonds, in opposite directions (−89 cm^{-1}). The same types of frequency modes were found for the *cis* isomer (N═N torsion at −165 cm^{-1} and coupled N—C torsions at −91 cm^{-1}). Nevertheless, additional negative frequencies were recorded for *cis*-azobenzene: −581 cm^{-1}, assigned to N═N stretching, and −1148 cm^{-1}, referring to a complex molecular vibration that couples C—N═N and N═N—C scissoring

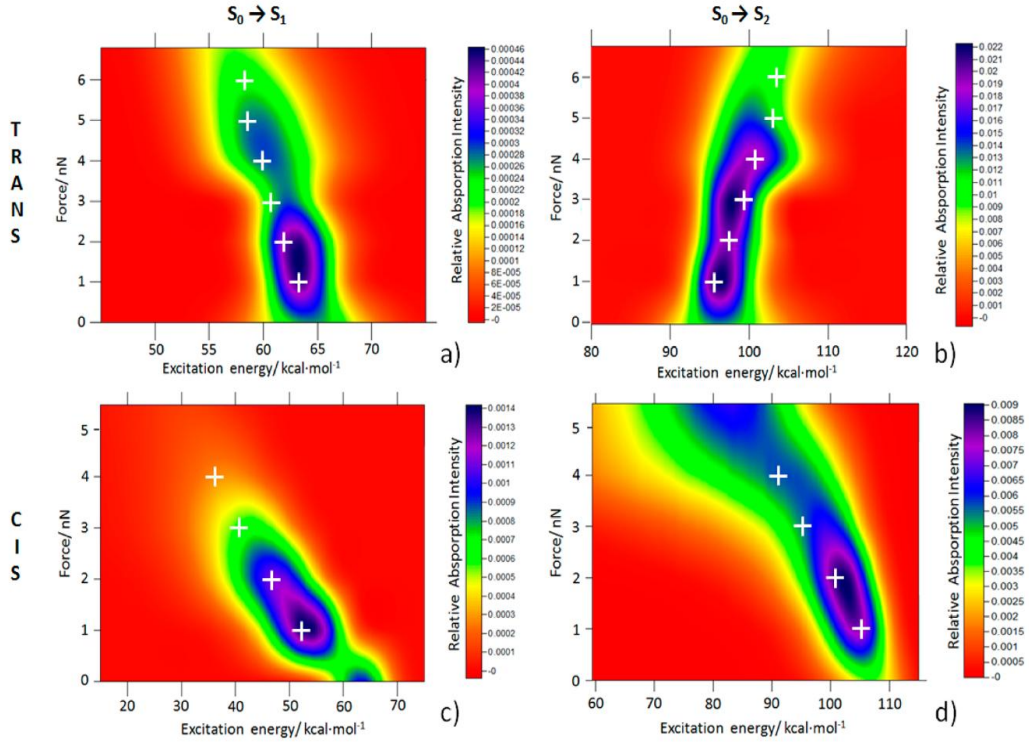

Figure 8. *Trans-* (top) and *cis-* (bottom) azobenzene absorption spectra when applying different elongation forces. The results are shown for $S_0 \rightarrow S_1$ $^1(n,\pi^*)$ (on the left: a, c) and $S_0 \rightarrow S_2$ $^1(\pi,\pi^*)$ (on the right: b, d) electronic transitions, by image plots where the relative absorption intensity is color mapped. White crosses indicate the optimized structures under stress.

with stretching of the phenyl moieties along the N—C bond direction. Hence, *trans* and *cis* S_2 PESs are rather different, and this can be further demonstrated by projecting the Hessian difference matrix ($\mathbf{H}_{S2} - \mathbf{H}_{S0}$): the eigenvalues related to the *cis* isomer indicate a direct participation of the angles defined by carbon atoms within the phenyl rings. Moreover, as for $S_0 \rightarrow S_1$, the higher frequency values found for the *cis* isomer indicate a larger curvature of the S_2 PES than for the *trans* isomer, again determining a higher amplitude of the excitation energy shift.

Force constrained optimizations are in agreement with the data obtained by dynamics: bathochromic and hypsochromic shifts are qualitatively reproduced, with dynamics underestimating the observed shift in absorption energy.

In order to estimate the error associated with the analytic ground state dynamics, a single point calculation (at the CAM-B3LYP/6-311+G(d,p) level) was performed on 100 geometries randomly selected for each trajectory, and its ground state energy was compared to the predicted energy by correlation graphs: the linear regression R^2 parameters are *ca.* 0.9 or higher for *trans*-azobenzene, while lower R^2 values (0.7−0.8) are recorded for *cis*-azobenzene when applying external forces higher than 1 nN. Nevertheless, in all cases a remarkable correlation was found for the excitation energy ($R^2 \sim 1$; see Supporting Information for details). This could be due to the fact that both ground and excited state energies are affected by almost the same error, finally leading to a correct excitation energy shift.

We should also notice that, since we are considering the intrinsic vibrational fluctuations of the system but neglecting the quantum vibronic states, we may expect nuclear quantum effects to displace the calculated absorption maxima. Nevertheless, pure quantum dynamics is unaffordable for a large molecule as azobenzene (with 66 internal degrees of freedom). Moreover, we do observe that the main contribution to the broadening of the absorption band is due to stretching modes of the carbon skeleton. Since the vibrational frequency for such kind of modes is of the order of $h\nu \sim kT$, it is not expected to find large differences between the proposed classical dynamics and quantum dynamics. Indeed, our results are in agreement with the experimental absorption spectra recorded without external force.[37,38]

Compression forces were also considered, finding out that modulation of the absorption energy is limited or, in some cases, not possible at all. More in detail, *trans*-azobenzene shows no modulation for the $S_0 \rightarrow S_1$ transition and a narrow modulation (3.5 kcal·mol^{-1} maximum absorption shift) for the $S_0 \rightarrow S_2$ transition, moreover limited to compression forces not higher than 0.75 nN. The *cis* isomer has a similar behavior, with maximum absorption shifts of 6 kcal·mol^{-1} ($S_0 \rightarrow S_1$) and 4 kcal·mol^{-1} ($S_0 \rightarrow S_2$), corresponding to a compression force of 0.5 nN. At higher forces no further modulation is recorded (see Supporting Information for details). These findings are in good accordance with experimental results, that report the capability to compress azobenzene (by atomic force microscopy) ensuring *trans*-to-*cis* photoswitching only up to 0.5 nN.[7]

Therefore, elongation would be preferred to compression forces, in order to obtain a higher modulation of the spectroscopical properties and, coupled to a higher deformation, a larger optomechanical work (see Figure 3). As a successful example, a DNA-based molecular motor containing

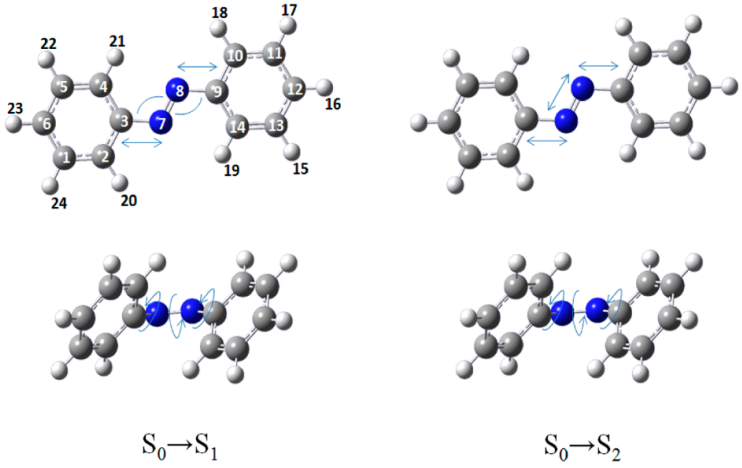

Figure 9. Internal coordinates (blue arrows) most involved in efficient modulation of the $S_0 \rightarrow S_1$ (left) and $S_0 \rightarrow S_2$ (right) excitation energies, for both *trans*- (top) and *cis*- (bottom) azobenzene.

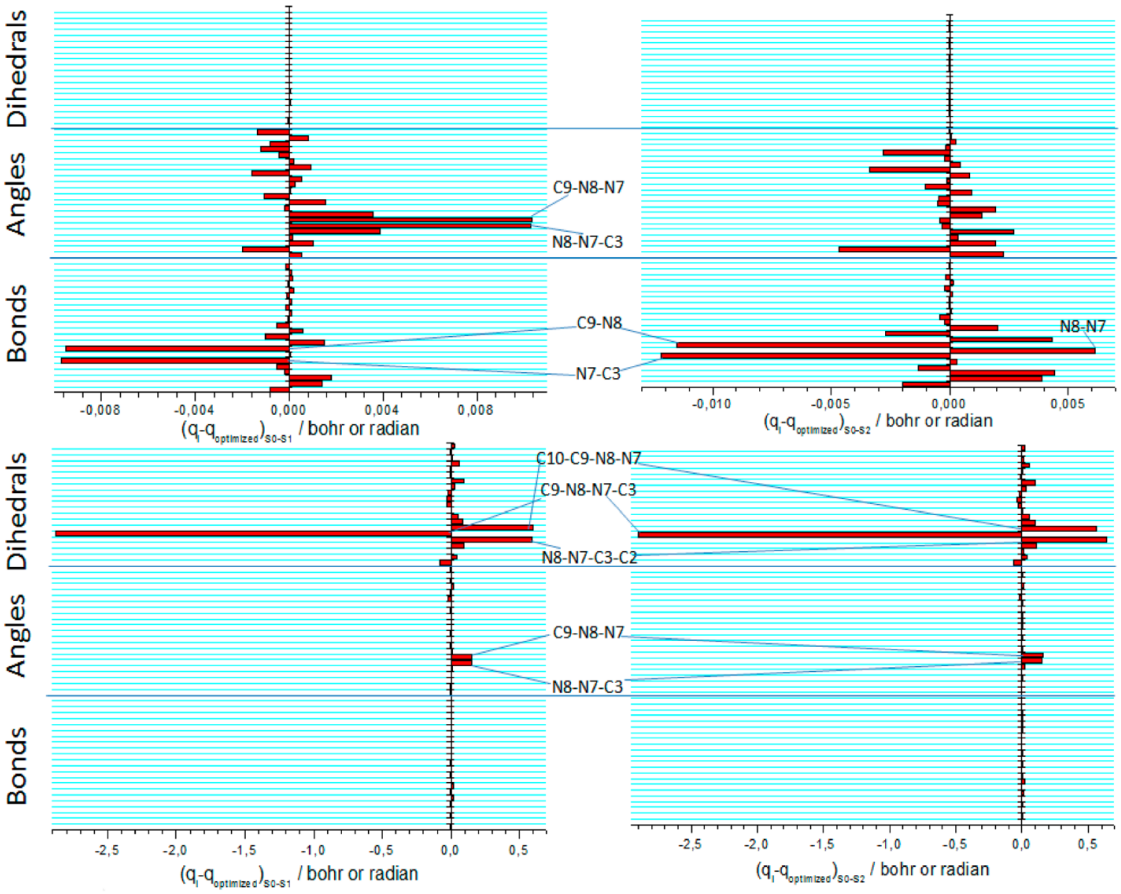

Figure 10. Contributions from each internal coordinate as a function of its variation from the equilibrium geometry (when applying 0.5 nN force), for both $S_0 \rightarrow S_1$ (left) and $S_0 \rightarrow S_2$ (right) vertical excitations. The most relevant coordinates are highlighted, corresponding mainly to angles and bonds for *trans*-azobenzene (top) and to dihedrals for *cis*-azobenzene (bottom). Refer to Figure 9 for atom numbering.

azobenzene as photoswitching unit was already proposed. Nevertheless, in this case the applied elongation forces are strongly limited (elastic limit at *ca.* 0.06 nN) by the fact that the DNA moiety can undergo unfolding.[54] We alternatively discuss the eventual inclusion of azobenzene in the main chain of a

dx.doi.org/10.1021/ct4007629 | *J. Chem. Theory Comput.* 2014, 10, 312−323

Journal of Chemical Theory and Computation Article

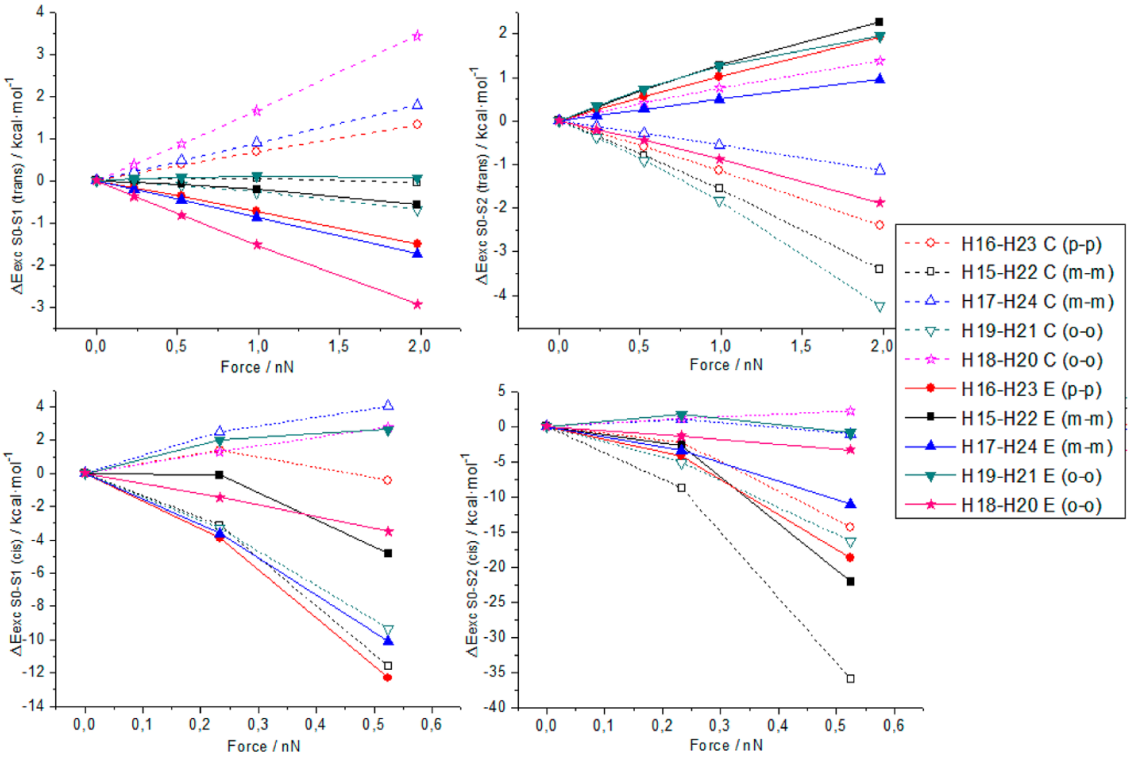

Figure 11. Excitation energy (CAM-B3LYP/6-311+G(d,p) level of theory) modulation as a function of external forces. Compression (C, dotted line) and elongation (E, thick line) is considered for *para*−*para* (p-p), *meta*−*meta* (m-m) and *orto*−*orto* (o-o) pair of forces applied to hydrogens (refer to Figure 9 for atom numbering). The results are shown for *trans* (top) and *cis* (bottom) isomers, including $S_0 \rightarrow S_1$ (left) and $S_0 \rightarrow S_2$ (right) electronic transitions.

polymer, where unfolding processes should not play a major role, generating a more convenient optomechanical cycle.

Structural Analysis. In the previous section, the results obtained by applying a pair of forces in *para* position with respect to the N═N moiety were discussed, showing how absorption properties can be modulated by the extent of the force applied. In this section a full structural analysis is performed, in order to determine (1) which molecular distortions are mainly responsible for absorption modulation and (2) which positions within the phenyl ring are the most suitable to efficiently produce such distortions, when a pair of external forces is applied (i.e., considering alternatives to the pair of force vectors in *para*−*para* configuration). Especially, the main coordinates involved in optimal modulation of the excited state energy gap ($\Delta E_{\text{exc S0–S1}}$; $\Delta E_{\text{exc S0–S2}}$) are shown in Figure 9, and the role of each internal coordinate is depicted in Figure 10.

We can therefore conclude that the C−N═N−C moiety is responsible for modulation of the excitation energy, being bond stretching and angle bending more relevant for the *trans* isomer, while torsions around dihedral angles are the leading contributions for the *cis* isomer. The variation of the excitation energy per force unit ($\Delta E_{\text{exc}}/\boldsymbol{F}^{\text{ext}}$) is within the range 2−2.5 kcal·mol^{-1}·nN^{-1} in the case of *trans*-azobenzene (up to 4 nN); while for *cis*-azobenzene the highest value (8 kcal·mol^{-1}·nN^{-1}) corresponds to ca. 0.5 nN, and decreases when applying higher forces (see Supporting Information for details).

Different pairs of force vectors were applied in all phenyl positions symmetric with respect to the center of inversion of the *trans* isomer, resulting in five possibilities: one pair in *para*−*para*, two pairs in *meta*−*meta* and two pairs in *orto*−*orto*. The results are shown in Figure 11.

Therefore, even though the application of external forces in *para* positions is a suitable choice (especially for bathochromic shifting the $S_0 \rightarrow S_1$ energy of the *cis* isomer), a more efficient modulation of the absorption energy is usually envisaged by forces applied in *meta*−*meta* or *orto*−*orto*. Moreover, it is in general possible to select the pair of forces depending on the desired (red or blue) shift, highlighting the red shifting capability of the pair applied at H_{15}−H_{22} (*meta*−*meta*) in compression mode to the *cis* isomer ($\Delta E_{\text{exc S0–S2}} \sim 36$ kcal mol^{-1}).

Toward a Linear Polymer Photoswitching Device. Two different operation modes were considered, applying forces at *para* positions (as for the dynamical study). Operation mode I: (1) elongation of the *trans* isomer, (2) *trans*-to-*cis* photoisomerization, (3) compression of the *cis* isomer, (4) *cis*-to-*trans* photoisomerization. Operation mode II: (1) elongation of the *cis* isomer, (2) *cis*-to-*trans* photoisomerization, (3) compression of the *trans* isomer, (4) *trans*-to-*cis* photoisomerization. Being the elastic limit of *trans*- and *cis*-azobenzene different in force applied and deformation gained, the two proposed operation modes give rise to a different maximum amount of work: operation mode I corresponds to 2.51×10^{-19} J, while operation mode II generates 3.69×10^{-19} J. These values refer to the single molecule. Nevertheless, if we consider *n* azobenzene units within a linear polymer chain (*n*: degree of polymerization), an elongation force can be applied

dx.doi.org/10.1021/ct4007629 | J. Chem. Theory Comput. 2014, 10, 312−323

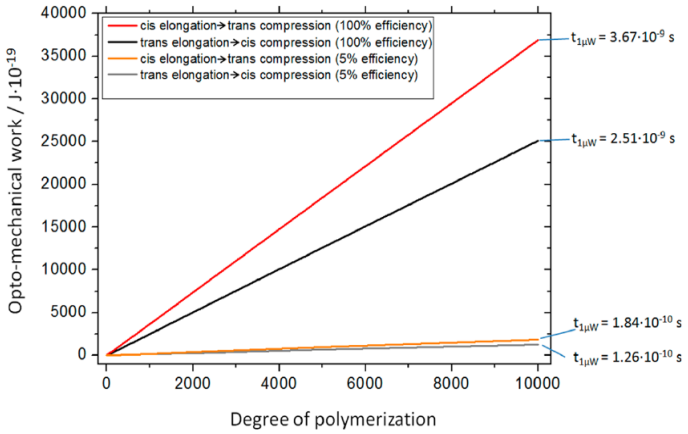

Figure 12. Estimation of the optomechanical work as a function of the degree of polymerization, assuming a linear polymer containing azobenzene units in its main chain. Operation mode I (*trans* elongation → *cis* compression) and II (*cis* elongation → *trans* compression) are shown, for a total efficiency of 100% and 5%, that takes into account the photoisomerization quantum yield during the cycle. For a 10 000 degree polymerization, the time required to perform a cycle in order to generate 1 μW power is calculated.

to both ends of the chain, producing an overall deformation n times larger with respect to the single molecule (assuming that all azobenzene units are in the same isomeric form). Experimentally, different methods were successfully applied in order to synthesize and characterize polymers bearing azobenzene moieties in their main chain.[13,21−24] Therefore, once clarified the optomechanical behavior of the single monomer, the work can be considered as a linear function of the degree of polymerization (Figure 12). This straightforward calculation corresponds to a device able to fully convert the optical excitation energy into mechanical work. Nevertheless, to complete a single optomechanical cycle a 5% quantum yield was experimentally estimated for azobenzene photoisomerization,[7,55] reducing the overall efficiency of the eventual device (see Figure 12). Especially, the work estimated by Holland et al. for an oligomer containing 10 azobenzene units, resulting from a first compression step (0.4 nN), is *ca.* 5×10^{-20} J.[55] In our work, the corresponding oligomer operating in modes I and II (i.e., undergoing elongation as first step) would correspond to *ca.* 12×10^{-20} J and 18×10^{-20} J, respectively, being a notable improvement.

Moreover, assuming a certain degree of polymerization and setting a target value for the power that could be produced by such a motor, the time required to perform an optomechanical cycle can be estimated. For example to obtain 1 μW power (scale of interest in nanotechnology[56]), a time between 1 and 2 $\times$ 10^{-10} s would be required by a linear polymer chain containing 10 000 azobenzene units, with a realistic efficiency of 5% (Figure 12).

Considering that azobenzene photoisomerization was proven to be an ultrafast process for both *cis*-to-*trans* (0.17 ps) and *trans*-to-*cis* (0.32 ps) conformational changes,[17,39] a full optomechanical cycle of *ca.* 0.5 ps (1 ps =10^{-12} s) can be estimated, leading to a low degree of polymerization to accomplish the requirements of a 1 μW motor: 40 in operation mode I and 27 in operation mode II. Increasing to 10000 the degree of polymerization, the corresponding power scales up to *ca.* 251 μW (mode I) and 369 μW (mode II).

As future perspectives, we can define four parameters by which work (and therefore power) can be improved: (i) degree of polymerization, (ii) maximum force applicable, (iii) maximum deformation (elongation and compression) length, (iv) quantum yield of the photoisomerization. While the first is a macromolecular parameter involving polymer chemistry, the other three parameters are characteristics of the single chromophore.

■ SUMMARY AND CONCLUSIONS

We presented new methodologies to simulate force spectroscopy experiments on single molecules, on the basis of optimization and classical dynamics on analytical potential energy surfaces. Large simulations (nanosecond time scale) were performed at a low computational cost, in order to reproduce electronic absorption spectra while applying a constant external force to both ends of the chromophore under study.

The proposed method was applied to azobenzene, one of the most studied photoswitches. Its mechanical properties were investigated by reproducing the corresponding stress−strain curves. This allowed to estimate the elastic limit and therefore the maximum forces which could be applied during the force spectroscopy simulations.

The resulting absorption spectra have shown the possibility to modulate the vertical excitation energy as a function of the elongation force and of the position within the molecule where it is applied, for both *trans* and *cis* isomers. This could be of interest for laser applications and optomechanical devices. Especially, we calculated the work generated by performing a single molecule optomechanical cycle, applying two different operation modes. After a comparison with available results in literature, an optomechanical motor based on a linear polymer bearing azobenzene units in its main chain was discussed, finally estimating the work and power eventually produced as a function of the degree of polymerization. Interestingly, we observe the possibility to produce power in the microwatt scale even at low degrees of polymerization.

■ ASSOCIATED CONTENT

Supporting Information

Absorption spectra while applying compression forces. Details of the developed methodologies. Analysis of the errors related to the ground and excited state energies. Numerical evaluation

of the oscillator strength. Cartesian coordinates of the most relevant structures along the ground state minimum energy path. Cartesian coordinates of the force constrained optimized structures. This material is available free of charge via the Internet at http://pubs.acs.org.

AUTHOR INFORMATION

Corresponding Authors

*Tel.: +34 91 885 2512. Fax: +34 918854763. E-mail: luisma.frutos@uah.es.

*E-mail: marco.marazzi@uah.es.

Present Address

[†]Department of Theoretical Chemical Biology, Institute for Physical Chemistry, Karlsruhe Institute of Technology, Kaiserstr. 12, 76131 Karlsruhe, Germany

Notes

The authors declare no competing financial interest.

ACKNOWLEDGMENTS

This research was supported by the Spanish MICINN grants CTQ2009-07120 and CTQ2012-36966. F.Z. is grateful to the Spanish MEC (Ministerio de Educación y Ciencia), and M.A.F.-G., D.R., and M.M. are grateful to the UAH (Universidad de Alcalá) for a doctoral fellowship.

DEDICATION

This work is dedicated to Prof. Obis Castaño on the occasion of his 70th birthday.

REFERENCES

(1) Hosono, N.; Kajitani, T.; Fukushima, T.; Ito, K.; Sasaki, S.; Takata, M.; Aida, T. *Science* **2010**, *330*, 808.

(2) Bleger, D.; Yu, Z.; Hecht, S. *Chem. Commun.* **2011**, *47*, 12260.

(3) *Molecular Switches*; 2nd ed.; Feringa, B. L.; Browneed, W. R., Eds.; Wiley-VCH: Weinheim, 2011.

(4) *Molecular Devices and Machines*; 2nd ed.; Balzani, V.; Credi, A.; Venturi, M., Eds.; Wiley-VCH: Weinheim, 2008.

(5) García-Iriepa, C.; Marazzi, M.; Frutos, L. M.; Sampedro, D. *RSC Adv.* **2013**, *3*, 6241.

(6) Turansky, R.; Konopka, M.; Doltsinis, N. L.; Stich, I.; Marx, D. *ChemPhysChem* **2010**, *11*, 345.

(7) Hugel, T.; Holland, N. B.; Cattani, A.; Moroder, L.; Seitz, M.; Gaub, H. E. *Science* **2002**, *296*, 1103.

(8) Shao, J.; Lei, Y.; Wen, Z.; Dou, Y.; Wang, Z. *J. Chem. Phys.* **2008**, *129*, 164111/1.

(9) Turansky, R.; Konopka, M.; Doltsinis, N. L.; Stich, I.; Marx, D. *Phys. Chem. Chem. Phys.* **2010**, *12*, 13922.

(10) Doltsinis, N. L.; Marx, D. *J. Theor. Comput. Chem.* **2002**, *1*, 319.

(11) Blanco-Lomas, M.; Samanta, S.; Campos, P. J.; Woolley, G. A.; Sampedro, D. *J. Am. Chem. Soc.* **2012**, *134*, 6960.

(12) Schierling, B.; Noel, A.-J.; Wende, W.; Hien, L. T.; Volkov, E.; Kubareva, E.; Oretskaya, T.; Kokkinidis, M.; Roempp, A.; Spengler, B.; Pingoud, A. *Proc. Natl. Acad. Sci. U. S. A.* **2010**, *107*, 1361.

(13) Sapich, B.; Vix, A. B. E.; Rabe, J. P.; Stumpe, J. *Macromolecules* **2005**, *38*, 10480.

(14) Ercole, F.; Davis, T. P.; Evans, R. A. *Polym. Chem.* **2010**, *1*, 37.

(15) Mahimwalla, Z.; Yager, K. G.; Mamiya, J.-i.; Shishido, A.; Priimagi, A.; Barrett, C. J. *Polym. Bull. (Heidelberg, Ger.)* **2012**, *69*, 967.

(16) Satzger, H.; Root, C.; Braun, M. *J. Phys. Chem. A* **2004**, *108*, 6265.

(17) Naegele, T.; Hoche, R.; Zinth, W.; Wachtveitl, J. *Chem. Phys. Lett.* **1997**, *272*, 489.

(18) Fujino, T.; Tahara, T. *J. Phys. Chem. A* **2000**, *104*, 4203.

(19) Fujino, T.; Arzhantsev, S. Y.; Tahara, T. *J. Phys. Chem. A* **2001**, *105*, 8123.

(20) Chang, C.-W.; Lu, Y.-C.; Wang, T.-T.; Diau, E. W.-G. *J. Am. Chem. Soc.* **2004**, *126*, 10109.

(21) Huang, H.-Y.; Lee, Y.-T.; Yeh, L.-C.; Jian, J.-W.; Huang, T.-C.; Liang, H.-T.; Yeh, J.-M.; Chou, Y.-C. *Polym. Chem.* **2013**, *4*, 343.

(22) Jaycox, G. D. *J. Polym. Sci., Part A: Polym. Chem.* **2005**, *44*, 207.

(23) Keum, C.-D.; Ikawa, T.; Tsuchimori, M.; Watanabe, O. *Macromolecules* **2003**, *36*, 4916.

(24) Howe, L. A.; Jaycox, G. D. *J. Polym. Sci., Part A: Polym. Chem.* **1998**, *36*, 2827.

(25) Davis, D. A.; Hamilton, A.; Yang, J.; Cremar, L. D.; Van, G. D.; Potisek, S. L.; Ong, M. T.; Braun, P. V.; Martinez, T. J.; White, S. R.; Moore, J. S.; Sottos, N. R. *Nature* **2009**, *459*, 68.

(26) Kryger, M. J.; Ong, M. T.; Odom, S. A.; Sottos, N. R.; White, S. R.; Martinez, T. J.; Moore, J. S. *J. Am. Chem. Soc.* **2010**, *132*, 4558.

(27) Lenhardt, J. M.; Ong, M. T.; Choe, R.; Evenhuis, C. R.; Martinez, T. J.; Craig, S. L. *Science* **2010**, *329*, 1057.

(28) Wolinski, K.; Baker, J. *Mol. Phys.* **2009**, *107*, 2403.

(29) Wolinski, K.; Baker, J. *Mol. Phys.* **2010**, *108*, 1845.

(30) Tuckerman, M. E.; Liu, Y.; Ciccotti, G.; Martyna, G. J. *J. Chem. Phys.* **2001**, *115*, 1678.

(31) Martyna, G. J.; Tuckerman, M. E.; Tobias, D. J.; Klein, M. L. *Mol. Phys.* **1996**, *87*, 1117.

(32) *Marvin 5.12.0*; ChemAxon: Budapest, Hungary, 2013; www.chemaxon.com.

(33) Brown, E. V.; Granneman, G. R. *J. Am. Chem. Soc.* **1975**, *97*, 621.

(34) Lednev, I. K.; Ye, T. Q.; Matousek, P.; Towrie, M.; Foggi, P.; Neuwahl, F. V. R.; Umapathy, S.; Hester, R. E.; Moore, J. N. *Chem. Phys. Lett.* **1998**, *290*, 68.

(35) Lednev, I. K.; Ye, T.-Q.; Hester, R. E.; Moore, J. N. *J. Phys. Chem.* **1996**, *100*, 13338.

(36) Hamm, P.; Ohline, S. M.; Zinth, W. *J. Chem. Phys.* **1997**, *106*, 519.

(37) Hamon, F.; Djedaini-Pilard, F.; Barbot, F.; Len, C. *Tetrahedron* **2009**, *65*, 10105.

(38) Bandara, H. M. D.; Burdette, S. C. *Chem. Soc. Rev.* **2012**, *41*, 1809.

(39) Ishikawa, T.; Noro, T.; Shoda, T. *J. Chem. Phys.* **2001**, *115*, 7503.

(40) Pederzoli, M.; Pittner, J.; Barbatti, M.; Lischka, H. *J. Phys. Chem. A* **2011**, *115*, 11136.

(41) Toniolo, A.; Ciminelli, C.; Persico, M.; Martinez, T. J. *J. Chem. Phys.* **2005**, *123*, 234308/1.

(42) Cembran, A.; Bernardi, F.; Garavelli, M.; Gagliardi, L.; Orlandi, G. *J. Am. Chem. Soc.* **2004**, *126*, 3234.

(43) Monti, S.; Orlandi, G.; Palmieri, P. *Chem. Phys.* **1982**, *71*, 87.

(44) Ciminelli, C.; Granucci, G.; Persico, M. *Chem.—Eur. J.* **2004**, *10*, 2327.

(45) Gagliardi, L.; Orlandi, G.; Bernardi, F.; Cembran, A.; Garavelli, M. *Theor. Chem. Acc.* **2004**, *111*, 363.

(46) Conti, I.; Garavelli, M.; Orlandi, G. *J. Am. Chem. Soc.* **2008**, *130*, 5216.

(47) Klug, R. L.; Burcl, R. *J. Phys. Chem. A* **2010**, *114*, 6401.

(48) Becke, A. D. *J. Chem. Phys.* **1993**, *98*, 1372.

(49) Lee, C.; Yang, W.; Parr, R. G. *Phys. Rev. B: Condens. Matter* **1988**, *37*, 785.

(50) Yanai, T.; Tew, D. P.; Handy, N. C. *Chem. Phys. Lett.* **2004**, *393*, 51.

(51) Frisch, M. J.; Trucks, G. W.; Schlegel, H. B.; Scuseria, G. E.; Robb, M. A.; Cheeseman; J. R.; Scalmani; G.; Barone; V.; Mennucci; B.; Petersson, G. A.; Nakatsuji, H.; Caricato, M.; Li, X.; Hratchian, H. P.; Izmaylov, A. F.; Bloino, J.; Zheng, G.; Sonnenberg, J. L.; Hada, M.; Ehara, M.; Toyota, K.; Fukuda, R.; Hasegawa, J.; Ishida, M.;Nakajima, T.; Honda, Y.; Kitao, O.; Nakai, H.; Vreven, T.; Montgomery, J. A., Jr.; Peralta, J. E.; Ogliaro, F.; Bearpark, M.; Heyd, J. J.; Brothers, E.; Kudin, K. N.; Staroverov, V. N.; Kobayashi, R.; Normand, J.; Raghavachari, K.; Rendell, A.; Burant, J. C.; Iyengar, S. S.; Tomasi, J.; Cossi, M.; Rega, N.; Millam, J. M.; Klene, M.; Knox, J. E.; Cross, J. B.; Bakken, V.; Adamo, C.; Jaramillo, J.; Gomperts, R.; Stratmann, R. E.; Yazyev, O.; Austin, A. J.; Cammi, R.; Pomelli, C.; Ochterski, J. W.; Martin, R. L.;

Morokuma, K.; Zakrzewski, V. G.; Voth, G. A.; Salvador, P.; Dannenberg, J. J.; Dapprich, S.; Daniels, A. D.; Farkas, O.; Foresman, J. B.; Ortiz, J. V.; Cioslowski, J.; Fox, D. J. *Gaussian 09*, Revision D.01; Gaussian, Inc.: Wallingford, CT, 2009.
(52) *Thermoplastics and Thermoplastic Composites*; 1st ed.; Biron, M., Ed.; Elsevier Ltd.: Oxford, 2007.
(53) Fernandez-Gonzalez, M. A.; Marazzi, M.; Lopez-Delgado, A.; Zapata, F.; Garcia-Iriepa, C.; Rivero, D.; Castano, O.; Temprado, M.; Frutos, L. M. *J. Chem. Theory Comput.* **2012**, *8*, 3293.
(54) McCullagh, M.; Franco, I.; Ratner, M. A.; Schatz, G. C. *J. Am. Chem. Soc.* **2011**, *133*, 3452.
(55) Holland, N. B.; Hugel, T.; Neuert, G.; Cattani-Scholz, A.; Renner, C.; Oesterhelt, D.; Moroder, L.; Seitz, M.; Gaub, H. E. *Macromolecules* **2003**, *36*, 2015.
(56) Wang, Z. L.; Wu, W. *Angew. Chem., Int. Ed.* **2012**, *51*, 11700.

6.3 Chapter Bibliography

Balaz, P.; Achimovicova, M.; Balaz, M.; Billik, P.; Cherkezova-Zheleva, Z.; Criado, J. M.; Delogu, F.; Dutkova, E.; Gaffet, E.; Gotor, F. J.; Kumar, R.; Mitov, I.; Rojac, T.; Senna, M.; Streletskii, A.; Wieczorek-Ciurowa, K., Hallmarks of mechanochemistry: from nanoparticles to technology. *Chem. Soc. Rev.* **2013**.

Beyer, M. K.; Clausen-Schaumann, H., Mechanochemistry: The Mechanical Activation of Covalent Bonds. *Chem. Rev.* **2005,** *105*, 2921-2948.

Blanco-Lomas, M.; Samanta, S.; Campos, P. J.; Woolley, G. A.; Sampedro, D., Reversible Photocontrol of Peptide Conformation with a Rhodopsin-like Photoswitch. *J. Am. Chem. Soc.* **2012,** *134*, 6960-6963.

Bléger, D.; Yu, Z.; Hecht, S., Toward optomechanics: Maximizing the photodeformation of individual molecules. *Chem. Commun.* **2011,** *47*, 12260–12266.

Caruso, M. M.; Davis, D. A.; Shen, Q.; Odom, S. A.; Sottos, N. R.; White, S. R.; Moore, J. S., Mechanically-Induced Chemical Changes in Polymeric Materials. *Chem. Rev.* **2009,** *109*, 5755-5798.

Ercole, F.; Davis, T. P.; Evans, R. A., Photo-responsive systems and biomaterials: photochromic polymers, light-triggered self-assembly, surface modification, fluorescence modulation and beyond. *Polym. Chem.* **2010,** *1*, 37-54.

Hammett, L. P., The Effect of Structure upon the Reactions of Organic Compounds. Benzene Derivatives. *J. Am. Chem. Soc.* **1937,** *59*, 96-103.

Helgaker, T.; Jorgensen, P.; Olsen, J., *Moleculat Electronic-Structure Theory*. JHON WILEY & SONS Great Britain, 2000.

Holland, N. B.; hugel, T.; Neuert, G.; Cattani-Scholz, A.; Renner, C.; Oesterhelt, D.; moroder, L.; Seitz, M.; Gaub, H. E., Single Molecule Force Spectroscopy of Azobenzene Polymers: Switching Elasticity of Single Photochromic Macromolecules. *Macromolecules* **2003,** *36*, 2015-2023.

Hugel, T.; Holland, N. B.; Cattani, A.; Moroder, L.; Seitz, M.; Gaub, H. E., Single-Molecule Optomechanical Cycle. *Science* **2002,** *296*, 1103-1106.

Marazzi, M.; López-Delgado, A.; Fernández-González, M. A.; Castaño, O.; Frutos, L. M.; Temprado, M., Modulating Nitric Oxide Release by S-Nitrosothiol Photocleavage: Mechanism and Substituent Effects. *The Journal of Physical Chemistry A* **2012,** *116*, 7039-7049.

McCullagh, M.; Franco, I.; Ratner, M. A.; Schatz, G. C., DNA-Based Optomechanical Molecular Motor. *J. Am. Chem. Soc.* **2011,** *133*, 3452-3459.

Sapich, B.; Vix, A. B. E.; Rabe, J. P.; Stumpe, J., Photoinduced Self-Organization and Photoorientation of a LC Main-Chain Polyester Containing Azobenzene Moieties. *Macromolecules* **2005,** *38*, 10480-10486.

Schierling, B.; Noel, A.-J.; Wende, W.; Hien, L. T.; Volkov, E.; Kubareva, E.; Oretskaya, T.; Kokkinidis, M.; Roempp, A.; Spengler, B.; Pingoud, A., Controlling the enzymatic activity of a restriction enzyme by light. *Proc. Natl. Acad. Sci. U. S. A.* **2010,** *107*, 1361-1366, S1361/1-S1361/4.

Stamler, J. S.; Jia, L.; Eu, J. P.; McMahon, T. J.; Demchenko, I. T.; Bonaventura, J.; Gernert, K.; Piantadosi, C. A., Blood Flow Regulation by S-Nitrosohemoglobin in the Physiological Oxygen Gradient. *Science* **1997,** *276*, 2034-2037.

Swain, C. G.; Lupton, E. C., Field and resonance components of substituent effects. *J. Am. Chem. Soc.* **1968,** *90*, 4328-4337.

Taft, R. W., Polar and Steric Substituent Constants for Aliphatic and o-Benzoate Groups from Rates of Esterification and Hydrolysis of Esters1. *J. Am. Chem. Soc.* **1952,** *74*, 3120-3128.

Wang, K.; Rangel, N. L.; Kundu, S.; Sotelo, J. C.; Tovar, R. M.; Seminario, J. M.; Liang, H., Switchable Molecular Conductivity. *J. Am. Chem. Soc.* **2009,** *131*, 10447-10451.

Wiggins, K. M.; Brantley, J. N.; Bielawski, C. W., Polymer Mechanochemistry: Force Enabled Transformations. *ACS Macro Letters* **2012,** *1*, 623-626.

Woodward, R. B., Structure and the Absorption Spectra of α,β-Unsaturated Ketones. *J. Am. Chem. Soc.* **1941,** *63*, 1123-1126.

Chapter 7: Photodynamical Behaviour of Molecular Devices

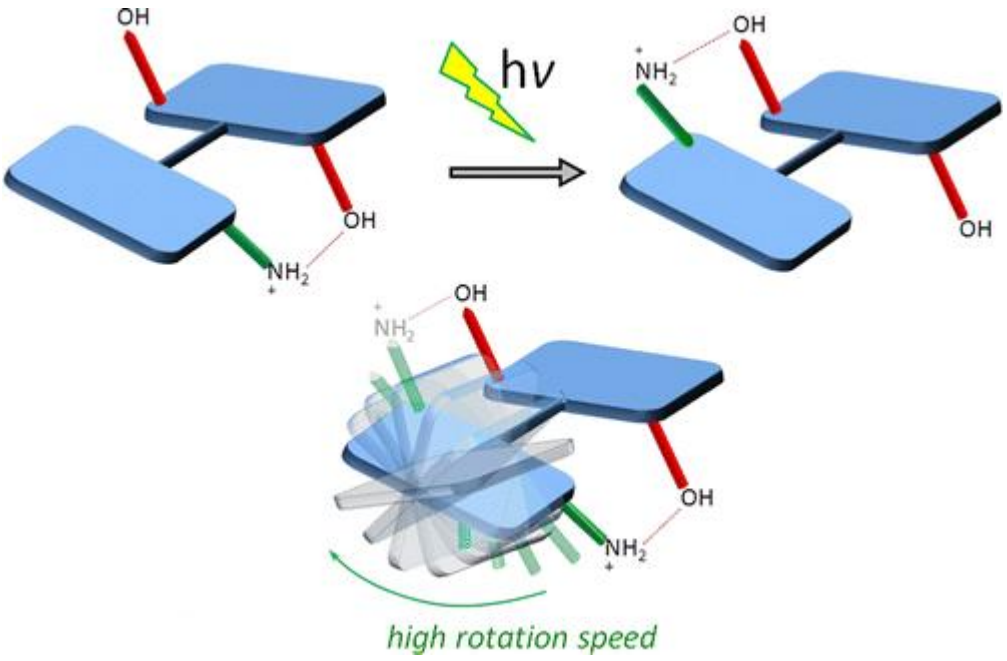

From the moment when the machine first made its appearance it was clear to all thinking people that the need for human drudgery, and therefore to a great extent for human inequality, had disappeared. If the machine were used deliberately for that end, hunger, overwork, dirt, illiteracy, and disease could be eliminated within a few generations. And in fact, without being used for any such purpose, but by a sort of automatic process -- by producing wealth which it was sometimes impossible not to distribute -- the machine did raise the living standards of the average human being very greatly over a period of about fifty years at the end of the nineteenth and the beginning of the twentieth centuries.

But it was also clear that an all-round increase in wealth threatened the destruction -- indeed, in some sense was the destruction -- of a hierarchical society.

1984. George Orwell.

7.1 Introduction

The accomplishment of a molecular device which uses geometrical transformations, as the driving force to generate a periodic motion which result in an autonomous power generation at molecular scale, has been a major goal in molecular engineering. The design of such devices requires a careful consideration of the many physical details involved in such devices, as the nature of the energy required to carry out the geometrical transformation, the automation of the cyclic power generation, as well as the requirements in terms of structure and chemical reactivity that the candidates molecules should have, etc.

7.1.1 Molecular Switches and Motors

The design and construction of molecular device by the bottom-up strategy (i.e. from atoms to molecular devices) is a major goal of nanotechnology. Molecular switches and motors are essential parts of molecular machines, and full understanding of its mechanisms and dynamical properties is of fundamental importance. These devices convert energy supply into mechanical energy, leading to a controlled motion (Feringa 2007). Photoinduced processes are well suited to use as input energy for molecular devices, because it does not produce waste products and the devices can operate in autonomous fashion (Balzani, et al. 2009, Cnossen, et al. 2012).

Photoswitches are bi-stable (state A and B) chromophores of special interest in the design and fabrication of optomechanical devices, since the absorption of light at a certain wavelength by state A is usually followed by a large structural change, which makes possible to reach state B. Then a second pulse of light (or thermal relaxation step), commonly at a different wavelength, reverse the process defining a pathway from state B back to state A (Balzani, et al. 2008, Feringa and Browneed 2011). Especially, switches based on photoisomerization are commonly applied to solve a variety of scientific and engineering problems, ranging from protein conformation control to photocatalysis, from molecular data storage to foldamers (Dong, et al. 2012). In all these cases, photoisomerization provides an efficient (*i.e.* ultrafast time scale) way to switch a process ON and OFF (Garcia-Iriepa, et al. 2013). Moreover, we can take advantage of the photoswitching property of a chromophore by generating optomechanical work in a single molecule device, operating switching cycles in a periodic mode, and therefore

leading to the eventual design and fabrication of optomechanical motors (Holland, et al. 2003).

Of particular interest are the optomechanical materials, which are based on direct conversion of light (applied as input), into macroscopic motion. This behaviour depends on the molecular structure of the material itself. Especially, soft organic materials were successfully designed as optomechanical responsive systems (*e.g.* oligomers and polymers) where the presence of one or more chromophore units is essential to ensure light absorption, which constitutes the first necessary event to promote the subsequent conformational and/or chemical modification underlying mechanical motion (Bleger, et al. 2011, Hosono, et al. 2010).

In this thesis it is presented a series of rules for designing photoswitches and photoactive motors based on existing chromophores like the protonated Schiff base chromophores of rhodopsins, remarking the use of hydrogen bonds in setting up the unidirectional rotation.

7.2 Results

The mechanism of photoswitches is the interconversion between the two possible states, on/off, while the performance of molecular motors involves a continuous, repetitive and unidirectional rotary movement of 360 degrees. Therefore, in the design of molecular motors is crucial to promote the unidirectional rotation of the device, and among the possible effect that can induce unidirectional rotations, it has been found that a chiral environment induce an asymmetric gradient which induces a unidirectional rotation (Albu, et al. 2009, Liu and Morokuma 2012, Yamaki, et al. 2005).

In the contributions presented in this section, there was explored a set of efficient photoswitches, based on the retinal chromophore, which are then taken as framework to the design of novel molecular motors, where the unidirectional rotation is caused by an initial torsion induced by hydrogen-bonds with chiral properties. It is important to emphasize that while molecular motors based on helical structured like diarylethenes (ter Wiel, et al. 2003), need four steps to complete a cycle (two photochemical and two

thermal steps), we propose molecular motors performing a cycle in two identical photochemical steps.

Such molecular devices should fulfil some specifications: the molecule should be planar with several conjugated π double bonds; a $\pi \rightarrow \pi^*$ electronic transition should be involved in order to induce a Z-E photoisomerization; it must be ensured that the optical brilliant state is the first accessible excited state or that the low lying excited states are similar to the bright state electronic nature, avoiding undesired photochemical pathways.

In order to show that the proposed molecular system meets the aforementioned conditions, it is firstly given a detailed description of the nature of the excited states.

Subsequently non-adiabatic molecular dynamics (NAMD) were performed to provide a dynamical picture of the molecular motor behaviour. The aims of the simulation were to provide statistical evidence of the unidirectional rotation, while the non-adiabatic algorithm was in charge of proving that not low lying state hinder the performance of the device. It was also possible to compute the mean time that the device spends in each involved electronic state, during a cycle of operation. Besides, the molecular dynamics simulations provided a detail description of the change in the geometrical coordinates involves in the photoinduced cycle, as for example the dihedral angle involves in the rotation.

7.2.1.1 Chiral hydrogen bond environment providing unidirectional rotation in photoactive molecular motors

THE JOURNAL OF PHYSICAL CHEMISTRY Letters

Letter

pubs.acs.org/JPCL

Chiral Hydrogen Bond Environment Providing Unidirectional Rotation in Photoactive Molecular Motors

Cristina García-Iriepa,[†,‡] Marco Marazzi,[†] Felipe Zapata,[†] Alessio Valentini,[†] Diego Sampedro,*[,‡] and Luis Manuel Frutos*[,†]

[†]Departamento de Química Física, Universidad de Alcalá, E-28871 Alcalá de Henares, Madrid, Spain

[‡]Departamento de Química, Centro de Investigación en Síntesis Química (CISQ), Madre de Dios 51, E-26006 Logroño, Spain

Supporting Information

ABSTRACT: Generation of a chiral hydrogen bond environment in efficient molecular photoswitches is proposed as a novel strategy for the design of photoactive molecular motors. Here, the following strategy is used to design a retinal-based motor presenting singular properties: (i) a single excitation wavelength is needed to complete the unidirectional rotation process (360°); (ii) the absence of any thermal step permits the process to take place at low temperatures; and (iii) the ultrafast process permits high rotational frequencies.

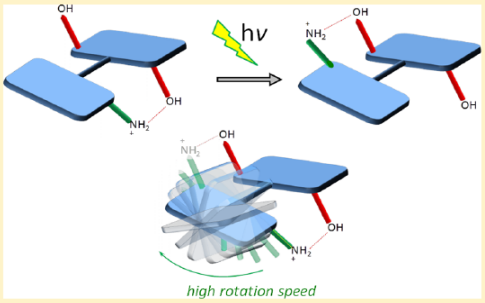

SECTION: Spectroscopy, Photochemistry, and Excited States

Construction of molecular devices with specific atomic-level properties has been a fundamental aim of nanotechnology in the last decades, as demonstrated by the design of molecular switches[1,2] and motors,[3] regular two/three-dimensional rotor arrays,[4] nanocars,[5] gyroscopes,[6] and so forth. Among these devices, molecular motors are of special interest as the input energy is converted into a controlled motion (unidirectional rotation) that plays an important role in both artificial and biological systems. Examples of Nature's molecular motors are the ATP synthase, kinesine, myosine, and flagellar motors in bacteria, all of them being essential for life.[7] Furthermore, artificial molecular motors have been proposed as crucial parts of molecular-level machines, mimicking biological systems by performing a specific function. The most suitable approach for chemists to construct molecular motors is the bottom-up approach, that is, starting from atoms or small building blocks.[8]

The design of efficient molecular motors should satisfy the following criteria: the energy supplied has to be transformed into a unidirectional repetitive rotary movement of 360° (i.e. mechanical work), and repetition of a high number of cycles has to be ensured (i.e., fatigue resistance).[9] The unidirectionality can be achieved by a protein or chiral environment (such as a protein surrounding[10] or a helical structure[11]). For novel applications (microscopic movement, control of macroscopic properties of materials, supramolecular organization and assemblies),[12] these devices are required to perform rotation at a considerable speed with high quantum yields. In contrast to Brownian,[13] electrically,[14] or chemically[15] driven motors, photoactivated ones are greatly profitable due to the manifest advantages of light as the energy supply.[11b,16] Among these types of devices, the ones reported by Feringa et al., based on a helical structure, are the most studied.[11] They present high quantum yields and need four steps (two photochemical and two thermal) to complete a cycle. Whereas the photochemical steps (Z−E photoisomerizations around a carbon−carbon double bond) are extremely fast, the thermal ones are rate-limiting, decreasing the rotational frequency of these devices. Further structural and electronic modifications have enhanced this weakness, leaving in any case the thermal isomerization steps as the bottleneck of the overall mechanism.[11b,17] Indeed, further theoretical studies have offered new insights to reduce or eliminate the thermal helix inversion steps of the overall mechanism.[18]

The approach presented here for the rational design of photoactive molecular motors is based on the use of an efficient photoactive molecular switch as the starting unit, in which a chiral environment is introduced via hydrogen bonds in order to obtain a molecular motor. Indeed, the complete rotation of this novel molecular motor is achieved only by two photochemical steps (no thermal steps are involved in the mechanism).

Photoactive molecular switches undergo Z−E photoisomerization around a given C═C, yielding the conversion between both stable states (Z and E). In order to control the

Received: December 24, 2012
Accepted: March 29, 2013
Published: March 29, 2013

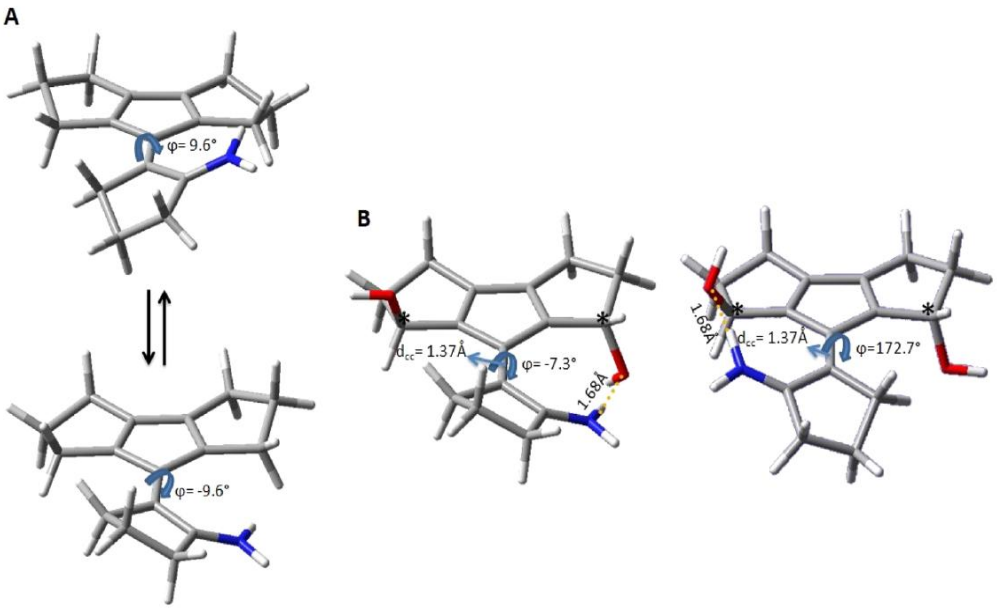

Figure 1. (A) Structure of the starting molecular photoswitch in its two possible conformations. Due to the same population for both isomers in the ground state, the system behaves as a photoswitch with no unidirectional rotation. (B) The corresponding derived molecular motor where the chiral hydrogen bond environment is introduced via −OH groups; the two symmetrically equivalent ground-state structures are shown, tailoring the two minima structures of the complete photocycle. Chiral carbon atoms with −OH are marked.

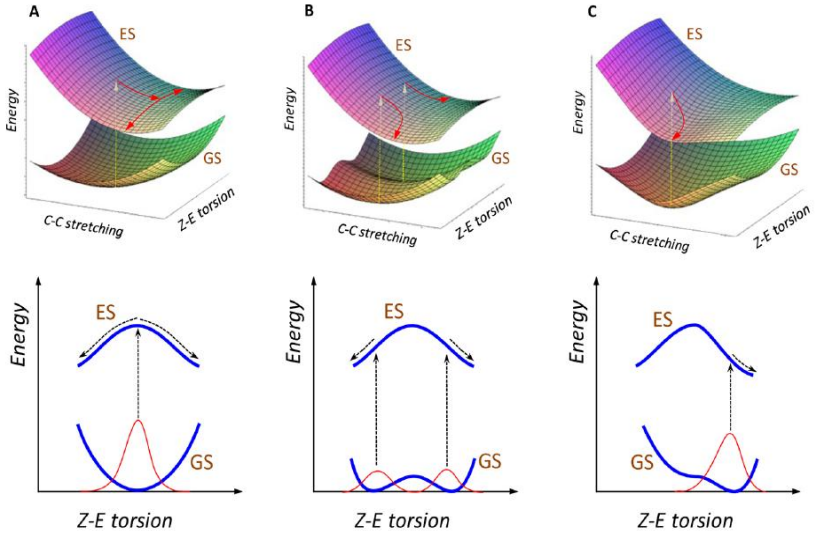

Figure 2. Schematic ground-state (GS) and excited-state (ES) PESs (up) and the corresponding distribution population on the ground state (down) for three different systems: (A) A planar photoswitch presenting a vanishing coupling between central bond torsion and stretching coordinates. Two rotation directions are possible in this case, and therefore, two minimum-energy paths bifurcate in the excited state at a transition state (noncontrolled rotational direction). (B) A nonplanar photoswitch showing two equivalent minima on the ground state, each one related to opposite rotation directions. (C) A photoactive molecular motor where the chiral hydrogen bond environment breaks the symmetry of the PES in both ground and excited states. The coupling between central bond torsion and stretching coordinates is not vanishing, inducing the torsion in a specific direction (controlled rotational direction).

photoreactivity of Z−E photoswitches, a general design strategy consists of blocking all but one double bond of the system by including them in rings of different size. Here, we use a molecular system exhibiting these characteristics, where only the central C═C bond linking two unsaturated rings is able to undergo Z−E photoisomerization. In this way, starting from a Z−E photoswitchable molecule with two equivalent ground-state minima (see Figure 1A), a chiral environment is introduced by including two hydroxyl groups linked to chiral carbon atoms, which permits formation of one hydrogen bond between the amino group and one of the two hydroxyl groups. Because the hydroxyl groups are linked to a chiral carbon atom,

we refer to this chemical ensemble as a chiral hydrogen bond environment (see Figure 1B). This chiral environment induces a guided pretwist around the C═C central bond in the ground state, leading to a single stable minimum on the ground state, which ultimately drives the unidirectional rotation in the excited state.

On the one hand, planar Z−E chromophores, as a retinal Schiff base photoswitch in gas and liquid phase, exhibit a $^1(\pi,\pi^*)$ photoactive excited electronic state.[19] Excitation to this electronic state is usually related to a vibrational excess[20] in the stretching modes involving the π system, provoking a bond length alternation of the conjugated backbone in the excited state. This vibrational energy is eventually transferred to the Z−E torsion mode involving molecular symmetry breaking and inducing the torsion in the excited state (i.e., stretching and torsion modes are not coupled in the case of strictly planar systems). The vibrational energy transfer takes place in many stretching cycles due to the lack of stretching−torsion coupling, which increases as the torsion becomes higher.[19a,21] Finally, a conical intersection (CI) with the ground state allows the torsion to be completed. In this situation, the evolution of the torsion coordinate in the excited state is not controlled, and the system can equally evolve in both possible directions (clockwise and counterclockwise). This noncontrolled torsion direction characterizes Z−E photoactive molecular switches.

Conversely, for nonplanar Z−E photoactive molecular switches, the existing coupling between stretching and torsion modes (i.e., the second derivative cross term) provokes the rapid flow of vibrational energy from excited stretching modes to torsional modes in the electronic excited state, contrary to the above-discussed planar systems. This is the case of retinal in rhodopsin, where the unidirectional rotation is guided especially by the surrounding amino acids of the opsin pocket, which provide a chiral environment.[10,22] This environment not only guides the rotation in the excited state but also accelerates the rotation due to the increase of the stretching−torsion coupling, making the Z−E isomerization process take place on the femtosecond time scale.[22,23]

The inclusion of the above-mentioned chiral hydrogen bond environment in the studied molecular photoswitch (see Figure 1B) modifies its force field, breaking the symmetry of the potential energy surfaces (PESs) along the torsion coordinate, giving rise to a single isomer instead of two isomers of the preceding photoswitch. This, in turn, as will be shown, ultimately permits the unidirectional rotation of the system.

In this regard, it is convenient to analyze the PESs (ground and optically bright states) corresponding to three different cases, planar photoswitches, nonplanar photoswitches, and the derived photoactive molecular motors, in order to realize what the initial rotation direction is after electronic excitation. Planar Z−E photoswitches present symmetrical PES profiles along the torsion coordinate; therefore, torsion is not controlled in any way, and two possible equivalent relaxation paths are accessible (see Figure 2A). Nevertheless, a photoswitch can exhibit nonplanarity, as is the case of the system studied here (see Figure 1A). For nonplanar switches, two equivalent conformations for each Z and E isomer may exist, and even if the torsion for each conformer were unidirectional, the equivalent population of both isomers in the ground state makes the system behave as a photoswitch (see Figure 2B). On the contrary, unidirectional rotation present in Z−E photoactive molecular motors is related to nonsymmetrical PESs in the excited and ground states along the torsion coordinate, with a single ground-state minimum and the rotation of the system being unidirectionally initiated in the excited state (see Figure 2C).

In order to ensure this unidirectional rotation, we generate a chiral hydrogen bond environment within a molecular photoswitch structure. This can be formally seen as a conversion from a photoswitch (Figure 1A) to a molecular motor (Figure 1B), which can be understood in terms of PESs. In contrast for the photoswitch (Figure 2B), there is no preference for the direction of rotation in the excited state; in chiral environments induced by a hydrogen bond, the symmetry is already broken in the ground state, which provokes the stabilization of the system along a specific torsion, resulting in a unidirectional rotation in the excited state (see Figure 2C).

Moreover, as will be shown, the strength of the hydrogen bond of the studied system is enough to correctly drive the torsion on the excited state but not so strong to block the rotation in this state, generating an intermediate and therefore quenching the process. Thus, the strength of the hydrogen bond could be critical in the design of an efficient motor, and it should be tuned for an optimal performance.

It should be noted that this design of a molecular motor with two symmetrically equivalent structures (for the initial and the 180° rotated isomers) would allow a continuous unidirectional movement using only a specific wavelength source. As a drawback, the experimental characterization of the molecular device would be difficult. From a practical point of view, this difficulty could be overcome through the modification of the basic design by including a group that could break the symmetry without altering the functioning of the motor.

For the study of the photochemical and photophysical properties of the proposed molecular motor, the multiconfigurational CASPT2//CASSCF[24] methodology has been employed with a 6-31G* basis set. The active space chosen is composed of all of the π and π^* orbitals (eight electrons in eight orbitals), therefore including all of the energy low-lying $^1(\pi,\pi^*)$ excited states. The stationary points have been determined by using analytical energy gradients computed at the CASSCF level and characterized by numerical frequency calculations at the same level of theory. Minimum energy paths (MEPs) were computed for the determination of the photoreaction mechanism, and crossings between electronic states were characterized by determining the derivative coupling (DC) and gradient difference (GD) vectors.[25] All calculations have been performed with MOLCAS 7.6[26] and the Gaussian 09[27] suite of programs.

The UV−visible absorption spectrum is characterized by a low-lying optically bright π,π^* excited state, S_2, exhibiting a dominant monoexcitation configuration with a large participation of the central carbons of the double bond in both, the occupied and the virtual orbitals involved in the excitation. The shape of these orbitals clearly indicates the rupture of the central carbon−carbon double bond in the excited state and the consequential favored torsion around this bond. The S_3 state has a similar electronic nature, showing a larger contribution of the configuration described by the $^1(\pi,\pi^*)$ central π double bond excitation. In fact, the $S_0 \rightarrow S_2$ and $S_0 \rightarrow S_3$ vertical excitations are close in energy (280 and 291 nm, respectively) with similar oscillator strengths (0.32 and 0.35, respectively).

Excitation of the system to the brightest states (S_3 and S_2) leads to similar profiles along the MEP, characterized by a steep energy variation along the increasing carbon−carbon central

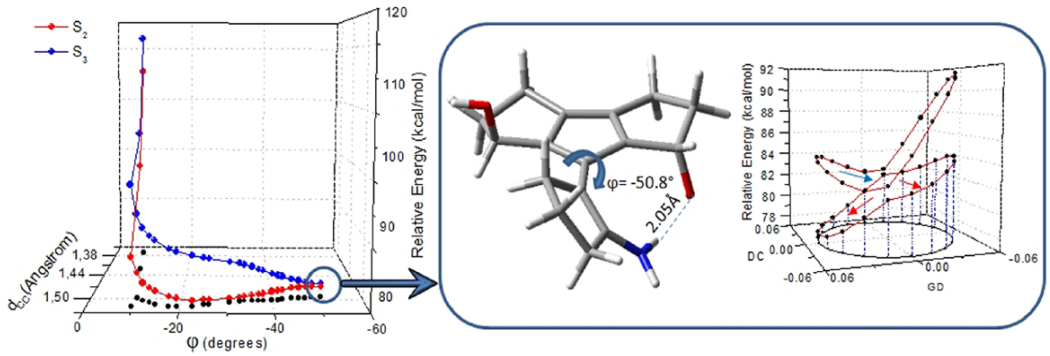

Figure 3. S_3 and S_2 energies along the MEP on S_3 after vertical excitation, represented as a function of the central bond torsion and stretching coordinates (left). The S_3/S_2 conical intersection structure is shown, as well as the S_3 and S_2 energy profiles around the tip of the conical intersection for a loop defined on the branching plane[28] with a 0.05 Åradius. The decay paths from S_3 (blue arrow) to S_2 (red arrows) are indicated.

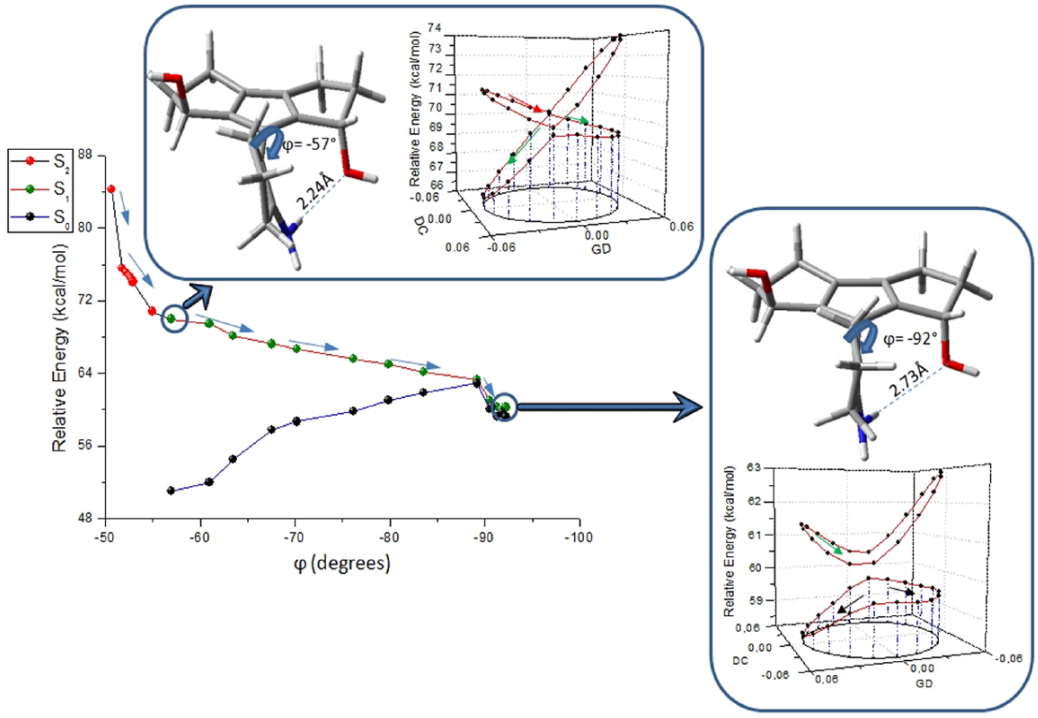

Figure 4. S_2, S_1, and S_0 energy profiles represented along the torsion coordinate for the two MEPs starting at the S_3/S_2 and S_2/S_1 conical intersections. The molecular structures of the conical intersections are displayed, showing, respectively, a very weak and a formally broken hydrogen bond, with central bond torsions of ∼−57 and −92°. The loop around the CI within the branching plane shows the topology of the CI; two possible paths are available for both CIs in the lower surface (S_1 and S_0), as shown by arrows, corresponding to torsion completion or abortion.

bond distance. This coordinate is significantly coupled with the torsion around the same bond in the direction guided by the hydrogen bond (see Figure 3). The coupling between the central bond stretching and torsion is essential, as discussed above, in controlling the unidirectional rotation. This allows the system to transfer the excitation energy, initially located in the stretching coordinates, to the torsional coordinate, inducing unidirectional rotation. Moreover, inverse (i.e., counterclockwise) rotation is not feasible due to the large energy barrier as a result of a double effect opposing this rotation, that is, hydrogen bond breaking and reversion of the already twisted torsion in the excited state (see the Supporting Information for details). The latter effect can be clarified by analyzing the excited-state PES along the torsional coordinate; for symmetric systems (see Figure 2A), the highest excited-state energy corresponds to a planar photoswitch, and torsion around this coordinate makes the energy decrease as a result of diradical repulsion; therefore, if the system is initially twisted at some degree of torsion, the reversion toward the planarity is energetically demanding, making the counterclockwise rotation unfavorable.

Relaxing along the torsional mode in S_3, the system reaches a low-sloped S_3/S_2 CI at ∼−51° of torsion with a vibrational excess of ∼22 kcal/mol. After decay to S_2, the system continues

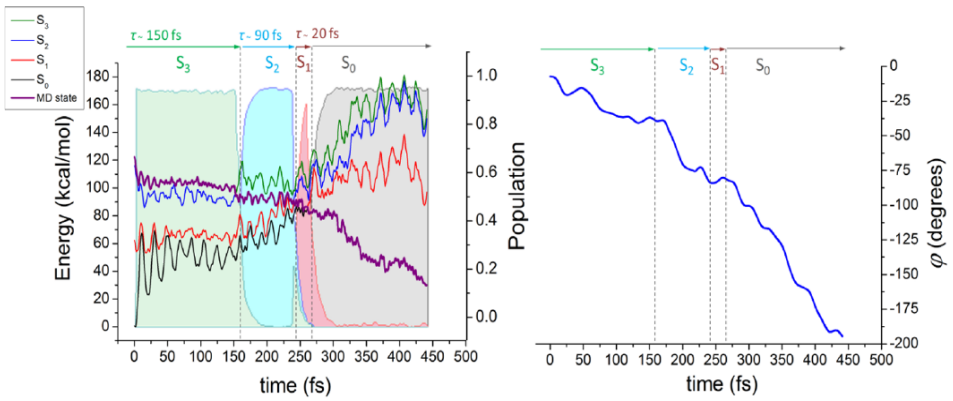

Figure 5. (Left) S_3, S_2, S_1, and S_0 relative energy profiles along the 0 K molecular dynamics simulation (lines, left scale). Populations of every state according to fewest switches algorithm are represented (background, right scale) by dashed filled profiles. Approximate state lifetimes are 150 fs for S_3, 90 fs for S_2, and 20 fs for S_1. S_0 is populated in ~260 fs. (Right) Central torsion angle (φ) evolution along the trajectory.

rotating because of a significant impulse along the rotation direction. It should be noted that no intermediate is found in the relaxation process, indicating that the hydrogen bond strength is large enough to guide the torsion after excitation but not so strong to block the rotation on the excited state.

The S_3/S_2 CI is characterized by a NH···O distance of ~2.0 Å. Once this point is reached, the system minimizes its energy by following two different bifurcating paths. The first one reaches a minimum-energy structure at 13 kcal/mol (CASPT2 level) below the S_3/S_2 CI, from where a low-lying transition state (3.8 kcal/mol at the CASPT2 level) permits it to continue the torsional process started in S_3. The second path directly continues the torsion started in S_3, breaking almost completely the hydrogen bond (see Figure 4). The linear impulse of the nuclei once it reaches the S_3/S_2 CI is expected to be enough to drive the torsion when following both paths, similarly to some highly efficient Z−E photoisomerizing systems like retinal in rhodopsin proteins.[7c,19a,29]

Relaxing along the increasing torsion S_2 pathway, the S_2 and S_1 states become rapidly degenerate in energy (see Figure 4). The crossing region between S_2 and S_1 states is reached when the torsion angle is ~−55°, with the NH···O hydrogen bond formally broken (2.24 Å). These S_2/S_1 CIs enhance the rotational motion, permitting the evolution of the system in the S_1 state, where the rotation is fulfilled at ~−92° (see Figure 4). At this point, the system intersects a third region of energy degeneration (the S_1/S_0 CI crossing region) that funnels the system into the ground state. The topology of these CIs is similar to those already described in many other Z−E photoisomerization processes.[19a,21,29b,30] From photon absorption to the S_1/S_0 CI, a total energy of ~43 kcal/mol (at the CASPT2 level) has been converted into vibrational excess mostly located into the torsional mode, resulting in almost twice the energy required for retinal isomerization in rhodopsin.[22]

From this last state crossing, the molecule can evolve along two different paths on the ground state, the first one completing the torsion and the second one aborting the rotation and recovering the initial structure (see the Supporting Information for more details). In both cases, the same initial structure is recovered due to the symmetric arrangement of the two equivalent hydrogen bonds; in the first case, the rotation is completed up to 180°, and in the second case, the rotation is aborted.

The resulting structure after 180° rotation is equivalent to the initial configuration. Therefore, the same rotational process can be fulfilled by absorption of a second photon, completing a 360° cycle by applying a monochromatic UV source with the corresponding wavelength. Moreover, as has been shown, there are no intermediates along the rotational path; therefore, the process is expected to be ultrafast. In addition, the large vibrational excess along the MEPs involving mainly the rotational coordinates makes the complete cycle process to be expected as highly efficient. Nevertheless, nonadiabatic molecular dynamics (NAMD) simulations are necessary in order to quantitatively predict the efficiency of the process.[31]

In order to provide a description of the photoisomerization dynamics, a single reference trajectory without initial kinetic energy (T = 0 K) has been computed by using Tully's fewest switches algorithm[31a] with decoherence correction[31c,32] working within MOLCAS.[33] This trajectory closely represents the photochemical behavior of the motor at very low temperatures, that is, in the absence of thermal energy boosting or quenching the isomerization.

From the obtained results, it can be concluded that photoisomerization is an efficient and an ultrafast process. Even without initial kinetic energy, the decay to the ground state is reached in ~260 fs with a torsion φ of ~−85° (see Figure 5), and the complete photoisomerization takes place in ~450 fs with a torsion φ of ~−190° (see the Supporting Information). The excited-state lifetimes can be estimated from the NAMD simulation; S_3, S_2, and S_1 have approximate lifetimes of ~150, 90 and 20 fs, respectively. According to the time scale of the photoisomerization (~0.5 ps), the rotation frequency is in the range of 10^{12} s^{-1} (terahertzs), which is, to our knowledge, the highest documented Z−E photoisomerization frequency of a photoactive artificial molecular motor.

In order to check the stability of the computed CAS(8,8)/6-31G* trajectory at room temperature,[34] a computationally more affordable 3-21G basis set was employed for the determination of 20 trajectories (see the Supporting Information for details). Although the PESs with both basis sets are qualitatively similar (see the Supporting Information), they present some differences. Specifically, the steepness of the PES along the MEPs is lower for 3-21G than that for 6-31G*.

This makes the 3-21G NAMDs slower (larger time scale photoisomerization) and less efficient due to the lesser impulse along the rotational coordinate (e.g., the 0 K NAMD with the 3-21G basis set does not fulfill the photoisomerization, contrary to the 6-31G* trajecotry). Nonetheless, 4 out of 20 trayectories (20%) give rise to the isomerization in a 1.5 ps time window, and more importantly, all of the computed trajectories provide unidirectional rotation after vertical excitation (i.e., counterclockwise rotation is forbidden). These results are in agreement with the 0 K 6-31G* NAMD as well as with the computed MEPs.

In conclusion, in this study, we present a novel concept for the design of photoactive molecular motors, the induction of unidirectional rotation by a chiral hydrogen bond environment. Indeed, molecular photoswitches could be converted into molecular motors by inducing a chiral environment through hydrogen bonds. This kind of design has some novel benefits in comparison to previously reported molecular motors; (i) both Z and E isomers can be designed in order to be structurally identical, as is the case of the present molecular motor (Figure 1). Therefore, a monochromatic light source can be applied to complete the whole photocycle (360°). (ii) Both Z to E and E to Z photoisomerizations take place in a single step without any energy barrier. Therefore, the process is expected to be ultrafast (taking less than 1 ps) and with radiative or quenching deactivations playing eventually a minor role. (iii) Any efficient molecular photoswitch can be transformed into an efficient photoactive motor by introducing the chiral hydrogen bond environment without modifying the chromophore electronic nature. (iv) The strength of the hydrogen bond(s) is tunable, facilitating the possibility to control the quantum yield of the process.

■ ASSOCIATED CONTENT

Supporting Information

Computational details, the excited-state initial rotation direction, molecular dynamics methods and trajectories, absorption spectra, the unidirectional rotation path, CASPT2 energy profiles, and Cartesian coordinates of the most relevant optimized structures are provided. Also given is the NAMD trajectory animation. This material is available free of charge via the Internet at http://pubs.acs.org.

■ AUTHOR INFORMATION

Corresponding Author

*E-mail: diego.sampedro@unirioja.es. Fax: +34 941 299 621. Tel: +34 941 299 647 (D.S.); luisma.frutos@uah.es. Fax: +34 91 885 4639. Tel: +34 91 885 2512 (L.M.F.).

Author Contributions

The manuscript was written through contributions of all authors. All authors have given approval to the final version of the manuscript.

Notes

The authors declare no competing financial interest.

■ ACKNOWLEDGMENTS

This research was supported by the Spanish MICINN Grants CTQ2009-07120 and CTQ2011-24800, Spanish MINECO Grant CTQ2012-36966, and the University of Alcalá UAH2011/EXP-041 Grant. C.G.-I. and M.M. are grateful to the UAH for a doctoral fellowship. L.M.F. acknowledges receipt of a "Ramon y Cajal" contract from MEC.

■ ABBREVIATIONS

CI, conical intersection; CASSCF, complete active space self-consistent field; CASPT2, complete active space perturbational theory to second order; MEP, minimum energy path; PES, potential energy surface; GS, ground state; ES, excited state; NAMD, nonadiabatic molecular dynamics

■ REFERENCES

(1) (a) Feringa, B. L.; van, D. R. A.; Koumura, N.; Geertsema, E. M. Chiroptical Molecular Switches. *Chem. Rev.* **2000**, *100*, 1789−1816. (b) Gust, D.; Moore, T. A.; Moore, A. L. Molecular Switches Controlled by Light. *Chem. Commun.* **2006**, 1169−1178. (c) Russew, M.-M.; Hecht, S. Photoswitches: from Molecules to Materials. *Adv. Mater. (Weinheim, Ger.)* **2010**, *22*, 3348−3360.

(2) García-Iriepa, C.; Marazzi, M.; Frutos, L. M.; Sampedro, D. *E/Z* Photochemical Switches: Syntheses, Properties and Applications. *RSC Adv.* **2013**, DOI: 10.1039/c2ra22363e.

(3) (a) Hernandez, J. V.; Kay, E. R.; Leigh, D. A. A Reversible Synthetic Rotary Molecular Motor. *Science* **2004**, *306*, 1532−1537. (b) Kelly, T. R. Progress toward a Rationally Designed Molecular Motor. *Acc. Chem. Res.* **2001**, *34*, 514−522. (c) Kelly, T. R.; Silva, R. A.; De, S. H.; Jasmin, S.; Zhao, Y. A Rationally Designed Prototype of a Molecular Motor. *J. Am. Chem. Soc.* **2000**, *122*, 6935−6949.

(4) (a) Zheng, X.; Mulcahy, M. E.; Horinek, D.; Galeotti, F.; Magnera, T. F.; Michl, J. Dipolar and Nonpolar Altitudinal Molecular Rotors Mounted on an Au(111) Surface. *J. Am. Chem. Soc.* **2004**, *126*, 4540−4542. (b) Michl, J.; Sykes, E. C. H. Molecular Rotors and Motors: Recent Advances and Future Challenges. *ACS Nano* **2009**, *3*, 1042−1048. (c) Horansky, R. D.; Magnera, T. F.; Price, J. C.; Michl, J. Artificial Dipolar Molecular Rotors. *Lect. Notes Phys.* **2007**, *711*, 303−330.

(5) (a) Akimov, A. V.; Nemukhin, A. V.; Moskovsky, A. A.; Kolomeisky, A. B.; Tour, J. M. Molecular Dynamics of Surface-Moving Thermally Driven Nanocars. *J. Chem. Theory Comput.* **2008**, *4*, 652−656. (b) Khatua, S.; Guerrero, J. M.; Claytor, K.; Vives, G.; Kolomeisky, A. B.; Tour, J. M.; Link, S. Micrometer-Scale Translation and Monitoring of Individual Nanocars on Glass. *ACS Nano* **2009**, *3*, 351−356. (c) Shirai, Y.; Osgood, A. J.; Zhao, Y.; Yao, Y.; Saudan, L.; Yang, H.; Chiu, Y.-H.; Alemany, L. B.; Sasaki, T.; Morin, J.-F.; Guerrero, J. M.; Kelly, K. F.; Tour, J. M. Surface-Rolling Molecules. *J. Am. Chem. Soc.* **2006**, *128*, 4854−4864.

(6) (a) Godinez, C. E.; Zepeda, G.; Garcia-Garibay, M. A. Molecular Compasses and Gyroscopes. II. Synthesis and Characterization of Molecular Rotors with Axially Substituted Bis[2-(9-triptycyl)ethynyl]-arenes. *J. Am. Chem. Soc.* **2002**, *124*, 4701−4707. (b) Dominguez, Z.; Khuong, T.-A. V.; Dang, H.; Sanrame, C. N.; Nunez, J. E.; Garcia-Garibay, M. A. Molecular Compasses and Gyroscopes with Polar Rotors: Synthesis and Characterization of Crystalline Forms. *J. Am. Chem. Soc.* **2003**, *125*, 8827−8837. (c) Escalante-Sanchez, E.; Rodriguez-Molina, B.; Garcia-Garibay, M. A. Toward Crystalline Molecular Rotors with Linearly Conjugated Diethynyl−Phenylene Rotators and Pentiptycene Stators. *J. Org. Chem.* **2012**, *77*, 7428−7434.

(7) (a) Stock, D.; Leslie, A. G. W.; Walker, J. E. Molecular Architecture of the Rotary Motor in ATP Synthase. *Science* **1999**, *286*, 1700−1705. (b) Shao, Q.; Gao, Y. Q. On the Hand-over-Hand Mechanism of Kinesin. *Proc. Natl. Acad. Sci. U.S.A.* **2006**, *103*, 8072−8077. (c) Sampedro, D.; Blanco-Lomas, M.; Rivado-Casas, L.; Campos, P. J. Retinal-Based Molecular Machines. In *Advances in Biomimetics*; George, A., Ed.; InTech: New York, 2011. (d) Kinbara, K.; Aida, T. Toward Intelligent Molecular Machines: Directed Motions of Biological and Artificial Molecules and Assemblies. *Chem. Rev.* **2005**, *105*, 1377−1400.

(8) Balzni, V.; Venturi, M.; Credi, A. *Molecular Devices and Machines: A Journey into the Nano World*; John Wiley & Sons: New York, 2003; p 500.

(9) Kelly, T. R.; Ed., Molecular Machines. In *Topics in Current Chemistry*; Springer: New York, 2005; p 236 and 262.

(10) (a) Crano, J. C. G.; Guglielmetti, R. J. *Organic Photochromic and Thermochromic Compounds*; Springer: New York, 1999. (b) Wolken, J. *Light Detectors, Photoreceptors, and Imaging Systems in Nature*; Oxfors University Press: New York, 1995.
(11) (a) Koumura, N.; Zijlstra, R. W.; van Delden, R. A.; Harada, N.; Feringa, B. L. Light-Driven Monodirectional Molecular Rotor. *Nature* **1999**, *401*, 152−155. (b) Feringa, B. L. In Control of Motion: From Molecular Switches to Molecular Motors. *Acc. Chem. Res.* **2001**, *34*, 504−513. (c) Feringa, B. L. The Art of Building Small: From Molecular Switches to Molecular Motors. *J. Org. Chem.* **2007**, *72*, 6635−6652.
(12) (a) de Jong, J. J. D.; Hania, P. R.; Pugzlys, A.; Lucas, L. N.; de Loos, M.; Kellogg, R. M.; Feringa, B. L.; Duppen, K.; van Esch, J. H. Light-Driven Dynamic Pattern Formation. *Angew. Chem., Int. Ed.* **2005**, *44*, 2373−2376. (b) de Jong, J. J. D.; Lucas, L. N.; Kellogg, R. M.; van Esch, J. H.; Feringa, B. L. Reversible Optical Transcription of Supramolecular Chirality into Molecular Chirality. *Science* **2004**, *304*, 278−281. (c) Pijper, D.; Feringa, B. L. Molecular Transmission: Controlling the Twist Sense of a Helical Polymer with a Single Light-Driven Molecular Motor. *Angew. Chem., Int. Ed.* **2007**, *46*, 3693−3696. (d) Eelkema, R.; Feringa, B. L. Reversible Full-Range Color Control of a Cholesteric Liquid-Crystalline Film by Using a Molecular Motor. *Chem.—Asian J.* **2006**, *1*, 367−369. (e) Eelkema, R.; Pollard, M. M.; Katsonis, N.; Vicario, J.; Broer, D. J.; Feringa, B. L. Rotational Reorganization of Doped Cholesteric Liquid Crystalline Films. *J. Am. Chem. Soc.* **2006**, *128*, 14397−14407. (f) Eelkema, R.; Pollard, M. M.; Vicario, J.; Katsonis, N.; Ramon, B. S.; Bastiaansen, C. W. M.; Broer, D. J.; Feringa, B. L. Molecular Machines: Nanomotor Rotates Microscale Objects. *Nature* **2006**, *440*, 163.
(13) (a) Astumian, R. D. Thermodynamics and Kinetics of a Brownian Motor. *Science* **1997**, *276*, 917−922. (b) Astumian, R. D.; Derenyi, I. A Chemically Reversible Brownian Motor: Application to Kinesin and NCD. *Biophys. J.* **1999**, *77*, 993−1002.
(14) (a) Seldenthuis, J. S.; Prins, F.; Thijssen, J. M.; van der Zant, H. S. J. An All-Electric Single-Molecule Motor. *ACS Nano* **2010**, *4*, 6681−6686. (b) Neumann, J.; Gottschalk, K. E.; Astumian, R. D. Driving and Controlling Molecular Surface Rotors with a Terahertz Electric Field. *ACS Nano* **2012**, *6*, 5242−5248.
(15) (a) Kelly, T. R.; Cai, X.; Damkaci, F.; Panicker, S. B.; Tu, B.; Bushell, S. M.; Cornella, I.; Piggott, M. J.; Salives, R.; Cavero, M.; Zhao, Y.; Jasmin, S. Progress toward a Rationally Designed, Chemically Powered Rotary Molecular Motor. *J. Am. Chem. Soc.* **2007**, *129*, 376−386. (b) Kelly, T. R.; De, S. H.; Silva, R. A. Unidirectional Rotary Motion in a Molecular System. *Nature* **1999**, *401*, 150−2.
(16) Rivado-Casas, L.; Sampedro, D.; Campos, P. J.; Fusi, S.; Zanirato, V.; Olivucci, M. Fluorenylidene−Pyrroline Biomimetic Light-Driven Molecular Switches. *J. Org. Chem.* **2009**, *74*, 4666−4674.
(17) (a) Pijper, D.; van Delden, R. A.; Meetsma, A.; Feringa, B. L. Acceleration of a Nanomotor: Electronic Control of the Rotary Speed of a Light-Driven Molecular Rotor. *J. Am. Chem. Soc.* **2005**, *127*, 17612−17613. (b) ter Wiel, M. K. J.; van Delden, R. A.; Meetsma, A.; Feringa, B. L. Increased Speed of Rotation for the Smallest Light-Driven Molecular Motor. *J. Am. Chem. Soc.* **2003**, *125*, 15076−15086.
(18) (a) Amatatsu, Y. Theoretical Design of a Light-Driven Molecular Rotary Motor with Low Energy Helical Inversion: 9-(5-Methyl-2-phenyl-2-cyclopenten-1-ylidene)-9H-fluorene. *J. Phys. Chem. A* **2011**, *115*, 13611−13618. (b) Amatatsu, Y. Theoretical Design of a Fluorene-Based Light-Driven Molecular Rotary Motor with Constant Rotation. *J. Phys. Chem. A* **2012**, *116*, 10182−10193.
(19) (a) Sampedro, D.; Migani, A.; Pepi, A.; Busi, E.; Basosi, R.; Latterini, L.; Elisei, F.; Fusi, S.; Ponticelli, F.; Zanirato, V.; Olivucci, M. Design and Photochemical Characterization of a Biomimetic Light-Driven Z/E Switcher. *J. Am. Chem. Soc.* **2004**, *126*, 9349−9359. (b) Sinicropi, A.; Martin, E.; Ryazantsev, M.; Helbing, J.; Briand, J.; Sharma, D.; Leonard, J.; Haacke, S.; Cannizzo, A.; Chergui, M.; Zanirato, V.; Fusi, S.; Santoro, F.; Basosi, R.; Ferre, N.; Olivucci, M. An Artificial Molecular Switch That Mimics the Visual Pigment and Completes Its Photocycle in Picoseconds. *Proc. Natl. Acad. Sci. U.S.A.* **2008**, *105*, 17642−17647. (c) Lumento, F.; Zanirato, V.; Fusi, S.; Busi, E.; Latterini, L.; Elisei, F.; Sinicropi, A.; Andruniow, T.; Ferre, N.; Basosi, R.; Olivucci, M. Quantum Chemical Modeling and Preparation of a Biomimetic Photochemical Switch. *Angew. Chem., Int. Ed.* **2007**, *46*, 414−420. (d) Bonacic-Koutecky, V.; Koehler, J.; Michl, J. Prediction of Structural and Environmental Effects on the S_1-S_0 Energy Gap and Jump Probability in Double-Bond cis−trans Photoisomerization. A General Rule. *Chem. Phys. Lett.* **1984**, *104*, 440−443. (e) Bonacic-Koutecky, V.; Koutecky, J.; Michl, J. Neutral and Charged Diradicals, Zwitterions, Funnels on the S_1 Hypersurface and Proton Translocation; Their Importance for the Optical Process and Other Photochemical and Photophysical Processes. *Angew. Chem.* **1987**, *99*, 216−236.
(20) The vibrational excess is calculated as the energy difference from the S_3 vertical absorption (Franck−Condon region) to the current point considered on the potential energy surface.
(21) (a) Garavelli, M.; Celani, P.; Bernardi, F.; Robb, M. A.; Olivucci, M. The $C_5H_6NH_2^+$ Protonated Schiff Base: An Ab Initio Minimal Model for Retinal Photoisomerization. *J. Am. Chem. Soc.* **1997**, *119*, 6891−6901. (b) Léonard, J.; Schapiro, I.; Briand, J.; Fusi, S.; Rossi Paccani, R.; Olivucci, M.; Haacke, S. Mechanistic Origin of the Vibrational Coherence Accompanying the Photoreaction of Biomimetic Molecular Switches. *Chem.—Eur. J.* **2012**, *18*, 15296−15304.
(22) Frutos, L. M.; Andruniow, T.; Santoro, F.; Ferre, N.; Olivucci, M. Tracking the Excited-State Time Evolution of the Visual Pigment with Multiconfigurational Quantum Chemistry. *Proc. Natl. Acad. Sci. U.S.A.* **2007**, *104*, 7764−7769.
(23) (a) Schoenlein, R. W.; Peteanu, L. A.; Mathies, R. A.; Shank, C. V. The First Step in Vision: Femtosecond Isomerization of Rhodopsin. *Science* **1991**, *254*, 412−415. (b) Wang, Q.; Schoenlein, R. W.; Penteanu, L. A.; Mathies, R. A.; Shank, C. V. Vibrationally Coherent Photochemistry in the Femtosecond Primary Event of Vision. *Science* **1994**, *266*, 422−424.
(24) Finley, J.; Malmqvist, P.-A.; Roos, B. O.; Serrano-Andres, L. The Multi-State CASPT2 Method. *Chem. Phys. Lett.* **1998**, *288*, 299−306.
(25) The DC vector measures the distortion of the system providing the maximum coupling between the electronic states involved in the crossing. The GD vector measures the distortion of the system leading to the largest variation of the energy difference between the two electronic states involved in the crossing.
(26) Aquilante, F.; De Vico, L.; Ferre, N.; Ghigo, G.; Malmqvist, P.-a.; Neogrady, P.; Pedersen, T. B.; Pitonak, M.; Reiher, M.; Roos, B. O.; Serrano-Andres, L.; Urban, M.; Veryazov, V.; Lindh, R. MOLCAS 7: The Next Generation. *J. Comput. Chem.* **2010**, *31*, 224−247.
(27) Frisch, M. J.; Trucks, G. W.; Schlegel, H. B.; Scuseria, G. E.; Robb, M. A.; Cheeseman, J. R.; Scalmani, G.; Barone; V.; et al. *Gaussian 09*, revision B.01; Gaussian, Inc.: Wallingford, CT, 2009.
(28) The branching plane is the plane spanned by the nonadiabatic coupling vectors (i.e., gradient difference and derivative coupling vectors) where energy degeneracy between the crossing states is left.
(29) (a) Dartnall, H. J. The Visual Pigment of the Green Rods. *Vision Res.* **1967**, *7*, 1−16. (b) Burghardt, I.; Hynes, J. T. Excited-State Charge Transfer at a Conical Intersection: Effects of an Environment. *J. Phys. Chem. A* **2006**, *110*, 11411−11423. (c) Rivado-Casas, L.; Blanco-Lomas, M.; Campos, P. J.; Sampedro, D. Photochemical Characterization of Biomimetic Molecular Switches. *Tetrahedron* **2011**, *67*, 7570−7574.
(30) Garavelli, M.; Bernardi, F.; Olivucci, M.; Vreven, T.; Klein, S.; Celani, P.; Robb, M. A. Potential-Energy Surfaces for Ultrafast Photochemistry: Static and Dynamic Aspects. *Faraday Discuss.* **1998**, *110*, 51−70.
(31) (a) Tully, J. C. Molecular Dynamics with Electronic Transitions. *J. Chem. Phys.* **1990**, *93*, 1061−1071. (b) Craig, C. F.; Duncan, W. R.; Prezhdo, O. V. Trajectory Surface Hopping in the Time-Dependent Kohn−Sham Approach for Electron−Nuclear Dynamics. *Phys. Rev. Lett.* **2005**, *95*, 163001/1−163001/4. (c) Jaeger, H. M.; Fischer, S.; Prezhdo, O. V. Decoherence-Induced Surface Hopping. *J. Chem. Phys.* **2012**, *137*, 22A545/1−22A545/14.

(32) Granucci, G.; Persico, M. Critical Appraisal of the Fewest Switches Algorithm for Surface Hopping. *J. Chem. Phys.* **2007**, *126*, 134114−134125.
(33) Code implemented by Valentini, A.; Frutos, L.M. working with MOLCAS 7.6 (see ref 26) CASSCF wave functions and energies.
(34) Initial conditions were obtained by sampling the phase space for the minimum-energy structure on S_0 with 1 ns dynamics. The dynamics were performed using a Nosé−Hoover chain of thermostats with T = 300K (see the Supporting Information for additional details).

7.2.1.2 Molecular design concepts: towards highly efficient photoactive molecular motors

Molecular Design Concepts Towards Highly Efficient Photoactive Molecular Motors

Cristina Garcia-Iriepa,[1,2] Marco Marazzi,[1] Felipe Zapata,[1] Alessio Valentini,[1] Diego Sampedro[2,] and Luis Manuel Frutos[1,*]*

[1] Unidad de Química Física, Universidad de Alcalá, E- 28871 Alcalá de Henares, Madrid, Spain. Fax: +34 91 885 4639; Tel: +34 91 885 2512

[2] Departamento de Química, Centro de Investigación en Síntesis Química (CISQ), Madre de Dios, 51, E-26006, Logroño, Spain. Tel: +34 941 299 647

AUTHOR EMAIL ADDRESS: diego.sampedro@unirioja.es; luisma.frutos@uah.es

ABSTRACT

Essential guidelines for the design of novel photoactive *Z-E* molecular motors are described. More specifically, the introduction of a chiral hydrogen bond environment into efficient molecular photoswitches was explored as a novel approach for the design of molecular motors with enhanced properties: the complete 360° rotation is achieved by only two photochemical steps (no thermal steps). This design strategy is described by analyzing the complete photocycle of such kind of *Z-E* molecular motors, exemplifying these guidelines with the rational design of a photoactive molecular motor already studied (*J. Phys. Chem. Lett.* **2013**, *4*, 1389). Concretely, we analyze (i) the election of the starting photoswitch based on its electronic and structural properties, including the role of the ground state conformations, the relation between structure and optical properties, as well as the factors controlling the photoswitch rotation performance; also (ii) the strategy for the inclusion of the chiral hydrogen bond environment providing unidirectional rotation is discussed, focusing specially on the effect of the hydrogen bond in the ground state pre-twist and also on its effect in the excited state reaction path. Finally (iii) we review the complete photoisomerization mechanism in order to provide a whole picture of the process.

INTRODUCTION

The design and construction of molecular machines is tightly associated with technology and industry advances. Accordingly, in the last decades nanotechnology focused on the development of machines with increased capacity and minimized size. This resulted in the construction of molecular assemblies of different size, shape, structure, function and use. To reach this aim, two approaches are possible, namely the *top-down* or the *bottom-up*.[1,2] Whereas the first one is based on the miniaturization of the components, the second one makes use of atoms or molecules to build devices, being a suitable deal for chemists.[3]

Molecular machines are designed to perform a specific task and therefore certain properties have to be satisfied in order to be useful devices. For ideal devices, the conversion of energy into mechanical work (motion), an easily monitorizable cycle at a short time scale, a cyclic process and being autonomous are some required features.[4] The advantages of using light as the energy supply are well known: there are no waste products, it is easily controlled by modern optical instruments (*e.g.* precise wavelength selection) and it shows high temporal and spatial resolution. Hereby, in this study we select light as the energy supply and *Z-E* photoisomerization as the chemical reaction (among pericyclic reactions, tautomerization, dissociation, electronic transfer, etc).[5-10]

Among the different synthesized molecular devices, either molecular switches or motors perform an essential function in molecular machines. In general, molecular switches are molecules that can be interconverted by an

energy supply between two (meta-) stable states. These devices have been broadly studied to control common processes (*e.g.* ion complexation, catalysis, peptide folding, electronic properties, etc.)[11-17] and as building blocks for the construction of rotary motors.[18-20] Several types of photoinduced switches have been studied, such as azobenzene,[21] diarylethenes,[22] green fluorescent protein chromophore analogues[23] and derivatives of the protonated Schiff base chromophore of rhodopsins[24-26] (for a complete review on the topic see ref. [27]). Whereas the direction of rotation experienced by molecular switches is usually neither controlled nor relevant, molecular motors are characterized by a unidirectional rotation of 360 degrees, making the design and mechanism of these devices more sophisticated and consequently, less investigated.

Examples of efficient molecular motors are found in Nature as: ATP synthase, a biological rotary motor that uses ATP and transmembrane electrochemical gradients as energy supplies,[28,29] kinesine and myosine, molecular assemblies which move in a linear fashion along a track by consumption of ATP.[30-32] These models are a highly suitable starting point for the design of novel artificial and efficient molecular motors. The first examples of molecular motors were described by Kelly *et al.*[33] (chemical motor) and Feringa *et al.*[34] (photoinduced motor), both in 1999. Since then, numerous structures have been proposed as molecular motors leading to a continuous growing of this nanotechnology field.

The main difference between molecular switches and motors is the unidirectional character of the motion. This fact can be achieved by introduction of a chiral environment in the structure, which imposes an efficient unidirectionality. A chiral environment can be achieved by protein surroundings as in rhodopsin,[35,36] by a helical structure as in diarylethenes[22,37] or, as we recently proposed,[38] by the induction of an initial torsion due to the formation of a chiral hydrogen bond environment (*i.e.* one of the chemical groups involved in the hydrogen bond is covalently bonded to a chiral carbon atom). Helical-shaped structures as overcrowded alkenes are the most studied models.[22,34,37] In this case, the unidirectional rotation of 360 degrees is complete with high quantum yields in two photochemical (ultrafast processes) and two thermal steps. Thermal steps limit the rotational rate and decrease the speed regarding to a fully photochemical process. This weakness has been improved by structural and electronic changes, nevertheless thermal isomerization steps always cause the slowing of the overall mechanism.[22,39,40]

With this idea in mind, we proposed a novel type of molecular motor with unidirectional rotation achieved by a chiral hydrogen bond environment, and ensuring a 360 degrees cycle by only two photochemical steps promoted by the same excitation wavelength.[38] This approach not only contributes to increase the motor speed, but it also allows applying a single monochromatic light during the rotation.

COMPUTATIONAL METHODS

The ground state conformational study has been performed by Møller–Plesset perturbation theory to the second order (MP2)[41,42] with a 6-31G* basis set. Specifically, all possible minima conformations of the molecular motor and all transition states that connect them were computed (see Supporting Information). Frequency calculations of all these stationary points were performed at the same level of theory.

All the photochemistry and photophysics calculations were carried out by MS-CASPT2//SA-CASSCF methodology[43] (State Average-Complete Active Space Self Consistent Field, with correction to the energy by Multi State-Perturbation Theory to second order), with a 6-31G* basis set. All π and π* orbitals were included in the active space, corresponding to 8 electrons in 8 orbitals. In order to determine the excited state relaxation pathway after excitation, minimum energy paths (MEPs) were calculated by applying the steepest descent algorithm in force constant weighted Cartesian coordinates with a step size of 0.02 Å. The crossings between electronic states (*i.e.* conical intersections, CIs) were characterized by calculating the gradient

difference (GD) and derivative coupling (DC) vectors (see Supporting Information).[44] In addition, the topology of the crossing was depicted by a scan of 20 geometries forming a circle of radius 0.05 Å around the CI, generated by a linear combination of the GD and DC vectors. The energy for each scan point was calculated at the SA-CASSCF level. Finally, single–point energies of the most relevant structures determined at the CASSCF level of theory was calculated at the CASPT2 level, in order to introduce the dynamic electron correlation. The dynamical behavior was studied by means of non-adiabatic molecular dynamics (NAMD), applying the Tully's fewest switches algorithm[45] with decoherence correction for the surface hop,[46,47] as implemented by us.[48] All calculations have been performed with MOLCAS 7.6[49] and Gaussian 09[50] suite of programs.

RESULTS

A novel photoinduced molecular motor based on chiral environment provided by hydrogen bonds has been recently reported.[38] Even though it is the first example of this kind of photoactive molecular motors, general underlying molecular design concepts can be extracted and set as general rules in the design of new photoactive devices. Here we reveal these general ideas and exemplify them by a particular molecular motor model.

First, we analyze the ideal characteristics of an efficient *Z-E* photoswitch, the starting point in the photoactive molecular motor design. Second, we design and study a molecule fulfilling the desired characteristics based on the retinal Schiff base. Afterwards, the general strategy for the inclusion of a chiral environment providing unidirectional rotation to a photoswitch is discussed and exemplified by the study of the static and dynamical photochemical properties of an efficient molecular motor. Finally, the general photoinduced unidirectional rotation mechanism is summarized.

Efficient *Z-E* Photoswitches: General Considerations. Despite the capital relevance of molecular *Z-E* photoswitches rational design, general rules for their molecular design are not well-established, regarding both the molecular and the electronic structure. Here we present some guides for the specific design of planar or nearly planar *Z-E* molecular photoswitches which are the starting point in the design of an efficient photoactive molecular motor. In the present study we considered photoswitches which are restricted to be chromophores, therefore the absorbed photon is the energy source for the *Z-E* photoisomerization. Nevertheless, even if the chromophore could be excited by other mechanism (i.e. energy transfer), the arguments presented along the text would remain valid.

Firstly, the photoswitch to be designed has to be planar or nearly planar, with several conjugated π double bonds formed by sp^2 atoms such as carbon atoms or quaternized nitrogen atoms, since they are able to keep the planarity of the system. We focus on this type of switches as they are the most common *Z-E* photoswitches,[51,52] nevertheless other kind of photoactive switches not covered in this study could be eventually considered for the design of a molecular motor. It is also possible to include terminal carbonyl or amino groups. Furthermore, it is well known that the length of the π-conjugated system determines to a great extent the excitation energy, where the general trend is that the larger the π-system length, the more red-shifted is the absorption.[53] Based on these general choices for the molecular design, different possibilities arise for potential photoswitches, and the election of the specific starting system becomes mainly a task of imagination and creativity. On the contrary, another strategy (usually safer) is to modify existing efficient photoswitches, either artificial or natural.[52,54] We will follow the latter strategy, being our selected photoswitch based on the retinal chromophore.

On one hand, let us consider the excitation process. The nature of the electronic transition needs to involve the π-system, *i.e.* $^1(\pi,\pi^*)$, typically producing some degree of bond length alternation in the excited state, where nearly double bonds become nearly single and *vice versa*.[55] This kind of excitation could induce some formal double bond to undertake *Z-E* photoisomerization. In order to avoid *Z-E*

photoisomerizations along different double bonds, a widely used strategy is to block all but one double bond, usually integrating them into conformationally rigid rings (*i.e.* five member rings).[26] Nevertheless, this kind of compounds with only one isomerizable double bond does not necessarily undertake the desired photoisomerization. On the contrary, it can be possible for the system to decay to the ground state in many other undesired ways (usually internal conversion or fluorescence emission).

In the following, we analyze the electronic properties of a generic system that fulfils the above described structural requirements. Moreover, some general characteristics essential to design an efficient *Z-E* photoswitch are provided. Three main factors are analyzed: i) electronic excitation nature ii) population probability of the target electronic excitation, and iii) influence of underlying electronic states.

i) Regarding the electronic excitation nature, the desired transition has necessarily to involve a bonding to antibonding π transition where the main contribution is due to the atoms involved in the selected double bond (*i.e.* C=C bond). A large contribution of the molecular orbitals of the selected bond would result in a large bond length alternation. Therefore, once selected the system to study, the first step is to identify the electronic transition nature in order to understand its potential photoswitching efficiency.

ii) Nevertheless, the identified transition (*i.e.* HOMO-LUMO transition) not necessarily corresponds to an accessible electronic state. For instance, this transition could be mainly an optically dark transition. A simple inspection of the molecular orbitals (MO) involved in the transition can provide much information without the necessity of a precise determination of the absorption spectrum. If we consider an ideal planar system with a central double bond, the bonding MO (*i.e.* HOMO) is A" symmetry (Cs point group) as well as the antibonding MO (*i.e.* LUMO). Therefore, the electronic excited state has also A' symmetry as a result of the A" x A" product. Also the "*x*" coordinate defining the axis placed along the sigma CC bond (*i.e.* "*x*" axis) has A' symmetry, making the transition dipole integral ($\int \psi_f x \psi_i$) not vanishing since the product A' x A' x A' corresponds to the totally symmetric representation, A' (Figure 2S). It is therefore clear that a strong contribution of the π-bonding MO to the antibonding MO configuration of the isomerizing double bond to the electronic excitation corresponds to an optically bright state.[56,57]

iii) Finally, it is well known that after an electronic excitation, a system can undergo different processes. Specially, if excited states of lower energy exist, the photoisomerization process could be deactivated. This situation becomes clear if we consider a system where the bright state is not the first electronic excited state and there are low lying excited states with different electronic nature. In this case, different crossings can provide alternative photochemical pathways since the potential energy surfaces topology is markedly different due to the different electronic state nature. This situation has to be overcome in the design of photoactive molecular motors ensuring that the bright state is the first excited state or that the electronic nature of low lying excited states is similar to the bright state electronic nature, avoiding undesired photochemical pathways.

Initial Design of a *Z-E* Photoswitch. As aforementioned, in this study we follow a usually safe strategy for the design of an efficient photoswitch: the modification of an existing model. Among the wide variety of reported photoswitches, we select as framework a minimal model of the protonated Schiff base chromophore of rhodopsins,[24-26] constituted by three double bonds (PSB3, Figure 1).

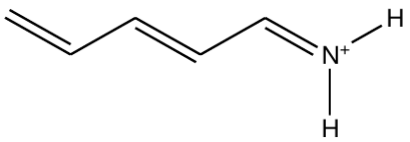

Figure 1. Structure of the selected chromophore, the protonated Schiff base of three double bonds.

Once selected the chromophore nature, we increase the conjugation degree of the systemby adding new double bonds in order to ensure an energetically accessible red-shifted absorption. Moreover, we select the desirable photoisomerizable double bond (the one in the middle of the chromophore structure) and integrate the other double bonds into rings to avoid competitive photoisomerization processes. As ring conformational equilibra are also competitive processes, we choose five member rings since they are the most conformationally rigid ones. Following these guides, we are able to design a potentially efficient photoswitch which structure is shown in Figure 2. The dihedral angle, φ, is defined as the 1 2 3 4 dihedral. Due to the steric hindrance (or effect) between hydrogens in the quaternized imine moiety and the ones in the opposite ring, two equivalent minima exist in the ground state with φ and –φ degrees respectively.[38]

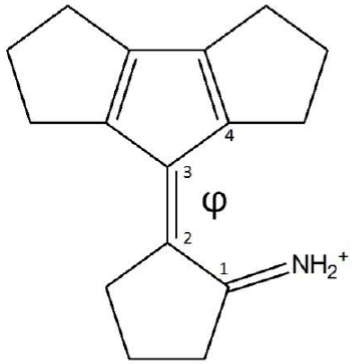

Figure 2. Photoswitch final structure.

Photoswitch Absorption Spectrum. The proposed molecular switch presents two optically dark states (oscillator strengths below $1 \cdot 10^{-2}$, see Table 1) being the two lowest-energy singlet excited states, S_1 and S_2. These states are described by a monoexcitation and a double excitation, respectively, from a π orbital of the cyclopentadiene unit to the π* of the central double bond (see Figure 1S). Moreover, the lowest-lying optically bright state corresponds to S_3, with relatively high oscillator strength of 0.66. The electronic transition nature of this state is a monoexcitation from the bonding π to the antibonding π* of the photoisomerizable double bond (see Figure 1S). The $S_0 \rightarrow S_3$ absorption energy is 89.4 kcal·mol^{-1} (at the CASPT2 level), so it can be populated irradiating with a light source around 320 nm of wavelength.

State	Transition	E_{CASPT2}/kcal ·mol^{-1} (nm)	f
S_1	$^1(\pi,\pi^*)$	35.5 (810)	$2.7 \cdot 10^{-3}$
S_2	$^1(\pi,\pi^*)$	88.2 (324)	$2.3 \cdot 10^{-2}$
S_3	$^1(\pi,\pi^*)$	89.4 (320)	0.66

Table 1. CASPT2 vertical excitation energies and oscillator strengths of the designed photoswitch.

Switch Motion Performance. The design of an efficient molecular switch is essential to ensure the efficiency of the molecular motor. Hence, the photochemistry of the proposed photoactive molecular switch was studied to evaluate its efficiency, both mechanistically and dynamically.

As described in the "Photoswitch Absorption Spectrum" section, the optically lowest-lying bright excited state is S_3. After excitation, the system relaxes along the stretching mode, by elongation of the central bond (from 1.37 Å to 1.51 Å). As the molecular switch minima (there are two equivalent minimum energy ground state structures) are non-planar structures, the torsion is partially coupled to the stretching modes (*i.e.* bond length variation makes torsion gradient component to vary), inducing rotation to start before elongation is completed. The system relaxes along the torsion coordinate up to *ca.* -73 degrees, reaching a S_3/S_2 CI (Figure 3). After the crossing, the system continues rotating until *ca.* -91 degrees as it reaches a S_2/S_1 CI and a S_1/S_0 CI almost as a triple crossing (Figure 4). From this point, the system can evolve completing 180 degrees of torsion or recovering the starting structure, aborting the process (Figure 5).

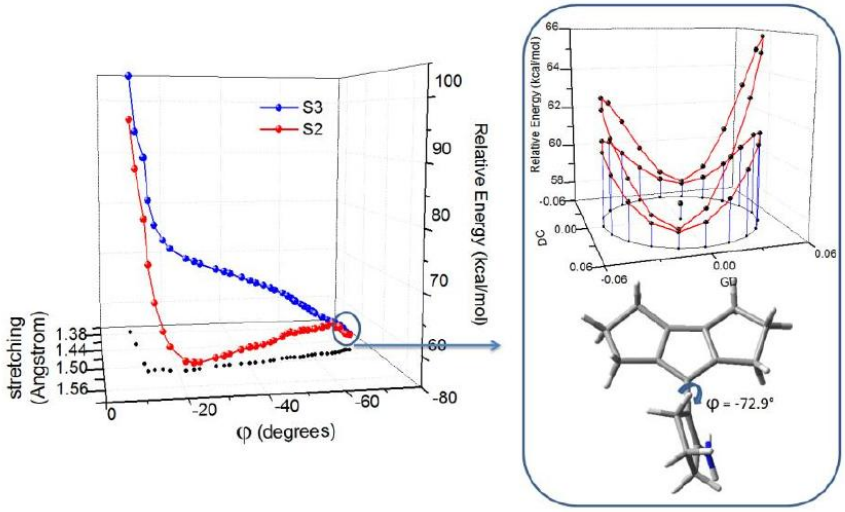

Figure 3. S_3 CASSCF energy profile along the MEP as a function of the central bond stretching and torsion coordinates (left). The S_3/S_2 conical intersection structure and topology are shown (right).

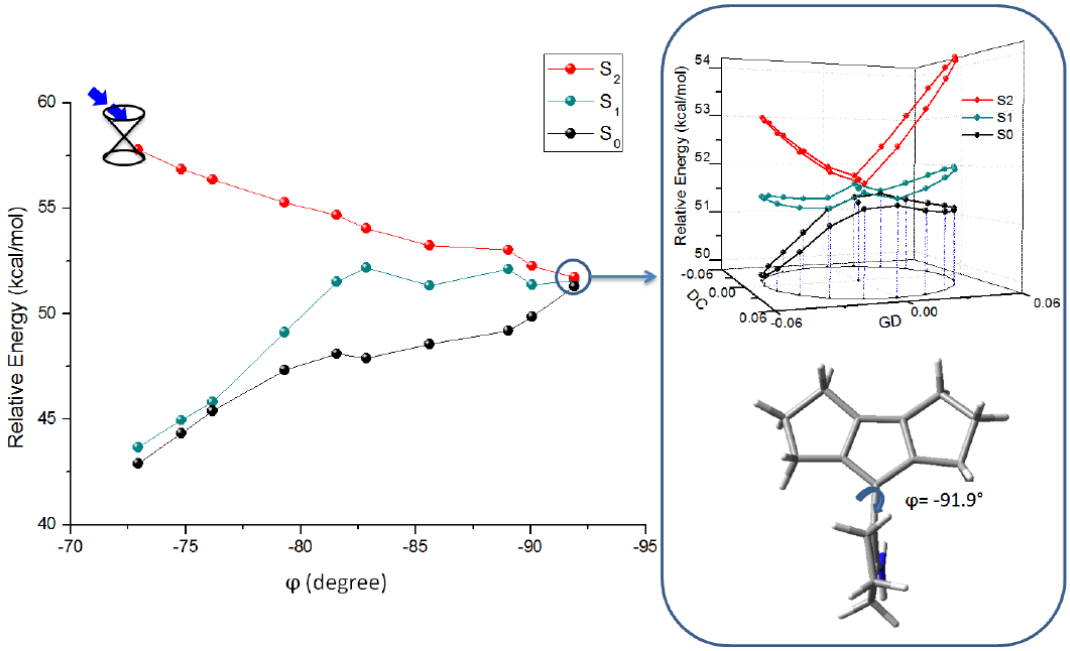

Figure 4. S_2, S_1 and S_0 CASSCF energy profiles along the MEP as a function of the central bond torsion coordinate (left). The S_2/S_1 and S_1/S_0 conical intersection structure and topologies are shown (right).

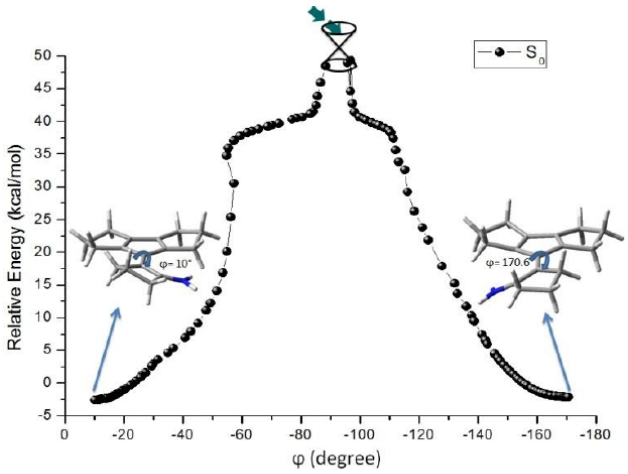

Figure 5. Ground state relaxation from the S_1/S_0 CI showing both paths, aborting and completing the torsion mechanism.

Moreover, the efficiency of this model switch has been studied by means of non-adiabatic molecular dynamics (NAMD) simulations.[45,46,58] A single reference trajectory at T = 0 K (*i.e.* without initial kinetic energy) was performed, in order to study the feasibility of the process. Indeed, if shown to be possible when no initial kinetic energy is included, the proposed mechanism is expected to remain efficient at T > 0 K since MEP as well as NAMD indicate that it is the most relevant photorreaction. The results indicate that photoisomerization is an efficient and ultrafast process for this photoswitch model, being the dynamics in close agreement with the minimum energy paths. The NAMD simulation indicates that the ground state is reached in ~ 215 fs with a torsion angle, φ, of ~ 100º, and the photoisomerization is finally completed in ~ 350 fs. Moreover, the lifetimes of each excited state can be estimated from the NAMD simulation; being S_3 the

longest lived excited state with a lifetime of ~ 135 fs, whereas S_2 has an approximate lifetime of ~ 75 fs and S_1 exists only for ~ 6 fs. This is in agreement with the crossings found along the MEP, with S_2/S1 CI and S_1/S_0 CI really close in energy and structure (Figure 6).

Conversion of Photoswitch into a Photoactive Motor: Structural Modifications for the Inclusion of a Chiral Hydrogen Bond Environment.

Starting from an efficient *Z-E* photoswitch, *i.e.* a molecule that photoisomerizes in both directions, clockwise or counterclockwise, additional structural modifications have to be done in order to make the system to rotate unidirectionally, *i.e.* to convert the switch into a motor. This unidirectionality is usually achieved by providing a chiral environment as it has been reported.[22,35-37] Whereas, we have adopted a novel approach based on the generation of a specific chiral hydrogen bond environment.[38] The structure design of this photoactive molecular motors family focuses on the introduction of polar groups (*e.g.* hydroxyl groups) connected to chiral carbon atoms.

Here, some general guidelines are described for the inclusion of a chiral hydrogen bond environment. First, it has been taken into account that two hydrogen bonds are formed – and also two broken- along the whole rotation mechanism (360º). Therefore the motor structure should have at least three polar groups (*e.g.* OH, NH_3^+) capable of hydrogen bond interaction. Once selected the polar groups to be included in the photoswitch, we have to ensure the right orientation and space proximity between those groups, to allow the interaction establishment. Moreover, to achieve a unidirectional rotation, at least one of the two polar groups involved in the hydrogen bond has to be a chiral atom substituent (*e.g.* placed in a chiral carbon atom). In addition, as the polar groups inserted could have atoms with non bonding electrons (*e.g.* N, O, etc.), it is preferable to avoid their conjugation with the chromophore in order to preserve its nature and efficiency (Figure 7).

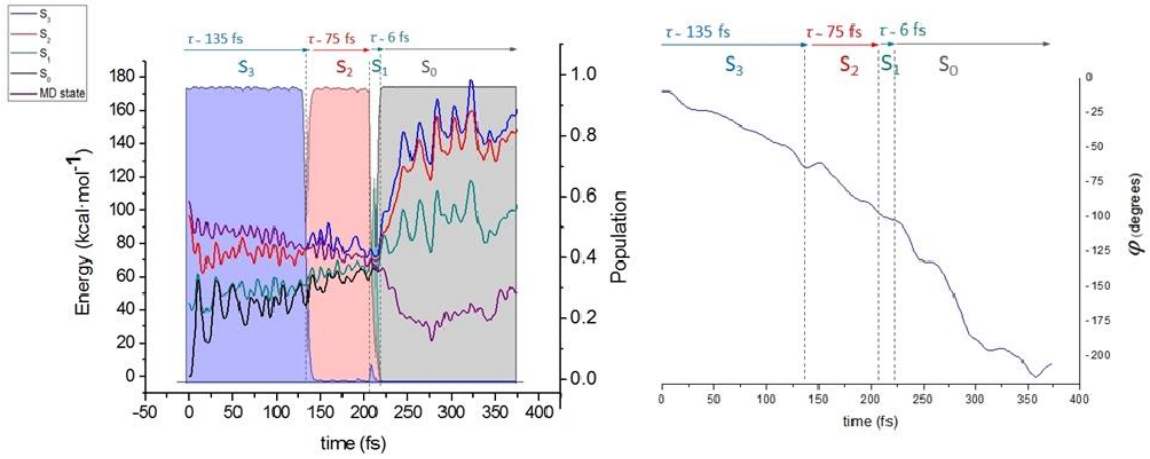

Figure 6. (Left) S_3, S_2, S_1, and S_0 CASSCF relative energy profiles and population along the NAMD simulation at 0 K. (Right) Torsion φ evolution along the molecular dynamic simulation.

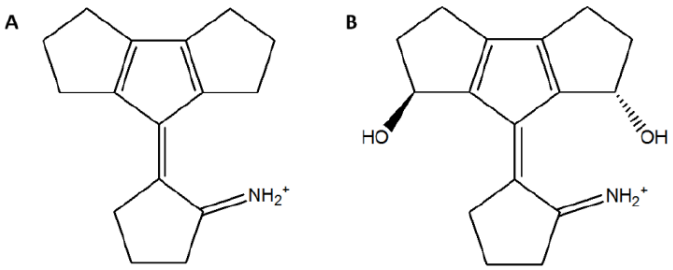

Figure 7. (**A**) Structure of the starting molecular photoswitch. **(B)** Structure of the molecular motor derived following the guidelines described above, where the chiral hydrogen bond environment is introduced via hydroxyl groups.

Hydrogen Bond Role in the Ground State: Global Minimum and Unidirectionality.

The structure modifications included in the photoswitch structure have a clear influence on the molecule force field. Regarding the ground state, the chiral hydrogen bond environment leads to a single ground state minimum on the corresponding motor potential energy surface (PES). Whereas, the photoswitch exhibits two equivalent global minima in the ground state (Figure 8). This fact is closely related with the unidirectional and non-controlled rotation that motor and switch, respectively, undergo when photoexcited. On one hand, the non-controlled rotation of the molecular photoswitch is due to the clockwise photoisomerization of one minimum structure and the counterclockwise photoisomerization of the other ground state minimum structure. Hence, the photoswitch global motion is not unidirectional. On the other hand, the chiral hydrogen bond formation leads to a single global minimum in the ground state of the molecular motor, therefore allowing photoisomerization only in one direction.

Moreover, it is noteworthy that the formation of the hydrogen bond (by introduction of hydroxyl groups, in this study) should maintain a non-zero initial rotation, φ, in the ground state. Any torsion from the planar structure implies the central double-bond to be partially broken, which is compensated by the stabilization due to the hydrogen bond formation. Therefore, the ground state geometry is a balance between both effects.

In addition, the structure of the molecular motor fulfilling the described design guidelines is constrained to a large extent, due to the lack of single bonds with free rotation. However, the presence of rings or polar groups (*i.e.* hydroxyl groups) with conformational freedom can lead to different stable conformers in the ground state. Their structure should be analyzed in order to check that they perform an identical unidirectional motion. In our case of study, the structure presents five-membered rings and hydroxyl groups with conformational freedom. The structure includes two different parts: three fused five-membered rings (stator) and a cyclopenteniminium (rotor) linked by a carbon-carbon double bond. This situation leads to different stable conformers (local minima) of the motor in the ground state (Figure 9).

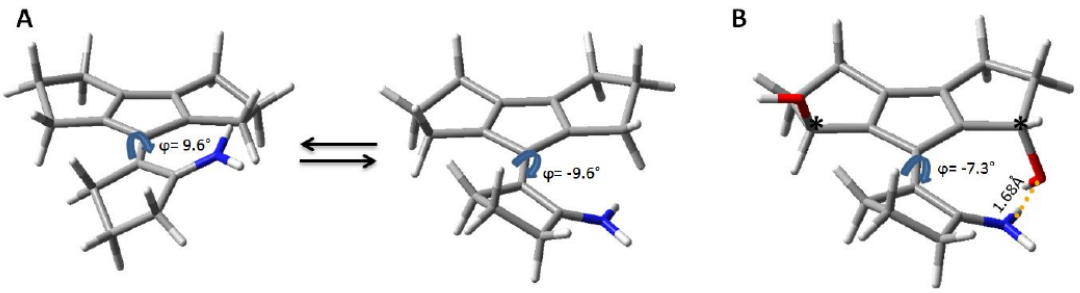

Figure 8. (A) Photoswitch global minima structure in the ground state. **(B)** Motor global minimum structure in the ground state (chiral carbons marked with *).

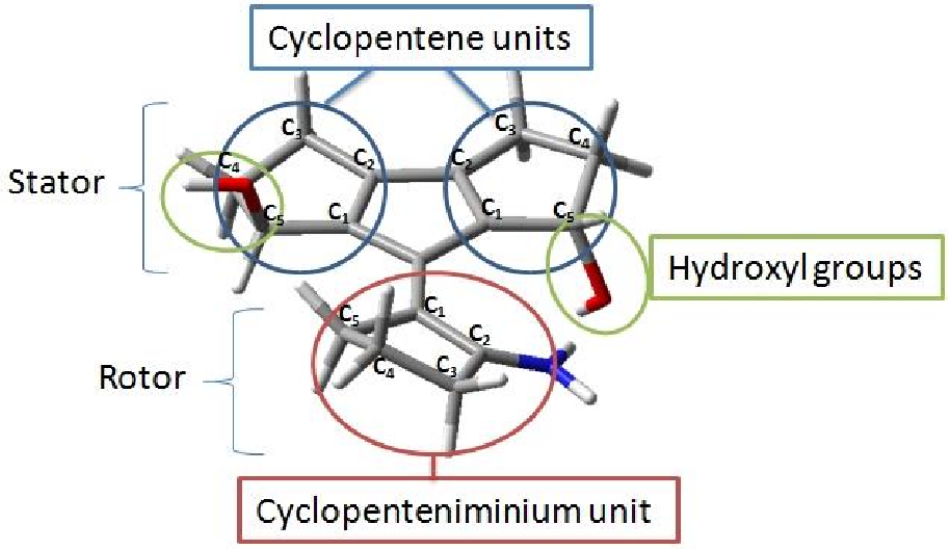

Figure 9. The three units with conformational freedom included in the molecular motor structure. Stator and rotor frameworks are indicated.

Regarding to the cyclopentene fragments, it is known that their equilibrium structure is non planar, being the carbon atom opposite to the double bond, C_4, out of the plane of the other four carbon atoms.[59-61] This ring bending mode is generally known as the ring-puckering vibration and it is said that the structure is puckered at equilibrium. For this fragment two minima are reported in the ground state with positive or negative puckering angle (the angle between the planes defined by $C_1C_2C_3C_5$ coplanar atoms and $C_3C_4C_5$) which are connected by a low energy (below 1.0 kcal·mol^{-1}) transition state, which corresponds to a planar ring structure (Figure 10a). For the cyclopenteniminium unit, it can be reasoned in a similar way as the structure presents two sp^2 C atoms. As there is not an endocyclic double bond, the carbons $C_1C_2C_3C_5$ are not coplanar but it is observed that the carbon C_4 tilts out (up or down) regarding to the other carbons. In this way, two minima are found in the ground state connected by a low energy (below 2.3 kcal·mol^{-1}) transition state, which is an almost planar structure (Figure 10b).

Finally, some motor conformers differ in the spatial arrangement of the hydroxyl groups. For each group two stable conformations are found in which the OH fragment is pointing inwards or outwards of the cyclopentene ring. These conformers are characterized by HCOH dihedral angles around 177 and 60 degrees (Figure 10c).

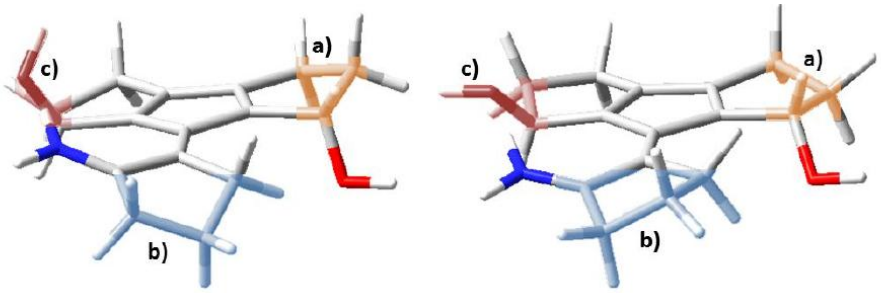

Figure 10. Possible conformational changes for a) cyclopentene units, b) cyclopenteniminium unit and c) hydroxyl groups.

Among all possible combinations of the conformations, it is noteworthy that only a few are stable structures (13 out of 32). Five of these minima represent the 95% of the total population at room temperature, whereas the other eight conformers constitute the remaining 5% (see Supporting Information). Analyzing the structure of the most stable conformers, we can conclude that the initial torsion induced by the hydrogen bond formation indicates the same rotation direction for all of them: from -7.3 to -0.57 degrees (Figure 11).

This fact ensures that although it exists a conformational equilibrium in the ground state, all the most relevant stable conformers rotate in an identical unidirectional way avoiding the efficiency reduction caused by the existence of structures rotating in the opposite sense. In order to check the pattern behavior proposed, the absorption spectrum and the minimum energy path from the Franck–Condon structure are computed for the five most stable conformers. The results indicate that all of them exhibit the same electronic transition nature (see Tables 1S, 2S, 3S, 4S and 5S of the Supporting Information) and rotate unidirectionally in the same sense (Figure 11).

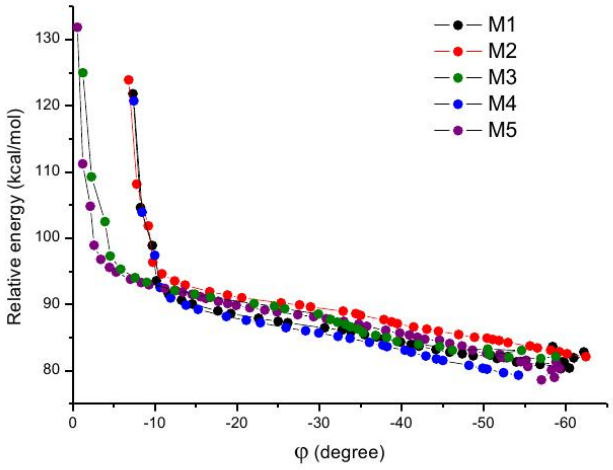

Figure 11. MEPs on the excited bright state of the five most stable conformers (M1 to M5) which represent 95% of the total population.

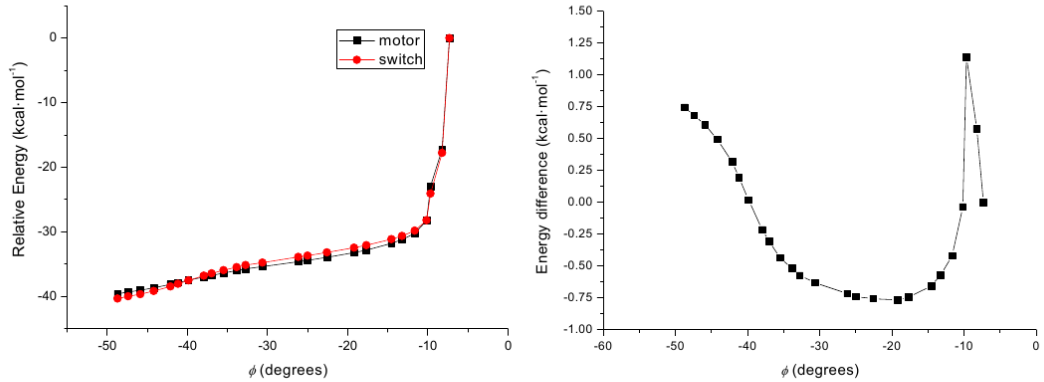

Figure 12. (left) Motor and switch S_3 energy profile along the motor MEP. (right) Energy difference (motor minus switch) along the same path.

Role of the Hydrogen Bond in the Excited State: Torsion Acceleration and Retention.

The excited state evolution of the molecular motor is clearly dictated by the presence of the chiral hydrogen bond environment, as it is the key factor providing the unidirectional rotation after excitation, as discussed above. Nevertheless, the effect of the hydrogen bond, even if essential, is not limited to provide a pre-twisted ground state structure inducing a unidirectional rotation in the excited state. On the contrary, this interaction has a significant impact on the excited state reaction path, as the PESs are now modified by the formation or rupture of the hydrogen bond. In order to gain physical insight into this effect, it is possible to compare the PESs along the excited state path of both, the switch (where everything but the hydrogen bond interaction is kept) and the motor. This study would permit to easily separate the effect of the hydrogen bond. Figure 12 shows relative energy profiles along S_3 path for the molecular motor and the molecular switch (where the hydroxyl groups are removed), *i.e.* the switch profile presented in Fig. 12 corresponds to a path mimicking the motor MEP. Therefore, the energy difference between both energy profiles accounts for the role of the hydrogen bond in the excited state.

The energy difference shown in Figure 12 (right) is a direct measurement of the hydrogen bond effect into the motor excited state energies, since the motor and the switch geometries are virtually identical except for the presence of the OH group. Also, since the evolution of the motor in the excited state is driven by the electronic changes in the chromophore (with a π,π^* state character), and the hydrogen bond does not affect the excitation, its influence on the MEP can be understood as the effect of an external force affecting in some extent the torsion. In order to quantify this effect, the energy difference between both profiles (Figure 12, right) can provide useful information. On one hand, the energy difference becomes negative in the region from φ ~ -10º to φ ~ -40º. In this region of the MEP the motor is stabilized in comparison to the switch. This can be explained in terms of hydrogen bond formation: for this torsion interval the hydrogen bond is formed and the rotation is enhanced with respect to the switch. Moreover, the highest stabilization is reached at *ca.* 20 degrees torsion, indicating that the stabilization of the motor reaches its maximum for this torsion. On the other hand, also considering this regionof the MEP, it can be seen that the force exerted by the hydrogen bond over the torsion (determined by the slope of the tangent line in the right graph of Figure 12) is initially positive (*i.e.* speeding the torsion) up to *ca.* -20º. From this torsion to *ca.* -40º, the force exerted by the hydrogen bond retains the torsion, reaching a maximum force value for this torsion angle, which corresponds to an inflection point in the energy difference plot, indicating that the hydrogen bond is offering its maximal resistance to be broken. Once the system reaches the latter torsion value (φ ~ -40º), the net effect of the hydrogen bond along the torsion results in a positive retention (the motor goes to higher energies than the

up to *ca.* -20º. From this torsion to *ca.* -40º, the force exerted by the hydrogen bond retains the torsion, reaching a maximum force value for this torsion angle, which corresponds to an inflection point in the energy difference plot, indicating that the hydrogen bond is offering its maximal resistance to be broken. Once the system reaches the latter torsion value (φ ~ -40º), the net effect of the hydrogen bond along the torsion results in a positive retention (the motor goes to higher energies than the corresponding structure equivalent to the switch). For torsion values larger than -40º the motor torsion is therefore unfavorable because this change in the torsion implies the necessity of the hydrogen bond breaking, which ultimately implies the rotating moiety to perform a certain amount of work provided by the absorbed photon. Consequently, a small part of the absorbed photon energy is employed in breaking the hydrogen bond in the retention part of the MEP, while the previous torsion acceleration part provides an initial impulse that helps to increase the unidirectional rotation.

This influence of the hydrogen bond in the excited state path is also reflected in the dynamical behavior of both, the motor and the switch. Since the hydrogen bond, close to the conical intersection (*ca.* -90º), is almost broken, the motor torsion will be always retained in some extent in comparison to the switch, and the expected excited state lifetimes will be larger in the motor than in the switch. In fact, the S_3, S_2 and S_1 lifetimes are *ca.* 150fs, 90fs and 20fs for the motor, while for the switch the same lifetimes corresponds to *ca.* 135fs, 75fs and 6fs respectively. The lifetimes are shifted by *ca.* +15fs for each excited state as a result of the torsion impediment provoked by the hydrogen bond.

Summarizing, the effect of the hydrogen bond in the motor torsion on the excited state can be essentially understood in terms of an external force provoked by the hydrogen bond and acting over the torsion coordinate. Initially, the torsion is accelerated (φ < -40º) in the excited state involving an additional kinetic energy of *ca.* 0.75 kcal/mol, while the retention of the torsion in a second step (φ > -40º) involves *ca.* 1.5 kcal/mol. It has to be noted that the energy difference between the two parts of the evolution on the excited state (*ca.* 0.75 kcal/mol) is not enough to completely block the torsion. Nevertheless, the hydrogen bond should be carefully selected in the design process in order to guarantee that is not strong enough to yield a large retention force impeding completely the rotation and blocking therefore the Z-E isomerization. In this regard, the maximal force exerted by the hydrogen bond along the torsion is located at the inflection point of the energy difference force representation (Figure 12, right) and should be a good parameter to understand the strength of the hydrogen bond.

General Photoisomerization Mechanism.

This novel family of molecular motors performs a simple and efficient unidirectional motion of 360 degrees. From the slightly rotated, φ degrees, minimum in the ground state the system is irradiated. After excitation to the optically bright state -the $^1(\pi,\pi^*)$ vertical transition to the CC central double bond- the system minimizes the energy along the stretching coordinate (*i.e.* bond length alternation) coupled with the torsion one. Then, the molecule continues rotating upon reaching a conical intersection with the ground state. After decay to the ground state, the motor completes the half rotation cycle, 180 + φ degrees. The complete cycle (360 + φ degrees) is accomplished after vertical excitation of the photoproduct, 180 + φ (Figure 13)[38].

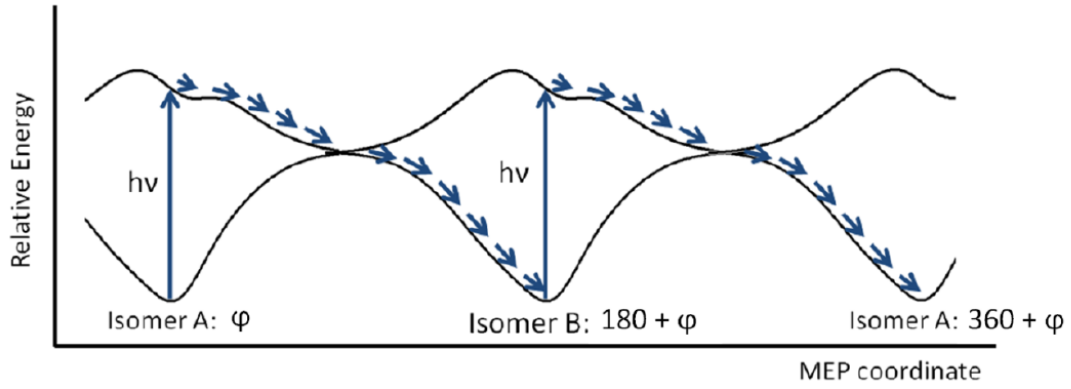

Figure 13. Photocyclization mechanism of novel molecular motors based on two photochemical steps with an initial hydrogen bond induced rotation of φ degrees.

Therefore, the full cycle can be achieved by absorption of a second photon of the same wavelength. This means that applying a monochromatic UV source, the molecular motor rotates in a unidirectional way completing the full cycle. The torsional mechanism and photochemistry of the second half cycle is exactly the same as the one described for the first half cycle.

CONCLUSIONS

A set of general guidelines are given for the design of an efficient *Z-E* photoactive molecular motor by introducing a chiral hydrogen bond environment into a photoactive switch. First, we provide some ideal properties for the starting photoswitch in order to behave properly: the electronic excitation should be mainly constituted by the π-π* transition of the isomerizable double bond, while the photoisomerization around the other double bonds should be blocked. Then, we show how to include the chiral environment providing unidirectional rotation and describe the aspects controlling the efficiency of this type of motors: pre-twisted structure in the ground state, unidirectional rotation after excitation to the optically bright state, and weak enough hydrogen bond in order to prevent stable intermediates in the excited state.

The complete design process of a photoactive motor is exemplified by a system based on the retinal chromophore. Both, the photochemistry and photophysics of a photoactive molecular motor and switch related in structure have been analyzed. The comparative study provides some keys to understand the molecular switch conversion into a molecular motor:

– the chiral environment generated by hydrogen bond formation is essential to ensure unidirectional rotation as only one global minimum is stable in the ground state, characterized by initial torsion.

– compared to the molecular switch, the hydrogen bond presence in the molecular motor retains the torsion motion as the CIs are reached at lower torsion values and the photoisomerization process is *ca.*100 fs slowed.

– the hydrogen bond is strong enough to guide the torsion but not too strong to avoid the photoisomerization process.

– these novel molecular motors are also characterized by an improved overall mechanism (*i.e.* no thermal steps are necessary to complete the 360° cycle; the time scale of the complete process is less than 1 ps, being faster than any other motor reported[62-64]).

ACKNOWLEDGMENT

This research was supported by the Spanish MINECO/FEDER grants CTQ2011-24800 and CTQ2012-36966, and Project CCG2013/EXP-089 for the University of Alcalá (UAH). C.G.I. and F.Z. are grateful to the Spanish MEC, A.V. and M.M. acknowledge the UAH for a doctoral fellowship.

SUPPORTING INFORMATION PARAGRAPH

Ground state conformational study. Molecular motor absorption spectrum. Gradient Difference (GD) and Derivative Coupling (DC) vectors of each conical intersection. CASPT2//CASSCF molecular switch energy profile. Photoproducts ground state geometries.

REFERENCES

(1) Iqbal, P.; Preece, J. A.; Mendes, P. M.; John Wiley & Sons Ltd.: 2012; Vol. 8, p 3589.

(2) Balzani, V. *Pure Appl Chem* **2008**, *80*, 1631.

(3) Balzani, V.; Credi, A.; Venturi, M. *Phys World* **2004**, *17*, 39.

(4) Kelly, T. R.; Editor *Molecular Machines. [In: Top. Curr. Chem., 2005; 262]*; Springer, 2005.

(5) Antonov, L.; Deneva, V.; Simeonov, S.; Kurteva, V.; Nedeltcheva, D.; Wirz, J. *Angew. Chem., Int. Ed.* **2009**, *48*, 7875.

(6) Sliwa, M.; Letard, S.; Malfant, I.; Nierlich, M.; Lacroix, P. G.; Asahi, T.; Masuhara, H.; Yu, P.; Nakatani, K. *Chem. Mater.* **2005**, *17*, 4727.

(7) Rosario, R.; Gust, D.; Hayes, M.; Springer, J.; Garcia, A. A. *Langmuir* **2003**, *19*, 8801.

(8) Rosario, R.; Gust, D.; Garcia, A. A.; Hayes, M.; Taraci, J. L.; Clement, T.; Dailey, J. W.; Picraux, S. T. *J. Phys. Chem. B* **2004**, *108*, 12640.

(9) Li, H.; Fahrenbach, A. C.; Coskun, A.; Zhu, Z.-X.; Barin, G.; Zhao, Y.-L.; Botros, Y. Y.; Sauvage, J.-P.; Stoddart, J. F. *Angew. Chem., Int. Ed.* **2011**, *50*, 6782.

(10) Gosztola, D.; Niemczyk, M. P.; Wasielewski, M. R. *J. Am. Chem. Soc.* **1998**, *120*, 5118.

(11) Shinkai, S.; Nakaji, T.; Nishida, Y.; Ogawa, T.; Manabe, O. *J. Am. Chem. Soc.* **1980**, *102*, 5860.

(12) Jousselme, B.; Blanchard, P.; Gallego-Planas, N.; Delaunay, J.; Allain, M.; Richomme, P.; Levillain, E.; Roncali, J. *J. Am. Chem. Soc.* **2003**, *125*, 2888.

(13) Cacciapaglia, R.; Di, S. S.; Mandolini, L. *J. Am. Chem. Soc.* **2003**, *125*, 2224.

(14) Bredenbeck, J.; Helbing, J.; Sieg, A.; Schrader, T.; Zinth, W.; Renner, C.; Behrendt, R.; Moroder, L.; Wachtveit, J.; Hamm, P. *Proc. Natl. Acad. Sci. U. S. A.* **2003**, *100*, 6452.

(15) Renner, C.; Behrendt, R.; Sporlein, S.; Wachtveitl, J.; Moroder, L. *Biopolymers* **2000**, *54*, 489.

(16) Spoerlein, S.; Carstens, H.; Satzger, H.; Renner, C.; Behrendt, R.; Morader, L.; Tavan, P.; Zinth, W.; Wachtveitl, J. *Proc. Natl. Acad. Sci. U. S. A.* **2002**, *99*, 7998.

(17) Melloni, A.; Rossi, P. R.; Donati, D.; Zanirato, V.; Sinicropi, A.; Parisi, M. L.; Martin, E.; Ryazantsev, M.; Ding, W. J.; Frutos, L. M.; Basosi, R.; Fusi, S.; Latterini, L.; Ferre, N.; Olivucci, M. *J. Am. Chem. Soc.* **2010**, *132*, 9310.

(18) Ruangsupapichat, N.; Pollard, M. M.; Harutyunyan, S. R.; Feringa, B. L. *Nat. Chem.* **2010**, *3*, 53.

(19) Lubbe, A. S.; Ruangsupapichat, N.; Caroli, G.; Feringa, B. L. *J. Org. Chem.* **2011**, *76*, 8599.

(20) ter, W. M. K. J.; van, D. R. A.; Meetsma, A.; Feringa, B. L. *Org. Biomol. Chem.* **2005**, *3*, 4071.

(21) Conti, I.; Garavelli, M.; Orlandi, G. *J. Am. Chem. Soc.* **2008**, *130*, 5216.

(22) Feringa, B. L. *J. Org. Chem.* **2007**, *72*, 6635.

(23) Martin, M. E.; Negri, F.; Olivucci, M. *J. Am. Chem. Soc.* **2004**, *126*, 5452.

(24) Rivado-Casas, L.; Sampedro, D.; Campos, P. J.; Fusi, S.; Zanirato, V.; Olivucci, M. *J. Org. Chem.* **2009**, *74*, 4666.

(25) Sinicropi, A.; Martin, E.; Ryazantsev, M.; Helbing, J.; Briand, J.; Sharma, D.; Leonard, J.; Haacke, S.; Cannizzo, A.; Chergui, M.; Zanirato, V.; Fusi, S.; Santoro, F.; Basosi, R.; Ferre, N.; Olivucci, M. *Proc. Natl. Acad. Sci. U. S. A.* **2008**, *105*, 17642.

(26) Sampedro, D.; Migani, A.; Pepi, A.; Busi, E.; Basosi, R.; Latterini, L.; Elisei, F.; Fusi, S.; Ponticelli, F.; Zanirato, V.; Olivucci, M. *J. Am. Chem. Soc.* **2004**, *126*, 9349.

(27) Garcia-Iriepa, C.; Marazzi, M.; Frutos, L. M.; Sampedro, D. *RSC Adv.* **2013**, *3*, 6241.

(28) Yoshida, M.; Muneynki, E.; Hisabori, T. *Nat. Rev. Mol. Cell Biol.* **2001**, *2*, 669.

(29) Boyer, P. D. *Nature (London)* **1999**, *402*, 247.

(30) Vallee, R. B.; Hoeoek, P. *Nature (London, U. K.)* **2003**, *421*, 701.

(31) Tyreman, M. J. A.; Molloy, J. E. *IEE Proc.: Nanobiotechnol.* **2003**, *150*, 95.

(32) Schliwa, M.; Woehlke, G. *Nature (London, U. K.)* **2003**, *422*, 759.

(33) Kelly, T. R.; De, S. H.; Silva, R. A. *Nature (London)* **1999**, *401*, 150.

(34) Koumura, N.; Zijlstra, R. W.; van, D. R. A.; Harada, N.; Feringa, B. L. *Nature* **1999**, *401*, 152.

(35) Wolken, J. *Light Detectors, Photoreceptors, and Imaging Systems in Nature*; Oxfors U.Press USA, 1995.

(36) Crano, J. C. G., R.J. *Organic Photochromic and Thermochromic Compounds*; Springer, New York, 1999.

(37) Feringa, B. L. *Acc. Chem. Res.* **2001**, *34*, 504.

(38) Garcia-Iriepa, C.; Marazzi, M.; Zapata, F.; Valentini, A.; Sampedro, D.; Frutos, L. M. *J. Phys. Chem. Lett.* **2013**, *4*, 1389.

(39) Ter, W. M. K. J.; Van, D. R. A.; Meetsma, A.; Feringa, B. L. *J. Am. Chem. Soc.* **2003**, *125*, 15076.

(40) Pijper, D.; van, D. R. A.; Meetsma, A.; Feringa, B. L. *J. Am. Chem. Soc.* **2005**, *127*, 17612.

(41) Head-Gordon, M.; Pople, J. A.; Frisch, M. J. *Chem. Phys. Lett.* **1988**, *153*, 503.

(42) Moller, C.; Plesset, M. S. *Phys. Rev.* **1934**, *46*, 618.

(43) Finley, J.; Malmqvist, P.-A.; Roos, B. O.; Serrano-Andres, L. *Chem. Phys. Lett.* **1998**, *288*, 299.

(44) The DC vector measures the distortion of the system providing the maximum coupling between the electronic states involved in the crossing. The GD vector measures the distortion of the system leading to the largest variation of the energy difference between the two electronic states involved in the crossing.

(45) Tully, J. C. *J. Chem. Phys.* **1990**, *93*, 1061.

(46) Jaeger, H. M.; Fischer, S.; Prezhdo, O. V. *J. Chem. Phys.* **2012**, *137*, 22A545/1.

(47) Granucci, G.; Persico, M. *J. Chem. Phys.* **2007**, *126*, 134114/1.

(48) Code implemented by A. Valentini and L. M. Frutos working with MOLCAS 7.8 (see ref.49)

(49) Aquilante, F.; De, V. L.; Ferre, N.; Ghigo, G.; Malmqvist, P.-a.; Neograd y, P.; Pedersen, T. B.; Pitonak, M.; Reiher, M.; Roos, B. O.; Serrano-Andres, L.; Urban, M.; Veryazov, V.; Lindh, R. *J. Comput. Chem.* **2010**, *31*, 224.

(50) Frisch, M. J.; Trucks, G. W.; Schlegel, H. B.; Scuseria, G. E.; Robb, M. A.; Cheeseman; J. R.; Scalmani; G.; Barone; V.; Mennucci; B.; Petersson, G. A.; Nakatsuji, H.; Caricato, M.; Li, X.; Hratchian, H. P.; Izmaylov, A. F.; Bloino, J.; Zheng, G.; Sonnenberg, J. L.; Hada, M.; Ehara, M.; Toyota, K.; Fukuda, R.; Hasegawa, J.; Ishida, M. N., T.;; Honda, Y.; Kitao, O.; Nakai, H.; Vreven, T.; Montgomery, J. A., Jr.;; Peralta, J. E.; Ogliaro, F.; Bearpark, M.; Heyd, J. J.; Brothers, E.; Kudin, K. N.; Staroverov, V. N.; Kobayashi, R.; Normand, J.; Raghavachari, K.; Rendell, A.; Burant, J. C.; Iyengar, S. S.; Tomasi, J.; Cossi, M.; Rega, N.; Millam, J. M.; Klene, M.; Knox, J. E.; Cross, J. B.; Bakken, V.; Adamo, C.; Jaramillo, J.; Gomperts, R.; Stratmann, R. E.; Yazyev, O.; Austin, A. J.; Cammi, R.; Pomelli, C.; Ochterski, J. W.; Martin, R. L.; Morokuma, K.; Zakrzewski, V. G.; Voth, G. A.; Salvador, P.; Dannenberg, J. J.; Dapprich, S.; Daniels, A. D.; Farkas, O.; Foresman, J. B.; Ortiz, J. V.; Cioslowski, J.; Fox, D. J. *Gaussian 09* **2009** *revision B.01; Gaussian, Inc.: Wallingford, CT*.

(51) Feringa, B. L.; Editor *Molecular Switches*; Wiley-VCH, 2001.

(52) Rivado-Casas, L.; Blanco-Lomas, M.; Campos, P. J.; Sampedro, D. *Tetrahedron* **2011**, *67*, 7570.

(53) Neckers, D. C. *Mechanistic Organic Photochemistry*; Reinhold, 1967.

(54) Zanirato, V.; Pollini, G. P.; De Risi, C.; Valente, F.; Melloni, A.; Fusi, S.; Barbetti, J.; Olivucci, M. *Tetrahedron* **2007**, *63*, 4975.

(55) Griesbeck, A. G.; Mattay, J. *Mol. Supramol. Photochem.* **2005**, *12*, 1.

(56) Rohatgi-Mukherjee, K. K. *Fundamentals of Photochemistry*; Wiley Eastern Ltd., 1978.

(57) Suzuki, H. *Electronic Absorption Spectra, and Geometry of Organic Molecules; an Application of Molecular Orbital Theory*; Academic, 1967.

(58) Craig, C. F.; Duncan, W. R.; Prezhdo, O. V. *Phys. Rev. Lett.* **2005**, *95*, 163001/1.

(59) Davis, M. I.; Muecke, T. W. *J. Phys. Chem.* **1970**, *74*, 1104.

(60) Kunitski, M.; Knippenberg, S.; Gelin, M.; Riehn, C.; Dreuw, A.; Brutschy, B. *Phys. Chem. Chem. Phys.* **2010**, *12*, 8190.

(61) Saebo, S.; Cordell, F. R.; Boggs, J. E. *J. Mol. Struct.: THEOCHEM* **1983**, *13*, 221.

(62) Koumura, N.; Geertsema, E. M.; Meetsma, A.; Feringa, B. L. *J. Am. Chem. Soc.* **2000**, *122*, 12005.

(63) Klok, M.; Boyle, N.; Pryce, M. T.; Meetsma, A.; Browne, W. R.; Feringa, B. L. *J. Am. Chem. Soc.* **2008**, *130*, 10484.

(64) van, D. R. A.; ter, W. M. K. J.; Pollard, M. M.; Vicario, J.; Koumura, N.; Feringa, B. L. *Nature (London, U. K.)* **2005**, *437*, 1337.

7.3 Chapter Bibliography

Albu, N. M.; Bergin, E.; Yaron, D. J., Computational Design of a Light-Driven Molecular Motor. *The Journal of Physical Chemistry A* **2009,** *113*, 7090-7096.

Balzani, V.; Credi, A.; Venturi, M., *Molecular Devices and Machines*. 2nd ed.; Wiley-VCH: Weinheim, 2008.

Balzani, V.; Credi, A.; Venturi, M., Light powered molecular machines. *Chem. Soc. Rev.* **2009,** *38*, 1542-1550.

Bleger, D.; Yu, Z.; Hecht, S., Toward optomechanics: Maximizing the photodeformation of individual molecules. *Chem. Commun.* **2011,** *47*, 12260-12266.

Cnossen, A.; Hou, L.; Pollard, M. M.; Wesenhagen, P. V.; Browne, W. R.; Feringa, B. L., Driving Unidirectional Molecular Rotary Motors with Visible Light by Intra- And Intermolecular Energy Transfer from Palladium Porphyrin. *J. Am. Chem. Soc.* **2012,** *134*, 17613-17619.

Dong, H.; Zhu, H.; Meng, Q.; Gong, X.; Hu, W., Organic photoresponse materials and devices. *Chem. Soc. Rev.* **2012,** *41*, 1754-1808.

Feringa, B. L., The Art of Building Small: From Molecular Switches to Molecular Motors. *The Journal of Organic Chemistry* **2007,** *72*, 6635-6652.

Feringa, B. L.; Browneed, W. R., *Molecular Switches*. 2nd ed.; Wiley-VCH: Weinheim, 2011.

Garcia-Iriepa, C.; Marazzi, M.; Frutos, L. M.; Sampedro, D., E/Z Photochemical switches: syntheses, properties and applications. *RSC Advances* **2013,** *3*, 6241-6266.

Holland, N. B.; hugel, T.; Neuert, G.; Cattani-Scholz, A.; Renner, C.; Oesterhelt, D.; moroder, L.; Seitz, M.; Gaub, H. E., Single Molecule Force Spectroscopy of Azobenzene Polymers: Switching Elasticity of Single Photochromic Macromolecules. *Macromolecules* **2003,** *36*, 2015-2023.

Hosono, N.; Kajitani, T.; Fukushima, T.; Ito, K.; Sasaki, S.; Takata, M.; Aida, T., Large-Area Three-Dimensional Molecular Ordering of a Polymer Brush by One-Step Processing. *Science* **2010,** *330*, 808-811.

Liu, F.; Morokuma, K., Computational Study on the Working Mechanism of a Stilbene Light-Driven Molecular Rotary Motor: Sloped Minimal Energy Path and Unidirectional Nonadiabatic Photoisomerization. *J. Am. Chem. Soc.* **2012,** *134*, 4864-4876.

ter Wiel, M. K. J.; van Delden, R. A.; Meetsma, A.; Feringa, B. L., Increased Speed of Rotation for the Smallest Light-Driven Molecular Motor. *J. Am. Chem. Soc.* **2003,** *125*, 15076-15086.

Yamaki, M.; Hoki, K.; Ohtsuki, Y.; Kono, H.; Fujimura, Y., Quantum Control of a Chiral Molecular Motor Driven by Laser Pulses. *J. Am. Chem. Soc.* **2005,** *127*, 7300-7301.

Chapter 8: Summary and Conclusions

"Seven and a half million years our race has waited for this Great and Hopefully Enlightening Day!" cried the cheer leader. "The Day of the Answer!" Hurrahs burst from the ecstatic crowd. "Never again," cried the man, "never again will we wake up in the morning and think Who am I? What is my purpose in life? Does it really, cosmically speaking, matter if I don't get up and go to work? For today we will finally learn once and for all the plain and simple answer to all these nagging little problems of Life, the Universe and Everything!".

…There was a moment's expectant pause whilst panels slowly came to life on the front of the console. Lights flashed on and off experimentally and settled down into a business-like pattern. A soft low hum came from the communication channel. "Good morning," said Deep Thought at last. "Er ... Good morning, O Deep Thought," said Loonquawl nervously, "do you have ... er, that is ..." "An answer for you?" interrupted Deep Thought majestically. "Yes. I have."
... "There really is one?" breathed Phouchg. "There really is one," confirmed Deep Thought. "To Everything? To the great Question of Life, the Universe and Everything?" "Yes."

... "And you're ready to give it to us?" urged Loonquawl. "I am." "Now?" "Now," said Deep Thought. "Though I don't think," added Deep Thought, "that you're going to like it." "Doesn't matter!" said Phouchg. "We must know it! Now!" "Now?" inquired Deep Thought. "Yes! Now.

..." "Alright," said the computer and settled into silence again. "The Answer to the Great Question..."'Yes ...!" "Of Life, the Universe and Everything ..." said Deep Thought. "Yes ...!" "Is ..." said Deep Thought, and paused. "Yes ...!" "Is ..." "Yes ...!!!...?"

"Forty-two," said Deep Thought, with infinite majesty and calm.

The Hitchhiker's Guide to the Galaxy. Douglas Adams

In this thesis we have developed a series of theoretical and computational methodologies, which were subsequently applied to a set of chemical and biological relevant systems in the field of photochemistry. The phenomena considered in this thesis, can be described as follows:

- Dexter-type energy transfer mechanisms between a donor and an acceptor molecule have been studied with the aim of defining an energy transfer reaction coordinate. Special attention has been focused on nonvertical excitation triplet-triplet energy transfer (TET).
- Effect of external forces over the spectroscopical properties of molecular systems was studied. Understanding the force as an agent which can induce structural changes in the conformation of the molecule, being it a substituent or a direct applied mechanical force.
- Design of molecular devices using a bottom-up methodology, which operates in an autonomous fashion and in the case of molecular motor induces a unidirectional rotation, driven by hydrogen bonds.
- Chemiluminescence and bioluminescence phenomena were studied, using a minimal model of the 1,2-dioxetane family of composes, which are the intermediates responsible for the light emission after its decomposition.
- Fluorescent emission of the irisFP, was studied in order to identify the main structural factors which mainly influence the fluorescent emission at a given temperature.

The aforementioned phenomena were addressed using a set of developed methodologies which implies the use of standard *ab initio* methods as density functional theory (DFT), time dependent density functional theory (TD-DFT) and multiconfigurational methods (CASSCF, CASPT2).

Accordingly, it was developed the following methodologies:

- An algorithm to define an energy transfer reaction coordinate, which can assign a quantitative weight to the contribution of each internal coordinate to the global transfer process.
- A software for molecular dynamic simulation was developed, providing the following features: a Nosé-Hoover chain of thermostat to control the temperature,

a fewest switches algorithm for non-adiabatic surfaces hopping, several interfaces to perform “on the fly” molecular dynamics using Gaussian or Molcas, an interface to perform molecular dynamics using analytical PESs and finally a QM/MM interface which is currently under development.

- A guideline to design molecular switches and motors, which operates in a cycle driven by photochemical excitations of the same wavelength.

Chapter 9: Resumen y Conclusiones (Spanish Version)

"José Arcadio Buendía pasó los largos meses de lluvia encerrado en un cuartito que construyó en el fondo de la casa para que nadie perturbara sus experimentos. Habiendo abandonado por completo las obligaciones domésticas, permaneció noches enteras en el patio vigilando el curso de los astros, y estuvo a punto de contraer una insolación por tratar de establecer un método exacto para encontrar el mediodía. Cuando se hizo experto en el uso y manejo de sus instrumentos, tuvo una noción del espacio que le permitió navegar por mares incógnitos, visitar territorios deshabitados y trabar relación con seres espléndidos, sin necesidad de abandonar su gabinete. Fue ésa la época en que adquirió el hábito de hablar a solas, paseándose por la casa sin hacer caso de nadie, mientras Úrsula y los niños se partían el espinazo en la huerta cuidando el plátano y la malanga, la yuca y el ñame, la ahuyama y la berenjena. De pronto, sin ningún anuncio, su actividad febril se interrumpió y fue sustituida por una especie de fascinación. Estuvo varios días como hechizado, repitiéndose a sí mismo en voz baja un sartal de asombrosas conjeturas, sin dar crédito a su propio entendimiento. Por fin, un martes de diciembre, a la hora del almuerzo, soltó de un golpe toda la carga de su tormento. Los niños habían de recordar por el resto de su vida la augusta solemnidad con que su padre se sentó a la cabecera de la mesa, temblando de fiebre, devastado por la prolongada vigilia y por el encono de su imaginación, y les reveló su descubrimiento.

-La tierra es redonda como una naranja"

Cien años de Soledad. Gabriel García Márquez

El proyecto realizado en esta Tesis consiste en el desarrollo y aplicación de metodologías teóricas y computaciones, usadas en la descripción estática y dinámica de procesos fotofísicos y fotoquímicos de compuestos químicos y de interés biológico. Estas metodologías computacionales fueron implementadas aplicando técnicas punteras usadas en el campo de la ciencia de la computación.

La presente Tesis se compone de 4 bloques principales. El primero de estos bloques estudia el proceso de transferencia de energía intermolecular, especialmente transferencia de energía triplete. Por su parte, el segundo bloque examina los mecanismos y comportamiento dinámico de dos procesos biológicos fotoinducidos de intereses tecnológico. Mientras el tercer bloque consiste en el estudio del efecto de fuerzas externas sobre las propiedades espectroscópicas de los sistemas moleculares. Finalmente, el último bloque considera el diseño de dispositivos moleculares usando cambios conformacionales fotoinducidos en la generación de movimiento controlado.

9.1 Transferencia de Energía Triplete-Triplete

Terenin y Ermolaev fueron los primeros en observar que una molécula que absorbe luz a cierta longitud de onda puede inducir emisión de fosforescencia en otra que se encuentra en la misma solución, pero que sin la presencia de la primera especie, este evento no se presentaría (Terenin and Ermolaev 1956). Este fenómeno es denominado transferencia de energía triplete (TET).

El mecanismo de la TET consiste en un intercambio electrónico entre las dos moléculas implicadas (Förster 1965), suponiendo que existe una interacción electrostática entre el dador en estado excitado (D*) y el aceptor (A), esta interacción acopla la energía liberada por D* para excitar simultáneamente el aceptor, proceso que resulta en la formación de las especies D y A*, conservándose el momento de spin total. Este proceso ocurre con una velocidad que puede ser medida experimentalmente. Además, para que la TET tenga lugar, es necesario que las moléculas estén a una distancia cercana para que ocurra el intercambio electrónico. Esta distancia en general es menor de un nanómetro.

Como ha sido señalado en un estudio teórico (Frutos, Castaño et al. 2004), para una distancia dador-aceptor determinada, la diferencia de energía entre los estados triplete del dador y aceptor (suponiendo un acoplamiento débil) esta modulada por activación térmica de determinadas coordenadas moleculares de los reactivos, lo que permite que ambas energías sean iguales, permitiendo el proceso de transferencia de energía. Si se considera una energía constante para el dador (lo cual ocurre, por ejemplo, con un dador rígido por ejemplo), es posible determinar las coordenadas que regulan o modulan la activación térmica para un determinado aceptor (dador).

En la presente Tesis se desarrolla un algoritmo que permite identificar las principales coordenadas en el proceso de TET, además establece un formalismo para asignar valores numéricos a la aportación de cada coordenada interna del sistema, a la coordenada de reacción del sistema. Además, este desarrollo demuestra la posibilidad de separar las contribuciones del dador tanto como el aceptor, a la coordenada de reacción, cuantificando efectivamente el aporte de cada molécula en el proceso de TET (Zapata, et al. 2014).

El mentado formalismo fue aplicado al paradigmático caso del cis-estilbeno, que fue la primera molécula en la que se estudió el proceso de TET no vertical. El término de transferencia no vertical surge de la hipótesis usada para explicar el hecho que la velocidad de transferencia de energía para varios dadores son significativamente más altas en comparación con las cinéticas predichas por Sandros (Saltiel, et al. 1984, sandros 1964) .

El algoritmo mencionado permitió la identificación de las principales coordenadas involucradas en el proceso de transferencia de energía del cis-estilbeno. Se obtuvo, que el enlace central C1=C2 y las torsiones fenil-vinil (C1C2-C3C5 y C1C2-C4C6) indicadas en la Figura 9.1, son quienes en mayor medida regulan la diferencia de energía singlete-triplete, en la zona de déficits energético (Energía Aceptor > Energía dador). Este resultado está en desacuerdo con hipótesis previas acerca de la naturaleza del comportamiento no vertical (Brennan, et al. 1994, Catalán and Saltiel 2001).

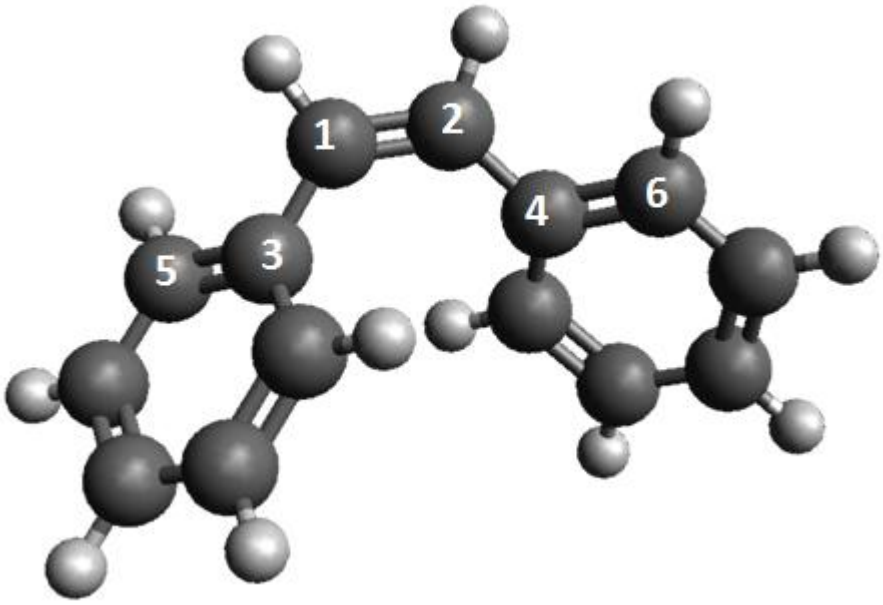

Figura 9.1. Representación esquemática del cis-estilbeno y numeración de los principales átomos involucrados en modular la diferencia de energía singlete-triplete.

Tras desarrollar el formalismo mencionado y corroborar su fiabilidad, es necesario ampliar el enfoque del problema de transferencia de energía puesto que la orientación dada hasta el momento corresponde a un análisis estático, sin embargo los procesos de transferencia de energía ocurren en fase condensada a una determinada temperatura. Es preciso entonces introducir los efectos dinámicos e investigar sus implicaciones en el proceso de transferencia de energía, y posteriormente su comparación con respecto a los análisis estático.

Para llevar a cabo un estudio dinámico fue desarrollada e implementada una metodología de simulación de dinámicas moleculares. La metodología se basa en la aproximación de Born-Oppenheimer, la cual supone que los núcleos atómicos se mueven en el campo electrostático medio causado por los electrones, desacoplando formalmente el moviente de núcleos y electrones. Además de ello esta metodología conlleva una representación clásica de los átomos cuya dinámica está gobernada por las leyes de Newton. De tal forma que el potencial necesario para integrar las ecuaciones de Newton, debe dar cuenta de las interacciones entre los átomos que conforman el sistema molecular.

Para obtener el potencial necesario para integrar las ecuaciones clásicas de movimiento, se recurrió a una aproximación cuadrática alrededor del punto Franck-Condon (utilizando el gradiente y el Hessiano). Esta extrapolación como fue demostrado, describe de forma realista el potencial en los entornos del punto de equilibrio, al mismo tiempo que permite un cálculo sencillo y rápido del gradiente molecular. Además de esto fue utilizado el algoritmo simpléctico Velociy-Verlet para integrar las ecuaciones de movimiento. Donde simpléctico se refiere a la propiedad de conservar el espacio de fases accesible a una determinada energía, sin perder o ganar energía por cuenta de errores numéricos acumulativos (Frenkel and Smit 2002).

Por otra parte, el proceso de transferencia de energía en solución se lleva a cabo a una temperatura determinada, de manera que el dador y aceptor estas en equilibrio térmico con el solvente. Por tanto para simular efectivamente estas condiciones es necesario introducir un termostato que intercambie constantemente energía con el sistema molecular. Para ello fueron implementadas las ecuaciones de la cadena de termostatos de Nosé-Hoover (Martyna, et al. 1992). Estos termostatos intercambian energía con el sistema molecular, de tal forma que las estadísticas resultantes de estas simulaciones pertenecen a las descritas por un ensamble canónico NVT, que describen correctamente el comportamiento de los sistemas moleculares a temperatura constante.

Esta metodología de dinámicas moleculares fue aplicada al estudio de uno de los pasos claves de la terapia fotodinámica, la transferencia de energía. En esta terapia es usado algún tipo de sensibilizador, generalmente un derivado de la porfirina que tiene un tiempo de vida media grande, para transferir la energía de excitación al oxígeno en estado fundamental triplete. El resultado de la transferencia es la formación de oxígeno singlete quien es el agente citotóxico responsable de la muerte celular (DeRosa and Crutchley 2002, Ethirajan, et al. 2011).

9.2 Mecanismos y Comportamiento Dinámico de Procesos Fotoinducidos en Sistemas Biológicos

Durante la elaboración de esta tesis doctoral se desarrolló un software que permite realizar simulaciones de dinámicas moleculares, bajo diferentes condiciones como: energía constante, temperatura constante y aplicación de fuerzas externas. Además, se implementó un algoritmo para dar cuenta de del comportamiento no adiabático dentro de las dinámicas moleculares, como se ha sdescrito en la sección previa.

Este conjunto de herramientas fue utilizado en el estudio dinámico de varios procesos fotoquímicos en sistemas modelo de interés biológico. A continuación se describe brevemente los resultados obtenidos.

9.2.1 Quimioluminiscencia y bioluminiscencia

El fenómeno de la quimioluminiscencia se refiere a la emisión de luz como resultado de la desactivación fluorescente de una molécula en estado excitado, la cual es producto resultante de una reacción química. Cuando este fenómeno se presenta en los seres vivos se llama bioluminiscencia.

Para el proceso de bioluminiscencia se ha encontrado que existe una familia de intermedios de reacción cíclicos, 1,2-dioxoetanos, que han sido señalados como los responsable de producir el fragmento en estado excitado responsable de la fotoemisión (Fraga 2008). Sin embargo, no existe aún un concenso sobre el mecanismo de formación del mismo. Además, algunos hechos como la relación fosforescencia/fluorescencia en la quimioluminiscencia todavía no se ha podido explicada satisfactoriamente.

Uno de los aspectos más interesantes en la descomposición del 1,2-dioxentane, es la aparición de una región dentro del espacio de fases denominada trampa entrópica (De Vico, et al. 2007). Este término se refiere a la situación donde los primeros cuatro estados singletes más bajos en energía e igualmente los primeros cuatro estados tripletes están degenerados en energía, en la región entorno al estado de transición que conlleva al rompimiento del enlace O-O.

Basados en la discusión anterior, en la presente tesis se lleva a cabo un conjunto de cálculos recurriendo a métodos configuraciones y estados con correcciones

perturbativas de segundo orden (MS-CASPT2), con el objetivo de proveer resultados claves que soporten en mecanismo biradicalario y su evolución en la trampa entrópica.

Además, dinámicas moleculares calculando el potencial "al vuelo" y usando el nivel de teoría CASSCF/ANO-RCC-VDZP, fueron llevadas a cabo para calcular el tiempo de vida medio de la molécula en la trampa entrópica en el estado fundamental. Además de esto, dado que el proceso de fosforescencia requiere una transferencia de población del estado fundamental al estado triplete, es necesario muestrear el espacio de fases en el estado fundamental con el objetivo de tener geometrías de referencia para futuros estudio de cruces entre sistemas.

9.2.2 Estudios QM/MM de la irisFP

En los últimos años, las proteínas fluorescentes (FPs) derivadas de la familia de proteínas verdes fluorescentes (GFP) han sido exitosamente aplicadas como marcadores biológicos (Wiedenmann and Nienhaus 2006), permitiendo la visualización de una amplia variedad de procesos, desde la expresión de los genes hasta el desarrollo celular y el movimiento de proteínas dentro de células vivas. Por otra parte, otras áreas tecnológicas como la microscopia óptica y fotónica aprovechan las características particulares de las FPs, lo que ha llevado al desarrollo de la nanoscopia óptica y el avance en dispositivos de almacenamiento de datos (Shaner, et al. 2007).

Estos logros han sido posibles gracias a la elevada resolución espacial y temporal ofrecida por las FPs, cuyas diferentes variedades pueden emitir diferentes colores e intensidades, dependiendo de la longitud de onda requerida para la irradiación.

Los estudios experimentales actuales se centran en la ingeniería genética (a través de la mutación genética dirigida) y de la caracterización estructural (mediante la espectroscopia de rayos X). Estas poderosas herramientas permiten la investigación sistemática del efecto de remplazar diferentes aminos ácidos en la estabilidad de la proteína y en el efecto deseado con respecto a la emisión y absorción de radiación, con respecto a FPs anteriores. Sin embargo, la mayoría de los intentos ha mostrado la inmensa dificultad de acertar cual mutación específica puede llevar a ciertos cambios en las propiedades biofísicas, siendo el entorno proteico del cromóforo altamente sensible al ambiente químico (puentes de hidrógeno, transferencia protónica, apilamiento π-π). En algunos casos una sola modificación de un aminoácido es suficiente para observar la variación espectroscópica esperada. En otros casos la modificación de amino ácido

conlleva de manera inesperada a la perdida casi completa de la emisión de fluorescencia, la cual puede ser recuperada luego de varias rondas de mutaciones aleatorias.

Sin embargo, la tarea de obtener una FP que pueda variar su absorción en la región del rojo (630-750nm), se ha convertido en el objetivo de números grupos de investigación dado que la mayoría de las FPs poseen un máximo de excitación en la región de los 400-588nm, Por lo que se requieren costosos láseres para llevar a cabo su fotoexcitación. Además, si se lograse que una FP absorbiese radiación cerca de los 640nm, un puntero de laser común podría ser usado como fuente, reduciendo el costo de las aplicaciones tecnológicas.

Por otra parte, estudios teóricos y computacionales han sido llevados a cabo con el fin de elucidar el mecanismo subyacente de fluorescencia, sugerido por los experimentos. Estudios de mecánica cuántica acoplados a los de mecánica molecular (QM/MM) han arrojado valiosa información sobre estos mecanismos. Sin embargo, el diseño racional de las propiedades fluorescentes de las FPs no se ha intentado hasta el momento, considerando las dificultades mencionadas.

Por lo tanto, En la presente Tesis se ha llevado a cabo un estudio preliminar sobre el cromóforo de la IrisFP embebido en un entorno QM/MM. Inicialmente se encontró un mínimo que daría cuenta de la observación experimental de fluorescente, puesto que los estudios teóricos en el vacío han mostrado que tal mínimo no existe. Así mismo, se caracterizó el entorno alrededor del mínimo y el área de intersección entre los dos primeros estados electrónicos singletes.

Con esta estructura de mínima energía se realizaron dinámicas moleculares, obteniéndose un espectro de fluorescencia teórico, comparable al espectro experimental descrito en la bibliografía (Adam, et al. 2008). Esta primera aproximación permitio aseverar la validez de la metodología usada, al mismo tiempo ha abierto el camino que permite estudiar sistematicamente las modifaciones en el entorno proteico (MM) y su repercusión sobre las propiedades espectroscopicas de tales mutaciones.

9.3 Respuesta fotoquímica al Estimulo de Fuerzas Externas

En el presente trabajo fue abordado el estudio estático y dinámico de las propiedades fotoquímicas de sistemas moleculares sometidos a fuerzas externas. Los estudios presentados en esta Tesis han permitido plantear nuevas metodologías con el fin

de predecir la modulación de propiedades espectroscópicas como resultados de la disrupción de las fuerzas externas en la topología de la superficie de energía potencial.

A continuación se describe brevemente tales metodologías.

9.3.1 Efecto del sustituyente

En la presente Tesis fue desarrollada una metodología para predecir la energía de excitación de un cromóforo sustituido, basado en las modificaciones geométricas inducidas por el sustituyente en el cromóforo de referencia. Para los cromóforos orgánicos, si el sustituyente no interacciona significativamente con la configuración electrónica responsable de la excitación, es entonces posible analizar el efecto del sustituyente sobre la longitud de onda absorbida, considerándo el sustituyente como una fuerza externa que modifica la geometría de equilibrio de la molécula de referencia.

Esta metodología pretende identificar las coordenadas moleculares responsables del cambio en la longitud de onda absorbida, utilizando una superficie modelo de tipo cuadrática. Se muestra, que tales coordenadas asociadas con el cambio de longitud de onda, están relacionadas con la distorsión perpendicular al gradiente molecular.

Esta Metodología se aplicó a la familia de S-nitrosotioles, utilizando geometrías de referencia a nivel CASPT2, obteniéndose las coordenadas responsables de la modulación de la energía de absorción. Así mismo, se evaluó la precisión del método al compararlo con cálculos ab initio y se discutió las causas de error.

9.3.2 Control opto-mecánico

El desarrollo de materiales a escala nanoscópica es uno de los retos actuales más abordados en la actualidad. De especial importancia son los materiales fotoactivos cuya configuración cambia al ser expuesto a la radiación electromagnética, convirtiendo la luz en movimiento microscópico. Entre de estos materiales se encuentran los interruptores fotosensibles, que están compuestos por cromóforos con dos estados estables, que pueden ser interconvertidos entre sí al absorber luz. Dado que el azobenceno presenta dos isómeros, cis y trans que pueden ser interconvertido entre sí por medio de la radiación electromagnética de diferentes longitudes de onda, resulta ser el candidato ideal para el desarrollo de dispositivos moleculares fotoactivos.

En la presente tesis se presenta un estudio teórico del efecto de fuerzas externas sobre las propiedades espectroscópicas con el objetivo de modular la absorción de un interruptor fotosensible en función de la fuerza externa aplicada, utilizando el azobenceno como interruptor. (Zapata, et al. 2013). Inicialmente, se llevó a cabo un estudio estático de la topología del azobenceno en estado fundamental fue llevado a cabo, pudiéndose determinar los valores extremos de fuerza a los que puede ser sometida sin que ocurre una disrupción irreversible en el sistema. Seguidamente una optimización a fuerzas externas constantes. Este procedimiento permitió identificar las geometrías moleculares más estables bajo una fuerza externa. Estas fuerzas son aplicadas como pares en las posiciones para de los anillos aromáticos.

Seguidamente, se llevaron a cabo dinámicas moleculares a fuerza externa constante, utilizando una aproximación cuadrática para el cálculo del gradiente. Dado que la representación cuadrática permite determinar el potencial de forma rápida, fue posible calcular en cada paso de integración, la energía para el estado fundamental y los dos estados excitados más bajos en energía S_1 y S_2, respectivamente. Con estos datos a disposición fue posible simular el espectro de absorción, construido como un histograma resultante de contar el número de energías de excitación ($S_0 \rightarrow S_1$ y $S_0 \rightarrow S_2$) que ocurren en un intervalo determinado durante las dinámicas. Al multiplicar cada entrada de este histograma por la fuerza del oscilador es posible obtener un espectro. Es importante notar que, un estudio estadístico (i.e. un muestreo aleatorio de geometrías tomadas de las dinámicas) fue llevado a cabo para identificar si existía una relación entra la energía de excitación para cada estado y la fuerza del oscilador, en el caso de existir tal relación se ajustó a una función para describirla, mientras en el caso de no existir alguna relación, la fuerza del oscilador utilizada corresponde a la media aritmética de los valores muestreados.

Los estudios dinámicos mostraron que no existe una modulación aparente cuando se aplican fuerzas de compresión para ambos isómeros. Sin embargo en el caso de fuerzas de extensión se ha encontrado que en el trans-azobenceno las fuerzas externas producen un desplazamiento batocrómico para la transición $S_0 \rightarrow S_1$, mientras que por el contrario, para la transición $S_0 \rightarrow S_2$ la aplicación de fuerza externa resulta en un desplazamiento hipsocrómico. Mientras que para el cis-azobenceno, las fuerzas externas producen un desplazamiento batocrómico para ambas transiciones. Seguidamente fueron identificadas

las coordenadas internas mayormente responsables en la modulación de la diferencia de energía para ambas transiciones, haciendo uso de las constantes de fuerza (i.e. Hessianos) obtenidas de las geometrías optimizadas a fuerza constate.

En este trabajo también se estudiaron posibles alternativas a la aplicación de fuerzas en posiciones diferente a posiciones para, encontrándose que las fuerzas aplicadas en posición meta podrían modular más eficientemente la diferencia de energía entre $S_0 \rightarrow S_1$ y $S_0 \rightarrow S_2$.

Finalmente, basado en los resultados previos se propone un polímero lineal que actúa como un interruptor fotosensible. Basados en los dos posibles modos de operación del polímero y en el grado de polimerización del mismo son propuestos valores teóricos para la cantidad de trabajo producido por unidad de tiempo.

9.4 Comportamiento Fotodinámico de Interruptores y motores moleculares

Los motores moleculares fotoactivos son dispositivos que tras la promoción a un estado electrónico excitado llevan a cabo un movimiento rotacional unidireccional, generalmente basado en una isomerización cis-trans de un doble enlace presente en la molécula (Garcia-Iriepa, et al. 2013). Este carácter unidireccional del movimiento rotatorio hace únicos a este tipo de dispositivos para distintas aplicaciones como el plegamiento de una macromolécula (Pijper and Feringa 2007), la generación de movimiento microscópico(Balzani, et al. 2009), etc.

Los motores moleculares propuestos hasta el momento (Feringa 2007), operan en ciclos de cuatros etapas: dos fotoquímicas (utilizando radiación electromagnética de dos diferentes frecuencias) y dos térmicas, siendo las etapas térmicas la limitación en la velocidad de rotación del motor. Además estos motores moleculares emplean estructurales helicoidales para asegurar la rotación unidireccional.

Una alternativa para mejorar el rendimiento de los motores moleculares ha sido propuesta (García-Iriepa, et al. 2013), en el cual se plantea una nueva estrategia para el diseño de motores moleculares con una alta velocidad de rotación, dado que dichos

motores operan a través de sólo dos etapas fotoquímicas (sin ninguna etapa térmica), las cuales son iniciadas con radiación electromagnética de la misma longitud de onda.

Estos nuevos motores moleculares deben presentar las siguientes características: a) su naturaleza electrónica deber ser tal que contenga un estado electrónico permitido que involucre la excitación de un enlace C=C; b) presencia de un enlace de hidrógeno quiral que sea lo suficientemente fuerte para producir la rotación unidireccional pero suficientemente débil para permitir la rotación en el estado excitado; c) la ausencia de mínimos de energía accesibles a la temperatura de reacción que permitan la formación de intermedios. En la Figura 9.2, se presenta un esquema de un posible motor molecular que cumple las mentadas condiciones mencionadas.

Con el objetivo de corroborar la naturaleza unidireccional del motor molecular propuesto, fueron llevadas a cabo simulaciones de dinámicas moleculares no adiabáticas. Estas simulaciones utilizan trayectorias clásicas para describir las regiones del espacio de fase donde el acoplamiento entre diferentes estados electrónicos es despreciable, mientras que el algoritmo de Tully (Tully 1990) es usado en las regiones donde el acoplamiento entre dos estados electrónicos es significativo. Se usó la implementación de este algoritmo descrita en (Valentini and Frutos 2012).

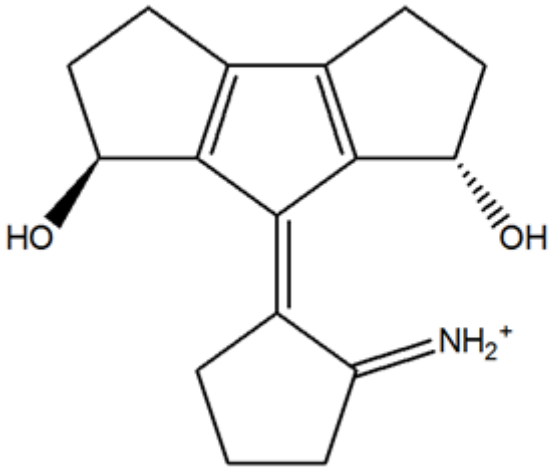

Figure 9.2. Posible motor molecular fotoactivo cuya rotación esta inducida por un enlace de hidrógeno que genera un entorno quiral.

9.5 Bibliografía

Adam, V.; Lelimousin, M.; Boehme, S.; Desfonds, G.; Nienhaus, K.; Field, M. J.; Wiedenmann, J.; McSweeney, S.; Nienhaus, G. U.; Bourgeois, D., Structural characterization of IrisFP, an optical highlighter undergoing multiple photo-induced transformations. *Proceedings of the National Academy of Sciences* **2008,** *105*, 18343-18348.

Balzani, V.; Credi, A.; Venturi, M., Light powered molecular machines. *Chem. Soc. Rev.* **2009,** *38*, 1542-1550.

Brennan, C. M.; Caldwell, R. A.; Elbert, J. E.; Unett, D. J., Nonvertical Triplet Excitation Transfer to Arylalkene Acceptors: Further Evidence That Double Bond Torsion Is Unimportant. *J. Am. Chem. Soc.* **1994,** *116*, 3460-3464.

Catalán, J.; Saltiel, J., On the Origin of Nonvertical Triplet Excitation Transfer: The Relative Role of Double-Bond and Phenyl-Vinyl Torsions in the Stilbenes. *The Journal of Physical Chemistry A* **2001,** *105*, 6273-6276.

De Vico, L.; Liu, Y.-J.; Krogh, J. W.; Lindh, R., Chemiluminescence of 1,2-Dioxetane. Reaction Mechanism Uncovered. *The Journal of Physical Chemistry A* **2007,** *111*, 8013-8019.

DeRosa, M. C.; Crutchley, R. J., Photosensitized singlet oxygen and its applications. *Coord. Chem. Rev.* **2002,** *233-234*, 351-371.

Ethirajan, M.; Chen, Y.; Joshi, P.; Pandey, R. K., The role of porphyrin chemistry in tumor imaging and photodynamic therapy. *Chem. Soc. Rev.* **2011,** *40*, 340-362.

Feringa, B. L., The Art of Building Small: From Molecular Switches to Molecular Motors. *The Journal of Organic Chemistry* **2007,** *72*, 6635-6652.

Förster, T., Delocalized excitation and excitation transfer. In *Modern Quantum Chemistry*, Sinanoglu, O., Ed. Academic Press: New York, 1965; pp 93-137.

Fraga, H., Firefly luminescence: A historical perspective and recent developments. *Photochemical & Photobiological Sciences* **2008,** *7*, 146-158.

Frenkel, D.; Smit, B., *Understanding Molecular Simulation*. second ed.; Academic Press: San Diego, 2002; Vol. 1.

Garcia-Iriepa, C.; Marazzi, M.; Frutos, L. M.; Sampedro, D., E/Z Photochemical switches: syntheses, properties and applications. *RSC Advances* **2013,** *3*, 6241-6266.

García-Iriepa, C.; Marazzi, M.; Zapata, F.; Valentini, A.; Sampedro, D.; Frutos, L. M., Chiral Hydrogen Bond Environment Providing Unidirectional Rotation in Photoactive Molecular Motors. *Journal of Physical Chemistry Letters* **2013,** *4*, 1389-1396.

Martyna, G. J.; Klein, M. L.; Tuckerman, M., Nosé-Hoover chains: The canonical ensemble via continuous dynamics. *The Journal of Chemical Physics* **1992,** *97*, 2635-2643.

Pijper, D.; Feringa, B. L., Molecular Transmission: Controlling the Twist Sense of a Helical Polymer with a Single Light-Driven Molecular Motor. *Angew. Chem. Int. Ed.* **2007,** *46*, 3693-3696.

Saltiel, J.; Marchand, G. R.; Kirkor-Kaminska, E.; Smothers, W. K.; Mueller, W. B.; Charlton, J. L., Nonvertical triplet excitation transfer to cis- and trans-stilbene. *J. Am. Chem. Soc.* **1984,** *106*, 3144-3151.

sandros, K., Transfer of Triplet State Energy in Fluid Solutions. III. Reversible Energy Transfer. *Acta Chem. Scand.* **1964,** *18*, 2355.

Shaner, N. C.; Patterson, G. H.; Davidson, M. W., Advances in fluorescent protein technology. *J. Cell Sci.* **2007,** *120*, 4247-4260.

Terenin, A.; Ermolaev, V., Sensitized phosphorescence in organic solutions at low temperature. Energy transfer between triplet states. *Transactions of the Faraday Society* **1956,** *52*, 1042-1052.

Tully, J. C., Molecular dynamics with electronic transitions. *The Journal of Chemical Physics* **1990,** *93*, 1061-1071.

Valentini, A.; Frutos, L. M., Tully's fewest switches algorithm with decoherence correction for the surface hop implemented in Molcas 7.6. 2012.

Wiedenmann, J.; Nienhaus, G. U., Live-cell imaging with EosFP and other photoactivatable marker proteins of the GFP family. *Expert Review of Proteomics* **2006,** *3*, 361-374.

Zapata, F.; Fernández-González, M. Á.; Rivero, D.; Álvarez, Á.; Marazzi, M.; Frutos, L. M., Toward an Optomechanical Control of Photoswitches by Tuning Their Spectroscopical Properties: Structural and Dynamical Insights into Azobenzene. *Journal of Chemical Theory and Computation* **2013,** *10*, 312-323.

Zapata, F.; Marazzi, M.; Castaño, O.; Acuña, A. U.; Frutos, L. M., Definition and determination of the triplet-triplet energy transfer reaction coordinate. *The Journal of Chemical Physics* **2014,** *140*, -.

Chapter 10: Appendices

"Cyberspace. A consensual hallucination experienced daily by billions of legitimate operators, in every nation, by children being taught mathematical concepts... A graphic representation of data abstracted from banks of every computer in the human system. Unthinkable complexity. Lines of light ranged in the nonspace of the mind, clusters and constellations of data. Like city lights, receding..."

Neuromancer. William Gibson.

10.1 A General Molecular dynamics interface program: HsDynamics

During this Ph.D. Thesis it was gradually developed a set of tools to carry out molecular dynamics and also some utilities to manage several important tasks as are: file parsing, calling of external electronic structure packages (Molcas, Gaussian, etc.), Input/Output processes and miscellaneous functions. Therefore it was developed a package called Hsdynamics to integrate the developed applications, taking advantage of the Haskell programming language and its libraries. The program can be run sequentially or using several CPUs to distribute the computations.

The code is under constant development and under a version control system, therefore it was not appended in the thesis, instead the latest version can be downloaded from here: https://github.com/felipeZ/Dynamics

The package structure is described in Figure 10.1, it provides a main module which initializes all the parameters required in the molecular dynamics and checks the input provided by the user. Once the molecule initial state has been successfully loaded, the control of the program is past to a loop in charge of performing the simulation. In another thread it is initialized a server logger which task is to receive messages from the main execution thread an do something with the message, for example write it in a file, print it in the standard output, send it to another machine with more memory, etc.

Subsequently the loop in charge of the simulation, calls the Dynamic module which executes the numerical integrations. The Dynamics module was built having performance as the main goal. Therefore it uses a library called REPA (REgular PArallel arrays), this library use a technique called parallel array fusion to calculate the numerical values of the arrays. The idea in the Dynamics module is to distribute the numerical integration in the available computing resources.

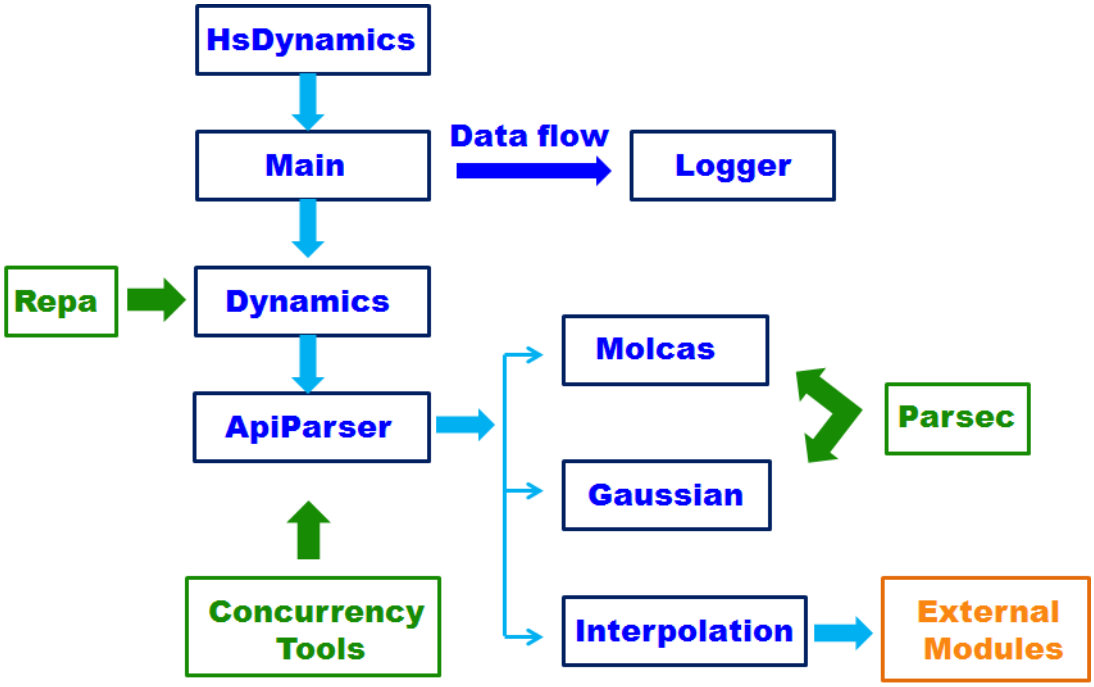

Figure 10.1. A diagram representing the structural organization of the HsDynamics software.

In order to compute the forces required by the integration of Newton's equation, an external electronic structure package is called to calculate the gradient "on the fly" or in the case of an interpolation some other modules should be called. The Dynamics module ApiParser presents an API (application programming interface) to the Dynamics client code in such a way that once it is specified which kind of calculation is intended ("on the fly" or interpolation) the Dynamics module asks for a force vector without noticing how is calculating, effectively isolating the numerical computation from the external packages.

On the other hand, the ApiParser module makes intensive use of the concurrency set of utilities offered by Haskell, mainly Async. The purposes of the ApiParser module is to call external packages, to write their input then to parse the corresponding output file and to read all the necessary parameters: gradients, energies and wave functions. The module also handles errors and closes the process smoothly if there is any problem.

Once the ApiParser module calls the external packages the resulting output must be read, even though this is quite a naïve method of communication between different software it enables fast development. It is important to notice that one of the deficiencies on computational chemistry is the lack of parsing tools, meaning a lack of a modular set of utilities which allow the structural analysys of output files, supporting an easy way to

lookup for important information. The vast majority of approaches in quantum chemistry are loops that searches for some keywords in a structureless stream of strings, which is a source of errors and very difficult to compose.

Our set of parsing modules offers a flexible collection of functions, which can be composed in more complex functions to form general parsing tools. In this sense, the modules Molcas and Gaussian, contains the utilities necessaries to recognize output structures of both computational packages and to record in a structure the most relevant information. Both of these modules were designed using the Parsec libraries of Haskell, which is a collection of several functions to create parsers.